COUPLING LINEARIZED FAR-FIELD BOUNDARY CONDITIONS WITH NONLINEAR NEAR-FIELD SOLUTIONS IN TRANSONIC FLOW

William S. Rowe and F. Edward Ehlers

Boeing Commercial Airplane Company
P.O. Box 3707
Seattle, WA 98124-2207

February 1988

Final Report
AFOSR Contract F49620-83-C-0118

Prepared for
United States Air Force
AIR FORCE OFFICE OF SCIENTIFIC RESEARCH
Building 410
Bolling Air Force Base
Washington, D.C. 20322

Boeing Document No. D6-52895

Unclassified

SECURITY CLASSIFICATION OF THIS PAGE

REPORT DOCUMENTATION PAGE

1a. REPORT SECURITY CLASSIFICATION: Unclassified	1b. RESTRICTIVE MARKINGS
2a. SECURITY CLASSIFICATION AUTHORITY	3. DISTRIBUTION/AVAILABILITY OF REPORT: Approved for public release; Distribution unlimited. Approved for public release; distribution unlimited.
2b. DECLASSIFICATION/DOWNGRADING SCHEDULE	
4. PERFORMING ORGANIZATION REPORT NUMBER(S): D6-52895	5. MONITORING ORGANIZATION REPORT NUMBER(S): AFOSR-TR- 88-0719
6a. NAME OF PERFORMING ORGANIZATION: Boeing Commercial Airplane Company; 6b. OFFICE SYMBOL (If applicable)	7a. NAME OF MONITORING ORGANIZATION: Air Force Office of Scientific Research
6c. ADDRESS (City, State and ZIP Code): P. O. Box 3707, Seattle, WA 98124-2207	7b. ADDRESS (City, State and ZIP Code): Building 410, Bolling Air Force Base, Washington, D.C. 20322
8a. NAME OF FUNDING/SPONSORING ORGANIZATION: AFOSR; 8b. OFFICE SYMBOL (If applicable): NA	9. PROCUREMENT INSTRUMENT IDENTIFICATION NUMBER: F49620-83-C-0118
8c. ADDRESS (City, State and ZIP Code): same as 7b.	10. SOURCE OF FUNDING NOS. — PROGRAM ELEMENT NO.: 61102F; PROJECT NO.: 2302; TASK NO.: B1; WORK UNIT NO.:
11. Coupling Linearized Far-Field Boundary Conditions With Nonlinear Near-Field Solutions in Transonic Flow	(U)
12. PERSONAL AUTHOR(S): Rowe, William S. and Ehlers, F. Edward	
13a. TYPE OF REPORT: Final Report; 13b. TIME COVERED: FROM 7/1/83 TO 2/29/88	14. DATE OF REPORT (Yr., Mo., Day): February 29, 1988; 15. PAGE COUNT: 172
16. SUPPLEMENTARY NOTATION	

17. COSATI CODES		
FIELD	GROUP	SUB. GR.

18. SUBJECT TERMS (Continue on reverse if necessary and identify by block number)
Unsteady Aerodynamics, Oscillating Wings, Transonic Flow, Flutter, Oscillating Airfoils

19. ABSTRACT (Continue on reverse if necessary and identify by block number)

Research has been conducted to evaluate the feasibility of coupling linearized far-field solutions with near-field finite difference equations to reduce the number of unknowns and thus the computer resources required in transonic flow calculations. For two-dimensional flow, changes to an existing finite difference program involved distributing sources on the grid boundary in order to obtain the proper far-field outgoing wave boundary conditions on a reduced grid. Validation of the matching procedure was made for zero thickness airfoils by comparison of the results with those of the kernel function method. For airfoils with finite thickness, a criterion based on the gradient of the flowfield Mach number was developed for establishing the minimum size finite difference region necessary for accurate unsteady calculations. Acceptable loading predictions were achieved for a 5:1 grid reduction ratio resulting in a 40% reduction in computer costs. This approach could not be applied directly to three-dimensional flow because of the large number of variables required in the exterior solution. However, it is shown that the number of unknowns can be reduced to a practical number by using both source and doublet distributions on the boundaries, describing these distributions with low-order polynomials, and using a least squares procedure to satisfy the matching conditions across the boundaries. Solutions for the flow over a wing of vanishing thickness were in very good

20. DISTRIBUTION/AVAILABILITY OF ABSTRACT: UNCLASSIFIED/UNLIMITED ☒ SAME AS RPT. ☒ DTIC USERS ☒	21. ABSTRACT SECURITY CLASSIFICATION: Unclassified
22a. NAME OF RESPONSIBLE INDIVIDUAL: Dr. Arje Nachman	22b. TELEPHONE NUMBER (Include Area Code): (202) 767-4937; 22c. OFFICE SYMBOL: NA

DD FORM 1473, 83 APR — EDITION OF 1 JAN 73 IS OBSOLETE.

Unclassified

SECURITY CLASSIFICATION OF THIS PAGE

19.

agreement with results from original finite difference technique and with the kernel function method. Solutions for a wing with thickness were in good agreement with results from the original finite difference technique. Since computing costs were reduced by as much as 95% of the cost for the original finite difference technique, the method of inner-outer matching is very promising. The pilot program used for this study is limited to rectangular wings.

FOREWORD

Contract F49620-83-C-0118 entitled "Coupling Linearized Far-Field Boundary Conditions with Nonlinear Near-Field Solutions in Transonic Flow" was sponsored by the Air Force Office of Scientific Research. The objective of this contract was to develop an efficient procedure for calculating pressure distributions and generalized forces in unsteady transonic flow for use in the evaluation of the flutter characteristics of aircraft.

Participants at the Boeing Commercial Aircraft Company include: Dr. Richard Ensminger, program manager; William S. Rowe, principal investigator; Dr. F. Edward Ehlers, and Warren H. Weatherill; all of the Flutter Research Group of the Structures Technology Department, Research and Development; and Dr. Roger Grimes of the Boeing Computer Services Company. The program manager for AFOSR was Dr. Anthony Amos of the Directorate of Aerospace Sciences.

This report describes the theoretical developments and validation studies accomplished during the course of the contract.

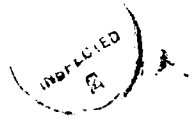

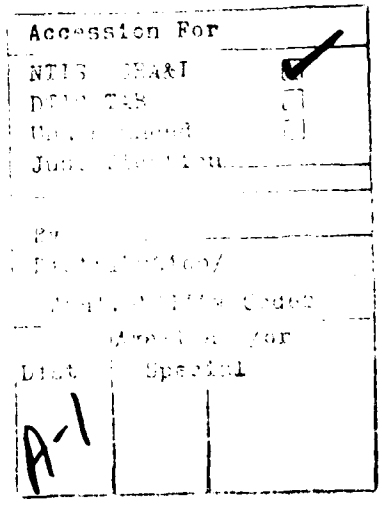

CONTENTS

CONTENTS (Concluded)

LIST OF FIGURES

LIST OF FIGURES (Concluded)

LIST OF TABLES

1.0 INTRODUCTION

Historically, flutter analysis of three-dimensional airplane configurations has been limited to the linearized (nonshock) flow regime where solutions are obtained for a relatively small number of unknowns. Unsteady loadings used in linearized flutter predictions are usually obtained by coupling assumed pressure distributions with a linearized kernel function to match the lifting surface normalwash boundary conditions. The number of unknowns is limited to the number of assumed pressure distributions that are distributed in a continuous fashion or applied as localized panel loadings over the lifting surfaces. Unsteady loadings obtained using panel methods (Doublet-Lattice or SOUSSA) usually limit the number of unknowns to some value that is less than 1000, even for a complicated 3D configuration. The number of unknowns to be evaluated in analysis using continuous pressure distributions is usually an order of magnitude less than that required in panel methods. That is, the number of unknowns is less than 100 when continuous pressures are used.

Transonic flutter predictions of some high aspect ratio wings have been successfully accomplished by applying experimental modification factors to the aerodynamic coefficients of linearized theory. Again, the number of unknowns to be evaluated is relatively small, and this problem size can be easily accepted on the relatively small core computers in use today. Transonic flutter predictions are needed early in the design stage to provide guidance for improving and validating airplane performance. It has been demonstrated that some high performance supercritical airfoils have severe flutter characteristics that need to be identified early in the design stage so that proper design changes can be applied to provide a stable flight system. It is nearly impossible to accurately represent unsteady surface pressures that contain an oscillating shock by means of a linear combination of assumed surface pressure distributions. Shocks that develop in transonic flows are not restricted to a localized region of the surface but extend out into the flow field away from the lifting surface and affect the entire flow field. Consequently, the velocity flow field around an airfoil having an embedded shock needs to be determined by a means that is more powerful than that used in nonshock flow analyses. A method that has proven successful in predicting the velocity field around an airfoil having attached shocks is one that determines the spatial variation of the velocity field from simultaneous solutions of the nonlinear differential equation evaluated at the intersections of a three-dimensional grid network that encompasses the airfoil. The number of unknowns to be evaluated in the 3D grid network may easily range up to 100,000 unknowns even for an analysis of an isolated lifting surface. The large number of unknowns taxes the limitations of present large core computers (such as the CRAY) when used in predicting unsteady loadings on isolated 3D surfaces. Consequently, unsteady loadings on complete 3D airplane configurations in unsteady transonic flow conditions must be deferred until extremelv large core computers are available in the future unless procedural modifications can be developed and applied to substantially reduce the number of solution unknowns.

2.0 NOMENCLATURE

a	Streamwise dimension of mesh region
b	Root semichord of wing or semichord of airfoil
C_p	Local pressure coefficient
f(x,y,t)	Instantaneous wing shape defined by $z_o = \delta f(x,y,t)$
f_o	Undisturbed wing or airfoil shape
f_1	Unsteady contribution to wing or airfoil shape
i,j,k	x,y,z subscripts and indices for points in the mesh
i	$\sqrt{-1}$
K	Transonic parameter, $(1 - M^2)/(M^2\varepsilon)$
M	Freestream Mach number
.,m	Mesh point indices
U_o	Freestream velocity
t	Time in units of b/U_o
x_o,y_o,z_o	Dimensionless physical coordinates
x',y',z'	Variables of integration
γ	Ratio of specific heats for air
ΔC_p	Jump in pressure coefficient
$\Delta\varphi_1$	Jump in φ_1 at plane of wing or vortex wake
$\Delta\varphi_{1te}$	Jump in φ_1, at wing trailing edge
δ	Thickness ratio
ε	$(\delta/M)^{2/3}$

2.0 NOMENCLATURE (Concluded)

λ_1	$\omega M/(1 - M^2)$
$\sigma(x,y)$	Source distribution over mesh boundary
φ	Complete, scaled perturbation velocity potential
φ_o	Steady scaled perturbation velocity potential
φ_1	Unsteady scaled perturbation velocity potential
ω	Reduced frequency

3.0 BACKGROUND INVESTIGATION

Given the difficulties resulting from the large number of unknowns required by current finite difference solution procedures, it is of interest to examine techniques for reducing the number of solution unknowns.

Numerical studies for this report began by using an existing finite difference computer program for unsteady transonic two-dimensional flow known as OPTRAN2 (ref. 1). The equations for OPTRAN2 are derived by simplifying the full time-dependent potential equations by assuming small disturbances and then separating the potential into steady and unsteady parts. The equation for the steady potential at high subsonic Mach numbers is the well-known nonlinear transonic equation. The equation for the unsteady potential, after assuming simple harmonic motion, is linear but with spatially varying coefficients which are functions of the steady potential. Shock motions are included as small motions about the steady-state location. Solutions are obtained either by direct solution or, for a limited range of Mach numbers and reduced frequency, by relaxation methods.

Unsteady loading predictions obtained from OPTRAN2 compare favorably with predictions obtained from other transonic computer programs such as the results of XTRAN2 (ref. 2), a "time-integration" procedure, as illustrated in Figure 1.

Results of one of the numerical excursions are shown in Figure 2, which presents a comparison of the velocity potential spatial variation above and below the wing plane (at the midchord station) for a flat plate and a NACA 64A010 airfoil section. The potential discontinuity across the finite thickness airfoil is greater than that obtained for the zero thickness airfoil. Spatial characteristics are quite similar at small distances away from the mean planes. A similar trend may also be observed for the spatial variation of the velocity potentials of the MBB-A3 airfoil section that is shown in Figure 3.

In both comparisons, the differences between potentials of finite thickness and zero thickness airfoils appear to be significant only in localized regions in the near vicinity of the airfoil. Effects of nonlinearities tend to diminish rapidly with increasing distance from the airfoil, so the potential distribution of the shock loaded finite thickness airfoil rapidly approaches the linearized solution of the zero-thickness airfoil. It appears that there is a substantial region of the finite difference grid network where the flowfield takes on linear characteristics that do not need to be evaluated by finite difference procedures. Consequently, the size of the grid network may be greatly reduced by taking advantage of the far-field linearity characteristics of the nonlinear solution by coupling an appropriate linear far-field solution with the nonlinear near-field solution. A schematic of such a modification procedure is shown in Figure 4.

The grid network would be reduced to some moderate size and the solution region would be separated into two parts. The linearized solution region outside of the network would extend to infinity from the outer boundary and the nonlinear solution region would be confined to the interior grid network. Sources (and perhaps doublets) of unknown strengths would be applied to the outer faces of the grid network in order to couple the two dissimilar solution regions. Solution coupling is obtained by matching both the velocity potential and its normal derivative on the interface boundary of the reduced size network.

Results of the preliminary investigation indicated that it may be possible to achieve a five-to-one reduction in the number of solution unknowns. A schematic (fig. 5) shows the network reduction that is thought to be possible for transonic analyses of isolated two-dimensional lifting surfaces.

4.0 OVERALL APPROACH

This research is directed toward determining the feasibility of coupling linearized far-field with nonlinear near-field solution procedures to reduce the size of finite differencing grid networks presently required in transonic analysis of three-dimensional airplane configurations.

The research is divided into two parts. The first part involves evaluating the feasibility of coupling two dissimilar solution procedures in the analysis of two-dimensional airfoil sections with an ultimate goal of demonstrating the capability of predicting unsteady loadings on a two airfoil (e.g., a wing-tail combination) problem. The second part consists of extending the analysis to three-dimensional lifting surfaces.

Existing finite difference computer programs developed to predict unsteady loadings on two-dimensional and three-dimensional isolated lifting surfaces are to be modified by inserting algorithms necessary to couple the linear and nonlinear solution procedures. The existing computer programs to be modified are the Boeing-developed programs designated as OPTRAN2 and OPTRAN3.

OPTRAN2 is a finite differencing program developed to evaluate unsteady loadings on two-dimensional airfoil sections due to infinitesimal oscillations about a steady angle of attack. Potential solutions may be obtained for zero-thickness or finite thickness airfoil sections. Viscosity effects are not accounted for in the program formulation; however, finite thickness loading predictions appear to be reasonable when compared with experimental data. Also, loading predictions for the zero-thickness case converge to values obtained from linearized theories that are known to be accurate.

OPTRAN3 is an extension of OPTRAN2 and has been formulated to predict unsteady transonic loadings on isolated three-dimensional wing configurations.

Major tasks involved in the two-dimensional investigation are identified as follows:

1. Develop analytical expressions for the far-field potentials due to sources (and perhaps doublets) distributed on the outer face of the grid network.
2. Develop necessary algorithms to couple the two-solution procedures, modify OPTRAN2, and check the program for accuracy of calculation.
3. Evaluate the validity of the coupling procedure by comparing computed results with exact predictions on a two-dimensional zero-thickness airfoil.
4. Compare predictions of the coupling procedure with results obtained from a full-grid analysis of OPTRAN2 applied to airfoils having attached shocks.
5. Demonstrate capability of predicting unsteady loadings on two airfoils in same flowfield (similar to a wing-tail combination).

Major tasks to be accomplished in the three-dimensional portion of this investigation are essentially the same as those described in the two-dimensional portion, with the exception that program modifications are to be applied to the finite span lifting surface program, OPTRAN3 and wing-tail combinations will not be included here.

5.0 TWO-DIMENSIONAL INVESTIGATION

5.1 ANALYTICAL DERIVATIONS

All analytical expressions necessary to couple two dissimilar solution regions have been derived and are given in Appendixes A, B, C, and D.

Expressions for the spatial variation of the velocity potentials caused by distributions of sources and/or doublets and the infinite wake are given in Appendix A.

Equations necessary to couple the linearized far-field potentials with the finite differencing near-field potentials are derived in Appendix B.

Appendix C contains the expressions used to evaluate the potential due to the infinite wake. The potentials due to the infinite wake are reduced to matrix coefficient form in Appendix D.

5.2 BASIC EQUATIONS EVALUATED BY OPTRAN2

Since the mathematical derivation of the method for the solution of the unsteady velocity potential for the flow about a harmonically oscillating wing is presented in Reference 1, the discussion here will be limited to a brief outline for the procedure for two dimensions. A more detailed discussion of the equations for three-dimensional flow is given in Appendix E. The complete nonlinear differential equation was simplified by assuming the flow to be a small perturbation from a uniform stream near the speed of sound. The resulting equation for unsteady flow is

$$[K - (\gamma-1)\varphi_t - (\gamma+1)\varphi_x]\,\varphi_{xx} + \varphi_{yy} - (2\varphi_{xt} + \varphi_{tt})/\varepsilon = 0, \tag{1}$$

where $K = (1 - M^2)/(M^2\varepsilon)$, M is the freestream Mach number of velocity U_o in the x direction, x and y are made dimensionless to the semichord b of the airfoil and the time t to the ratio b/U_o. With the airfoil shape as a function of time defined by the relation

$$y_0 = \delta f(x,t),$$

the linearized boundary condition becomes

$$\varphi_y = f_x(x,t) + f_t(x,t). \tag{2}$$

The quantity δ is associated with properties of the airfoil (such as maximum thickness ratio, camber, or maximum angle of attack) and is assumed to be small. The coordinate is scaled to the dimensionless physical coordinate y_o according to

$$y = \delta^{1/3} M^{2/3} y_0,$$

and ε is given in terms of δ by

$$\varepsilon = (\delta/M)^{2/3}.$$

The pressure coefficient is found from the relation

$$C_p = -2\varepsilon(\varphi_x + \varphi_t).$$

The preceding differential equation is simplified by assuming harmonic motion and by assuming the velocity potential to be separable into a steady-state potential and a potential representing the unsteady effects. We write for the perturbation velocity potential

$$\varphi = \varphi_0(x,y) + \varphi_1(x,y)e^{i\omega t} \tag{3}$$

and for the body shape

$$y_0 = \delta f(x,t) = \delta\,[f_0(x) + f_1(x)e^{i\omega t}].$$

Since the steady-state terms must satisfy the boundary conditions and the differential equation in the absence of oscillations, we obtain

$$[K - (\gamma + 1)\varphi_{0_x}]\varphi_{0_{xx}} + \varphi_{0_{yy}} = 0 \tag{4}$$

with

$$\varphi_{0_y} = f_0(x), \qquad y = 0, \qquad -1 \leq x \leq 1. \tag{5}$$

On the assumption that the oscillations are small and products of φ_1 may be neglected, equations (1) and (2) with the aid of equations (4) and (5) yield

$$\{[K - (\gamma + 1)\,\varphi_{0_x}]\,\varphi_{1_x}\}_x + \varphi_{1_{yy}} - (2i\omega/\varepsilon)\,\varphi_{1_x} + q\varphi_1 = 0, \tag{6}$$

where

$$q = \omega^2/\varepsilon - i\omega(\gamma - 1)\varphi_{0_{xx}}$$

subject to the wing boundary conditions

$$\varphi_{1_y} = f_{1_x} + i\omega f_1(x), \; y = 0, \qquad -1 \leq x \leq 1. \tag{7}$$

The differential equation of (6) is of a mixed type, being elliptic or hyperbolic whenever the steady state equation (4) is elliptic or hyperbolic. The finite difference equations are formulated by using central differencing in defining the y and z derivatives, whereas the x derivatives are evaluated using central differencing whenever the region is subsonic (having elliptic characteristics). Upstream (or backward) differences are applied in defining the x derivative at all hyperbolic stations.

The boundary condition requirement that the pressure be continuous across the wake from the trailing edge was found in terms of the jump in potential $\Delta\varphi_1$ to be

$$\Delta\varphi_1 = \Delta\varphi_{1_{te}} e^{-i\omega(x - x_{te})}, \tag{8}$$

where $\Delta\varphi_{1_{te}}$ is the jump in the potential at $x = x_{te}$ just downstream of the trailing edge and is determined to satisfy the Kutta condition that the jump in pressure vanish at the trailing edge. The quantity $\Delta\varphi_1$ is also used in the difference formulation for the derivative $\varphi_{1_{yy}}$ to satisfy continuity of normal flow across the trailing edge wake.

The system of equations that is solved by OPTRAN2 is the set of linear spatially variable coefficient equations given by equation (6), where only the unsteady part of the potential is being evaluated. The total potential given by equation (3) is composed of an unsteady part and a steady part.

OPTRAN2 does not solve for the steady potentials - that is, it evaluates only the unsteady potentials. Evaluation of the unsteady loadings on a finite thickness airfoil requires that the steady-state potential distribution be obtained from an external source for input to OPTRAN2. The steady-state program that has been used in this investigation is known as TSFOIL and is described in Reference 3.

Total potentials are obtained by adding the steady potentials of TSFOIL to the unsteady potentials of OPTRAN2. Solutions for the unsteady potentials are obtained by a direct solution since the equations are linear but have spatially variable coefficients.

5.3 MODIFICATION PROCEDURES APPLIED TO OPTRAN2

In the finite difference formulation for a boundary value problem of a partial differential equation, boundary conditions must be specified on the mesh boundaries to make the system of equations solvable. For the case of harmonic oscillations on a wing, the proper boundary conditions require outgoing waves. The far-field solution can be approximated by the classical linearized equation. The research described here is the investigation of prescribing singularity distributions on the mesh boundaries and matching the resulting outer solution with the inner finite difference formulation.

Sources are distributed along individual segments of the outer boundary (as shown in fig. 6) in order to provide continuity in the velocity potential and its normal derivative at the outer boundary.

Velocity potentials and their derivatives are calculated for each of the solution matching stations that are located on the boundary of the reduced sized grid network. The potential calculation involves evaluating the potential due to each of the triangular shaped source distributions and the potential due to the infinite wake.

The equation for the velocity potential for a control station derived in References 1 and 4 is given by

$$\varphi_1 = -\frac{e^{i\lambda_1 Mx}}{4i}\int_{-a}^{a}[\sigma_u\psi_u - \sigma_d\psi_d]\,dx' - \frac{e^{i\lambda_1 Mx}}{4i}\int_{-b}^{b}[\sigma_\ell\psi_\ell - \sigma_r\psi_r]\,dy' + \Delta\varphi_{1_{te}}\cdot\chi(x,y), \tag{9}$$

where $\psi = H_0^{(2)}\left[\lambda_1\sqrt{((x-x')^2 + K(y-y')^2)}\right]$ (a Hankel function)

$$\chi = -\frac{1}{4i}\int_1^\infty e^{-i\omega(x'-1)}\,\psi_y dx'.$$

The linear and nonlinear solutions are coupled together by equating potentials and normal derivatives at the boundaries. The coupling equations for the upstream boundary are given as:

$$\varphi_{1x} = (\varphi_{2j} - \varphi_{1j})/(x_2 - x_1) \tag{10}$$

$$\varphi_1 = (\varphi_{2j} + \varphi_{1j})/2, \tag{11}$$

where φ_{1j} and φ_{2j} are the perturbation potentials from the finite difference solution. Similar relations hold for the other three sides. Equations (9), (10), and (11) are discretized by prescribing the source distribution at mesh points along the mesh boundary as in Figure 6. In the first attempt, the integration

of equation (9) was performed numerically using a triangular basis function as shown in Figure 6. The use of this basis function centered at each point on the boundary yields a continuous piecewise linear distribution of the source strength over the boundaries, and resulting potentials are evaluated at the discrete mesh points. At first, the values of the kernel function were calculated at the mesh points on the boundary and interpolated quadratically at the midpoints to make an efficient program. A five point Simpson's rule was first tried to evaluate the individual integrals of the basis function potential. The combined equations for the inner flow and equations for the source distribution of the outer solution are inserted into a large matrix array (see fig. 7) and solved simultaneously.

It must be noted that a substantial amount of computing time is required in evaluating the coefficients of the potentials due to the source distributions and infinite wake. Nonetheless, it is anticipated that the overall number of CP seconds required by this grid reduction procedure will be less than that required for full grid analyses.

6.0 VALIDATION FOR ZERO THICKNESS AIRFOILS

Validation of this modification procedure is established by showing the capability for accurately predicting unsteady loadings on zero-thickness airfoils. It is then assumed that it can be accurately applied in analyses of finite thickness airfoils that are subjected to nonlinear flows.

The accuracy of predictions obtained from this OPTRAN2 modified procedure is established by comparing predictions obtained from a method developed by Bland (ref. 5) of NASA LRC that is known to be accurate.

Prior to making comparisons between the results with the revised procedure and exact results, an initial computer run was made to determine the prediction accuracy of the basic unmodified OPTRAN2 program. These results are shown in Figure 8. The continuous solid lines represent the prediction results of the BLAND (NASA LRC) (ref. 5) method and the open symbols represent the results obtained using the full 60 by 72 grid available in OPTRAN2. It is to be expected that small differences would be present since the full grid OPTRAN2 does not fully account for an infinite wake but has a wake that extends only 1-½ chordlengths downstream of the trailing edge. Nontheless, the predictions appear to be reasonably close for the most part and it is expected that small differences should exist between the full grid and modified grid analyses.

Program checkout was then initiated and a series of computer runs was obtained to assess the prediction accuracy of this modification procedure. Typical results of one of the grid reduction cases are shown in Figure 9.

It was evident that for this example the technique failed to provide reasonable predictions for the zero-thickness case, and one would expect to obtain poor correlation for analyses of the finite thickness case in mixed transonic flow conditions. Consequently, the program was reexamined for possible coding errors and/or limitations of the applied integration techniques in order to identify the cause of the lack of correlation.

Several coding errors were detected and the revised coding was inserted into the program. However, these corrections only modified the predicted results by a very small amount, which essentially resulted in revised predictions that were approximately the same as those shown in Figure 9. Integration accuracy checks were then conducted to evaluate the accuracy level of the integration procedure. As a result of this investigation, two program changes were made: (1) the basis function shown in Figure 6 was changed to one that is continuous in the first derivative as shown in Figure 10, and (2) Legendre-Gauss integration quadratures were inserted to replace the Simpson's Rule integration technique previously used. Logarithmically singular integrals were formulated in analytical form and were used in place of the quadrature techniques previously applied in this portion of the program.

Computer runs that followed these program changes result in the reasonable predictions that are shown for a typical case in Figure 11.

In order to evaluate the effect of the shape of the basis function on prediction results, the original piecewise continuous basis function was reinserted into the program and this change produced results that were almost identical with the results of Figure 11. Since the results are almost identical, it is evident that reasonable correlations may be achieved by using either one of the basis functions to define the distributions of externally applied source distributions. The more important conclusion is that the Simpson rule integration methods do not provide the integration accuracy necessary for good correlations.

After a series of computer runs, it was established that the minimum size grid network that can be used to provide accurate predictions of unsteady loadings on zero-thickness airfoils is a grid network that maintains at least four horizontal grid lines above and below the airfoil and at least four vertical grid lines spaced ahead of the leading edge and behind the trailing edge. The requirement of maintaining four grid lines above and below the surface coincides with using four grid points to calculate a second order derivative using finite differencing techniques.

Analysis results are shown in Figure 12 for a case where four grid lines are distributed above and below the surface and four grid lines are spaced ahead of and behind the airfoil. The grid size reduction ratio is approximately 10:1 and was achieved at a cost that is 52% of the cost required for a full grid OPTRAN2 analysis.

Prediction accuracy becomes unacceptable for cases where there are less than four grid lines distributed above and below the airfoil. An example of the accuracy deterioration that may result is shown in Figure 13 for a case where only three horizontal grid lines are distributed above and below the airfoil.

It appears that the largest reductions that can be achieved by coupling analytical and finite differencing techniques as applied to solutions of second order differential equations are limited to a 10:1 reduction of grid size and a 50% reduction of computer costs. These limiting values are applicable only to linear flow systems. Reduction ratios are expected to be substantially less for analyses involving nonlinear flows described in the next section.

7.0 VALIDATION FOR FINITE THICKNESS AIRFOILS

Validation investigations have been extended to determine the feasibility of reducing the size of grid networks associated with analyses of finite thickness airfoils subjected to nonlinear transonic flow conditions.

7.1 MODERATE SHOCK LOADING CONDITIONS

The investigation was extended to evaluate the feasibility of reducing the network grid size in the analyses of finite thickness airfoils having a moderate shock only on one side of the airfoil.

An initial investigation covered an analysis using a NACA 64A010 airfoil section oscillating in pitch about a 1-deg mean angle of attack at $M = 0.80$. Velocity potentials and Mach number variations for steady-state flow conditions were obtained from the output of TSFOIL in order to initiate the OPTRAN2 analysis. Spatial variations of the flow field Mach number obtained from TSFOIL are shown in Figure 14 in the form of Mach number contour plots. The background grid is not drawn to scale but is used to indicate the number of grid lines that were applied in the steady-state analysis. For this case, the upper and lower boundaries are located 12.73 chordlengths above and below the surface. The forward boundary is located 4.83 chordlengths ahead of the leading edge and the downstream boundary is located 4.89 chordlengths aft of the trailing edge. The numbers appearing in the margins represent the locations of the unsteady grid network relative to the steady-state network. The unsteady network has 30 horizontal grid lines above and below the surface and there are 12 vertical grid lines distributed ahead of the leading edge, 18 behind the trailing edge, and 42 are distributed over the length of the airfoil.

The Mach contour plot indicates that the flow characteristics ahead of and behind the airfoil deviate from remote conditions by only a small amount. This suggests that the forward and aft boundaries may be located very close to the leading and trailing edges similar to locations that were found to be appropriate in analyses of zero-thickness airfoils.

Even though shocks are not present in the region below the airfoil, it appears (from a rough plot of Mach number versus vertical distance) that the gradient of the Mach number may have nonlinear characteristics in a region that may extend 1/2 chordlength into the flow field below the lower surface. This will confine the location of the lower boundary to a region that is located at a distance that is at least 1/2 chordlength or greater below the lower surface.

From a plot of Mach number versus vertical distance above the airfoil, it appears that the gradient of the Mach number has linear characteristics at distances greater than .8 chordlength above the surface. This should prove to be the minimum distance that the upper boundary can be located relative to the upper surface for accurate predictions of unsteady loadings.

Results of a computer run made using the approximate boundary locations described above are shown in Figures 15 and 16. The predictions obtained from the coupling procedure are almost identical to those obtained by the full grid analysis method except for a small region near the midchord where minor differences exist for the out-of-phase loadings. One possible reason for the localized difference in predictions is that there may be spurious waves generated within the interior finite differencing grid. Spurious waves are generally caused by satisfying the boundary conditions only at discrete points instead of in a continuous manner around the exterior boundary. In order to evaluate this possible error source, the program was modified to include the effects of adding doublet distributions to the exterior of the grid boundary. The added doublets would allow using the additional boundary condition of setting $\varphi = 0$ in the interior grid region and eliminate any spurious waves in the finite differencing network. The predictions that resulted from this program modification were found to be almost the same as the results

obtained by the original formulation that made use of source distributions only. It was concluded that for this case, if spurious waves are in the inner grid, their effect was minimal and there is no need to apply additional doublet distributions to enhance the loading predictions.

Also, prediction differences observed in Figure 16 may be due to comparing the output of two programs that use different representations of the infinite wake. The full grid OPTRAN2 program takes into account the wake effects only over a distance of 1-½ chordlengths downstream of the trailing edge, whereas the coupling procedure uses the complete infinite wake. Prediction differences between OPTRAN2 and an "exact" program of NASA-LRC (as shown in fig. 8) are of the same order of magnitude as shown in Figure 16. Consequently, the coupling procedure results are accurate within the error bounds defined for the full grid OPTRAN2 analysis and therefore are judged to be acceptable.

A numerical investigation was then conducted in an attempt to develop a criterion that can be applied in defining optimum grid sizes to reduce computer costs. The investigation involved developing a plot of the spatial variation of the Mach number as a function of the vertical distance above the airfoil shown in Figure 17. This plot was constructed from the information contained in the upper regions of the flow field Mach contour plot of Figure 14. Then a series of computer runs was made for analysis cases where the upper boundary was varied while the forward, aft, and lower boundaries were maintained in the fixed locations defined in Figures 15 and 16. Prediction results obtained from these analyses were then judged to be acceptable or unacceptable in comparison with the reference predictions obtained from the full grid OPTRAN2 analyses. The location of the upper boundary relative to the upper surface of the airfoil for each analysis case was then identified on the Mach variation plot of Figure 17.

The demarcation zone that separates acceptable predictions from unacceptable predictions is denoted by the crosshatched region. The vertical line dividing acceptable from unacceptable results is not a single line of zero width but is a region having finite width where prediction accuracy gradually changes from unacceptable to acceptable. The width of the region was not determined in this study since this would require changing the vertical spacing of the horizontal grid lines that are "hardwired" into the basic program. However, it has been determined that the demarcation zone does not include the region where the upper boundary of the eight grid line case is located. This may be illustrated by examining the loading predictions for the eight grid line case shown in Figures 18 and 19 where the plotted results indicate that the predictions are unacceptable since large differences in predictions exist over the entire chordlength including the region containing the shock loadings.

Unsteady loading predictions shown in figures 20 and 21 were obtained for the smallest size grid network that can be used to provide acceptable results. The network size is identified as having nine grid lines above the surface, seven grid lines below the lower surface, four grid lines ahead of the leading edge, and four grid lines behind the trailing edge.

It should be noted that the analysis case contained within the demarcation zone and having predictions judged to be acceptable has a gradient of the Mach number given by

$$\Delta M/\Delta y = -0.156.$$

It may be coincidental but this value is nearly the numerical value of the upper limit for which linear terms can be used to approximate transcendental functions within 1% error bounds. It appears that one criterion that can be used to obtain accurate predictions is that the gradient of the Mach number on the outer boundaries must be equal to or less than the numerical value of the upper limit for which linear terms may be used to approximate transcendental functions within 1% error bounds.

The following numerical investigation is developed to evaluate the validity of using this criterion in analyses involving small shock loading conditions.

7.2 SMALL SHOCK LOADING CONDITIONS

The small shock loading analysis case was developed using a NACA 64A010 airfoil section oscillating in pitch about a mean angle of attack of 1-deg at M = 0.78. The same analysis procedures used in the previous case were applied to provide the plot of Figure 22, which represents the flow field Mach number variation in terms of Mach contour lines.

The region below the airfoil does not have enough information to identify how far the nonlinearities extend into the flow field. However, it is observed in comparing the locations of the Mach contour lines of Figures 14 and 22 that the contours for the small shock loading case extend a smaller distance into the lower flow field than do the contours of the moderate shock loading case. Consequently, the locations of forward, aft, and lower boundaries will be initially set at the boundary locations defined for the network of the moderate shock loading case.

The region above the airfoil has a sufficient number of contour lines to construct the plot of Mach number variation with respect to vertical distance from the airfoil shown in Figure 23. Then a series of computer runs was made for various upper boundary locations and the results were judged to be acceptable or unacceptable and noted as such by the demarcation zone shown on the plot of Figure 23. The demarcation zone that separates acceptable from unacceptable results is identified by the vertical crosshatched region.

Prediction differences become very large for cases where the location of the upper boundary lies to the left of the demarcation zone. For example, analysis results shown in Figures 24 and 25 were obtained for the first case located to the left of the demarcation zone. The predictions are judged to be unacceptable since they differ by approximately 10% over the region forward of the shock and the out-of-phase shock loading is underestimated by approximately 20%.

Once the accuracy limit of the upper boundary location was established, the lower boundary was moved to a new location and computer runs were conducted to identify the smallest size network that could be used to provide acceptable loading predictions for this analysis case. The unsteady loading predictions shown in Figures 26 and 27 represent predictions obtained for the smallest size network that can be used for providing accurate loadings. The network consists of nine horizontal grid lines above the surface, six below, four grid lines ahead of the leading edge, and four grid lines behind the trailing edge. The grid size reduction ratio that is achieved is greater than the 5:1 goal that was established at the beginning of this investigation.

It appears that the previously developed criterion is also valid for this analysis case since the gradient of the Mach number

$$\Delta M/\Delta y = -0.135$$

lies well below the upper limit of the numerical values for which linear terms may be used to approximate transendental functions within small error bounds.

A final check on the approximation of the criterion is made by examining its effect in predicting loadings for systems subjected to symmetrical shock loadings.

7.3 SYMMETRICAL SHOCK LOADINGS

The symmetrical shock loading case was developed for a NACA 64A010 airfoil section oscillating about a 0-deg mean angle of attack at M = 0.825. The flow field Mach number variation obtained from

TSFOIL is shown in Figure 28 in a form of Mach contour plots. Symmetrical shock loadings extend a distance of .43 chordlength into the flow field above and below the surface.

Upper and lower grid line boundaries for a series of runs were noted on the plot of Figure 23 which shows the spatial variation of Mach number with respect to distances above and below the airfoil. A more detailed plot of Mach number versus distance above the wing is shown in Figure 29. Included in this figure is a crosshatched region indicating a demarcation between acceptable and unacceptable results based on comparisons with OPTRAN2. The demarcation line is located in a region where the value of the gradient of the Mach number with respect to the vertical coordinate, $\Delta M/\Delta y$, equals -0.15, and lies within the numerical upper limit where linear terms can still be used to approximate transcendental functions within 1% error bounds. Results obtained for the case of having nine grid lines above and below the airfoil are shown in Figure 30 and 31. Differences in the loading predictions appear to be within acceptable error bounds of Figure 8. Consequently, the results are judged to be acceptable.

Prediction differences rapidly attenuate to zero for cases exceeding nine grid lines above and below the airfoil. Also, prediction differences become very large for networks that have less than nine grid lines above and below the surface.

It is important to note that the reason for requiring a minimum of nine grid lines distributed above and below the airfoil for this analysis case is due to the fact that the ninth grid line (which defines the outer boundary location) happens to be located at a vertical station that has a Mach number gradient value that is contained within the acceptable numerical range for which linear terms may be used to approximate transcendental functions.

8.0 TWO AIRFOIL SOLUTION

Unsteady harmonic oscillation of two airfoils in the same flow field was investigated to evaluate the feasibility of reducing the size of finite differencing grid network required for a total two airfoil system analysis. Each airfoil was encased with a separate grid network having its own individual source distributions applied to the outer surface of each network.

The size of the grid network surrounding each airfoil was chosen to correspond to a size that was previously found to be suitable for analysis of a single airfoil. The analysis was developed using a NACA 64A010 airfoil section oscillating at a reduced frequency of $k = 0.30$ about a 1-deg mean angle of attack for $M = 0.80$.

Unsteady interaction effects between the two airfoils is taken into account by having the boundary conditions of each network prescribed in such a way that the total combined source distribution influences each of the grid regions. Interaction effects between the two airfoils influence only the externally applied source distributions, which in turn effect the boundary conditions on external surfaces of the networks to change the loadings on the individual airfoils.

The boundary condition on the main airfoil was chosen to be the same as that used in a single airfoil analysis—pitching about the leading edge. The second airfoil was maintained in a stationary position to act as a reflector for the waves generated by the main airfoil. Computer programs are not available to provide steady-state flow solutions for the combined two airfoil analysis. Consequently, we applied the single surface steady-state TSFOIL results to each individual airfoil. That is, we represented the steady-state flow conditions acting on the two airfoils in a manner that assumed there were no interaction effects existing between the two airfoils. Unsteady loading predictions resulting from applying this assumption will be in error since steady-state shock location will not be properly defined. However, even with these shortcomings, the feasibility of the solution matching technique can be evaluated to determine its effectiveness in reducing grid size requirements in analyses of multiple airfoil systems.

Program checkout included making several runs to assess the interaction influence between vertically spaced airfoils. This verified that the unsteady loadings limited out to the same loadings obtained for the analysis of an isolated airfoil when spatial separation became large.

Main surface unsteady loadings obtained for the two airfoil systems are compared with single surface loadings in Figures 32 and 33, where airfoils are horizontally separated by a distance of 1.5 chordlengths and vertically separated a distance of .5 chordlength.

The reflector airfoil has a substantial influence on the loading developed on the forward surface. This may be due to the fact that two-dimensional disturbances decay more slowly than do three-dimensional disturbances. For two-dimensional flow, the disturbances decay in proportion to $\exp(-i\omega r)/\sqrt{r}$, and in 3-dimensional flows they are proportional to $\exp(-i\omega r)/r$. The shock location (predicted by the dual airfoil system) remains in the same position as that predicted of the single airfoil, since its position was determined by the steady-state solution.

In reality the second airfoil would have altered the steady-state shock location from the single airfoil solution, and this would have been reflected in the unsteady solution as well.

However, the reflecting airfoil does have an influence on moving the shock. At the location of the steady-state shock position, a jump in the unsteady potential usually occurs across the shock. As an example, Figure 34 shows a plot of the distribution of the jump in unsteady potential across the airfoil.

We see that a jump in this quantity occurs at x = 0.18, the location of steady state-shock. From equation D-3 in Reference 6, this jump in potential is seen to be a measure of the oscillation of the shock position. When the motion of the shock is given by

$$x = x_1 e^{i\omega t},$$

the complex amplitude of the shock is given by the relation

$$x_1 = [\varphi_1]/[\varphi_{ox}].$$

The notation [ ] denotes jump across the shock. The quantity$[\varphi_{ox}]$ is proportional to the pressure jump across the shock and is thus a measure of the shock strength. Figure 35 shows a plot of the jump in unsteady potential across the shock as a function of streamwise distance between centers of the two airfoils as the second airfoil is moved along the horizontal line y = 1.5 where y = 0 is the location of the main airfoil. The amplitude of oscillation of the moving shock wave varies in a sinusoidal fashion and decays as the second airfoil is moved aft.

Timing results are not available, since the solution matrix of OPTRAN2 has not been modified to allow evaluation of a two airfoil system. However, a grid size reduction ratio of 5.21:1 has been achieved for the two airfoil system, and this value lies well within the reduction ratio goal established at the beginning of this investigation.

8.1 COMMENTS ON THE GRADIENT OF MACH NUMBER

It was determined, after a series of numerical investigations, that acceptable unsteady loading predictions may be achieved for all cases where the gradient of the Mach number (taken in a direction normal to the boundaries) never exceeds a value of

$$\Delta M/\Delta y = -.170.$$

It appears that this value is near the maximum value for which linear terms may be used to approximate transcendal functions within small error bounds. This corresponds to the evaluation slopes of derivatives within small error bounds.

Since this convergence criterion has proven to be valid for all cases investigated, it appears that it could be applied in any type of finite differencing procedure to ensure reliable loading predictions.

9.0 THREE-DIMENSIONAL INVESTIGATION

For the current method, the original finite difference grid with simple outgoing wave boundary conditions is replaced with a smaller grid and an exterior distribution consisting of sources and doublets on the boundaries of the truncated finite difference region. In the two-dimensional investigation, the source and doublet distribution, with outgoing wave far-field conditions, was represented by a set of localized functions applied about a set of control points. These control points were aligned with the rows and columns that make up the finite difference mesh and lie halfway between the outermost row and the first interior row for each boundary. The interior finite difference potential was matched with the amplitude and the normal derivative of the potential from the externally applied functions during the solution process.

As presented above, this new procedure proved successful for two-dimensional flow. In extending this procedure to the three-dimensional problem, it is necessary to distinguish between the setting up of the coefficient matrix and the solution of the coefficient matrix for the vector of unknowns. For the original finite difference procedure, the cost of setting up the large but sparse coefficient matrix was small compared to that required to solve for the unknowns. However, in the current procedure, calculation of the coefficients associated with exterior distributions is quite different. For each control point there is a source (and doublet) distribution to be calculated due to every other control point. Consequently, the dominating cost for the new procedure is that of evaluating the influence functions associated with the exterior distributions rather than cost associated with solving the simultaneous equations. It was found that for the two-dimensional problems presented above, approximately 80% of the cost of a run was for evaluating and summing the influence functions to form the coefficient matrix. This problem will become even more acute for three-dimensional configurations.

For instance, consider the three-dimensional grid network that encompasses the wing and a portion of the wake as shown in Figure 36. The total number of unknowns that exist for a solution of OPTRAN3 would be

$$(I_m - 2)(J_m - 1)(K_m - 2) = 42 \times 19 \times 30 = 23{,}940 \text{ unknowns}$$

If the outer boundaries are located halfway between X_1 and X_2 fo he forward boundary, and between X(43) and X(44) for the aft boundary, with the lower boundary located halfway between Z_1 and Z_2 and upper boundary located between Z(31) and Z(32), with the outboard boundary located between Y(19) and Y(20) then the number of control stations available to provide solution matching is given by 2 x 19 x 30 + 2 x 19 x 42 + 30 x 42 = 3,996 grid points available to satisfy the solution matching procedures. However, the number of influence functions needed to be evaluated would be the square of this number, which would be 15,968,016 influence function evaluations, if individual loading functions were to be applied at each control station of the original outer boundary of the grid network. The number of influence functions calculations would still be large even if the grid size were reduced to one-half the number of grid stations in each coordinate direction. The number of influence functions calculations would then amount to approximately 7,984,008 which would be a prohibitive number of functions to be evaluated and would defeat the cost reduction purpose of the research.

The number of influence functions to be calculated may be reduced by extending the source and doublet distributions over larger regions; in particular, it has been determined that low-order global functions may be used to represent the distributions on each boundary face. Figure 37 presents the velocity potential distribution on the outer boundaries of a grid network as calculated using the original finite difference procedure. These distributions must be matched in amplitude and normal derivative with potentials generated by the source and doublet distributions. The potential distributions on the upper, lower, and outboard boundaries are smooth and continuous, and may be generated by source and

doublet distributions described using a few low-order polynomials. Potential distributions on the forward and aft boundaries may be generated using low-order polynomials coupled with the discontinuous potential distributions that are generated by the wake.

Although the number of unknowns have been reduced, an adequate number of control (or matching) points may be retained by making use of least squares error procedures. Care must be taken to select the most appropriate distributions, the minimum number of matching points, and the location of these points to obtain optimum results.

Thus, in order to attain a more cost-effective procedure in the three-dimensional program the following tasks were undertaken to modify the OPTRAN3 program:

1. Develop an accurate numerical procedure evaluating the potential due to the doublet sheet of the infinite wake shed from the wing trailing edge
2. Derive relations for matching the finite difference potentials and normal derivatives with the potentials and normal derivatives of the applied sources and doublets in order to satisfy boundary conditions on the outer grid boundaries
3. Devise a least-squares error procedure for selecting the values of the parameters of the assumed source and doublet distributions used to match the finite difference solution

The result of rewriting OPTRAN3 to implement the above ideas is a pilot program for calculating the pressure distributions over harmonically oscillating rectangular wings in transonic flows. This program is called TRINX3 for TR(ransonic-)IN(ner-e)X(terior-matching,-)3(-dimensional).

9.1 EQUATIONS EVALUATED BY OPTRAN3

The finite difference equations applicable to the interior solution region are given in Appendix E. A brief discussion is presented to describe how the unsteady flow can be represented by a small perturbation about the steady flow condition. The derivation parallels the write-up of the two-dimensional flow equations with the exception that additional equations are given for the inclusion of the spanwise variable and the source and doublet distributions are represented by global rather than local functions.

9.2 EQUATIONS EVALUATED BY TRINX3

Expressions given in Appendix F have been developed for the evaluation of potentials at an arbitrary field point due to the source and doublet distributions applied to the exterior boundaries of the grid network. Potential equations which have been developed for each exterior face of the grid boundary are coupled with a zero potential interior boundary condition to provide potential and normal derivatives from the grid solution which are directly related to the doublet and source values from the exterior solutions. The form of the exterior solution is chosen to represent the outgoing wave.

Procedures used to couple the linear exterior solution with the interior finite difference equations are set forth in Appendix G. The relationship between the interior and exterior potentials are developed from equating potentials and normal derivatives to satisfy the boundary conditions on the surface that separates the two solution procedures.

Appendix H provides a description of the least-squares error solution procedure used to obtain the best approximation of matching surface boundary conditions. The function to be minimized is composed of two parts. The first part represents the sum of the squares of the terms that provide continuity between the inner and outer solutions, and the second part is the sum of squares of the terms that vanish in the region that is interior of the grid boundary. Least squares solutions are obtained from satisfying a set of simultaneous equations developed from taking derivatives of the error function with respect to the parameters associated with the exterior applied source and doublet distributions.

The form of the global functions for the source and doublet distributions on the grid boundaries is

$$X^m Y^n$$

where m and n are integers which may also be zero. The integrals of the product of these polynomial terms and the fundamental point source and doublet functions over the grid boundaries for each of the solution matching points are formed into arrays. Appendix I defines these arrays.

A numerical means for evaluating the potential due to the doublet distribution of the infinite wake is contained in Appendix J. The potential induced by the wake that extends beyond the finite differencing grid network is defined as

$$\phi_w(x,y,z) = \frac{1}{4\pi} \int_{-y_t}^{y_t} \exp\big(i\omega(a_2 - x)\big)\Delta\phi_1\left(a_2, y'\right)dy' \cdot$$

$$\int_{a_2}^{\infty} \exp\big(-i\omega(x' - x)\big)\big(\partial\psi_1/\partial z'\big)dx'$$

where $\psi_1 = \exp\left(-i\lambda\left(R_1 + M\,(x' - x)\right)\right)/R_1$

$$R_1^2 = (x - x')^2 + (y - y')^2 + (z - z')^2$$

$$\lambda = \omega M/(1 - M^2)$$

The above infinite integral is identified as being the kernel function of the potential integral and may be reduced to a more recognizable form by combining the exponentials and separating the integral into two parts which results in the expression

$$\text{Kernel} = \frac{\partial}{\partial z'} \int_o^{\infty} \frac{\exp\left[-i\bar{\omega}\,(\tau + M(\tau^2 + r^2)^{1/2})\right]}{(\tau^2 + r^2)^{1/2}}\,d\tau + \frac{\partial}{\partial z'} \int_o^{x_o} \frac{\exp\left[i\bar{\omega}\,(\tau - M(\tau^2 + r^2)^{1/2})\right]}{(\tau^2 + r^2)^{1/2}}\,d\tau$$

where $\bar{\omega} = \lambda/M; \quad \tau = (x - x')$

It is to be noted that the above form of the kernel function is identical with that Watkins, Runyan, and Woolston (ref. 7), with the exception that the above kernel applies a single derivative to each of the integral terms and the kernel of Reference 7 applies two derivatives. The difference between using one or two derivatives depends on the objectives being sought. A single derivative provides a velocity potential and an application of an additional derivative will define a velocity field. Thus the expressions for the kernel function defining a potential field or a velocity field only differ by an application of a single derivative. Consequently, the kernel function used in the wake potential calculations is the kernel function of Reference 7 multiplied by the vertical coordinate, z.

For points in the region of integration, the source has a 1/r singularity. After subtracting terms containing the singularity from the integrands, we can perform the integration numerically. The value of the integration of the source over the region is then found by adding the closed form integration of the 1/r terms. The theory is described in detail in Appendix K.

Accuracy checks have been conducted to ensure that this form of the kernel function will provide reasonably accurate potentials due to the infinite wake. The spanwise variation of the wake chordwise integral in Figure 38 indicates that its largest value is generated at the control station and rapidly diminishes in value in the spanwise direction. The spanwise integration procedure has been formulated to provide sufficient accuracy by subdividing the interval into several small intervals and applying Legendre integration quadrature procedures to each integration interval. A numerical test was conducted to evaluate the accuracy of the analytic formulation and algorithm expressions in calculating the potential distribution due to the infinite wake. The numerical test was one of calculating the potential on the downstream face of the grid network and comparing the values of the discontinuity in potential across the wing plane with the discontinuity in potential input from the wing trailing edge. The potential discontinuity calculated at the wing plane should be equal to the discontinuity value input from the trailing edge of the wing if the kernel function has been accurately formulated and programmed.

The results plotted in Figure 39 indicate that the limiting value of the potential discontinuity across the wing plane does become equal to the input discontinuity value as z approaches zero at the wing plane. As a consequence of the above, it is assumed that the potential distributions required at the aft boundary can be accurately generated by a combination of source and doublet distributions described by a few low-order polynomial functions coupled with the discontinuity distribution discussed above.

A study was made to estimate what form the source and doublet polynomial distributions should take to adequately describe the potential and its normal derivatives on the boundary of the grid region. The jump in potential on the aft face of the grid region is taken care of by the trailing wake. If we subtract the contribution of the wake, the resulting source and doublet distributions that satisfy the boundary conditions will be continuous.

From a solution of the complete finite difference equations using the ADI method, the potential was calculated on selected grid boundaries for a Mach number of 0.82 and an angle of attack of 1 deg. A modified potential was then calculated by subtracting out the potential induced by the wake aft of the downstream boundary. The relatively smooth behavior of this modified potential is shown in Figures 40 through 43. The real part of the modified potential is plotted versus the spanwise variable for several values of the vertical coordinate for the downstream boundary in Figure 40. In this figure, large gradients in the potential were limited to the immediate neighborhood of the wingtip. Examples of modified potential distributions in the vertical direction are presented in Figures 41 and 42. In Figure 41, on the upstream boundary, the variation in both the real and imaginary parts of the modified potential is smooth except in the immediate vicinity of the wing plane. Here, the potential and its first derivatives are continuous across the wing plane but show large gradients in the derivative of the potential with respect to z. In Figure 42, on the downstream boundary, there are large gradients in both the modified potential and its derivative with respect to z. Moreover, subtracting out the wake contribution does not eliminate the rapid variations near the wing plane z = 0. This is easily seen from Figure 43 where the potential on the aft plane from the finite difference solution is compared with the wake contribution and with the modified potential resulting from subtracting the wake contribution from the finite difference potentials. This would indicate that a fairly high-order polynomial is needed to represent the source and doublet distributions for properly matching the interior grid solution and exterior linearized solution. However, experience has shown that good results may be obtained with a polynomial of the form

$$a_1 z + a_2 z^3$$

for the z variation when the flow is symmetric.

The potential distribution on the upper and lower grid boundaries was found to be very smooth. It was also found that the pattern for the normal derivative on the grid boundaries was essentially the same as the potential distribution. The results of the study are shown in Figure 37 where a typical source (or doublet) distribution is sketched on the boundaries of the grid region.

10.0 MESH PATTERNS AND DISTRIBUTION POLYNOMIALS FOR THE VALIDATION STUDIES

The configuration used for the validation studies is an aspect ratio 8 rectangular wing at a Mach number of 0.82 oscillating harmonically at a reduced frequency of 0.3 based on the semichord. The basic finite difference mesh is 44 x 20 x 32 grid that, when used with OPTRAN3 with the two different point distributions discussed below, resulted in pressure distributions that matched well with corresponding distributions from the kernel function routine RHO4 (refs. 8 and 9). For the basic mesh, the upstream, downstream, outboard, lower, and upper boundaries are at $x = -2.5$, $x = 3.0$, $y = 12.78$, $z = -4.5$, and $z = +4.5$, with the leading and trailing edges, and the wingtip at $x = -1.0$, $x = 1.0$, and $y = 8.0$ respectively. For the wing of vanishing thickness, the grid points were concentrated about the leading and trailing edges and the wingtip. For the thickness case, points were also concentrated about the shock location at the root, $x = 0.1$. The mesh patterns for the x-z and x-y planes for the thickness problem are shown in Figures 44 and 45. For reduced frequencies significantly smaller than 0.3, all boundaries would have to be moved out to obtain satisfactory results with OPTRAN3.

The truncated grids for TRINX3 were obtained by simply eliminating planes of mesh point from this basic grid. Thus a mesh of 32 x 17 x 16 was obtained by removing six y-z planes of mesh points adjacent to the upstream and downstream boundaries, four x-y planes of points adjacent to the upper and lower boundaries, and x-z planes of points adjacent to the outboard boundary. Since the mesh points are not uniformly spaced, reduction in the size of the finite difference solution region is not directly related to the reduction in number of grid points.

A second problem that must be addressed is the solution of the polynomials used to represent the source and doublet distributions on the outer boundaries of the finite difference mesh. It is currently assumed that the geometric characteristics of the velocity potential distributions on the boundaries as calculated with OPTRAN3 should be directly reflected in the polynomials used for the source and doublet distributions. With this in mind, the source and doublet distributions were selected to have the same forms. In the vertical direction, the terms

$$z \text{ and } z^3$$

were selected on the upstream, downstream, and outboard grid boundary faces. Because of symmetry about the root chord in the spanwise variable, the terms

$$y^0, y^2, \text{ and } y^4$$

were applied to the upstream, downstream, upper, and lower faces of the grid boundary. For the streamwise variation, we chose

$$x^0, x, \text{ and } x^2$$

On the upstream face, for example, this yields the product terms

$$z, zy^2, zy^4, z^3, z^3y^2, \text{ and } z^3y^4$$

leading to six parameters. Similarly six parameters result on the downstream face. On the outboard grid boundary we have

$$z, xz, x^2z, z^3, xz^3, \text{ and } x^2z^3$$

and on the lower and upper boundaries we chose

$$x^0y^0,\ y^2,\ y^4,\ x,\ xy^2,\ xy^4,\ x^2,\ x^2y^2,\ \text{and}\ x^2y^4$$

leading to nine parameters. Thus a total of 72 parameters associated with both sources and doublets is required.

Finally, another advantage of using both sources and doublets for the exterior solution is that it allows for the decoupling of the boundary points used for the inner-outer matching from the grid points used for the finite difference solution. The problem size, then, is reduced not only in the number of unknown coefficients used to define the distribution polynomials, but also in the number of points at which the matching conditions, using the least squares procedure, is applied. For the validation studies, 12 points were used in the streamwise direction, and eight points were used in both the spanwise and vertical directions. Thus, 96 control points were used on the outboard boundary and 64 were used on each of the four remaining boundaries. The points were uniformly spaced for all but one run. For the one case in the flat plate study in which the points were concentrated about the wing plane, a geometric progression algorithm was used to arrange points vertically.

11.0 VALIDATION STUDIES FOR A WING OF VANISHING THICKNESS

Validation studies for a wing of vanishing thickness consist of correlating pressure distributions calculated with the new inner-outer matching program, TRINX3, the original finite difference program, OPTRAN3, and the kernel function program RHO4 of References 8 and 9. The configuration used for these studies is an aspect ratio 8 rectangular wing at a Mach number of 0.82 oscillating harmonically at a reduced frequency of 0.3.

The first results, presented in Figures 46 and 47, compare pressure coefficients from RHO4 and from TRINX3 for two different grids, a 32 x 17 x 16 and a 32 x 17 x 12. The smaller grid has two less x-y planes of points both above and below the wing, with the upper and lower boundaries being correspondingly closer to the wing surface. Only the root chord and the second chord in from the tip are presented, since results for the intermediate chords are very similar. The agreement of the 32 x 17 x 16 grid with RHO4 is excellent. The smaller grid doesn't agree with RHO4 quite as well near the trailing edge of the wing. An earlier run with a grid size of 30 x 17 x 16, differing from the 32 x 17 x 16 grid by moving eight columns in from the aft boundary instead of six, showed a large deviation from the RHO4 solution in the vicinity of the trailing edge. This was corrected by moving the aft boundary two columns downstream, and the comparisons are shown in Figures 48 and 49.

From Figure 40 it would appear that a better match with lower order polynomials could be accomplished if the upstream and downstream grid boundaries were divided into two panels at the wingtip, y_t, with the origin of the polynomials at y_t. In Figures 50 and 51, pressures from the one- and two-panel method are compared. Also included on the graphs are results for the control points concentrated somewhat closer to the wing plane. The results of all three methods that use a 32 x 17 x 16 grid are in close agreement, but with the single-panel method yielding somewhat better results. Concentrating the points near the plane z = 0 improved the two-panel method.

It has been noted in earlier studies that for small reduced frequencies the grid boundaries for the finite difference solutions using OPTRAN3 had to be moved further from the wing to get accurate results for the imaginary part of the pressure coefficient distribution. Figures 52 and 53 present results for a reduced frequency of 0.01 and compares pressures from TRINX3, OPTRAN3, and RHO4. The TRINX3 and OPTRAN3 problem setups are those used to obtain satisfactory results at a reduced frequency of 0.3. It is seen that the matching procedure yields better agreement for the imaginary parts with RHO4 than OPTRAN3, indicating that TRINX3 has significantly better far-field boundary conditions.

12.0 VALIDATION FOR A WING WITH THICKNESS

To test the matching procedure for the flow over a wing with thickness in which the flow contains a local supersonic region with a shock, we chose the same planform as for the flat plate, but with NACA 64A010 airfoil sections. For a reference solution, we chose a Mach number of 0.82 with zero angle of attack. The steady state potential distribution required as input to OPTRAN3 and to TRINX3 was computed using XTRAN3S (Ref. 10). Since the flow is symmetric, a solution from OPTRAN3 can be obtained with a moderate cost by solving one-half the grid. The solution using OPTRAN3 for a reduced frequency of k = 0.3 required 206 cp seconds. A full-grid solution would require about eight times this amount, making the cost prohibitive. Using the same source and doublet polynomials and the same reduced grid of 32 x 17 x 16 as for the flat plate, the TRINX3 solution required only 72 cp seconds. This is about 5% of the cost of a full OPTRAN3 solution.

In order for the matching procedure to be valid, the Mach number on the points inside the truncated upper and lower boundaries must at least be subsonic. This means that the array

$$U_{ijk} = K \cdot (\gamma + 1)\phi_{o\ ijk}$$

where K is like 1-M for M, the local Mach number, close to one, and thus must have all positive values on the points just inside the upper and lower grid boundaries. On the vertical plane x(19), the supersonic zone extends the farthest away from the wing surface at the root. The value of U along this column of points, U(I=14, J=2, K), is plotted in Figure 54. Moving in eight points from the original upper and lower grid boundaries defines the z region where U(I,J,K) at the point just inside the grid boundaries is always positive, since the point Z(10) just inside the grid region is seen to be positive. However, moving in nine points from the original upper and lower grid boundaries, we find that U at the point Z(11) is negative. Figure 55 presents a map of the Mach number in the full 44 x 20 x 32 grid. The inner lines show the 32 x 17 x 16 grid, and it is seen that this is the closest one can move the boundary of the grid region so that the value of U is always positive and thus the Mach number is less than one. Calculations with the 32 x 17 x 14 grid showed poor agreement with OPTRAN3. Thus it appears that 8 points is the maximum one can move the upper and lower grid boundary inward for this particular problem.

Figures 56 to 59 show the comparison of results from OPTRAN3 and the TRINX3 solution with the 32 x 17 x 16 grid and an additional solution where the upper and lower grid boundaries are moved in seven rows instead of eight. The agreement between the three solutions is seen to be good. The two solutions from the matching procedure, TRINX3, are nearly the same as we should expect.

Near the wingtip, in the vicinity of the trailing edges, there appears a dip in the real part (fig. 58). This was eliminated by moving the downstream boundary two more columns aft as is seen in Figures 60 and 61, which compare the pressure coefficients from the 32 x 17 x 16 grid with results from the 34 x 17 x 16 grid. This dip was also noted in the flat plate problem (see figs. 48 and 49) where it was eliminated in similar fashion. However, it appears that the aft boundary must be moved farther aft from the trailing edge for the thickness case than for the flat plate. Increasing the number of grid planes in the streamwise direction only increases the computing time linearly with the number of grid points, while increasing the number of x-z and x-y planes causes the computing time to increase as the cube of the number of mesh points.

We also made calculations using the method in which the upstream and downstream grid boundaries are divided at the wingtip into two panels, with the origin of the spanwise variable at the tip. Figures 62 to 65 show the comparison of the single with the two-panel method and with OPTRAN3. The two methods are in close agreement. The two-panel method gives results that are in somewhat better agreement with OPTRAN3. The same polynomials for the source and doublets are used in each of the two panels as in the single-panel method. Consequently, there are more parameters in the two-panel case.

13.0 SUMMARY AND CONCLUSIONS

The intent of this research was to evaluate the feasibility of a procedure for reducing the overall cost of using a harmonic finite difference procedure for analyzing nonlinear transonic flow. This was to be accomplished by reducing the number of unknowns by using a smaller finite difference solution volume (a smaller number of mesh points) with a better far-field boundary condition achieved by distributing sources and doublets on the outer boundaries to define a linear exterior flowfield.

The research was divided into two parts. The first part consisted of developing a solution matching procedure for two-dimensional flow analyses, and the second part extended the analysis capability to three-dimensional flow conditions.

The solution matching procedure that was developed for the two-dimensional flow analyses was one of reducing the size of the grid network of the original finite difference program, OPTRAN2, in both the horizontal and vertical direction and applying source distributions, with the proper outgoing wave characteristics, in a piecewise continuous fashion on the outer boundaries of the reduced grid.

Inner and outer solutions were matched by equating the potentials and normal derivatives of the inner and outer solutions at the control station locations on the outer boundary. The number of piecewise continuous potential functions applied to the outer boundary was equal to the number of control stations. Thus, an exact match in both amplitude and normal derivative of the potential could be attained at each boundary control station. This exact match in the zero thickness analysis case allowed the solution unknowns to be reduced by a factor of 10:1 and reduced the computer usage costs by a factor of 2:1. A 5:1 reduction in solution unknowns and a 40% reduction in computer costs were achieved for the finite thickness transonic flow analysis cases. The inconsistency between the reduction in computer usage costs and the reduction in the number of solution unknowns is due to the additional calculations required to evaluate the arrays of influence coefficients due to the potentials applied to the outer boundary.

It appears that a 2:1 cost reduction is the best that can be achieved for the exact solution matching case.

The solution procedure was changed in the three-dimensional case, since an exact match would require an excessive amount of additional calculations that would negate the reduction of computer usage costs.

Computer costs may be reduced significantly without compromising accuracy by using global functions to represent the continuous distributions of both sources and doublets on the outer boundaries of the finite difference region and solving for the unknowns using a least squares procedure for matching conditions across these boundaries. The solution obtained using the matching procedure applied to the analysis of a rectangular wing of vanishing thickness of aspect ratio 8 at a Mach number of 0.82 and a reduced frequency of $k = 0.3$ is in very good agreement with results from the full-grid finite difference solution and the kernel function method. For small frequencies, the matching procedure yielded results that were better than those from the finite difference procedure, indicating a more accurate far-field representation. The solutions using the matching procedure for the flow over a wing with thickness of the same planform but with a NACA 64A010 airfoil section, gave results in good agreement with the finite difference procedure. The results indicate that reductions of 90% to 95% (from an estimated 1600 to 80 seconds for the problems considered here) in computing costs can be achieved by the inner-outer matching procedure.

It appears that this solution matching procedure does provide a viable means of reducing computer usage costs. The initial application of this procedure is very promising, but further tests should be made to identify the optimum number and location of boundary points, the polynomials for the representation

of source and doublet distributions, and the location of grid boundaries to provide a further reduction in costs. As derived, the method is applicable only to rectangular wings, although wings with small sweep angles could be treated by constructing the grid in the manner of W. Schmidt (ref. 11). For wings of large sweep and taper, the basic approach is feasible, but integration over the grid boundaries must incorporate the swept-wing transformation, in which the leading and trailing edges of the wing are coordinate lines.

14.0 REFERENCES

1. Ehlers, F. E.: "A Finite Difference Method for the Solution of the Transonic Flow Around Harmonically Oscillating Wings," NASA CR-2257, January 1974.

2. Rizzetta, D. P. and Chin, W. C.: "Effect of Frequency in Unsteady Transonic Flow," AIAA Journal, Vol. 117, pp. 779-781, July 1979.

3. Stahara, S. S.: "Operational Manual for Two-Dimensional Transonic Code," NASA CR3064, 1978.

4. Ehlers, F. E.; Sebastian, J. D.; and Weatherill, W. H.: "An Investigation of Several Factors Involved in a Finite Difference Procedure for Analyzing the Transonic Flow About Harmonically Oscillating Airfoils and Wings," NASA CR-159143, 1979.

5. Bland, S. R.: "Development of Low Frequency Kernel Function Aerodynamics for Comparison with Time Dependent Finite Difference Methods," NASA Technical Memorandum 83283, May 1982.

6. Ehlers, F. E.; Weatherill, W. H.; and Yip, E. L.: "Development and Application of Algorithm for Calculating the Transonic Flow About Harmonically Oscillating Wings," NASA CR-17376, 1984.

7. Watkins, C. E.; Runyan, H. L.; and Woolston, D. S.: "On the Kernel Function of the Integral Equation Relating Lift and Downwash Distributions of Oscillating Finite Wings in Subsonic Flow," NACA Report 1234, 1956.

8. Rowe, W. S.; Winther, B. A.; and Redman, M. C.: "Prediction of Unsteady Aerodynamic Loadings Caused by Trailing Edge Control Surface Motions in Subsonic Compressible Flow — Analysis and Results," NASA CR-2003, March 1972.

9. Redman, M. C.; Rowe, W. S.; and Winther, B. A.: "Prediction of Unsteady Aerodynamic Loadings Caused by Trailing Edge Control Surface Motions in Subsonic Compressible Flow — Computer Program Description," NASA CR-112015, March 1972.

10. Borland, C. J. and Rizzetta, D. P.: "Transonic Unsteady Aerodynamics for Aeroelastic Applications — Vol. I: Technical Development Summary," AFWAL TR 80-3107, April 1982.

11. Schmidt, W.; Rohlfs, R.; and Vanino, R.: "Some Results Using Relaxation Methods for Two- and Three-Dimensional Transonic Flows." Presented at the Fourth International Conference on Numerical Methods in Fluid Dynamics, Boulder, Colorado, June 24-28, 1974.

12. Watkins, C. E.; Woolston, D. S.; and Cunningham, H. J.: "A Systematic Kernel Function Procedure for Determining Aerodynamic Forces on Oscillating or Steady Finite Wings at Subsonic Speeds," NASA Technical Report R-48, 1959.

13. Abromowitz, M., and Stegun, I. A.: "Handbook of Mathematical Functions," Dover Publications Inc., New York, 1965.

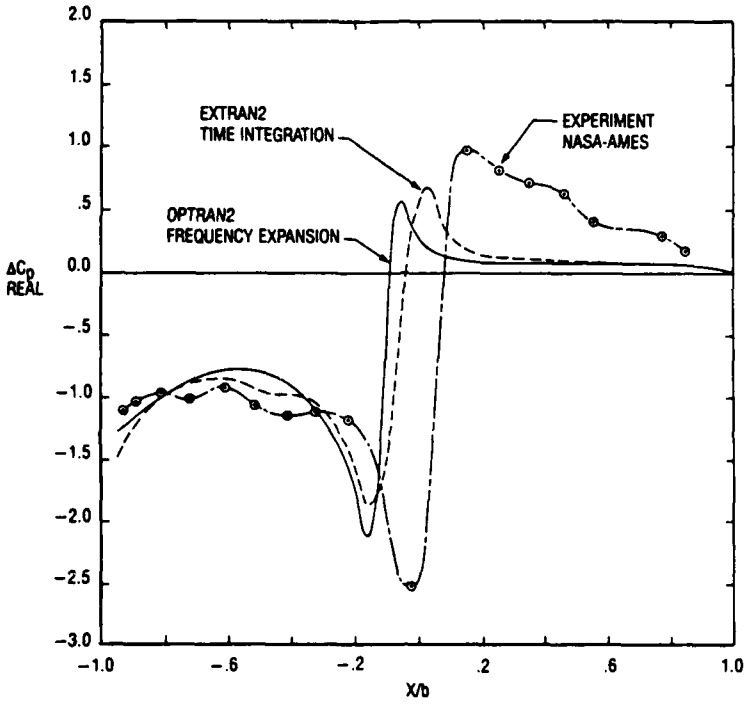

Figure 1. Comparison of Theoretical and Experimental Pressure Coefficients Obtained Using a NACA 64A010 Airfoil Oscillating 0.05 Semichord in Plunge at M = 0.80 and k = 0.151.

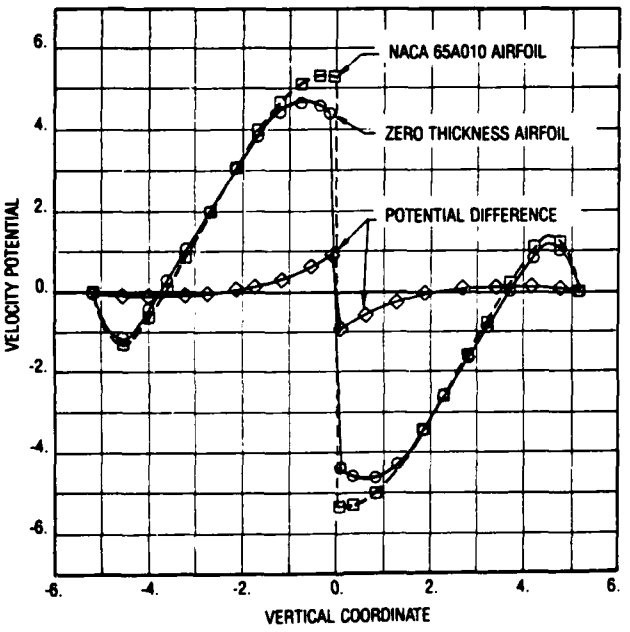

Figure 2. Spatial Variations of Velocity Potentials on a Flat Plate and a NACA 64A010 Airfoil Section.

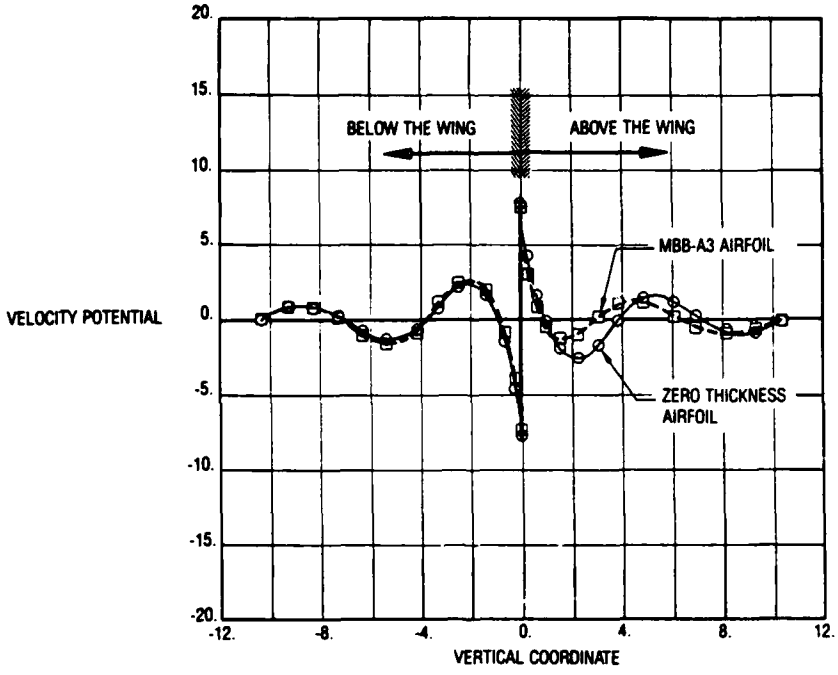

Figure 3. Spatial Variations of Velocity Potentials on a Flat Plate and MBB-A3 Airfoil Section.

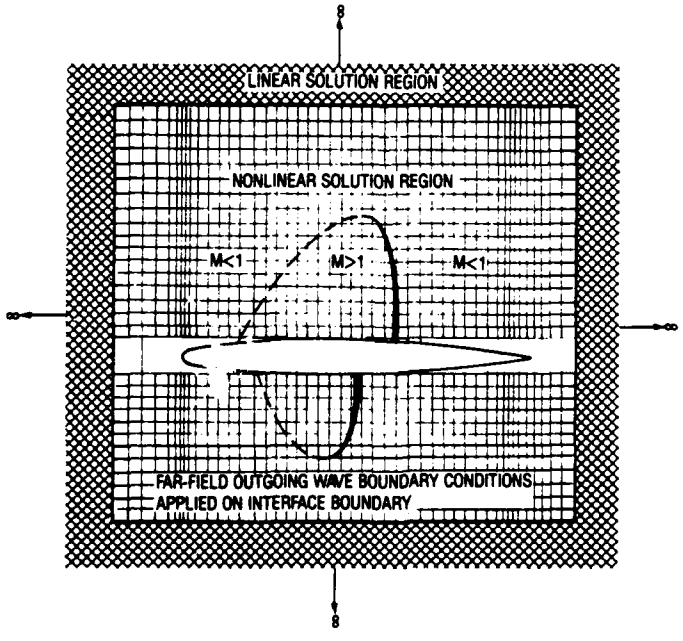

Figure 4. Suggested Modification of Transonic Solution Procedures.

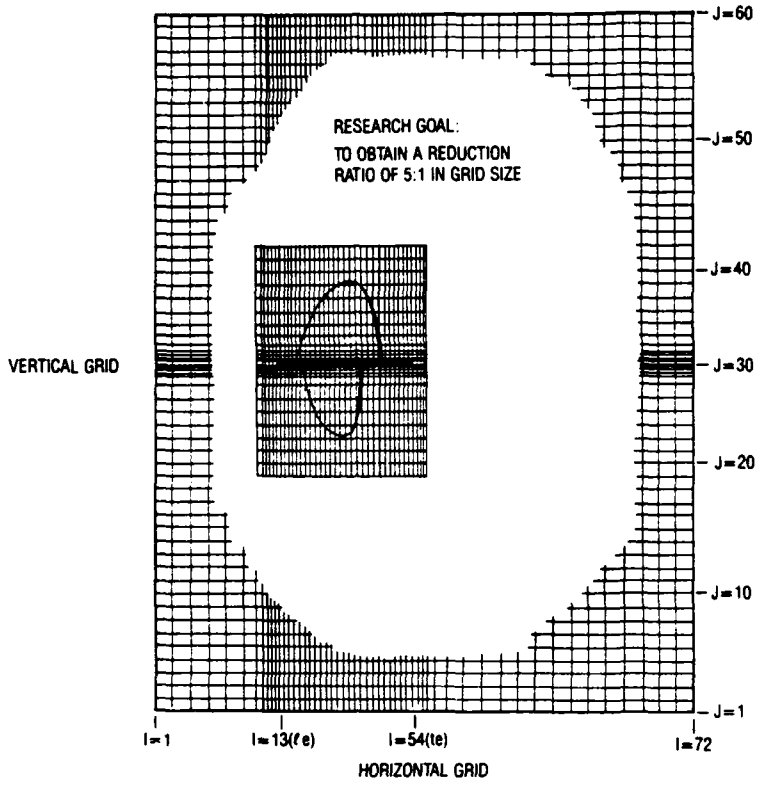

Figure 5. Schematic of Anticipated Reduction in Grid Size that May Result From Solution Matching.

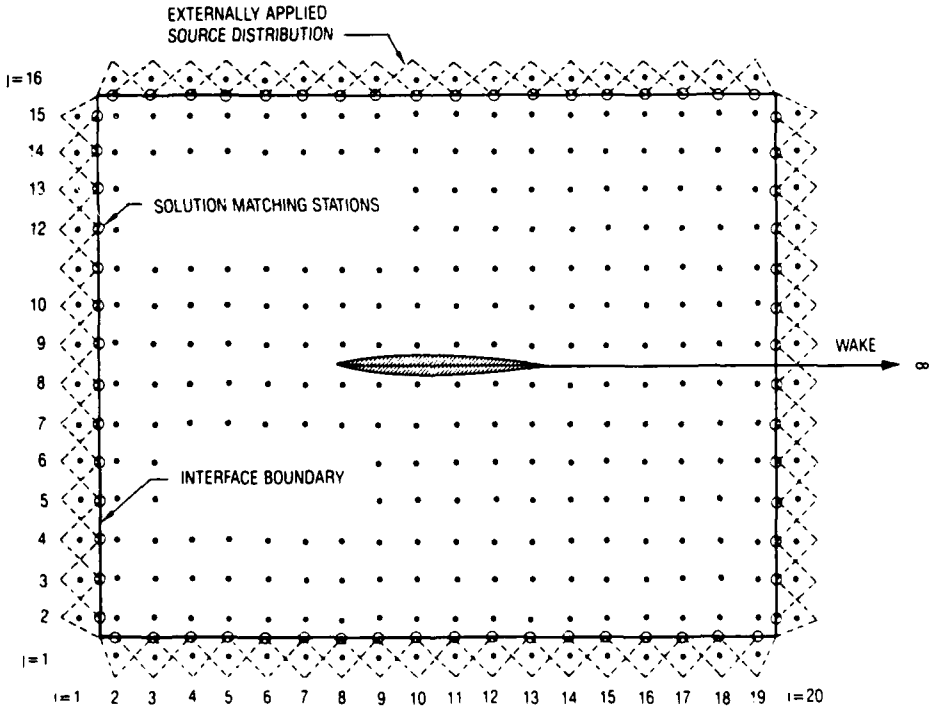

Figure 6. Notation and Geometry Modifications Applied in Solution Matching Procedure.

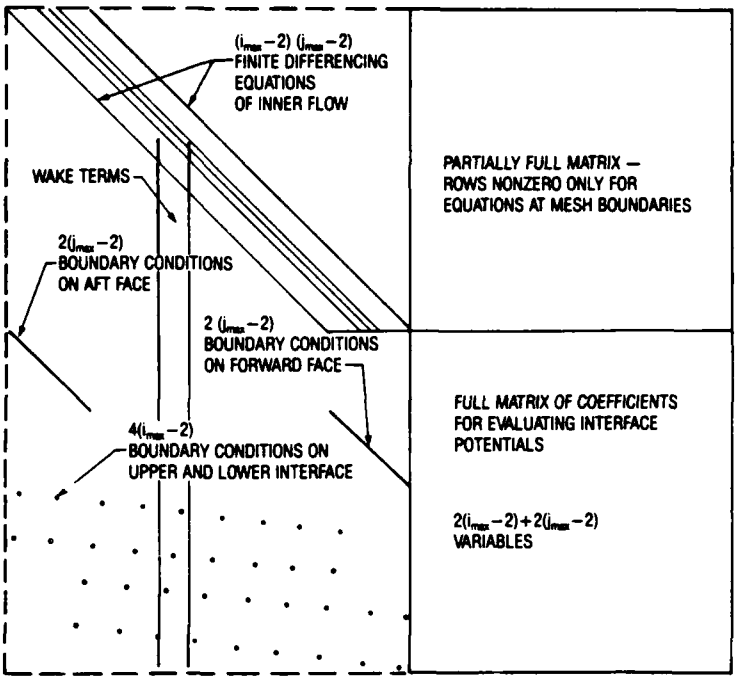

Figure 7. Schematic of the Coefficient Matrix Used in Combining Inner and Outer Solutions.

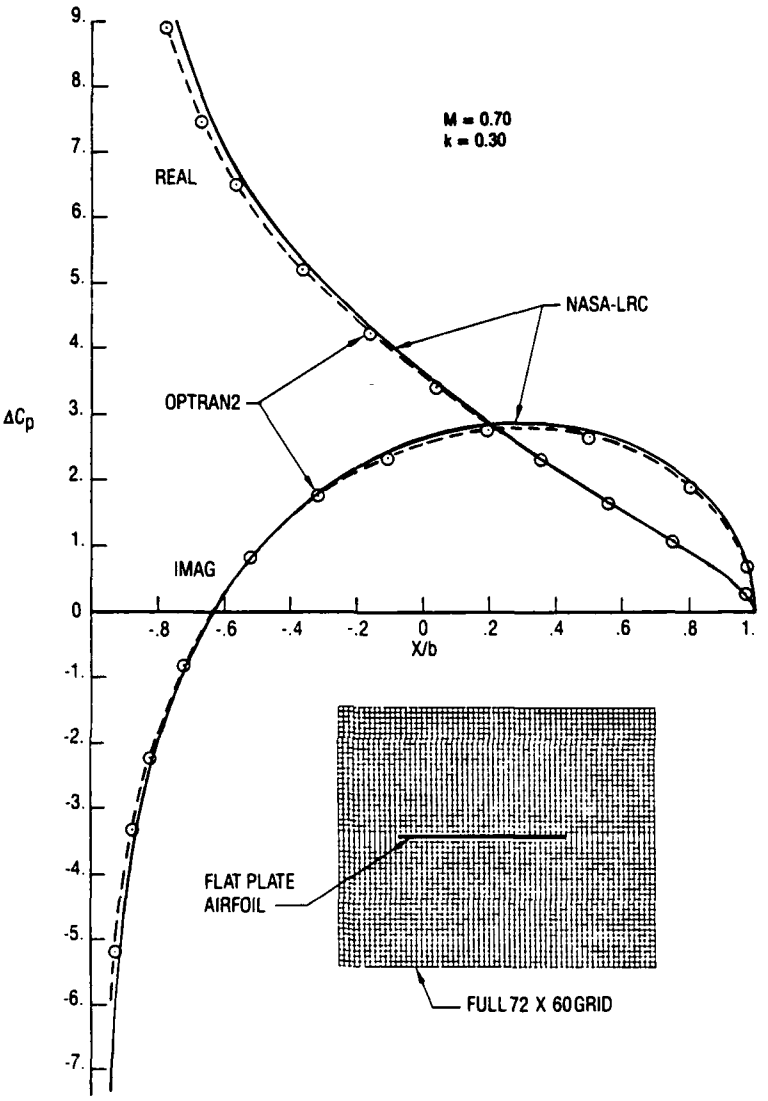

Figure 8. Comparison of Pressure Coefficients that Establish a Standard of Reference Error Bounds.

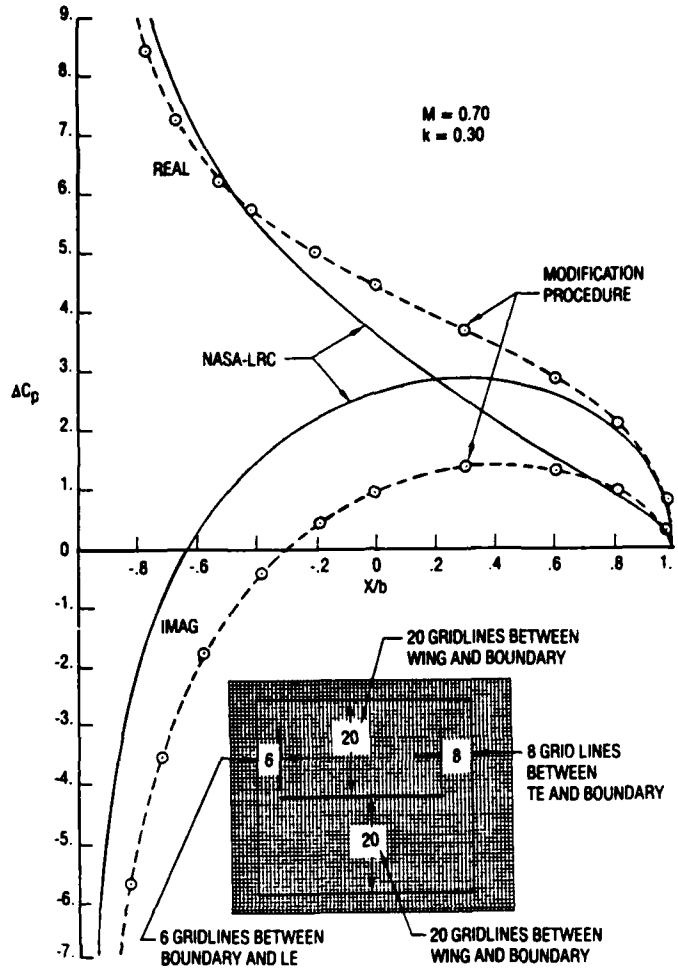

Figure 9. Pressure Coefficient Comparison Developed During Initial Checkout of Modification Procedure.

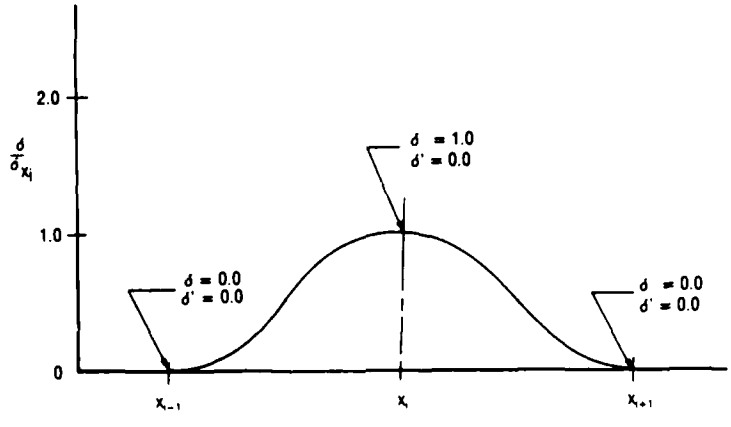

Figure 10. Basis Function Developed to Maintain First Derivative Continuity of Externally Applied Source Distributions.

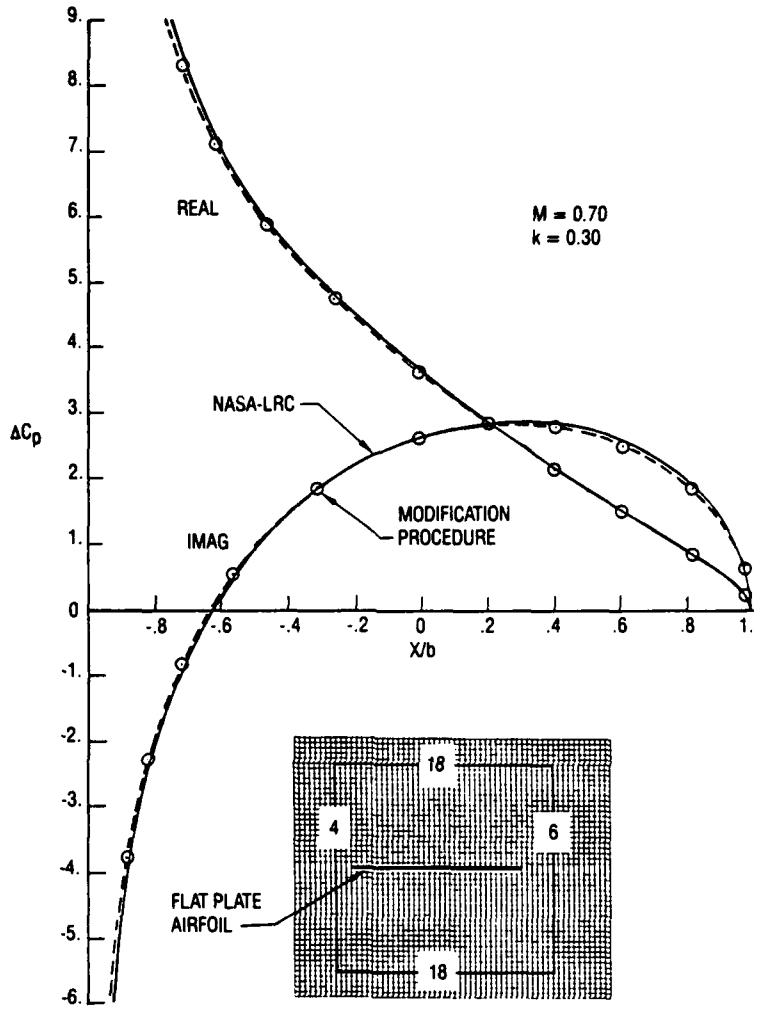

Figure 11. Comparison of Pressure Coefficients Obtained Using Gaussian Integration Procedures and the First Derivative Continuous Basis Function.

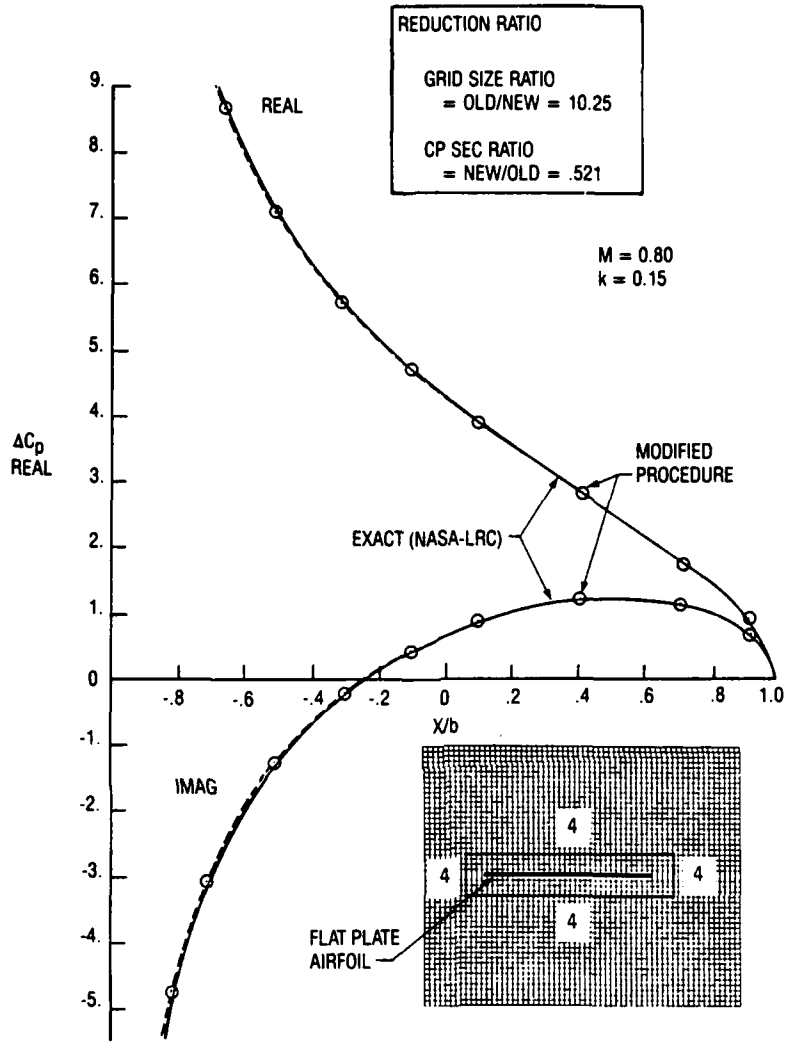

Figure 12. Comparison of Pressure Coefficients Developed for a Minimum Size Grid Network Having Four Gridlines Above and Below the Airfoil.

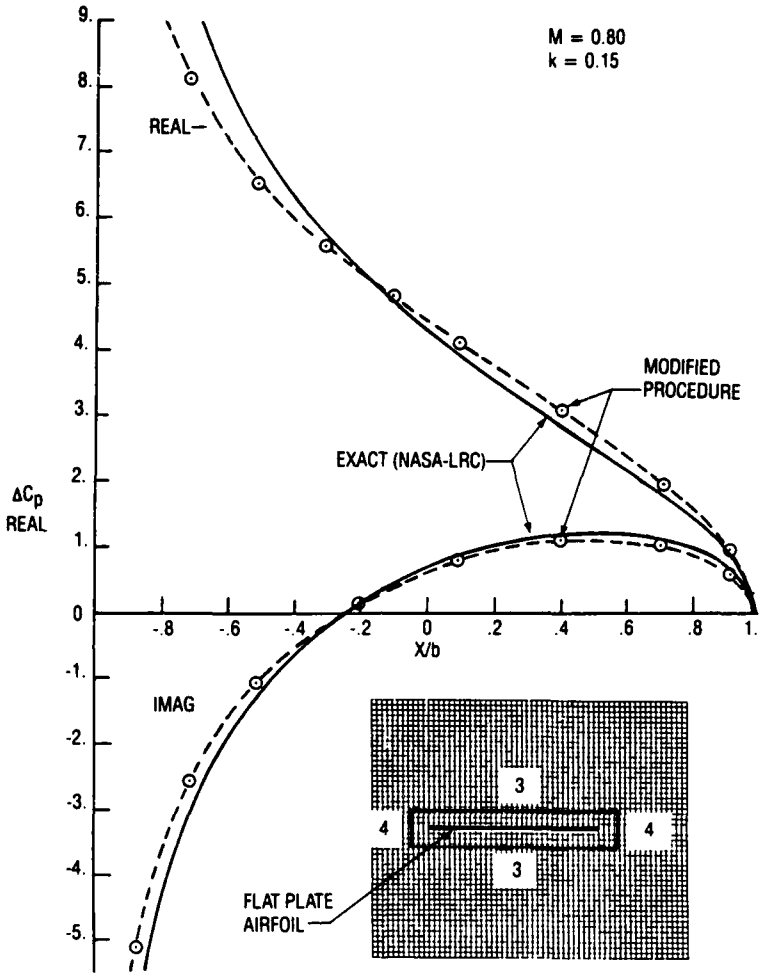

Figure 13. Comparison of Pressure Coefficients Developed for a Network Having Three Gridlines Above and Below the Airfoil.

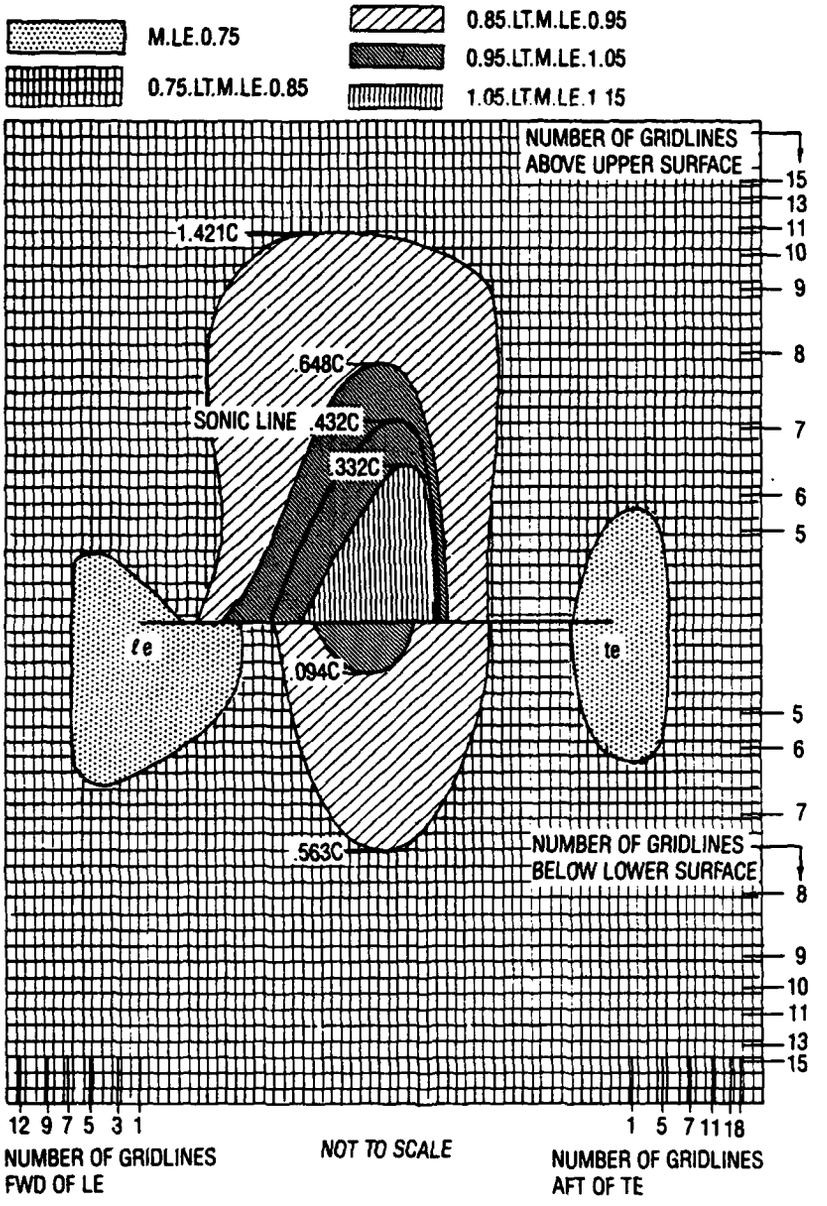

Figure 14. Steady Flow Field Mach Number Variation for a NACA 64A010 Airfoil at a 1° Angle of Attack with M = 0.80.

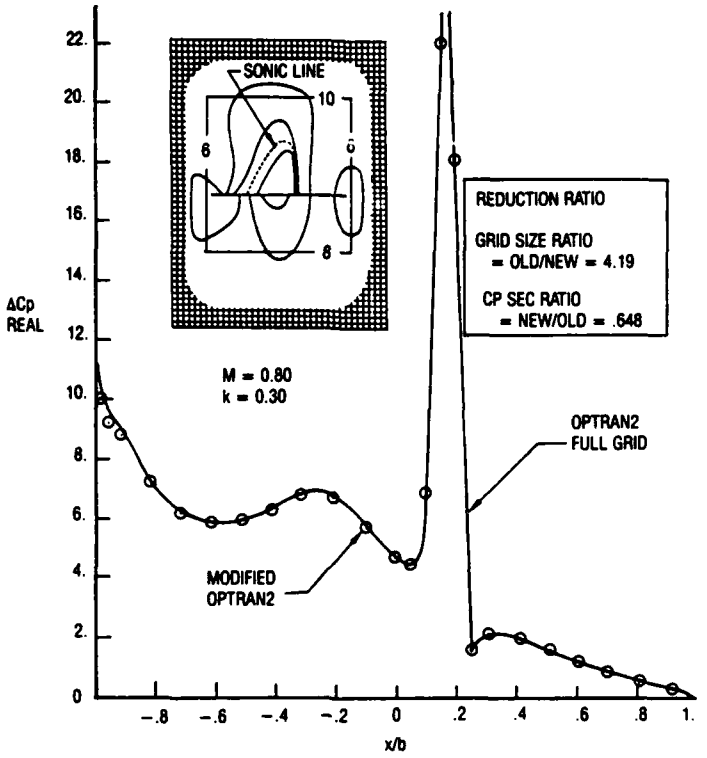

Figure 15. Real Part of the Unsteady Pressure Coefficients Obtained for Oscillations About a 1° Mean Angle of Attack at M = 0.80.

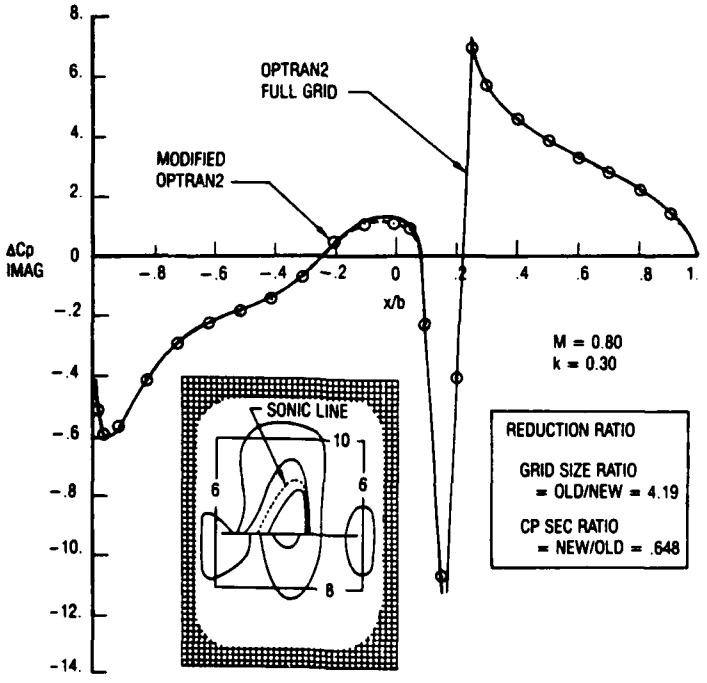

Figure 16. Imaginary Part of Unsteady Pressure Coefficients Obtained for Oscillations at About a 1° Mean Angle of Attack at M = 0.80.

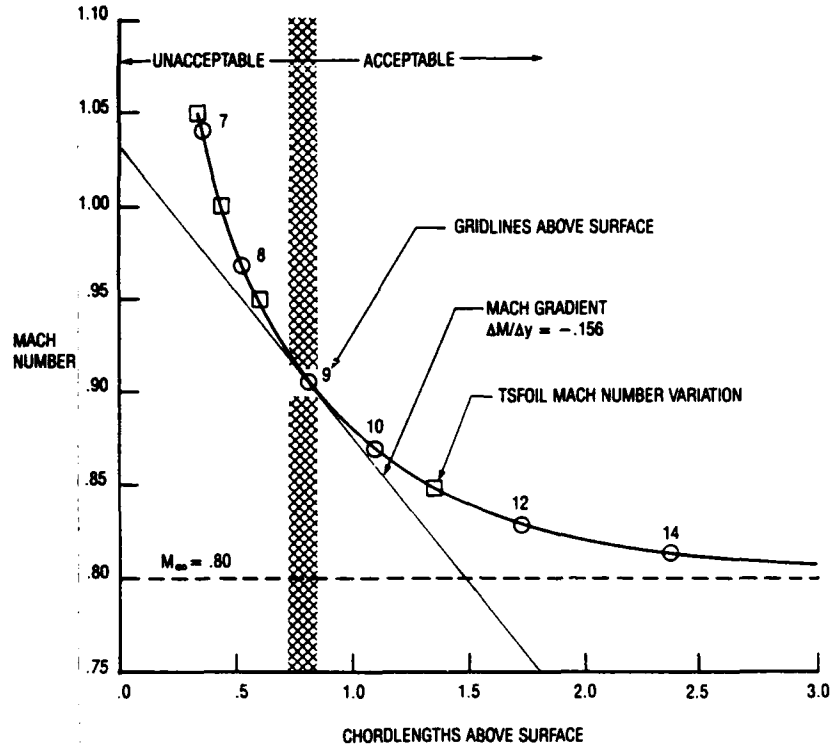

Figure 17. Mach Number Variation as a Function of the Distance Above the Airfoil for M = 0.80.

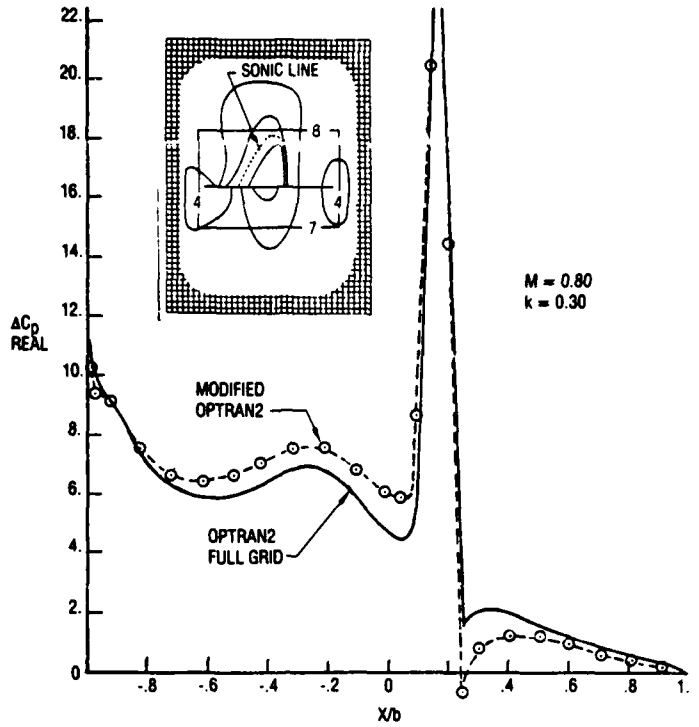

Figure 18. Real Part of Pressure Coefficients Developed for a Case Where the Upper Boundary is Located in a Region Having Nonlinear Mach Number Characteristics.

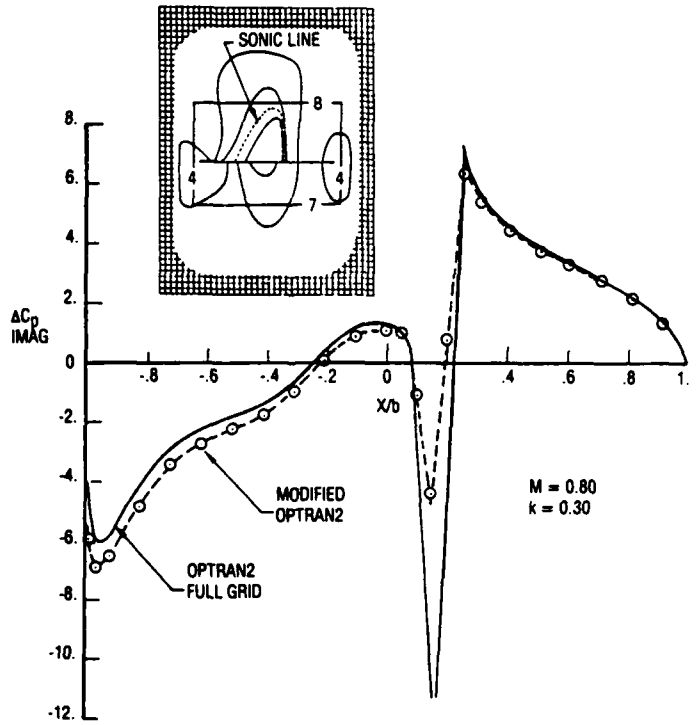

Figure 19. Imaginary Part of Pressure Coefficients Developed for a Case Where the Upper Boundary Intersects a Region of Nonlinear Mach Number Characteristics.

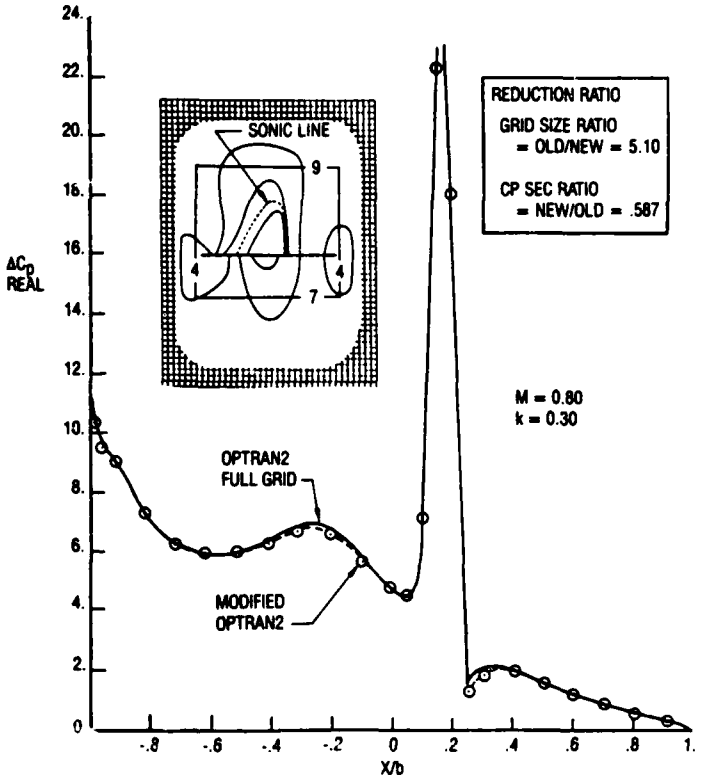

Figure 20. Real Part of Pressure Coefficients for a Case Where the Upper Boundary is Located in the Demarcation Zone.

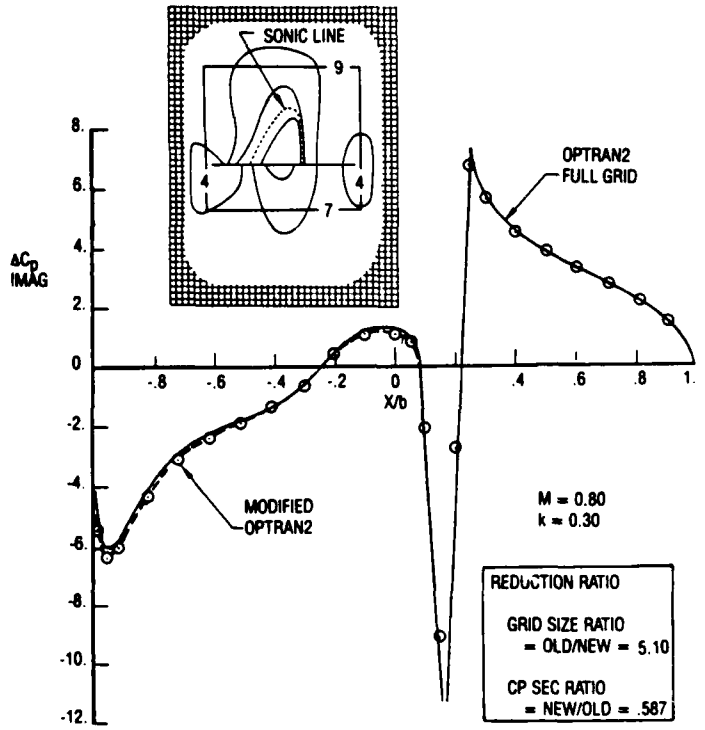

Figure 21. Imaginary Part of Pressure Coefficients Where Upper Boundary is Located in the Demarcation Zone.

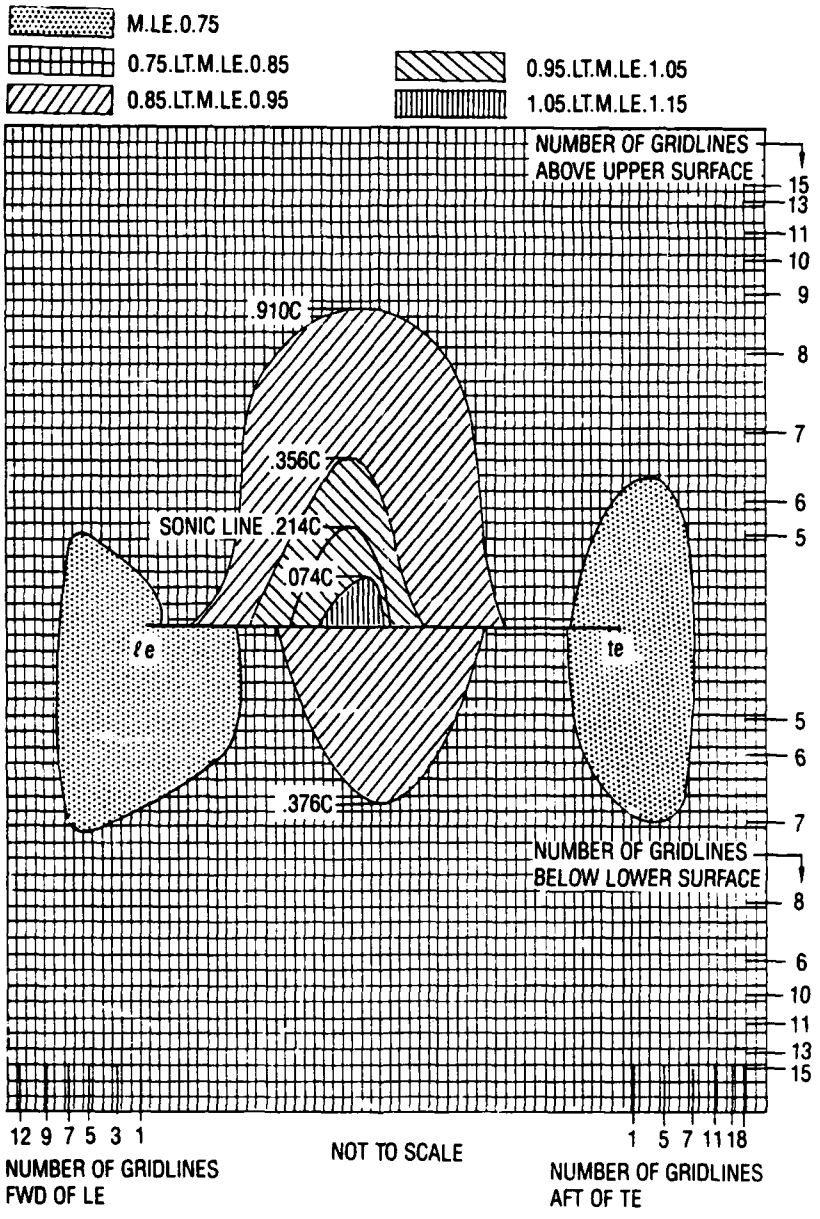

Figure 22. Steady Flow Field Mach Number Variation for a NACA 64A010 Airfoil at a 1° Angle of Attack With M = 0.78.

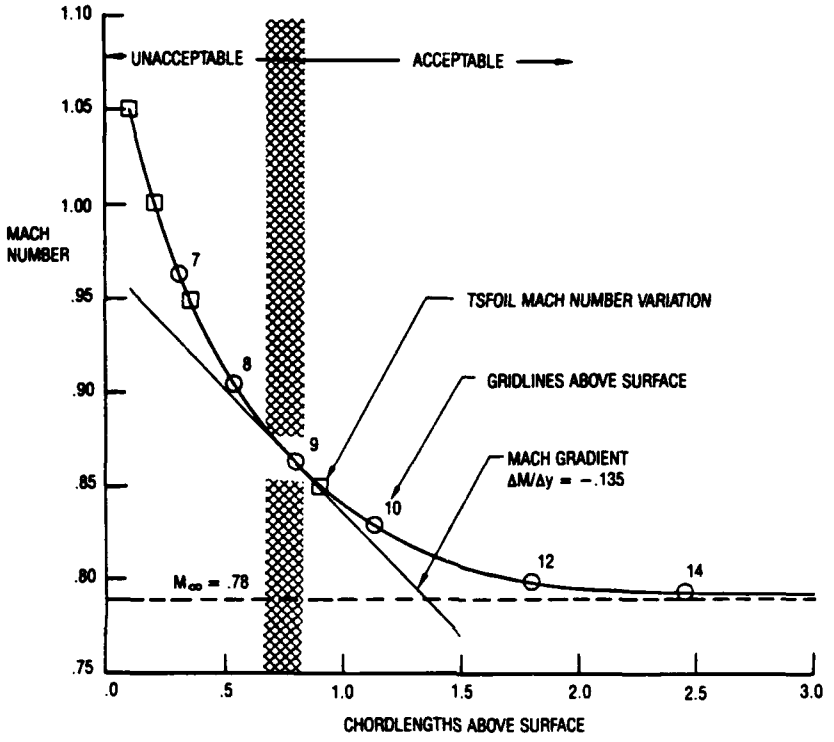

Figure 23. Mach Number Variation as a Function of the Distance Above the Airfoil for M = 0.78.

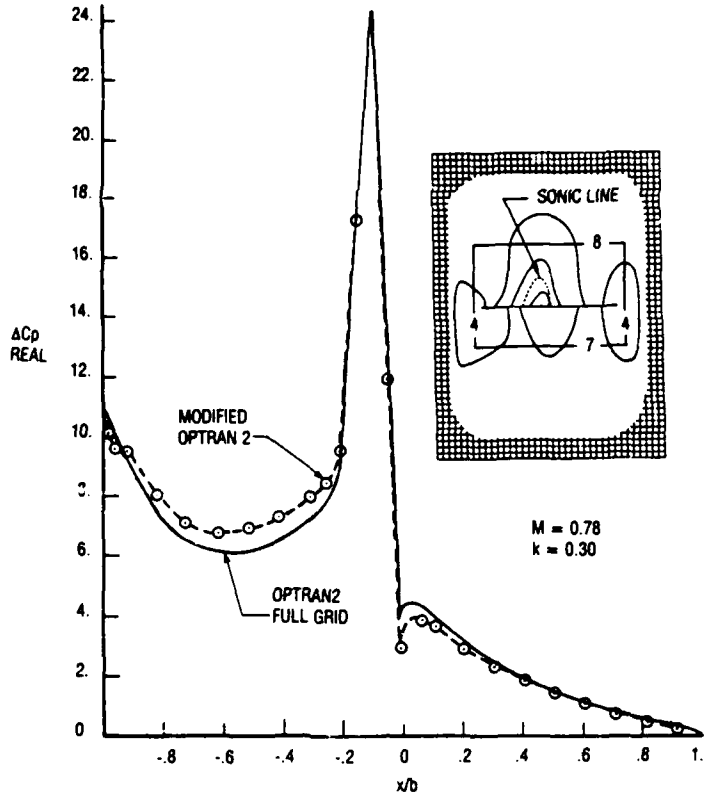

Figure 24. Real Part of Pressure Coefficients Where the Upper Boundary Intersects a Region of Nonlinearities.

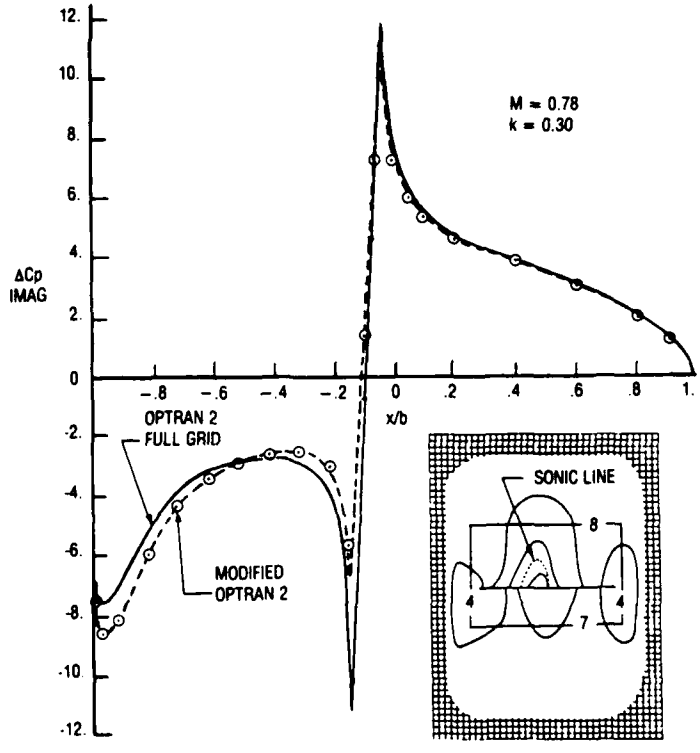

Figure 25. Imaginary Part of Pressure Coefficients for a Network Where the Upper Boundary Intersects a Nonlinear Region.

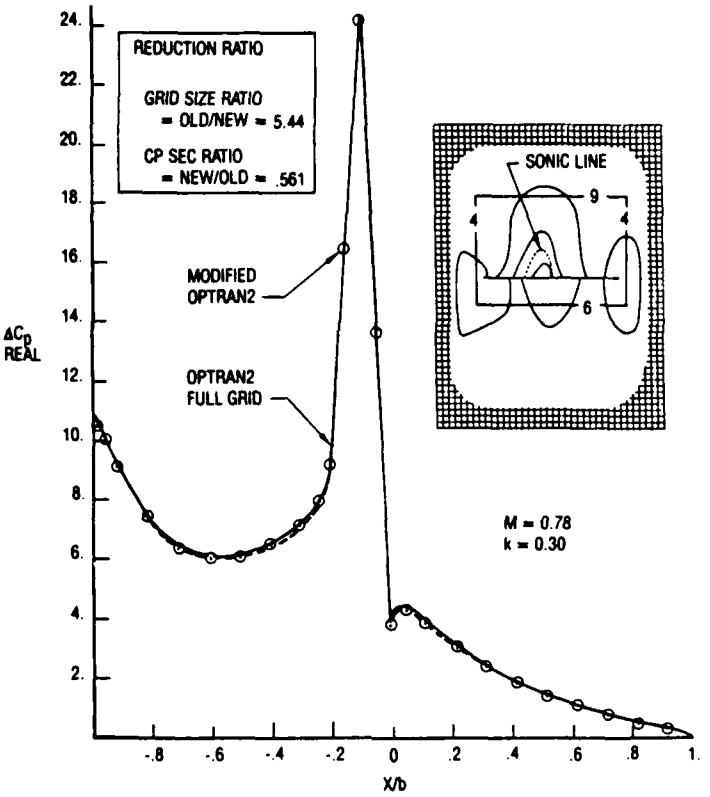

Figure 26. Real Part of Pressure Coefficients Obtained for the Upper Boundary Located in the Demarcation Zone for M = 0.78.

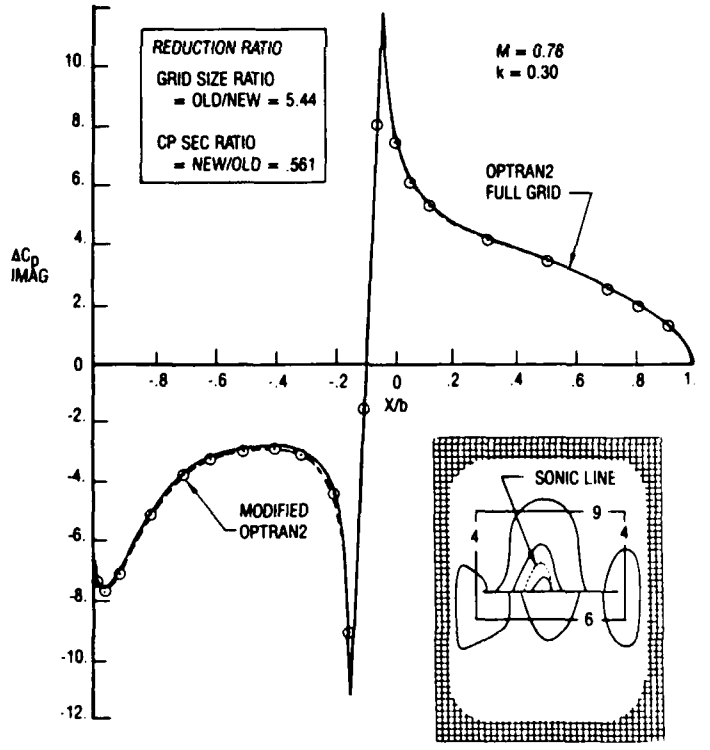

Figure 27. Imaginary Part of Pressure Coefficients Obtained for the Upper Boundary Located in the Demarcation Zone for M = 0.78.

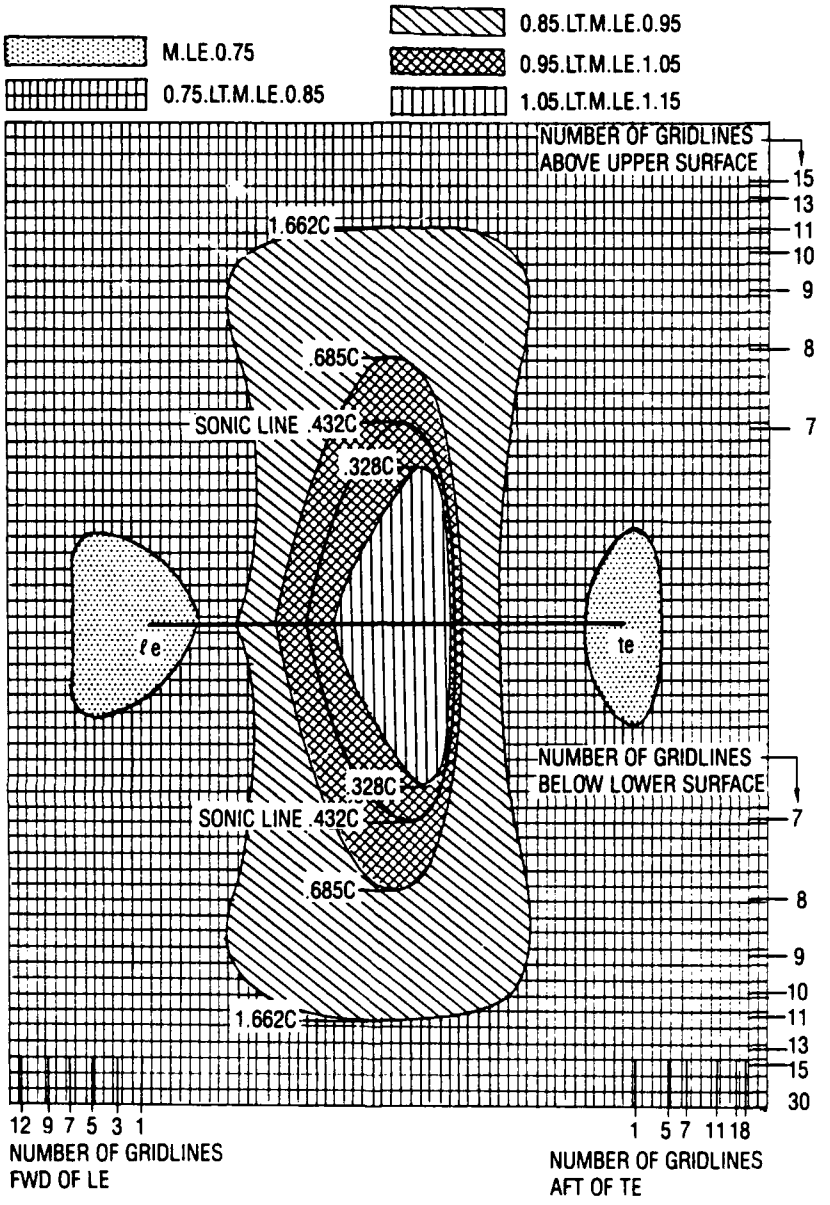

Figure 28. Steady Flow Field Mach Number Variation for a NACA 64A010 Airfoil at 0° Angle of Attack With M = 0.825.

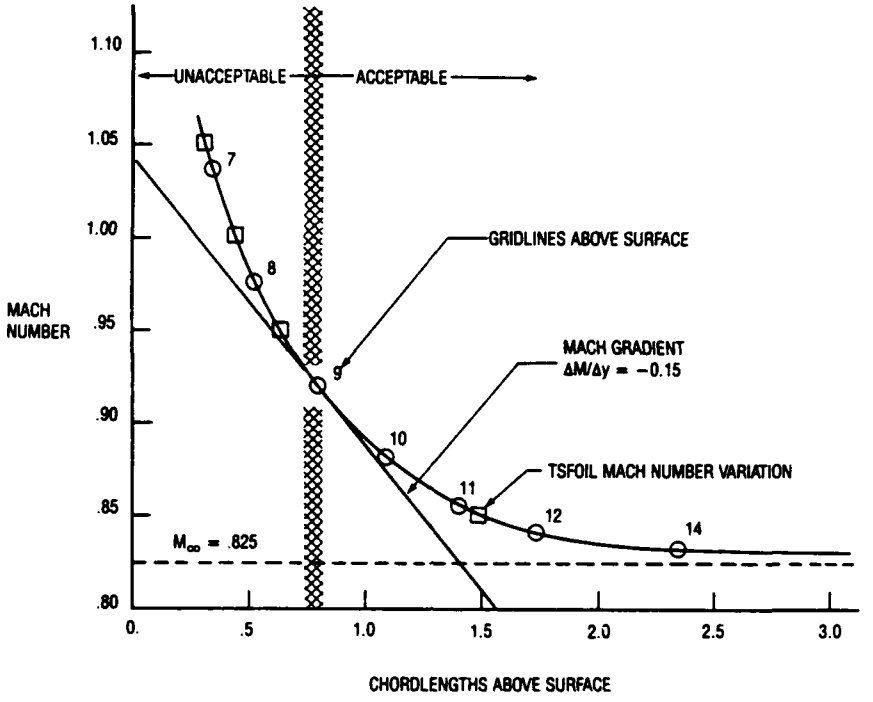

Figure 29. Mach Number Variation as a Function of Distance Above and Below the Airfoil for M = 0.825.

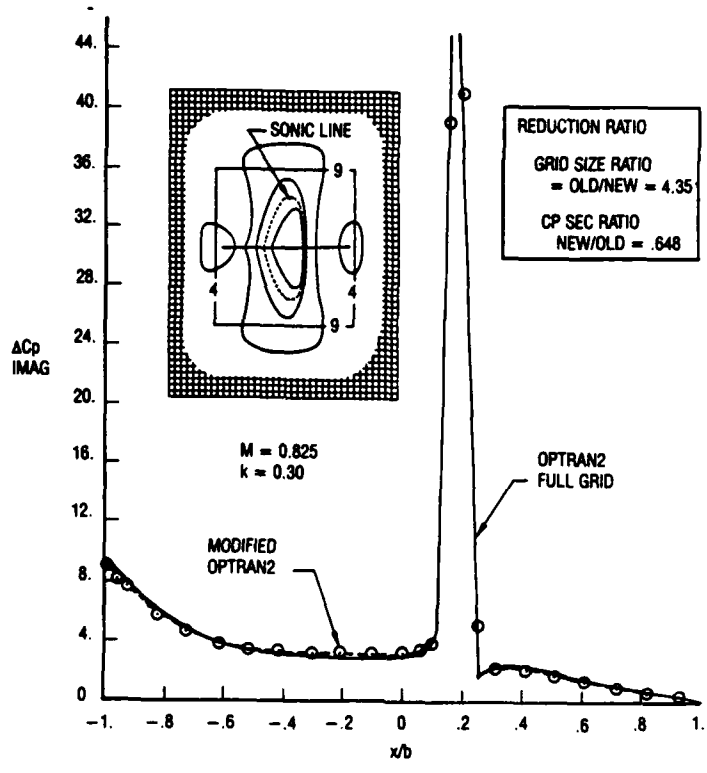

Figure 30. Real Part of Pressure Coefficients Obtained for Upper and Lower Boundaries Located in the Demarcation Zone With M = 0.825.

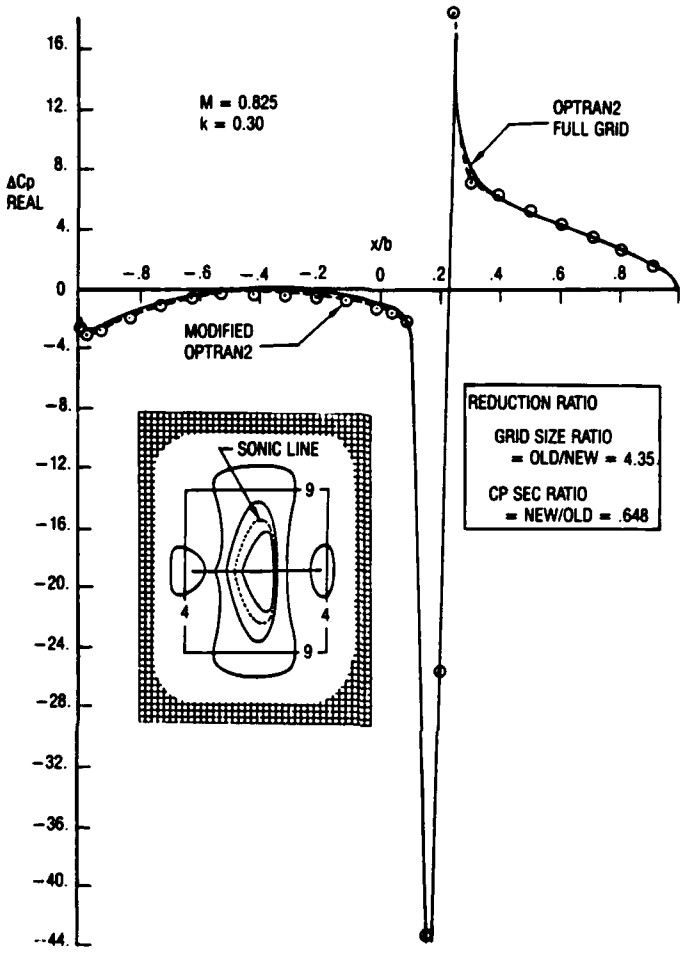

Figure 31. Imaginary Part of Pressure Coefficients Obtained for Upper and Lower Boundaries Located in the Demarcation Zone With M = 0.825.

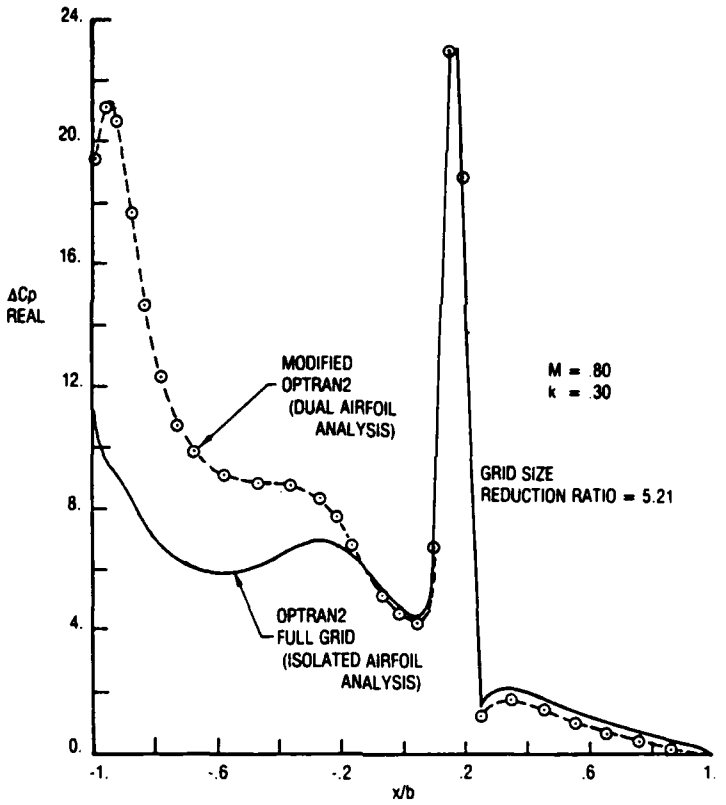

Figure 32. Real Part of the Pressure Coefficients Developed on the Leading Airfoil of a Two Airfoil System Compared With Coefficients Developed on an Isolated Airfoil.

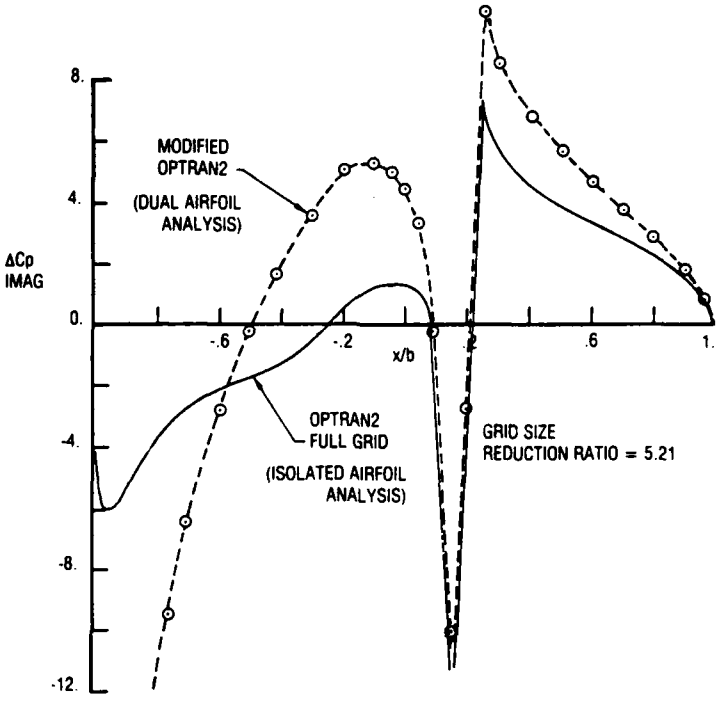

Figure 33. Imaginary Part of the Pressure Coefficients Developed on the Leading Airfoil of a Two Airfoil System Compared With Coefficients Developed on an Isolated Airfoil.

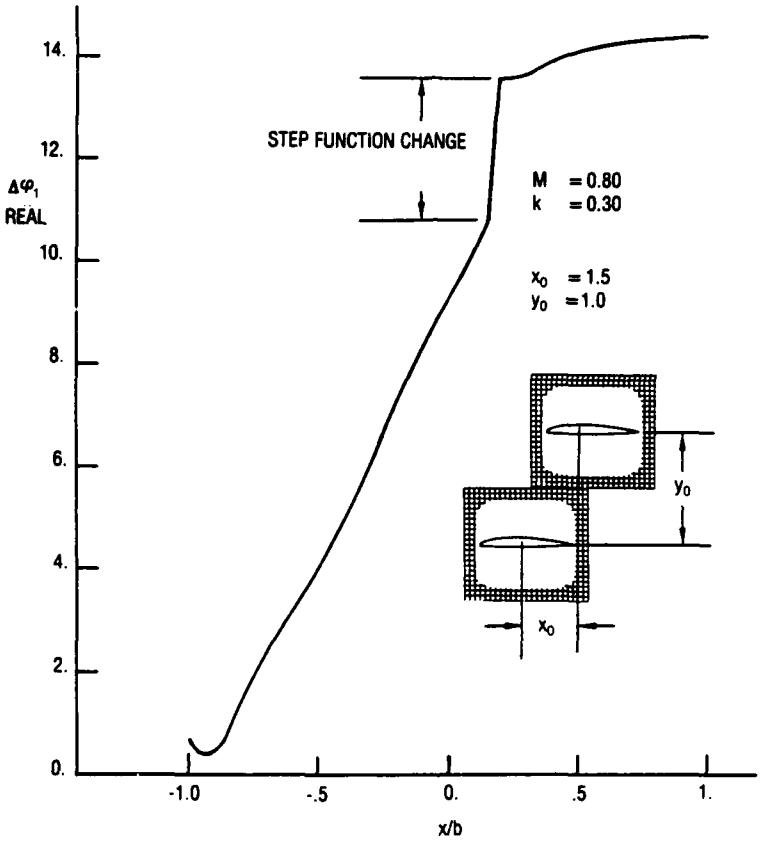

Figure 34. Variation of Velocity Potential as a Function of Distance Along the Chordlength of the Leading Airfoil.

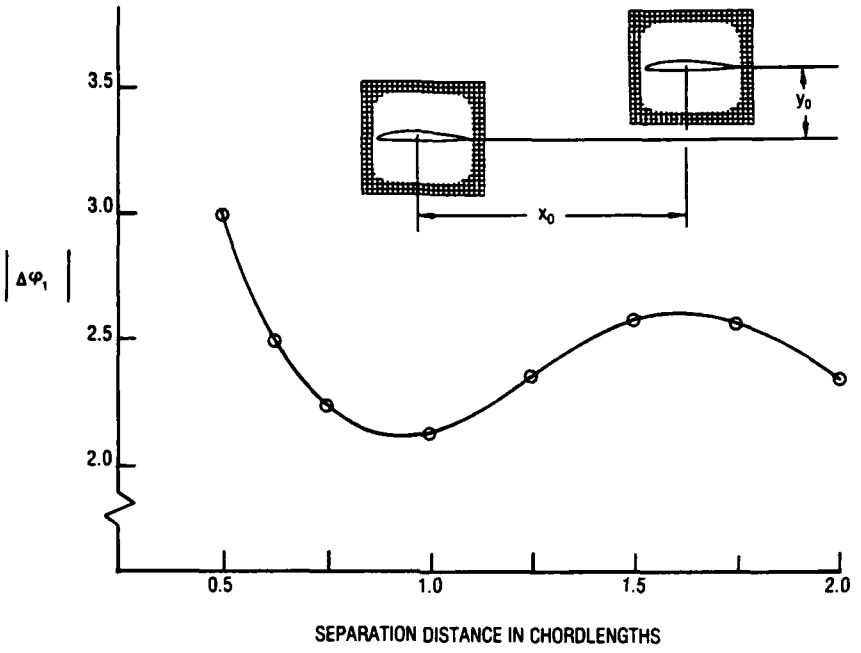

Figure 35. Velocity Potential Variation as a Function of Airfoil Separation Distance.

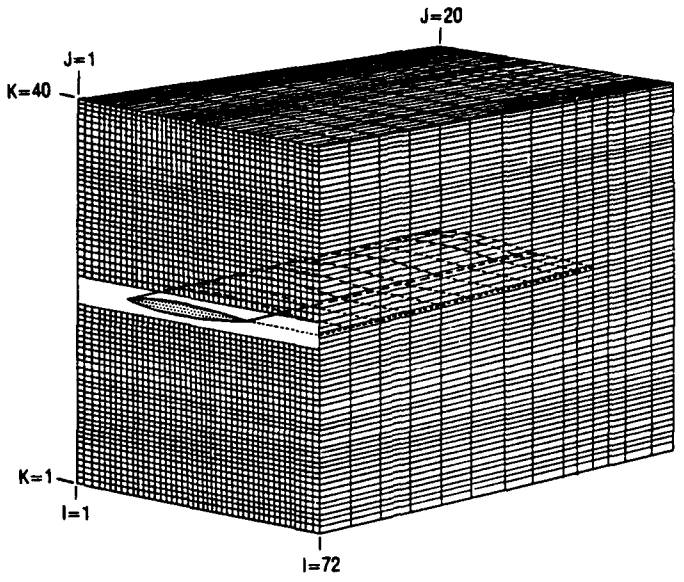

Figure 36. Finite Span Wing and Partial Wake Embedded in Grid Network.

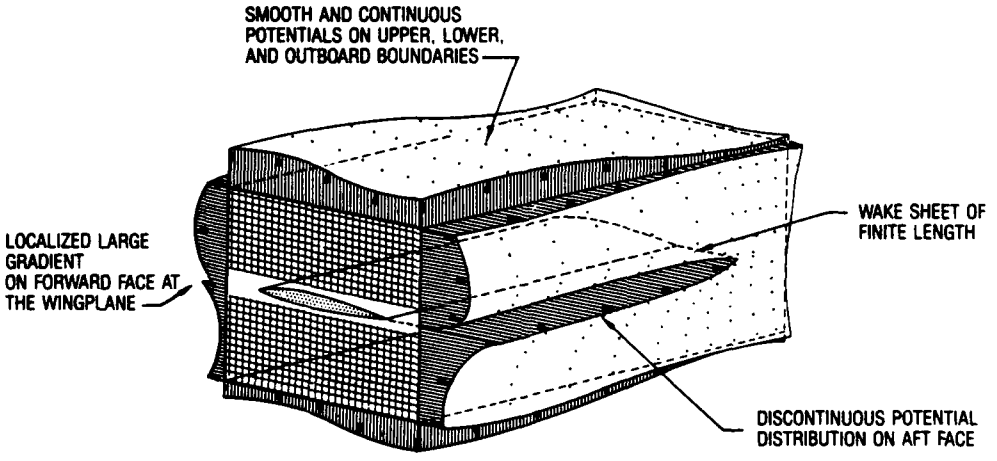

Figure 37. Velocity Potential Distributions Evaluated on the Outer Boundaries Due to the Interior Finite Difference Solution.

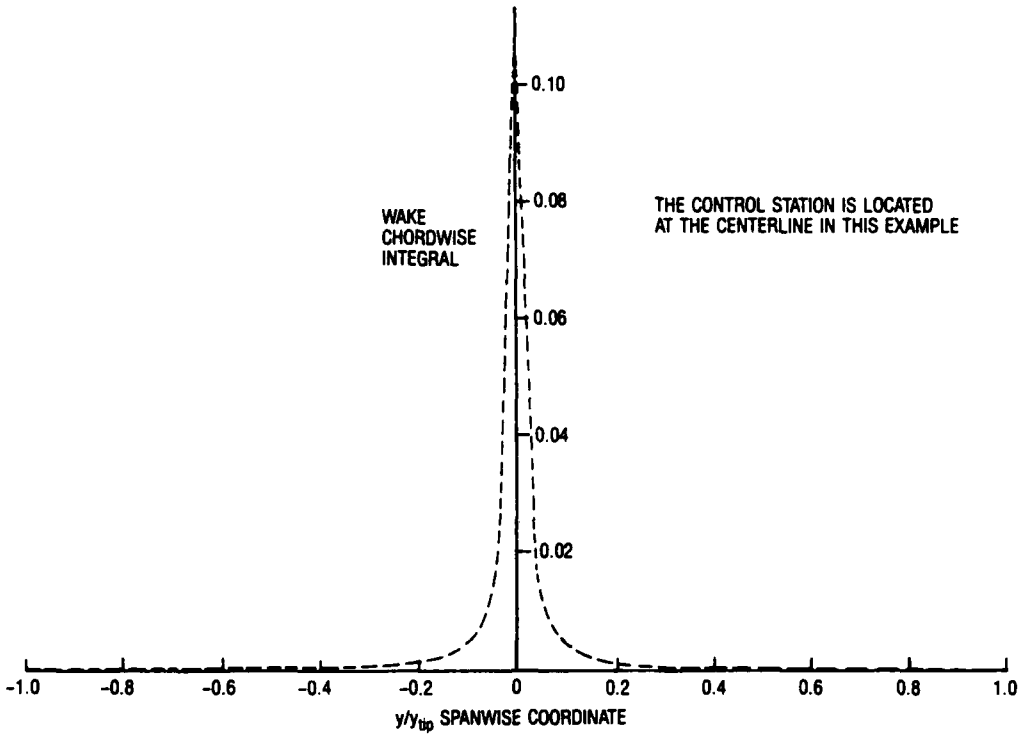

Figure 38. Spanwise Variation of the Wake Integral on the Z Plane Located a Distance of 0.078 Chord Lengths Above the Wingplane.

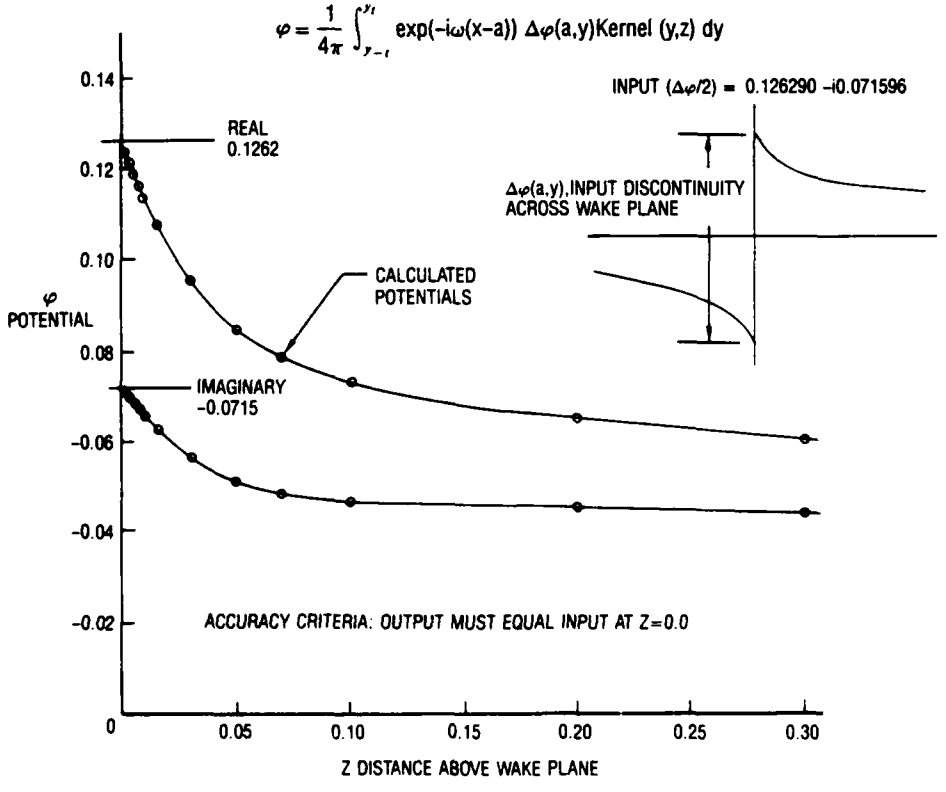

Figure 39. Accuracy Check of Wake Integral Evaluation.

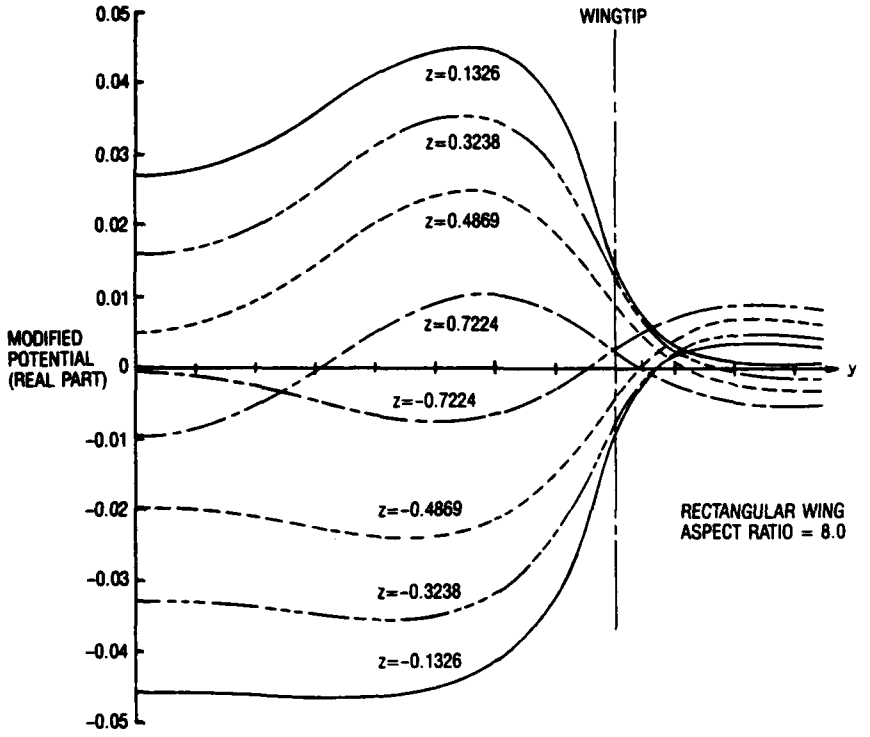

Figure 40. Typical Variation of Modified Potential for Several Values of z; Downstream Boundary, Real Part.

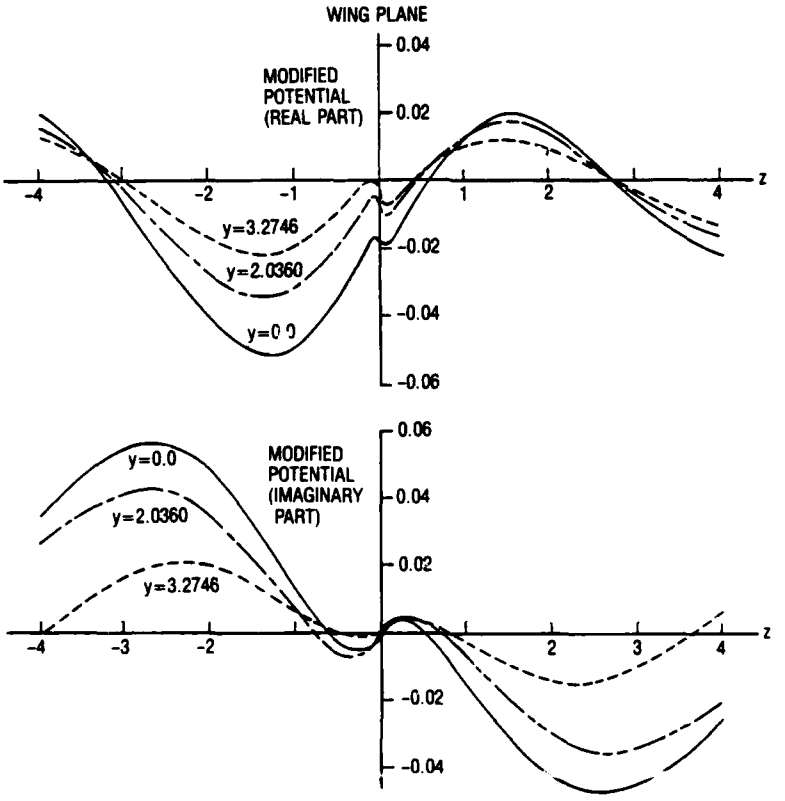

Figure 41. Variation of Modified Potential; Upstream Boundary.

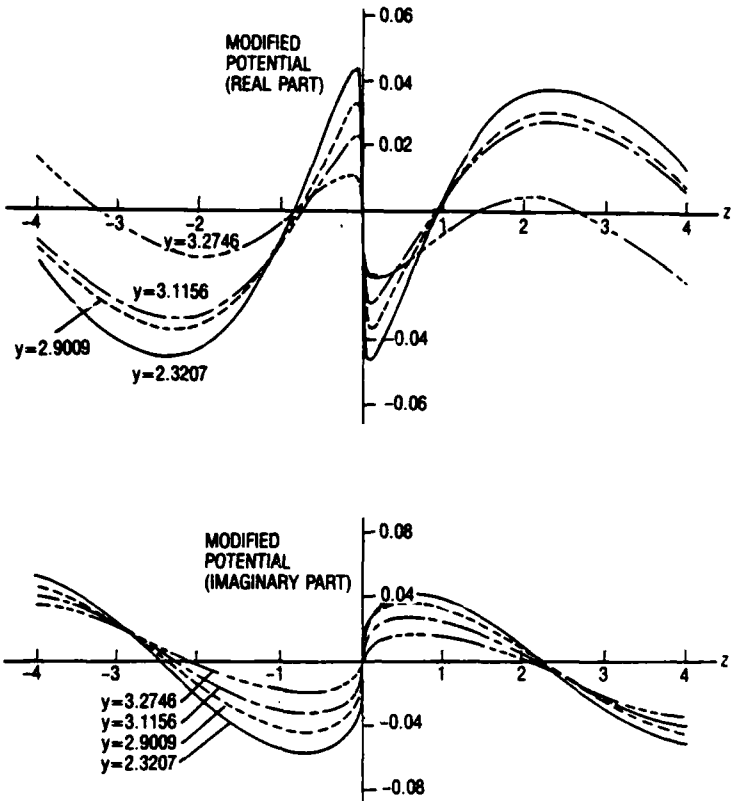

Figure 42. Typical Variation of the Modified Potential With z for Several Spanwise Stations; Downstream Boundary.

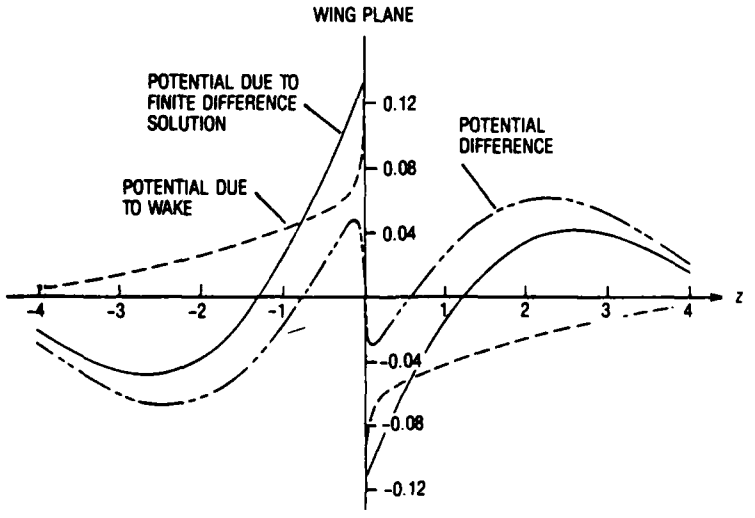

Figure 43. Comparison of Full, Modified, and Wake-Induced Potentials; Variation With z on Downstream Boundary.

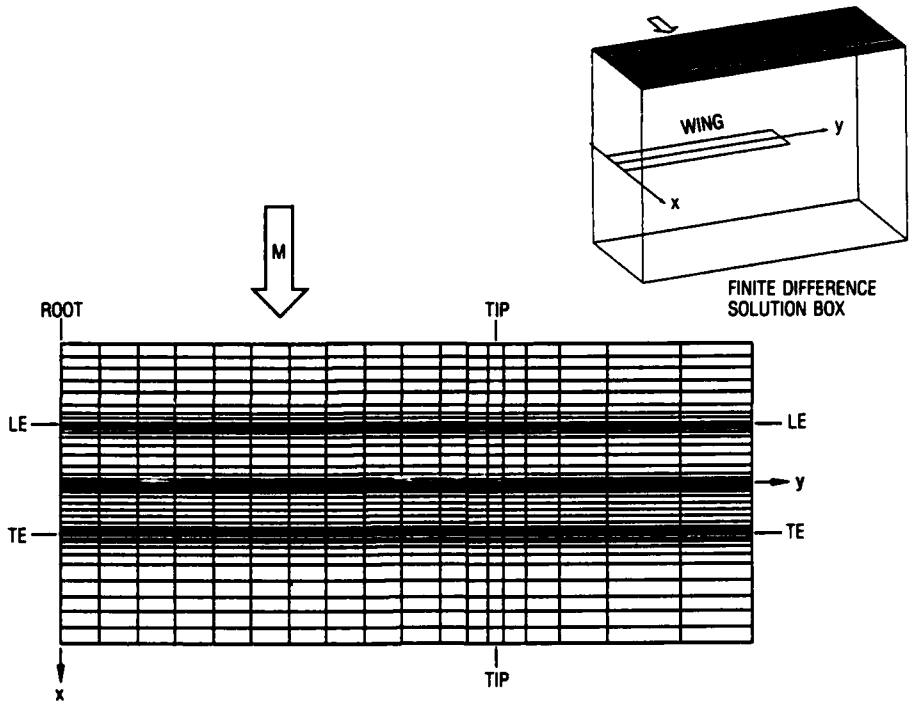

Figure 44. Basic Grid Pattern, x-y Plane

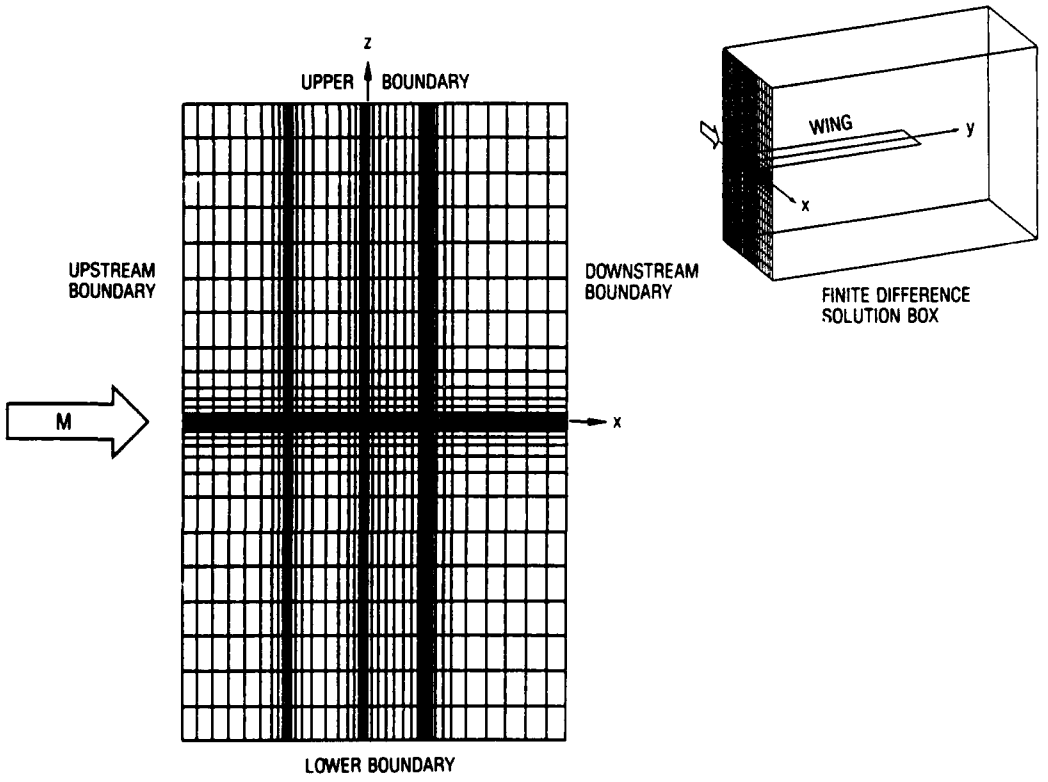

Figure 45. Basic Grid Pattern, x-z Plane

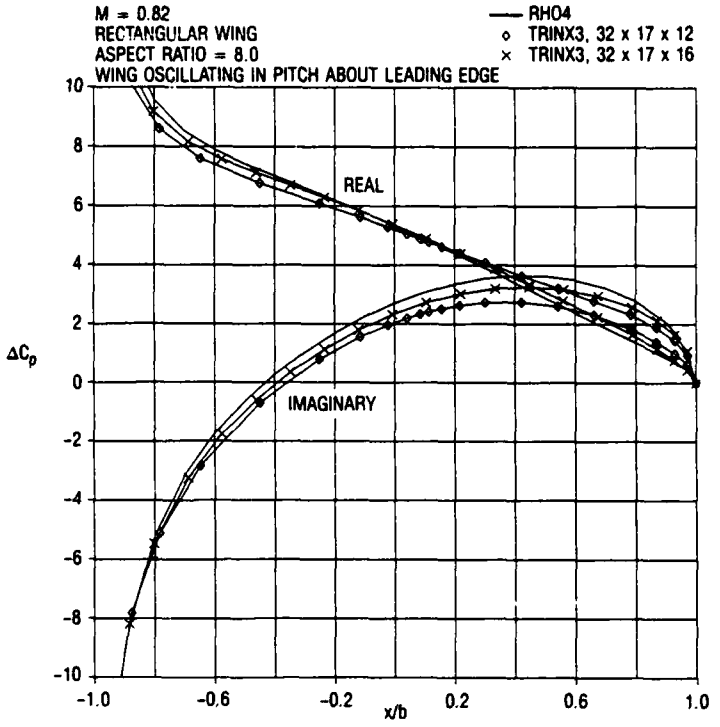

Figure 46. Comparison of Pressure Coefficients From RHO4 and TRINX3 With Two Grids; Flat Plate, k=0.3, Root.

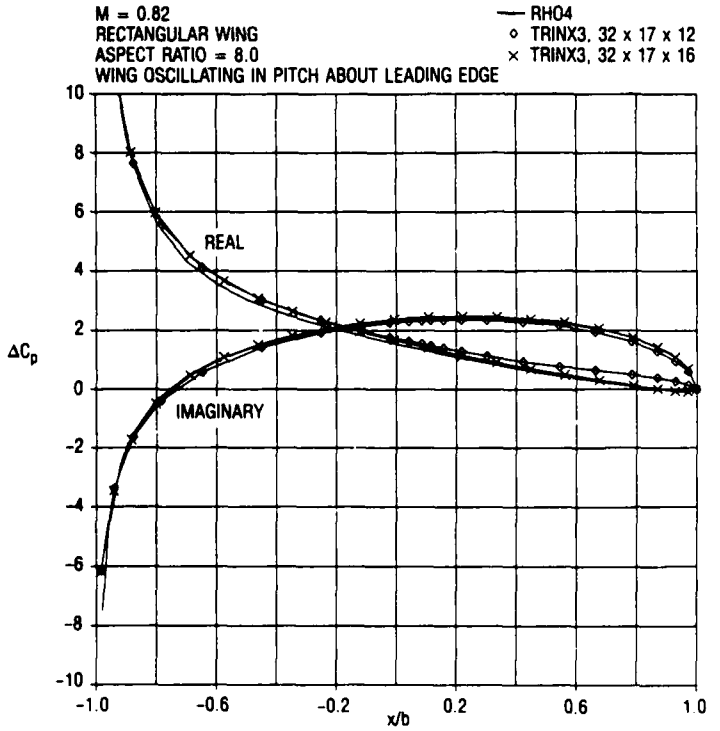

Figure 47. Comparison of Pressure Coefficients From RHO4 and TRINX3 With Two Grids; Flat Plate, k=0.3, η=0.94

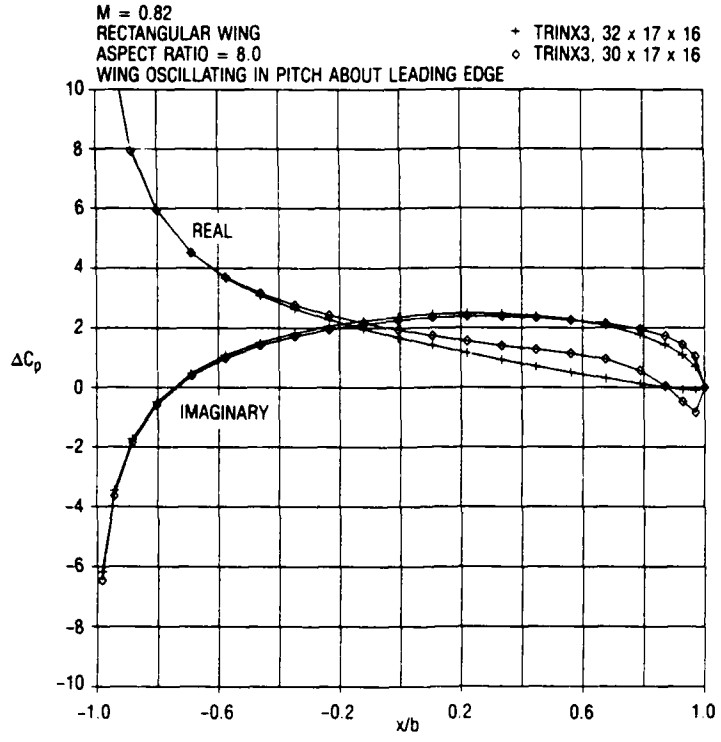

Figure 48. Comparison of Pressure Coefficients From Two TRINX3 Solutions Illustrating Effect of Moving the Downstream Boundary Aft; Flat Plate, k=0.3, Root.

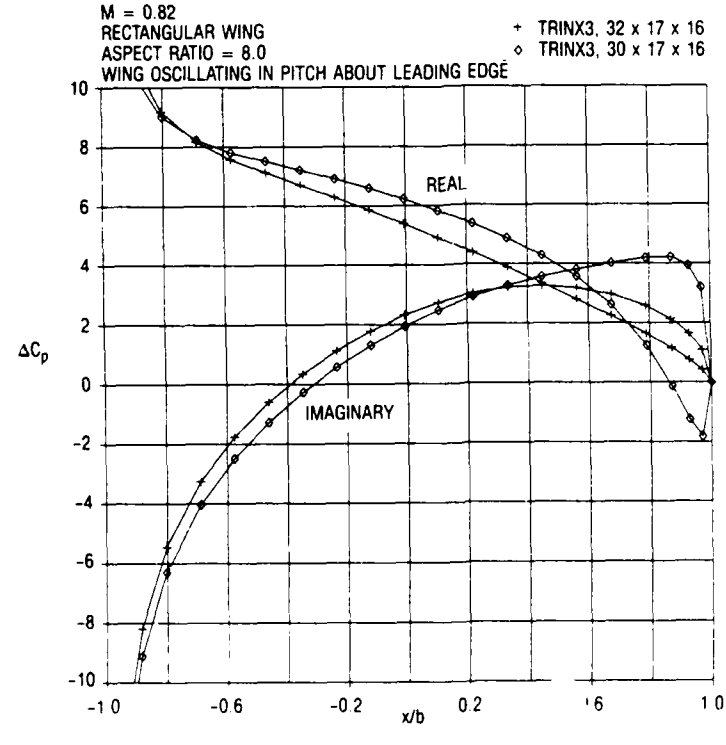

Figure 49. Comparison of Pressure Coefficients From Two TRINX3 Solutions Illustrating Effect of Moving the Downstream Boundary Aft; Flat Plate, k=0.3, η=0.94.

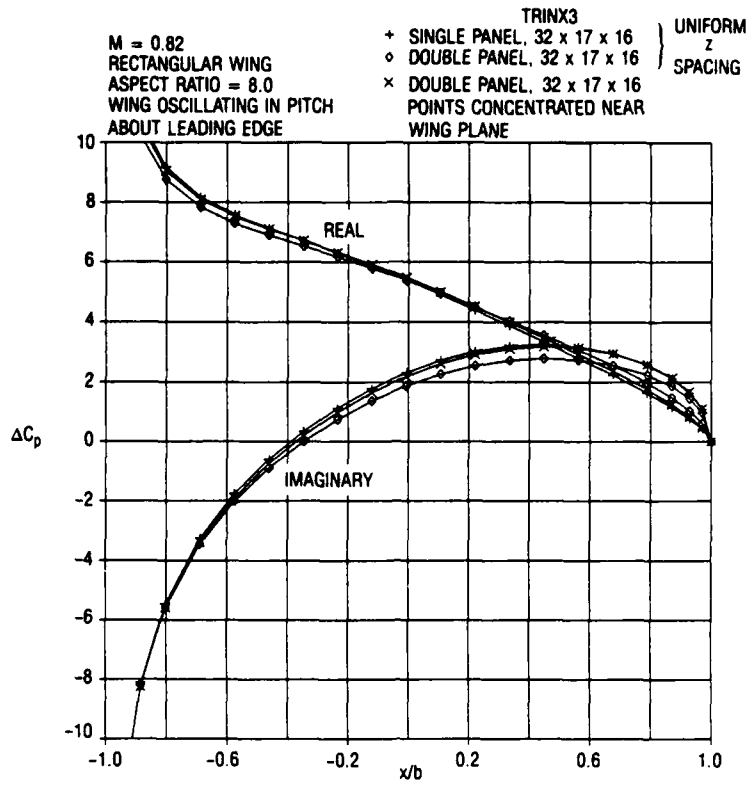

Figure 50. Comparison of Pressure Coefficients From Three TRINX3 Cases; Flat Plate, k=0.3, Root.

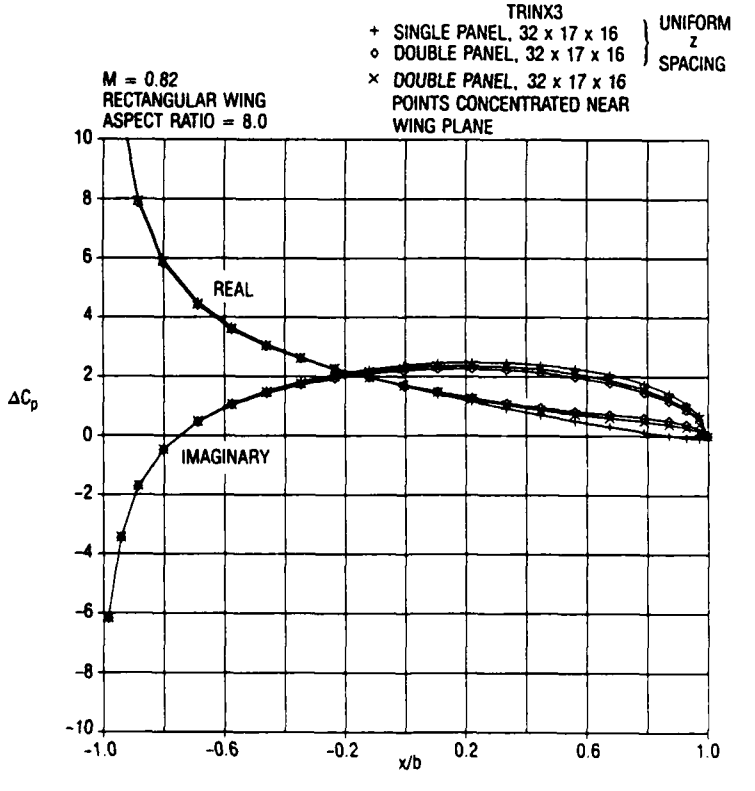

Figure 51. Comparison of Pressure Coefficients From Three TRINX3 Cases; Flat Plate, k=0.3, η=0.94.

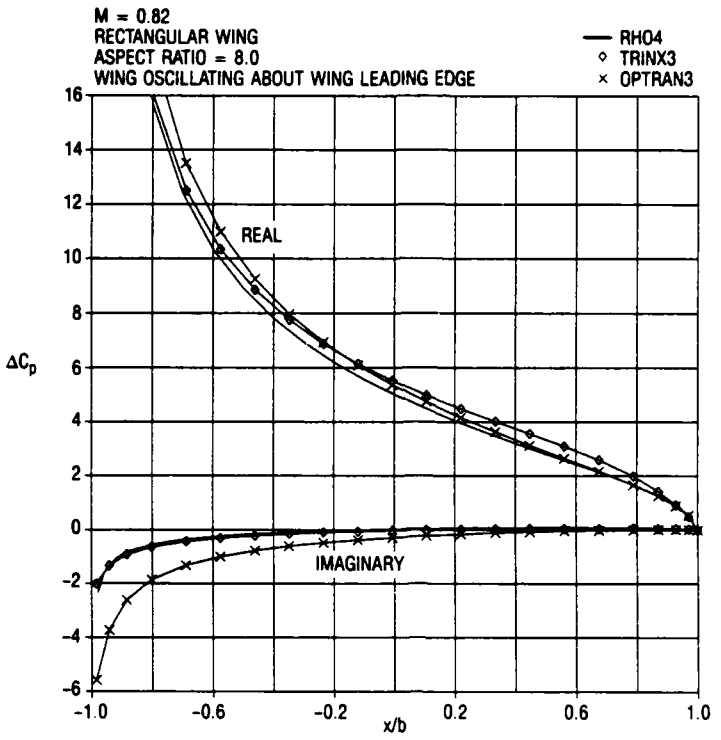

Figure 52. Comparison of Pressure Coefficients From RHO4, TRINX3, and OPTRAN3; Flat Plate, k=0.01, Root.

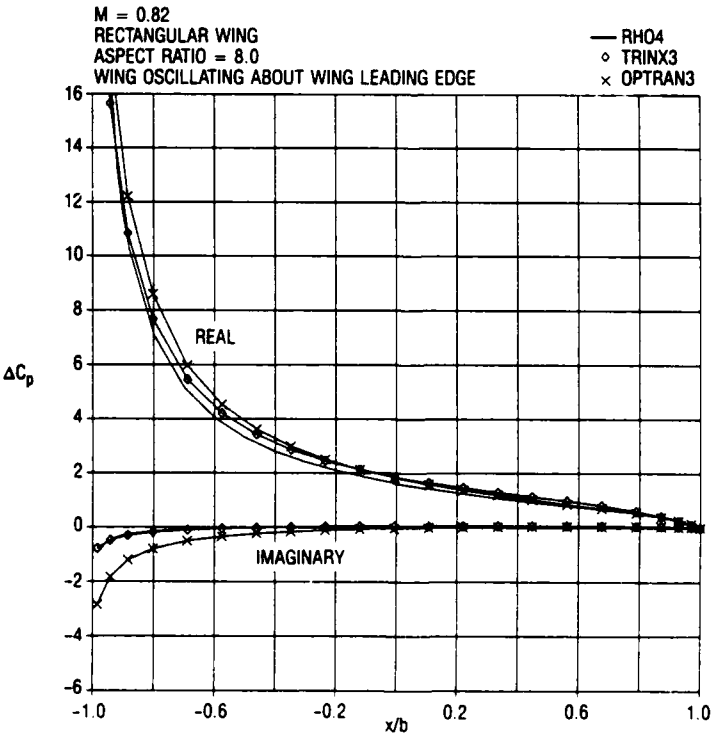

Figure 53. Comparison of Pressure Coefficients From RHO4, TRINX3, and OPTRAN3; Flat Plate, k=0.01, η=0.94.

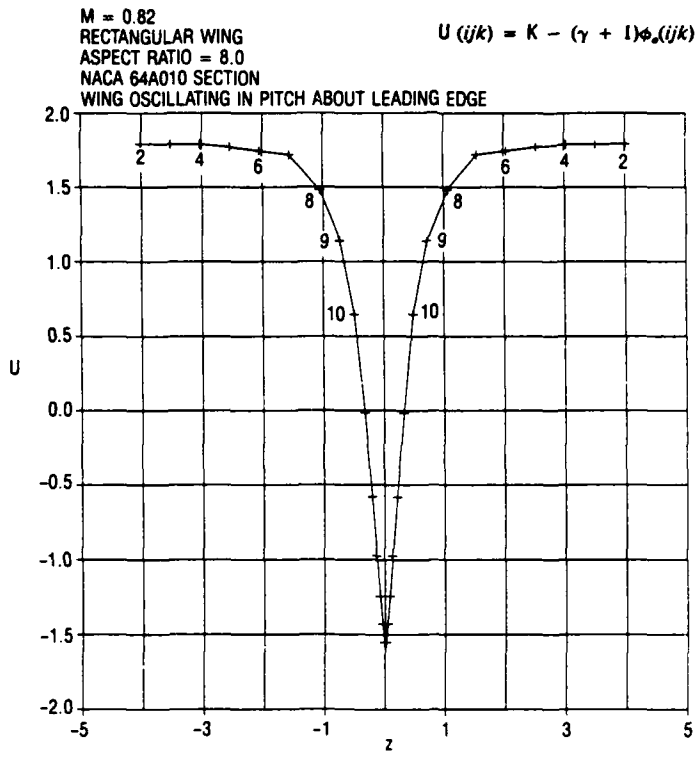

Figure 54. Typical Variation of U With z; Column of Points on Wing at Root.

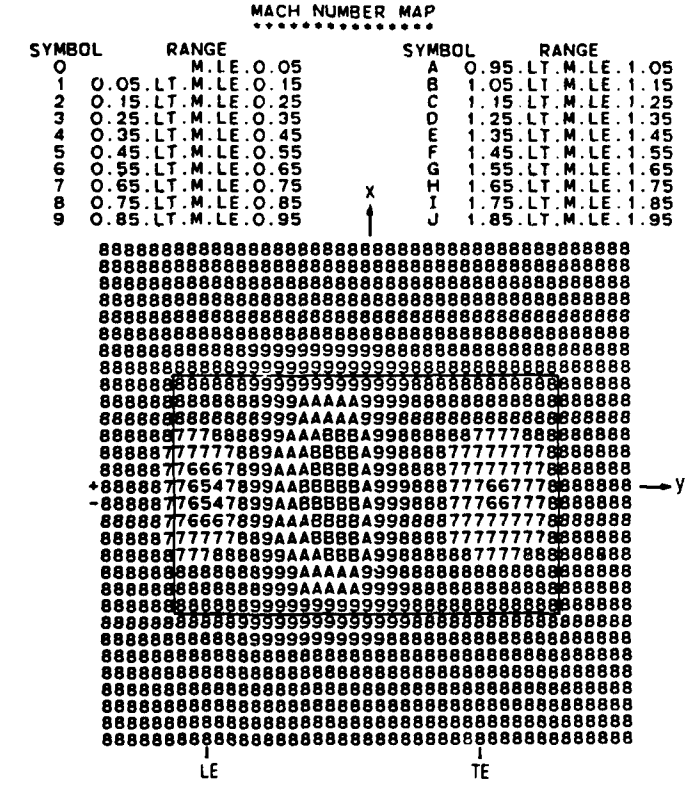

Figure 55. Steady Flow Mach Number Variation; Streamwise Plane at Root.

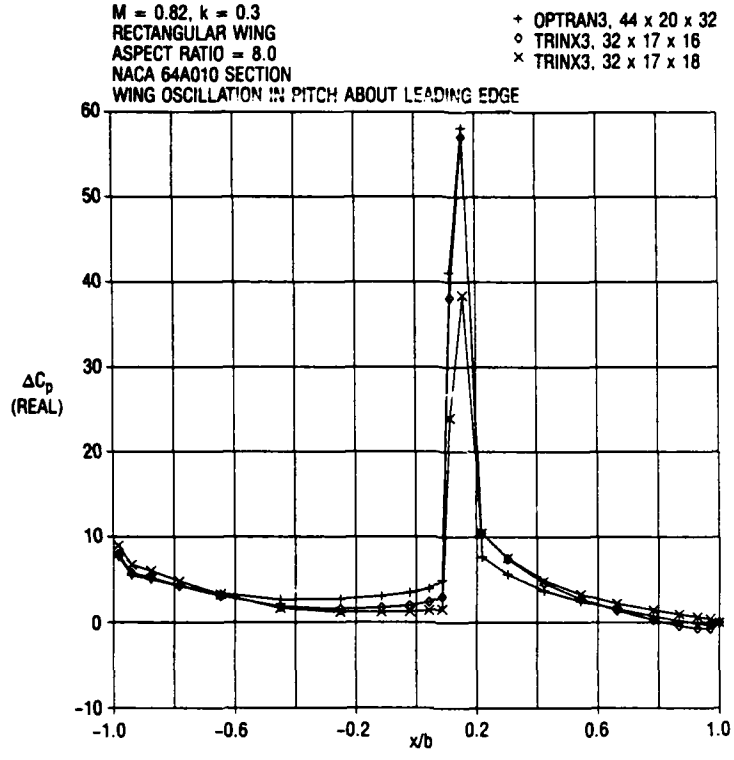

Figure 56. Comparison of Pressure Coefficients From TRINX3 and RHO4; Real Part, Root.

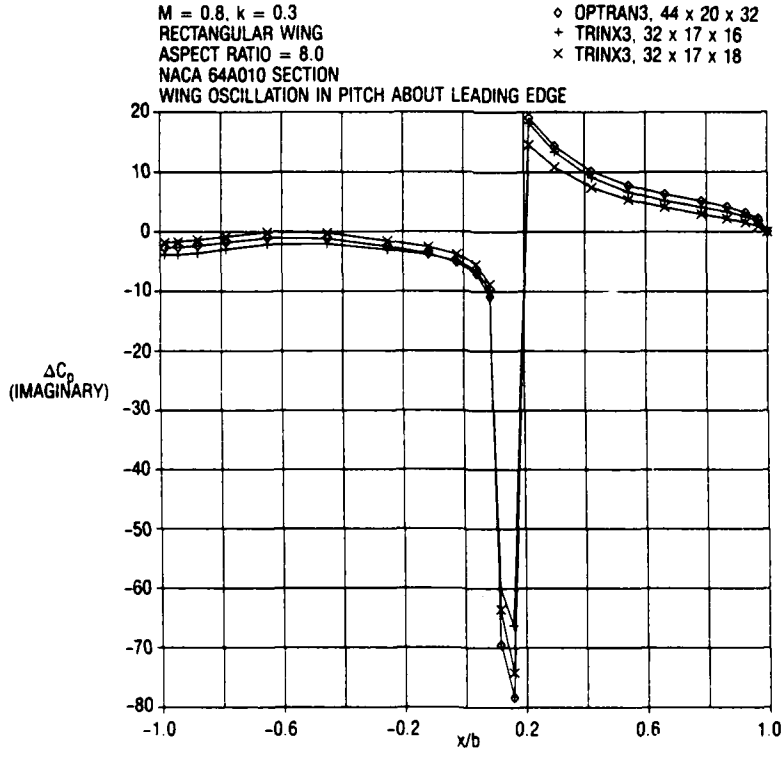

Figure 57. Comparison of Pressure Coefficients From TRINX3 and RHO4; Imaginary Part, Root.

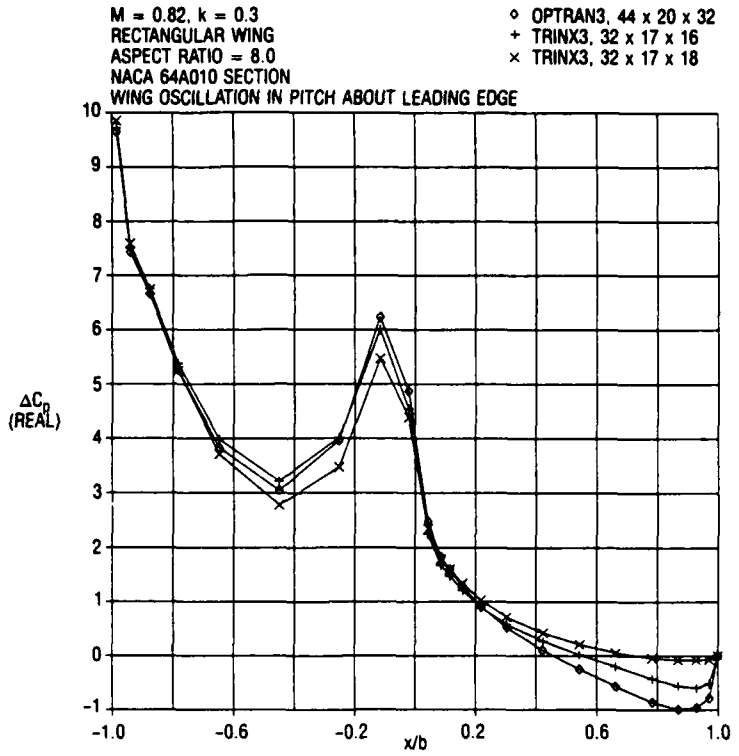

Figure 58. Comparison of Pressure Coefficients From TRINX3 and RHO4; Real Part, η=0.94.

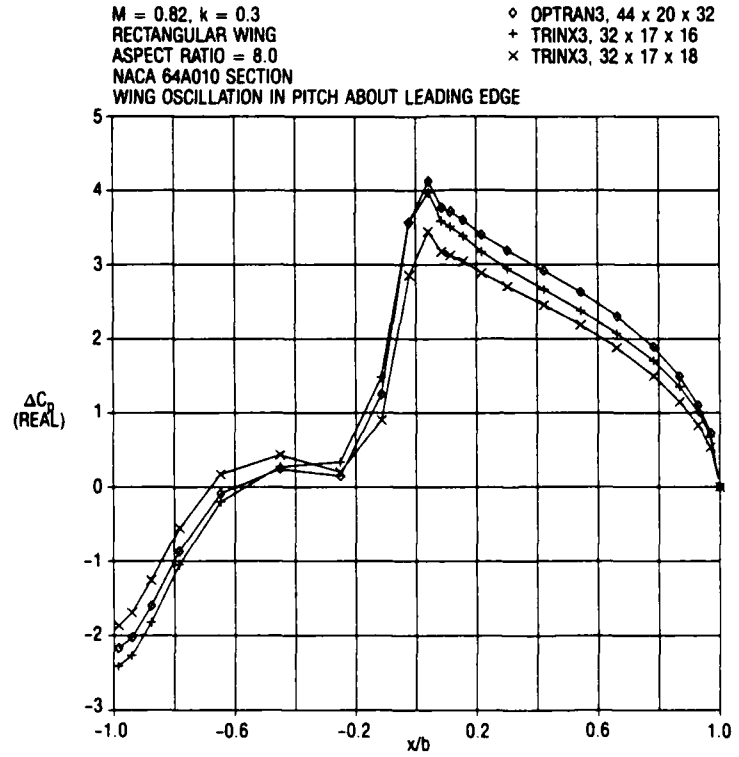

Figure 59. Comparison of Pressure Coefficients From TRINX3 and RHO4; Imaginary Part, η=0.94.

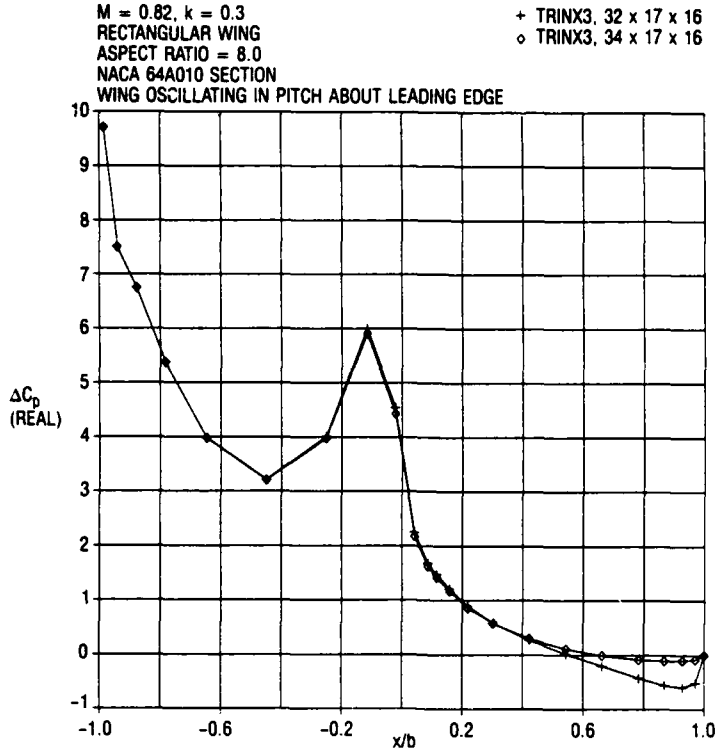

Figure 60. Comparison of Pressure Coefficients From TRINX3 for Two Grids; Real Part, η=0.94.

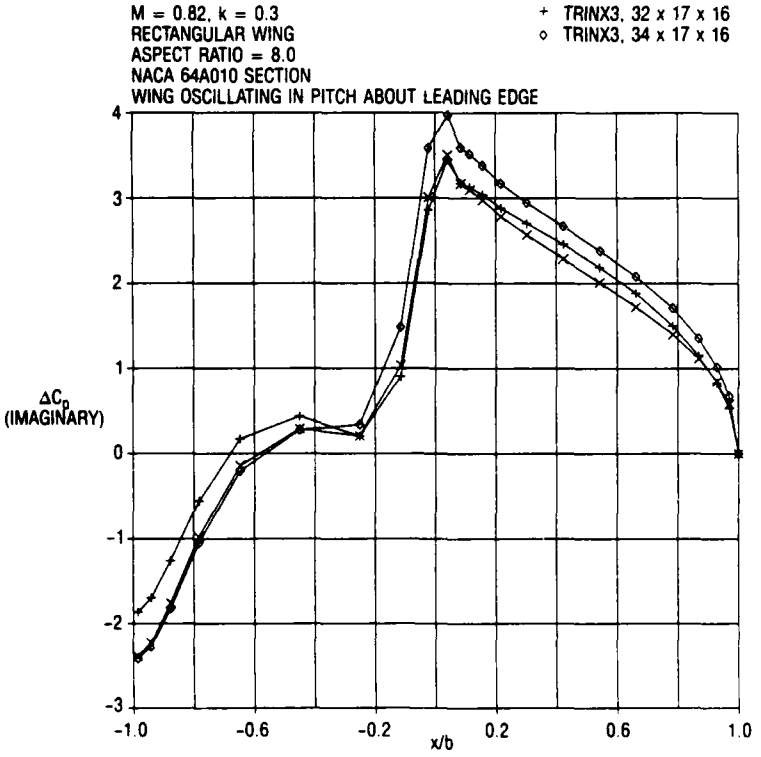

Figure 61. Comparison of Pressure Coefficients From TRINX3 for Two Grids; Imaginary Part, η=0.94.

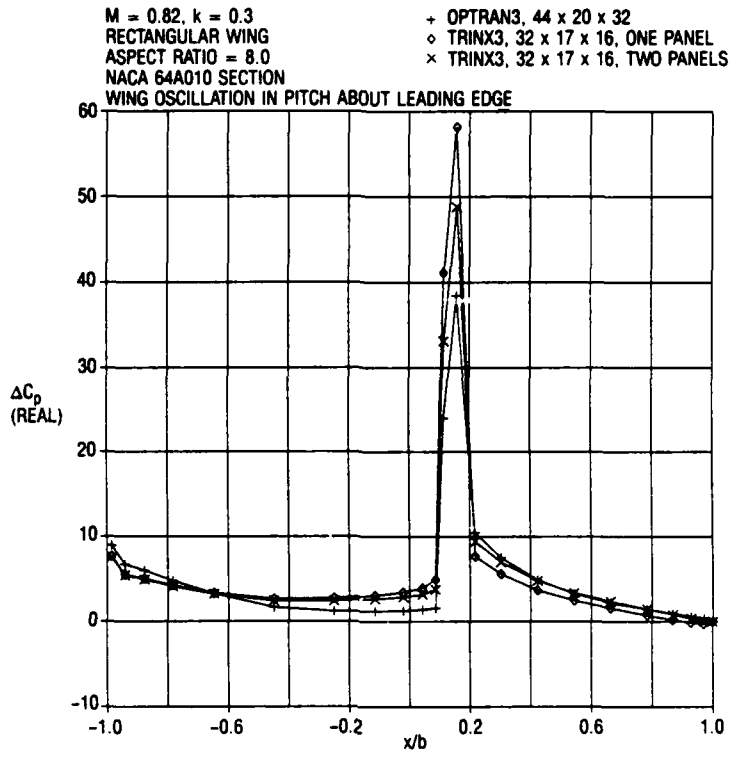

Figure 62. Comparison of Pressure Coefficients From TRINX3 for One and Two Panel Procedures; Real Part, Root.

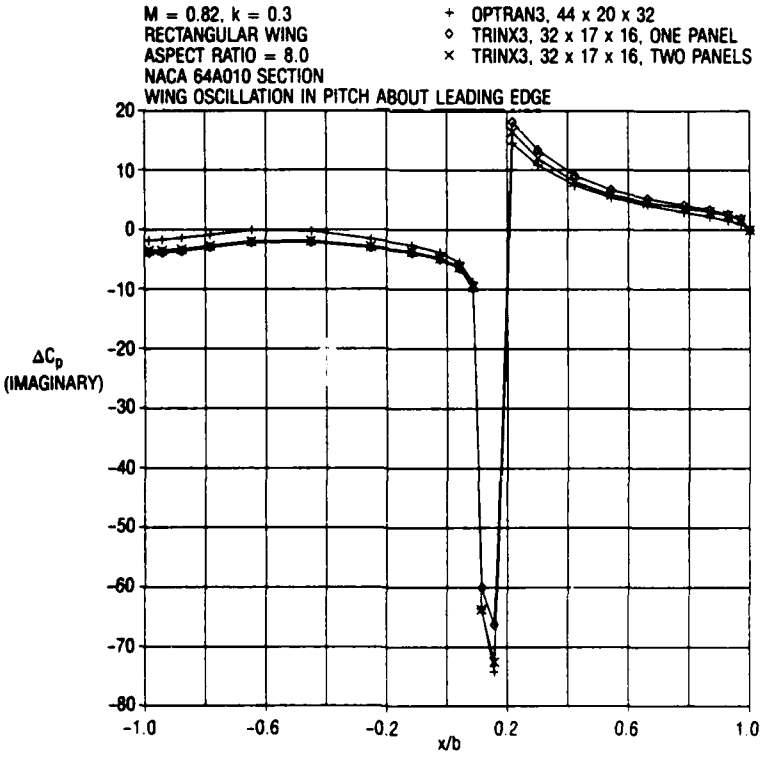

Figure 63. Comparison of Pressure Coefficients From TRINX3 for One and Two Panel Procedures; Imaginary Part, Root.

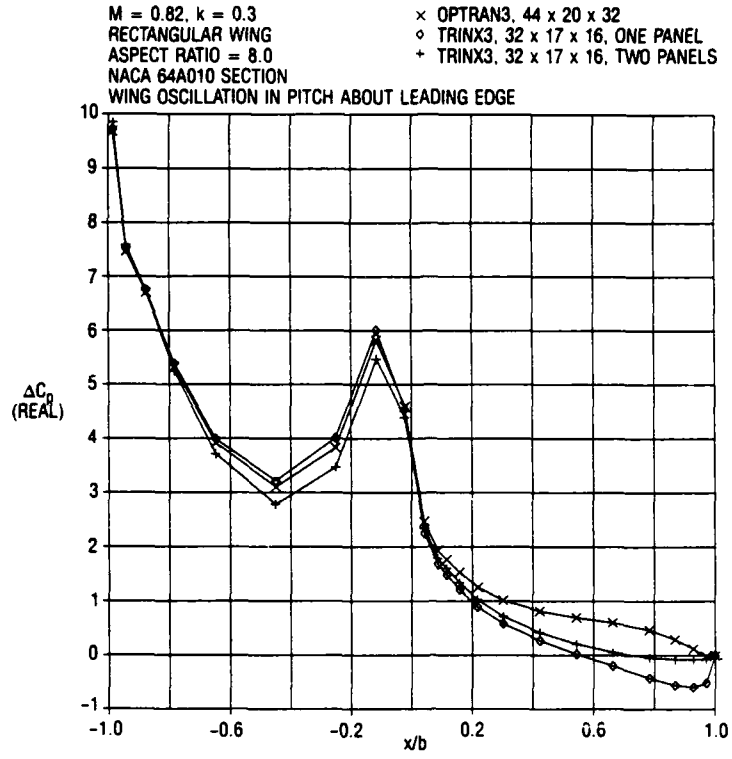

Figure 64. Comparison of Pressure Coefficients From TRINX3 for One and Two Panel Procedures; Real Part, η=0.94.

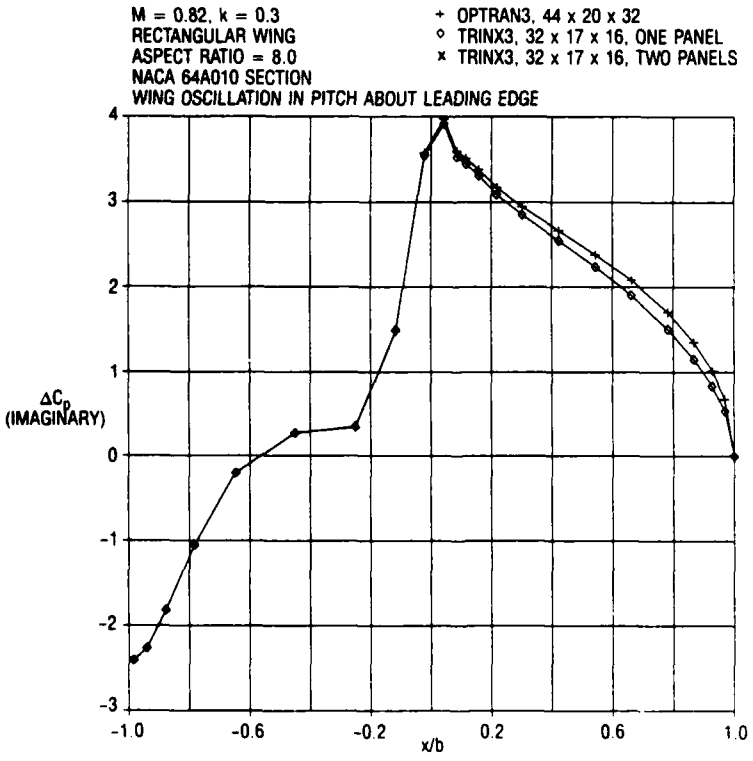

Figure 65. Comparison of Pressure Coefficients From TRINX3 for One and Two Panel Procedures; Imaginary Part, η=0.94.

APPENDIX A

DERIVATION OF VELOCITY POTENTIAL FUNCTIONS FOR THE OUTER SOLUTION COMPOSED OF SOURCE AND DOUBLET DISTRIBUTIONS FOR TWO-DIMENSIONAL FLOW

To derive the form of the outer solution, we consider the region outside the finite differencing grid network. The partial differential equation for the unsteady potential may be written as

$$\varphi_{1x_1x_1} - 2i\lambda_1 M\varphi_{1x_1} + \varphi_{1yy} + \lambda_1^2(1 - M^2)\varphi_1 = \frac{\gamma + 1}{K}(\varphi_{0x_1}\varphi_{1x_1})_{x_1} + i\omega\frac{(\gamma - 1)}{K}\varphi_1\varphi_{0x_1x_1}, \quad \text{(A1)}$$

where $x_1 = x$, and $y_1 = y_1\sqrt{K}$; $\lambda_1 = \omega M/(1-M^2)$

The terms on the right-hand side become less significant with increasing distance from the transonic zone and will be neglected in the outer solution derivation. We make use of Green's theorem to obtain the outer solution by the following procedures.

We choose a singular function,

$$\psi(X_1, Y_1), \quad \text{(A2)}$$

which satisfies $L(\psi) = 0$ for

$$L = \frac{\partial^2}{\partial X_1^2} - 2i\lambda_1 M\frac{\partial}{\partial X_1} + \frac{\partial^2}{\partial Y_1^2} + \lambda_1^2(1 - M^2). \quad \text{(A3)}$$

The function ψ is singular at $X_1 = Y_1 = 0$;

$$\begin{aligned} X_1 &= x_1 - x_1', \\ Y_1 &= y_1 - y_1', \end{aligned} \quad \text{(A4)}$$

where the primes denote the variables of integration, and x_1, y_1 is the reference station.

Consider the surface integral

$$\int_S (\psi L(\varphi_1) - \varphi_1 L(\psi))\, ds, \quad \text{(A5)}$$

with the surface S being the region outside of the region of the following sketch that includes a circle of vanishing radius centered about the reference point x_1, y_1. since $L(\varphi_1) = L(\psi) = 0$, the integral of equation 5 vanishes.

Note: Unless otherwise stated, references made in Appendices A, B, C, and D to equations in these appendices do not include the appendix letter or parenthesis. For example, in Appendix A, equation (A5) would be referred to as "equation 5."

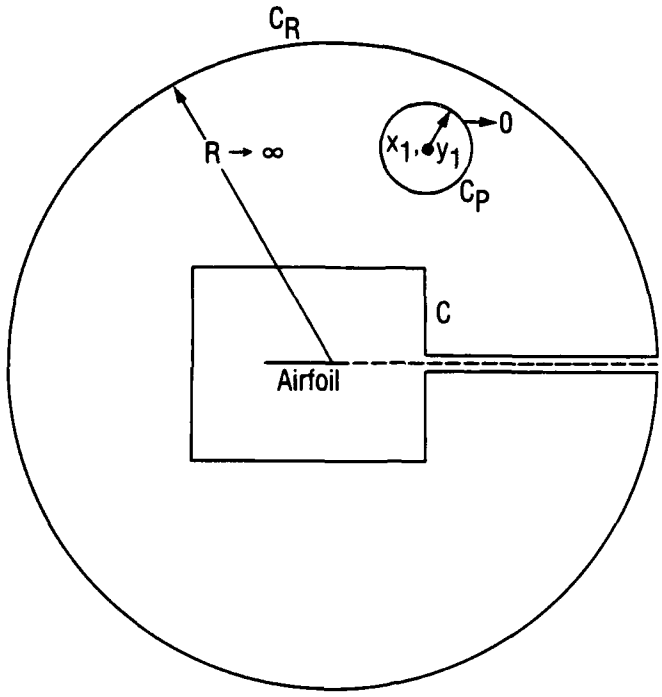

Figure A-1.—Area Integration for Green's Theorem

Expanding the integrand of equation 5 results in the equation

$$\int_S \{\psi[\varphi_{1x_1'x_1'} - 2i\lambda_1 M\varphi_{1x_1'} + \varphi_{1y_1'y_1'} + \lambda_1^2(1 - M^2)\varphi_1] - \varphi_1[\psi_{1x_1'x_1'} + 2i\lambda_1 M\psi_{1x_1'} + \psi_{1y_1'y_1'} + \lambda_1^2(1 - M^2\psi_1]\}\, ds = 0, \tag{A6}$$

where use has been made of the relationships

$$\psi_{1X_1X_1} = \psi_{1x_1'x_1'},$$

$$\psi_{1X_1} = -\psi_{1x_1'}$$

and

$$\psi_{1Y_1Y_1} = \psi_{1y_1'y_1'}.$$

Rearranging the terms yields the expression

$$\int_S \{[\psi\varphi_{1x_1'x_1'} - \varphi_1\psi_{x_1'x_1'}] - 2i\lambda_1 M[\varphi_1\psi_{x_1'} + \varphi_{1x_1'}\psi] + [\psi\varphi_{1y_1'y_1'} - \varphi_1\psi_{y_1'y_1'}]\}\, ds = 0,$$

which is suitable for evaluating the integrals of Green's theorem when it is put in the following form:

$$\int_S \left\{\frac{\partial}{\partial x_1'}[\psi\varphi_{1x_1'} - \varphi_1\psi_{x_1'}] - 2i\lambda_1 M\frac{\partial}{\partial x_1'}(\varphi_1\psi) + \frac{\partial}{\partial y_1'}[\psi\varphi_{1y'} - \varphi_1\psi_{y_1'}]\right\} ds = 0. \tag{A7}$$

The surface integrals are converted to line integrals (contour integrals) by using Green's theorem.

$$\int_S \frac{\partial A}{\partial x_1'}\, ds = \int_{C+C_p} A\, n_{x_1}\, d\ell$$

and (A8)

$$\int_S \frac{\partial A}{\partial y_1'}\, ds = \int_{C+C_p} A\, n_{y_1}\, d\ell,$$

where C represents the contour around the grid network and infinite wake, and C_p represents the contour around the circle of vanishingly small radius located at x_1, y_1. The integral around the external circle of radius R vanishes as R approaches infinity. Applying equations 8 to equation 7 yields

$$\int_{C+C_p} \left\{ \psi\, \frac{\partial \varphi_1}{\partial n} - \varphi_1 \frac{\partial \psi}{\partial n} - 2i\lambda_1 M\, \varphi_1 \psi n_x \right\} d\ell = 0. \tag{A9}$$

We now derive the expression for ψ, using the equation

$$\psi_{X_1X_1} - 2i\lambda_1 M\, \psi_{X_1} + \psi_{Y_1Y_1} + \lambda_1^2 (1 - M^2)\, \psi = 0.$$

We remove the first derivative term by using the transformation

$$\psi\,(X_1, Y_1) = \exp\,(i\lambda_1 M\, X_1)\, \psi_0\,(X_1, Y_1), \tag{A10}$$

where $\psi_0\,(X_1, Y_1)$ satisfies the Helmholtz equation

$$\psi_{0X_1X_1} + \psi_{0Y_1Y_1} + \lambda_1^2 \psi_0 = 0.$$

Then let $\psi_0 = \psi_0(r)$ (where $r = \sqrt{(X_1^2 + Y_1^2)}$) be substituted into the Helmholtz equation to obtain he the differential equation

$$\psi_{0rr} + \psi_{0r}/r + \lambda_1^2\, \psi_0 = 0,$$

which is recognized as being a Bessel equation.

We choose the solution of this equation to be the Hankel function of the second type,

$$\psi_0(r) = H_0^{(2)}\,(\lambda_1 r). \tag{A11}$$

This Hankel function may be approximated for large values of r by the expression

$$\psi_o(r) \sim \exp\,(-i\lambda_1 r)/\sqrt{r}, \tag{A12}$$

which has characteristics of an outgoing wave whose magnitude approaches zero as r tends to infinity.

We now integrate around the small circle centered at x_1,y_1, using an approximation for the Hankel function that is valid for small r, that is,

$$H_0^{(2)}\,(\lambda_1 r) \approx -\frac{2i}{\pi}\, \ell n\,(r). \tag{A13}$$

Since $\psi_n = \psi_r$ for the circle, the integration of the line integral about the point x_1, y_1 yields

$$\lim_{r\to 0} \int_{-\pi}^{\pi} \psi \frac{\partial \varphi_1}{\partial r} r d\theta = 0 \tag{A14}$$

$$\lim_{r\to 0} \int_{-\pi}^{\pi} \psi_r \varphi_1 r d\theta = -4i\varphi_1(x_1,y_1). \tag{A15}$$

Inserting equations 14 and 15 into equation 9 results in

$$\varphi_1(x_1,y_1) = \frac{1}{4i} \int_C \left[\psi \frac{\partial \varphi_1}{\partial n} - \varphi_1 \frac{\partial \psi}{\partial n} - 2i\lambda_1 M \varphi_1 \psi n_x\right] d\ell, \tag{A16}$$

where the contour C consists of a clockwise circuit around the rectangle and the upper and lower sides of the wake. Note that $\partial\varphi_1/\partial n$ is continuous across the wake. Therefore, equation 16 becomes

$$\varphi_1(x_1,y_1) = \frac{1}{4i} \oint_{\square} \left[\psi \frac{\partial \varphi_1}{\partial n} - \varphi_1 \frac{\partial \psi}{\partial n} - 2i\lambda_1 M \varphi_1 \psi n_x\right] d\ell,$$

$$+ \frac{1}{4i} \int_a^{\infty} \Delta\varphi_1 \frac{\partial \psi}{\partial y'} dx', \tag{A17}$$

where a is the x coordinate of the right-hand boundary of the grid region, and $\Delta\varphi_1$ represents the jump in potential across the wake.

The jump in potential must satisfy the condition that the pressure be continuous across the wake; that is,

$$\Delta\varphi_{1x} + i\omega\Delta\varphi_1 = 0$$

or

$$\Delta\varphi_1 = \Delta\varphi_a \exp(i\omega(a-x)). \tag{A18}$$

We now insert equation 10 and equation 18 into equation 17 and also regroup the terms to obtain the expression

$$\varphi_1(x_1,y_1) = \frac{\exp(i\lambda_1 M x_1)}{4i} \oint_{\square} \exp(-i\lambda_1 M x_1') \left[\left(\frac{\partial \varphi_1}{\partial n} - 2i\lambda_1 M \varphi_1 n_{x'}\right) \psi_0 - \varphi_1 \frac{\partial \psi_0}{\partial n} \right] d\ell$$

$$- \frac{\Delta\varphi_a}{4i} \exp(i\lambda_1 M x_1) \int_a^{\infty} \exp(-i\lambda_1 M x_1') \exp(-i\omega(x_1'-a)) \left.\frac{\partial \psi_0}{\partial y_1}\right|_{y_1'=0} dx'. \tag{A19}$$

This equation is put into a shorter form by noting that ψ_0 and $\partial\psi_o/\partial n$ represent sources and doublets and that the multiplier coefficients are strength distributions designated as

$$\sigma = \exp(-i\lambda_1 m x_1') \left[\frac{\partial \varphi_1}{\partial n} - 2i\lambda_1 m \varphi_1 n_x \right] \tag{A20}$$

and

$$\mu = -\exp(-i\lambda_1 m x_1')\, \varphi_1.$$

Thus equation 18 is reduced to a form given by

$$\varphi_1(x_1,y_1) = \frac{\exp(i\lambda_1 M x_1)}{4i} \oint_{\square} \left[\sigma\psi_0 + \mu \frac{\partial \psi_0}{\partial n} \right] d\ell$$

$$- \frac{\Delta\varphi_a}{4i} \exp(i\lambda_1 M x_1) \int_a^{\infty} \exp(-i\omega(x_1'-a)) \exp(-i\lambda M x_1') \left. \frac{\partial \psi_0}{\partial y_1} \right|_{y_1'=0} dx'. \tag{A21}$$

where

$$\psi_0 = H_0^{(2)}(\lambda_1 \sqrt{((x_1-x_1')^2 + (y_1-y_1')^2)})$$

$$= H_0^{(2)}(\lambda_1 \sqrt{((x-x')^2 + K(y-y')^2)})$$

Equation 19 is the final form of the equation used to define the potential distribution in the region outside the finite differencing grid network.

APPENDIX B

DEVELOPMENT OF THE EQUATIONS FOR COUPLING LINEARIZED FAR-FIELD POTENTIALS WITH THE FINITE DIFFERENCE NEAR-FIELD POTENTIAL FOR TWO-DIMENSIONAL FLOW

We establish a source distribution on the boundary of the finite difference mesh and match the solution from this source distribution plus the infinite wake with the finite difference solution. Let the exterior solution be given by the sum of the potentials due to source distribution on the exterior boundary and the potential due to the wake.

$$\varphi_e = \exp(i\lambda_1 Mx)\,\psi(x,y) + \varphi_w, \tag{B1}$$

where

$$\psi(x,y) = -\frac{1}{4i}\int_{a_1}^{a_2} \{\sigma_u(x')\ell_o(u_u) + \sigma_d(x')\ell_o(u_d)\}\,dx'$$

$$-\frac{1}{4i}\int_{b_1}^{b_2} \{\sigma_\ell(y')\ell_o(u_\ell) + \sigma_r(y')\ell_o(u_r)\}\,dy'. \tag{B2}$$

φ_w is the potential due to the wake. Here $\sigma(x')$ and $\sigma(y')$ denote the source distribution in the y = constant and x = constant boundaries of the mesh, respectively. The u variables with the subscripts are defined by

$$u_u = (\lambda_1/2)^2\,\{(x-x')^2 + K(y-b_2)^2\},$$

$$u_d = (\lambda_1/2)^2\,\{(x-x')^2 + K(y-b_1)^2\},$$

$$u_\ell = (\lambda_1/2)^2\,\{(x-a_1)^2 + K(y-y')^2\}, \tag{B3}$$

and

$$u_r = (\lambda_1/2)^2\,\{(x-a_2)^2 + K(y-y')^2\}.$$

The subscript u denotes the upper boundary; d, the lower boundary; ℓ, the left boundary; and r, the right boundary. The functions $\ell_n(u)$ are related to the Hankel function of the second kind by

$$\ell_n(u) = (2/z)^n\,H_n^{(2)}(z), \tag{B4}$$

Note: Unless otherwise stated, references made in Appendices A, B, C, and D to equations in these appendices do not include the appendix letter or parenthesis. For example, in Appendix A, equation (A5) would be referred to as "equation 5."

where $u = (z/2)^2 = (\lambda_1/2)^2 [(x-x')^2 + K(y-y')^2]$. (B5)

Then $z = \lambda_1 \sqrt{((x-x')^2 + K(y-y')^2)}$. The function $\ell_n(u)$ has the following property:

$$\ell_n'(u) = -\ell_{n+1}(u). \tag{B6}$$

Continuity must be maintained in the potential distribution and in its normal derivative across the interface boundary that separates near-field and far-field equations. These conditions applied to the upstream boundary at $x = a_1$ and $y = y_j$ are expressed as

$$\frac{\varphi_{2j} - \varphi_{1j}}{x_2 - x_1} = \left.\frac{\partial \varphi_e}{\partial x}\right|_{x=a_1} \tag{B7}$$

and

$$\frac{\varphi_{2j} + \varphi_{1j}}{2} = \varphi_e \Big|_{x=a_1}$$

These relations may be combined in the more convenient form

$$\varphi_{2j} = \varphi_e + \Delta x_1 \, \varphi_{e_x}/2$$

and

$$\varphi_{1j} = \varphi_e - \Delta x_1 \, \varphi_{e_x}/2, \tag{B8}$$

where $\Delta x_1 = x_2 - x_1$.

Similarly, on the downstream boundary $x = a_2$, the boundary conditions become

$$\frac{\varphi_{i_m j} - \varphi_{i_{m-1}}}{x_{i_m} - x_{i_{m-1}}} = \varphi_{ex}(a_2, y_j) \tag{B9}$$

and

$$\frac{\varphi_{i_m j} + \varphi_{i_{m-1} j}}{2} = \varphi_e(a_2, y_j),$$

or

$$\varphi_{i_m j} = \varphi_e(a_2, y_j) + \Delta x_m \, \varphi_{ex}(a_2, y_j)/2$$

and (B10)

$$\varphi_{i_{m-1} j} = \varphi_e(a_2, y_j) - \Delta x_m \, \varphi_{ex}(a_2, y_j)/2.$$

On the upper boundary, $y = b_2$, we have

$$(\varphi_{ij_m} - \varphi_{ij_{m-1}}) / (y_{jm} - y_{j_{m-1}}) = \varphi_{ey}(x_i, b_2)$$

and (B11)

$$(\varphi_{ij_m} + \varphi_{ij_{m-1}}) / 2 = \varphi_e(x_i, b_2),$$

and these simplify to

$$\varphi_{ij_m} = \varphi_e(x_i, b_2) + \Delta y_m \, \varphi_{ey}(x_i, b_2)/2$$

and (B12)

$$\varphi_{ij_{m-1}} = \varphi_e(x_i, b_2) - \Delta y_m \, \varphi_{ey}(x_i, b_2)/2,$$

where $\Delta y_m = y_{j_m} - (y_{j_{m-1}})$. y_{jm} and x_{im} are, respectively, the maximum values of y_j and x_i in the mesh.

Similarly, on the lower mesh boundary, $y = b_1$, we have

$$\varphi_{i2} = \varphi_e(x_i, b_1) + \Delta y_1 \, \varphi_{ey}(x_i, b_1)/2$$

and

$$\varphi_{i1} = \varphi_e(x_i, b_1) - \Delta y_1 \, \varphi_{ey}(x_i, b_1)/2, \quad \text{(B13)}$$

where $\Delta y_1 = y_2 - y_1$.

The Derivation of the Exterior Potential and Its Derivatives

We now evaluate the quantities φ_e, φ_{ex}, and φ_{ey} on the required boundaries. From equation (1), we have

$$\varphi_{ex} = \exp(i\lambda_1 Mx)\{\psi_x + i\lambda_1 M\psi\} + \varphi_{wx} \quad \text{(B14)}$$

and

$$\varphi_{ey} = \exp(i\lambda_1 Mx)\psi_y + \varphi_{wy}. \quad \text{(B15)}$$

Now

$$\psi_x = \frac{\lambda_1^2}{8i}\int_{a_1}^{a_2}[\sigma_u(x')\ell_1(u_u) + \sigma_d(x')\ell_1(u_d)](x-x')dx'$$

$$+\frac{\lambda_1^2}{8i}\int_{b_1}^{b_2}[\sigma_\ell(y')\ell_1(u_e)(x-a_1) + \sigma_r(y')\ell_r(u_r)(x-a_2)]dy'. \tag{B16}$$

Since we require ψ_x only on the left and right mesh boundaries, we take the limit as $x \to a_1$ from outside the mesh boundary, that is, for $x < a_1$. From page 49 of Reference 4, this is seen to be

$$\lim_{x \to a_1^-}\left\{\frac{\lambda_1^2}{8i}\int_{b_1}^{b_2}\sigma_e(y')(x-a_1)\ell_1(u_\ell)dy'\right\} = -\sigma_\ell(y)/(2\sqrt{K}). \tag{B17}$$

Also taking the limit as $x \to a_2$ from values outside the boundary, that is for $x > a_2$, we obtain

$$\lim_{x \to a_2^+}\left\{\frac{\lambda_1^2}{8i}\int_{b_1}^{b_2}\sigma_r(y')(x-a_2)\ell_1(u_r)dy'\right\} = +\sigma_r(y)/(2\sqrt{K}). \tag{B18}$$

Then on $x = a_1$ the derivative with respect to x becomes

$$\psi_x = \frac{\lambda_1^2}{8i}\int_{a_1}^{a_2}[\sigma_u(x')\ell_1(u_u) + \sigma_d(x')\ell_1(u_d)](a_1-x')dx'$$

$$-\sigma_\ell(y)/(2\sqrt{K}) + \frac{\lambda_1^2(a_1-a_2)}{8i}\int_{b_1}^{b_2}\sigma_r(y')\ell_1(u_r)dy', \tag{B19}$$

where

$$u_u = \lambda_1^2[(a_1-x')^2 + K(y-b_2)^2]/4, \tag{B20}$$

$$u_d = \lambda_1^2[(a_1-x')^2 + K(y-b_1)^2]/4,$$

and

$$u_r = \lambda_1^2[(a_1-a_2)^2 + K(y-y')^2]/4.$$

In a similar manner, the derivative with respect to x on the right-hand boundary, $x = a_2$, becomes

$$\psi_x = \frac{\lambda_1^2}{8i}\int_{a_1}^{a_2}[\sigma_u(x')\ell_1(u_u) + \sigma_d(x')\ell_1(u_d)](a_2-x')dx'$$

$$+\sigma_r(y)/(2\sqrt{K}) + \frac{\lambda_1^2(a_2-a_1)}{8i}\int_{b_1}^{b_2}\sigma\,(y')\ell_1(u\ )dy', \tag{B21}$$

where

$$u_u = \lambda_1^2[(a_2-x')^2 + K(y-b_2)^2]/4,$$

$$u_d = \lambda_1^2[(a_2-x')^2 + K(y-b_1)^2]/4, \tag{B22}$$

and

$$u_\ell = \lambda_1^2[(a_2-a_1)^2 + K(y-y')^2]/4.$$

Note that u_ℓ in equation 22 equals u_r in equation 20.

Differentiation with respect to y yields

$$\psi_y = \frac{\lambda_1^2 K}{8i}\int_{a_1}^{a_2}[\sigma_u(x')\ell_1(u_u)(y-b_2) + \sigma_d(x')\ell_1(u_d)(y-b_1)]\,dx' \tag{B23}$$

$$+\frac{\lambda_1^2 K}{8i}\int_{b_1}^{b_2}[\sigma_\ell(y')\ell_1(u\ ) + \sigma_r(y')\ell_1(u_r)]\,(y-y')dy'.$$

Taking the limit as $y \to b_2$ on the upper boundary for points outside the mesh, or $y > b_2$, leads to

$$\lim_{y\to b_2^+}\left\{\frac{\lambda_1^2 K}{8i}\int_{a_1}^{a_2}\sigma_u(x')\ell_1(u_u)(y-b_2)dx'\right\} = \sqrt{K(\sigma(x)/2)} \tag{B24}$$

as found on page 49 of Reference 4. The derivative with respect to y on the upper boundary then becomes

$$\psi_y = \sqrt{K(\sigma_u(x)/2)} + \frac{\lambda_1^2 K(b_2-b_1)}{8i}\int_{a_1}^{a_2}\sigma_d(x')\ell_1(u_d)dx' \tag{B25}$$

$$+\frac{\lambda_1^2 K}{8i}\int_{b_1}^{b_2}[\sigma_\ell(y')\ell_1(u_\ell + \sigma_r(y')\ell_1(u_r)](b_2-y')dy',$$

where

$$u_d = \lambda_1^2[(x-x')^2 + K(b_2-b_1)^2]/4,$$

$$u_\ell = \lambda_1^2[(x-a_1)^2 + K(b_2-y')^2]/4, \tag{B26}$$

and

$$u_r = \lambda_1^2[(x-a_2)^2 + K(b_2-y')^2]/4.$$

Similarly, for $y \to b_1$ and $y < b_1$,

$$\psi_y = \frac{\lambda_1^2 K(b_1-b_2)}{8i} \int_{a_1}^{a_2} \sigma_u(x')\ell_1(u_u)dx' - \sqrt{K}(\sigma_d(x)/2)$$

$$+ \frac{\lambda_1^2 K}{8i} \int_{b_1}^{b_2} [\sigma_\ell(y')\ell_1(u_\ell) + \sigma_r(y')\ell_1(u_r)](b_1-y')dy', \tag{B27}$$

where

$$u_u = \lambda_1^2[(x-x')^2 + K(b_2-b_1)^2]/4,$$

$$u_\ell = \lambda_1^2[(x-a_1)^2 + K(b_1-y')^2]/4, \tag{B28}$$

and

$$u_r = \lambda_1^2[(x-a)^2 + K(b_1-y')^2]/4.$$

We now represent the integration over the mesh boundaries in terms of the sum of integrals over the basis functions. For the source distribution over the upper mesh boundary, this can be expressed in the form

$$\int_{a_1}^{a_2} \sigma_u(x')\ell_0(u_u)dx' = \sum_{i=2}^{i_m-1} \sigma_{ui} \int_{x_{i-1}}^{x_{i+1}} \sigma_i(x')\ell_0(u_u)dx', \tag{B29}$$

where $\sigma_i(\ \ ')$ represents the equation for the first-derivative-continuous source distribution of figure 6. Thus:

$$\sigma_i(x') = 1 - 3(x_i-x')^2/\delta_i^2 + 2(x_i-x')^3/\delta_i^3 \text{ for } x_{i-1} \leqslant x' \leqslant x_i,$$

$$\sigma_i(x') = 1 - 3(x'-x_i)^2/\delta_{i+1}^2 + 2(x'-x_i)^3/\delta_{i+1}^3 \text{ for } x_i \leqslant x' \leqslant x_{i+1}, \tag{B30}$$

$$\delta_i = x_i - x_{i-1},$$

and σ_{ui} = unknown coefficient multiplier (to be determined).

For the summation in equation 29 to represent the limits a_1 to a_2, we must replace x_1 by $(x_1 + x_2)/2 \equiv a_1$ and x_{i_m} by $(x_{i_{m-1}} + x_{i_m})/2 \equiv a_2$. The coordinates y_1 and y_{j_m} must be changed in a similar manner.

Equation 30 has the property that the function σ_i and its first derivative are continuous. Note that $\ell_0(u) = H_0^{(2)}(\lambda_1 r)$, where r takes on the definition of

$$r = \sqrt{[(x-x')^2 + K(y_{j_m}-y_1)^2]} \tag{B31}$$

for the particular case of evaluating the potential on the upper boundary at x,y_{jm} due to sources distributed on the lower boundary at $y' = y_1$.

Then the integral in equation 29 takes the form

$$\int_{x_{i-1}}^{x_{i+1}} \sigma_i(x') H_0^{(2)}(\lambda_1 r)dx' = \int_{x_{i-1}}^{x_i} [1 - 3(x_i - x')^2/\delta_i^2 + 2(x_i - x')^3/\delta_i^3] H_0^{(2)}(\lambda_1 r)dx'$$

$$+ \int_{x_i}^{x_{i+1}} [1 - 3(x' - x_2)^2/\delta_{i+1}^2 + 2(x' - x_i)^3/\delta_{i+1}^3] H_0^{(2)} \lambda_1(r)dx'. \quad \text{(B32)}$$

In the first integral on the right-hand side of equation 32, we introduce the variable

$$t = (x_i - x')/\delta_i \text{ or } x' = x_i - t\delta_i. \quad \text{(B33)}$$

In the second integral, we let

$$t = (x' - x_i)/\delta_{i+1} \text{ or } x' = x_i + t\delta_{i+1}. \quad \text{(B34)}$$

Then the two integrals combine to give

$$\int_{x_{i-1}}^{x_{i+1}} \sigma_i(x') H_0^{(2)}(\lambda_1 r)dx' = \int_0^1 [1 - 3t^2 + 2t^3] \{\delta_i H_0^{(2)}(\lambda_1 \sqrt{[(x_i - x - t\delta_i)^2 + K(y_{jm} - y_1)^2}]$$

$$+ \delta_{i+1} H_0^{(2)}(\lambda_1 \sqrt{[(x_i - x + t\delta_{i+1})^2 + K(y_{jm} - y_1)^2}]\} dt. \quad \text{(B35)}$$

We perform this integration numerically by using a four-point Gaussian quadrature formula. Thus the integral becomes

$$\int_{x_{i-1}}^{x_{i+1}} \sigma_i(x') H_0^{(2)}(\lambda_1 r)dx' = \sum_{k=1}^{4} W t_k (1 - 3t_k^2 + 2t_k^3) \{\delta_i H_0^{(2)}(\lambda_1 \sqrt{[(x_i - x - t_k\delta_i)^2 + K(y_{jm} - y_1)^2}]$$

$$+ \delta_{i+1} H_0^{(2)}(\lambda_1 \sqrt{[(x_i - x + t_k\delta_{i+1})^2 + K(y_{jm} - y_1)^2}]\}. \quad \text{(B36)}$$

The formula can be further simplified by defining new weight functions,

$$\bar{W}_{tk} = (1 - 3t_k^2 + 2t_k^3) W_{t_k}, \quad \text{(B37)}$$

and we obtain

$$\int_{x_{i-1}}^{x_{i+1}} \sigma_i(x')H_0^{(2)}(\lambda_1 r)dx' = \sum_{k=1}^{4} \bar{W}_{tk}\{\delta_i H_0^{(2)}(\lambda_1\sqrt{[(x_i-x-t_k\delta_i)^2 + K(y_{jm}-y_1)^2}]$$

$$+ \delta_{i+1}H_0^{(2)}(\lambda_1\sqrt{[(x_i-x+t_k\delta_{i+1})^2 + K(y_{jm}-y_1)^2}]\}. \quad \text{(B38)}$$

We define a new variable in order to simplify the expressions. We let

$$X_{0kij\ell} = \int_{x_{i-1}}^{x_{i+1}} \sigma_i(x')H_0^{(2)}(\lambda_1\sqrt{[(x_k-x')^2 + K(y_j-y_\ell)^2}])dx', \quad \text{(B39)}$$

where the potential is evaluated at x_k, y_j for the source distribution located at $y=y_\ell$, and x' ranges between $x' = x_{i-1}$ and $x'=x_{i+1}$.

We now consider integration along the y axis analogous to equation 38 and obtain the expression with another new variable defined as

$$Y_{0ikj\ell} = \int_{y_{j-1}}^{y_{j+1}} \sigma_j(y')H_0^{(2)}(\lambda_1\sqrt{[(x_i-x_k)^2 + K(y-y')^2}])dy',$$

$$= \sum_{m=1}^{4} \bar{W}_{tm}\{\delta_j H_0^{(2)}(\lambda_1\sqrt{[(x_i-x_r)^2 + K(y_j-y_\ell-t_m\delta_j)^2}])$$

$$+ \delta_{j+1}H_0^{(2)}(\lambda_1\sqrt{[(x_i-x_k)^2 + K(y_j-y_\ell+t_m\delta_{j+1})^2}])\}, \quad \text{(B40)}$$

where the potential is being evaluated at x_i, y_ℓ due to the source distribution located at an x_k station, and y' ranges between $y'=y_{j-1}$ and $y'=y_{j+1}$.

Equations 38 and 40 can be put in the same form by noting that, in terms of the variables x and $\sqrt{K}$ y, the Hankel function is symmetric. Thus we write for equation 39

$$X_{0kij\ell} = \sum_{m=1}^{4} \bar{W}_{tn}\{H_0^{(2)}(\lambda_1\sqrt{[(x_i-x_r-t_m\delta_i)^2 + K(y_j-y)^2}])\delta_i$$

$$+ \delta_{i+1}H_0^{(2)}(\lambda_1\sqrt{[(x_i-x_k+t_m\delta_{i+1})^2 + K(y_j-y)^2}])\}. \quad \text{(B41)}$$

Hence, we have

$$X_{0kij\ell} = HSO(x_k, x_{i-1}, x_i, x_{i+1}, \sqrt{K}y_j, \sqrt{K}y_\ell, \lambda_1). \quad \text{(B42)}$$

where the zero implies that the $H_0^{(2)}(\zeta)$ Hankel function is being used.

The k represents the x station where the potential is being evaluated, $x=x_k$.
i represents the x′ location of the source distribution $x'=x_i$.
j represents the y′ location of the source distribution $y'=y_j$.
ℓ represents the y location where the potential is being evaluated, $y=y_\ell$.

Similarly, we write equation 40 in the form

$$Y_{0kij\ell} = \frac{1}{\sqrt{K}} \sum_{n=1}^{4} \bar{W}_{tk} \{\bar{\delta}_j H_0^{(2)}(\lambda_1\sqrt{[(\eta_j-\eta_\ell-t_n\bar{\delta}_j)^2 + (x_r-x_i)^2]})$$

$$+ \bar{\delta}_{j+1} H_0^{(2)}(\lambda_1\sqrt{[(\eta_j-\eta_\ell+t_n\bar{\delta}_{j+1})^2 + (x_k-x_i)^2]})\}, \tag{B43}$$

where

$$\eta = \sqrt{K}y; \ \bar{\delta}_j = \eta_j-\eta_{j-1}; \ \text{and} \ \bar{\delta}_{j+1} = \eta_{j+1}-\eta_j.$$

Comparing equations 41 and 43, we see that

$$Y_{0kij\ell} = \frac{1}{\sqrt{K}} \ HSO(\sqrt{K}y_\ell, \sqrt{K}y_{j-1}, \sqrt{K}y_j, \sqrt{K}y_{j+1}, x_i, x_k, \lambda_1). \tag{B44}$$

We now derive similar integration formulas for the integrals in equation 19. First consider the integral along the downstream boundary that contributes to the potentials on the upstream boundary given as

$$\bar{\sigma}_{rj} \int_{y_{j-1}}^{y_{j+1}} \sigma_j(y')\ell_1(u_r)dy'.$$

This is evaluated by inserting the definition of $\ell_1(u_r)$ that is given by equation 4 as

$$\ell_1(u) = 2H_1^{(2)}(\zeta)/\zeta,$$

where

$$\zeta = \lambda_1\sqrt{[(x_1-x_{i_m})^2 + K(y-y')^2]}.$$

In the subroutine call, the subscript is changed from 0 to 1 to denote that the integrand contains the function $H_1^{(2)}(\zeta)$ instead of $H_0^{(2)}(\zeta)$.

Hence we write

$$Y_{11i_m j\ell} = \int_{y_{j-1}}^{y_{j+1}} \sigma_j(y')\ell_1(u_r)dy' \tag{B45}$$

$$= \sum_{k=1}^{4} \bar{W}_{tk} \{2\delta_j H_1^{(2)}(\zeta)/\zeta + 2\delta_{j+1} H_1^{(2)}(\zeta_1)/\zeta_1\},$$

where

$$\zeta = \lambda_1 \sqrt{[(x_1 - x_{i_m})^2 + K(y_j - y_\ell - t_k\delta_j)^2]}$$

and

$$\zeta_1 = \lambda_1 \sqrt{[(x_1 - x_{i_m})^2 + K(y_j - y_\ell + t_k\delta_{j+1})^2]}. \tag{B46}$$

Similarly, the first integral in equation 25 becomes

$$\int_{a_1}^{a_2} \sigma_d(x')\ell_1(u_d)dx' = \sum_{i=2}^{i_m-1} \sigma_{di} \int_{x_{i-1}}^{x_{i+1}} \sigma_i(x')\ell_1(u_d)dx', \tag{B47}$$

and

$$\int_{x_{i-1}}^{x_{i+1}} \sigma_i(x')\ell_1(u_d)dx' = \sum_{n=1}^{4} \bar{W}_{tk} \{2\delta_i H_1^{(2)}(\zeta)/\zeta + 2\delta_{i+1} H_1^{(2)}(\zeta_1)/\zeta_1\}, \tag{B48}$$

where

$$\zeta = \lambda_1 \sqrt{[(x_i - x - t_n\delta_i)^2 + K(y_{j_m} - y_1)^2]} \tag{B49}$$

and

$$\zeta_1 = \lambda_1 \sqrt{[(x_i - x + t_n\delta_{i+1})^2 + K(y_{j_m} - y_1)^2]}.$$

Replacing y_1 and y_{j_m} by y_j and y_ℓ and x by x_k, we write for equation 48

$$X_{1kij\ell} = \int_{x_{i-1}}^{x_{i+1}} \sigma_i(x')\ell_1(u)dx' = HS1\,(x_k, x_{i-1}, x_i, x_{i+1}, \sqrt{K}y_j, \sqrt{K}y_\ell, \lambda_1). \tag{B50}$$

Also, equation 45 can be written as

$$Y_{1kij\ell} = \int_{y_{j-1}}^{y_{j+1}} \sigma_j(y')\ell_1(u)dy' = \frac{1}{\sqrt{K}} HS1\,(\sqrt{K}y_\ell, \sqrt{K}y_{j-1}, \sqrt{K}y_j, \sqrt{K}y_{j+1}, x_i, x_k, \lambda_1). \tag{B51}$$

We now consider the integrals in equation 21 that have a factor $(x_k - x')$ in the integrand:

$$\int_{a_1}^{a_2} \sigma_u(x')\ell_1(u)(x_k - x')dx' = \sum_{i=2}^{2m-1} \bar{\sigma}_{ui} \int_{x_{i-1}}^{i+1} \bar{\sigma}_i(x')\ell_1(u)(x_k - x')dx', \tag{B52}$$

where $u = \lambda_1^2[(x_k - x')^2 + K(y_j - y_\ell)^2]/4.$ (B53)

Inserting the expression for the first-derivative-continuous source distribution for σ_i yields

$$\int_{x_{i-1}}^{x_{i+1}} \sigma_i(x')\ell_1(u)(x_k - x')dx' =$$

$$\int_{x_{i-1}}^{x_i} [1 - 3(x_i - x')^2/\delta_i^2 + 2(x_i - x')^3/\delta_i^3]\ell_1(u)(x_k - x')dx' \tag{B54}$$

$$+ \int_{xi}^{x_{i+1}} [1 - 3(x' - x_i)^2/\delta_{i+1}^2 + 2(x' - x_i)^3/\delta_{i+1}^3]\ell_1(u)(x_k - x')dx'.$$

Introducing the variables of equations 33 and 34 leads to another variable $\tilde{X}_{1kij\ell}$, where 1 denotes the use of the Hankel function of order 1.

The k represents the x location where the potential is being evaluated, $x = x_k$.
i represents the x' location of the source distribution $x' = x_i$.
ℓ represents the y' location of the source distribution $y' = y_\ell$.
j represents the y location where the potential is being evaluated, $y = y_j$.

So that

$$\tilde{X}_{1kij\ell} = \int_{x_{i-1}}^{x_{i+1}} \sigma_i(x')\ell_1(u)(x_k - x')dx' \tag{B55}$$

$$= \int_0^1 [1 - 3t^2 + 2t^3]\{\delta_i(x_k - x_i + t\delta_i)\ell_1(u_0)$$

$$+ \delta_{i+1}(x_k - x_i - t\delta_{i+1})\ell_1(u_1)\}dt,$$

where

$$u_0 = \lambda_1^2[(x_k - x_i + t\delta_i)^2 + K(y_j - y_\ell)^2]/4 \tag{B56}$$

and

$$u_1 = \lambda_1^2[(x_k - x_i - \delta_{i+1})^2 + K(y_j - y_\ell)^2]/4.$$

By the Gaussian quadrature formula,

$$\tilde{X}_{1kij\ell} = \sum_{m=1}^{4} \bar{W}_{tm} \{\delta_i(x_k - x_i + t_m\delta_i)\ell_1, u_0$$

$$+\delta_{i+1}(x_k - x_i - t_m\delta_{i+1})\ell_1(u_1)\}] \tag{B57}$$

$$= HSX(x_k, x_{i-1}, x_i, x_{i+1}, \sqrt{K}y_j, \sqrt{K}y_\ell, \lambda_1), \tag{B58}$$

where

$$u_0 = \lambda_1^2 [(x_k - x_i + t_m\delta_i)^2 + K(y_\ell - y_j)^2]/4 \tag{B59}$$

and

$$u_1 = \lambda_1^2 [(x_k - x_i - t_m\delta_{i+1})^2 + K(y_\ell - y_j)^2]/4. \tag{B60}$$

Consider now the integrals in equation 23. We have

$$\int_{b_1}^{b_2} \sigma_\ell(y')\ell_1(u)(y-y')dy' =$$

$$\sum_{j=2}^{j_m-1} \bar{\sigma}_{\ell j} \int_{y_{j-1}}^{y_{j+1}} \sigma_j(y')\ell_1(u)(y-y')dy'; \tag{B61}$$

and, analogous to equation 40, we write

$$\int_{y_{j-1}}^{y_{j+1}} \sigma_j(y')\ell_1(u)(y_\ell - y')\,dy' =$$

$$= \sum_{n=1}^{4} \bar{W}_{tn} \left\{ \bar{\delta}_j \ell_1(u_0)(\eta_\ell - \eta_j + t_n\bar{\delta}_j) + \bar{\delta}_{j+1}\ell_1(u_1)(\eta_\ell - \eta_j - t_n\bar{\delta}_{j+1}) \right\} \tag{B62}$$

$$= \frac{1}{K} HSX(\sqrt{K}y_\ell, \sqrt{K}y_{j-1}, \sqrt{K}y_j, \sqrt{K}y_{j+1}, x_i, x_k, \lambda_1), \tag{B63}$$

where

$$u_0 = \lambda_1^2 \left[(x_i - x_k)^2 + (\eta_\ell + \eta_j + t_n\bar{\delta}_j)^2\right]/4, \tag{B64}$$

$$u_1 = \lambda_1^2 \left[(x_i - x_k)^2 + (\eta_\ell - \eta_j - t_n\bar{\delta}_{j+1})^2\right]/4, \tag{B65}$$

and

$$\bar{\delta}_j = \eta_j - \eta_{j-1}\,;\ \bar{\delta}_{j+1} = \eta_{j+1} - \eta_j. \tag{B66}$$

We can now write down the equation for ψ. Using equations 39 and 40, equation 2 can be written as

$$\psi(x_i, y_j) = -\frac{1}{4i}\sum_{k=2}^{i_m-1} \left[\sigma_{uk} X_{0ikj_{mj}} + \sigma_{dk} X_{0ik1j}\right]$$

$$-\frac{1}{4i}\sum_{k=2}^{J_m-1} \left[\sigma_{\ell k} Y_{0i1kj} + \sigma_{rk} Y_{0ii_{mkj}}\right], \tag{B67}$$

where now we designate x_1 and x_{i_m} as the x mesh boundary and y_1 and y_{j_m} as the y mesh boundary.

We now write the expressions for the normal derivatives required in the coupling procedure.

On the upstream boundary, where $x = a_1$, the x derivative defined by equation 19 is now given in summation form as

$$\psi_x(x_1,y_j) = \frac{\lambda_1^2}{8i}\sum_{i=2}^{i_m-1}\left[\sigma_{ui}\,\tilde{X}_{11ij_mj} + \sigma_{di}\,\tilde{X}_{11i1j}\right]$$

$$-\sigma_{\ell j}/(2\sqrt{K}) + \frac{\lambda_1^2(x_1 - x_{i_m})}{8i}\sum_{k=2}^{j_m-1}\left[\sigma_{rk}\,Y_{11i_mkj}\right]. \tag{B68}$$

Similarly, equation 21, which represents the x derivative on the downstream boundary, is reduced to a summation form given by

$$\psi_x(x_{i_m},y_j) = \frac{\lambda_1^2}{8i}\sum_{i=2}^{i_m-1}\left[\sigma_{ui}\,\tilde{X}_{1i_mij_mj} + \sigma_{di}\,\tilde{X}_{1i_mi1j}\right]$$

$$+\sigma_{rj}/(2\sqrt{K}) + \frac{\lambda_1^2(x_{i_m} - x_1)}{8i}\sum_{k=2}^{j_m-1}\left[\sigma_{\ell k}\,Y_{1i_m1kj}\right]. \tag{B69}$$

The y derivative on the upper boundary of equation 25 becomes

$$\psi_y(x_i,y_{j_m}) = \sqrt{K}\,\sigma_{ui}/2 + \frac{\lambda_1^2 K(y_{j_m} - y_1)}{8i}\sum_{k=2}^{i_m-1}\left[\sigma_{dk}\,X_{1ik1j_m}\right]$$

$$+\frac{\lambda_1^2 K}{8i}\sum_{j=2}^{j_m-1}\left[\sigma_{\ell j}\,\tilde{Y}_{1i1jj_m} + \sigma_{rj}\,\tilde{Y}_{1ii_mjj_m}\right]. \tag{B70}$$

The y derivative on the lower boundary ($y = y_1$) of equation 27 takes the form

$$\psi_y(x_i, y_1) = -\sigma_{di}\sqrt{K}/2 + \frac{\lambda_1^2 K(y_1 - y_{j_m})}{8i}\sum_{k=2}^{j_m-1}\sigma_{uk}\,X_{1ikj_m1}$$

$$+\frac{\lambda_1^2 K}{8i}\sum_{j=2}^{j_m-1}\left[\sigma_{\ell j}\,\tilde{Y}_{1i1j1} + \sigma_{rj}\,\tilde{Y}_{1ii_mj1}\right]. \tag{B71}$$

Having formulated the expressions of ψ, ψ_x, and ψ_y, we are ready to formulate the expressions that couple the linearized far-field equations with finite difference near-field equations on the boundary of the grid network.

We equate the potentials at stations of the finite differencing grid network that are located one station ahead and one station behind the forward boundary by the relationships given in equation 8, which are expanded to give the expressions

$$\varphi_{1j} = \exp(i\lambda_1 M x_1)\left[(1-i\lambda_1 M\Delta x_1/2)\,\psi(x_1,y_j) - \frac{\Delta x_1}{2}\,\psi_x(x_1,y_j)\right]$$

$$+ \varphi_w - \Delta x_1 \varphi_{w_x}/2 \tag{B72}$$

and

$$\varphi_{2j} = \exp(i\lambda_1 M x_1)\left[(1+i\lambda_1 M\Delta x_1/2)\,\psi(x_1,y_j) + \frac{\Delta x_1}{2}\,\psi_x(x_1,y_j)\right]$$

$$+ \varphi_w + \Delta x_1 \varphi_{w_x}/2.$$

Substituting equations 67 and 68 into the first of equations 72 leads to

$$\varphi_{1j} = \exp(i\lambda_1 M x_1)\left\{C_1\left[\sum_{i=2}^{i_m-1} \sigma_{ui} X_{01ij_mj} + \sigma_{di} X_{01ilj}\right)\right.$$

$$+ \sum_{k=2}^{j_m-1} (\sigma_{\ell k} Y_{011kj} + \sigma_{rk} Y_{01i_mkj})\Big] + \frac{\Delta x_i}{2}\,\frac{\sigma_{\ell j}}{2\sqrt{K}}$$

$$+ C_2\left[\sum_{i=2}^{i_m-1} \sigma_{ui}\,\tilde{X}_{11ij_mj} + \sigma_{di}\,\tilde{X}_{11ilj}\right) \tag{B73}$$

$$\left. + (x_1 - x_{i_m}) \sum_{k=2}^{j_m-1} \sigma_{rk} Y_{11i_mkj}\right]\Big\} + \varphi_w - \frac{\Delta x_1}{2}\,\varphi_{w_x},$$

where

$$C_1 = i(1+i\lambda_1\Delta x_1/2)/4 \text{ and } C_2 = i\lambda_1^2\Delta x_1/16. \tag{B74}$$

Here, $i = \sqrt{-1}$ instead of the subscript value.

The double subscripted sigmas of equation 73 represent the unknown coefficient multipliers of the individual source distributions that are distributed on the outer boundary shown in figure 8.

σ_{ui} is associated with the sources distributed on the upper boundary; σ_{di} is associated with the sources on the lower boundary; $\sigma_{\ell j}$ represents the source strengths on the upstream boundary; and σ_{rj} is applicable to the downstream boundary source strengths.

There are (i_m-2) variables on the upper and lower boundaries and (j_m-2) variables on upstream and downstream boundaries. The variables are numbered by beginning with the source distribution on the upper surface, followed by the sources distributed on the lower surface, then those on the upstream boundary, and ending with the distributions on the downstream boundary.

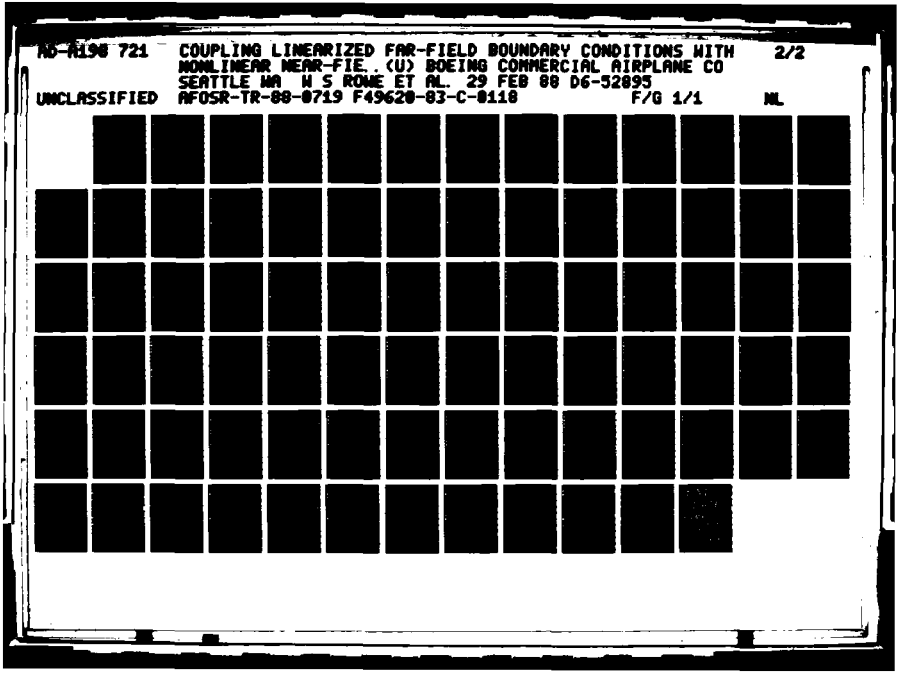
AD-A198 721 COUPLING LINEARIZED FAR-FIELD BOUNDARY CONDITIONS WITH 2/2
NONLINEAR NEAR-FIE..(U) BOEING COMMERCIAL AIRPLANE CO
SEATTLE WA W S ROWE ET AL. 29 FEB 88 D6-52895
UNCLASSIFIED AFOSR-TR-88-0719 F49620-83-C-0110 F/G 1/1 NL

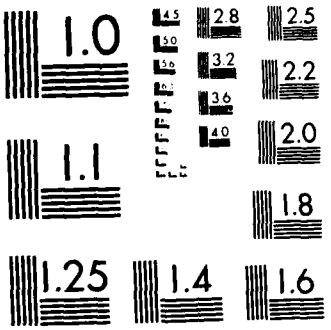
1.0
1.1
1.25
1.4
1.6
1.8
2.0
2.2
2.5
2.8
3.2
3.6
4.0
4.5
5.0
5.6

We replace the double subscripts by a single subscript k that progressively increases in value around the periphery of the boundary and is designated as

$$\sigma_{ui} \text{ for } 2 \leqslant i \leqslant i_m-1,\ \sigma_k;\ k=1 \text{ to } (i_m-2)$$

$$\sigma_{di} \text{ for } 2 \leqslant i \leqslant i_m-1,\ \sigma_k;\ k=(i_m-1) \text{ to } 2(i_m-2)$$

$$\sigma_j \text{ for } 2 \leqslant j \leqslant j_m-1,\ \sigma_k;\ k=2(i_m-2)+1 \text{ to } 2(i_m-2)+j_m-2$$

$$\sigma_{rj} \text{ for } 2 \leqslant j \leqslant j_m-1,\ \sigma_k;\ k=2(i_m-2)+j_m-1 \text{ to } 2(i_m+j_m-4). \tag{B75}$$

Thus the total number of source variables is seen to be

$$NS = 2(i_m-2) + 2(j_m-2). \tag{B76}$$

We designate the coefficient of σ_n in the nth equation as

$$w(m,n).$$

Hence the equation 73 may be written for the $j-1$ equation, for $2 \leqslant j \leqslant (j_m-1)$, as

$$\varphi_{1j} = \sum_{k=1}^{NS} W(j-1,k)\sigma_k + \varphi_w - \Delta x_1 \varphi_{wx}/2.$$

The $W(j-1,k)$ terms are coefficient multipliers of source strengths for equations that define the potentials at stations located one station forward of the upstream boundary.

$$W(j-1,i-1) = \exp(i\lambda_1 M x_1)\,[C_1 X_{01ij_mj} + C_2\,\tilde{X}_{11ij_mj}]\,;\ 2 \leqslant i \leqslant i_m-1$$

$$W(j-1,i_{max}+i-3) = \exp(i\lambda_1 M x_1)[C_1 X_{01i1j} + C_2\,\tilde{X}_{11i1j}]\,;\ 2 \leqslant i \leqslant i_m-1$$

$$W(j-1,2i_{max}+k-5) = \exp(i\lambda_1 M x_1)[C_1 Y_{011kj} + \Delta x_1 \delta_{ik}/(4\sqrt{k})]\,;\ 2 \leqslant k \leqslant j_m-1 \tag{B77}$$

$$W(j-1,2i_{max}+j_{max}+k-7) = \exp(i\lambda_1 M x_1)[C_1 Y_{01i_mkj} + (x_1-x_i)C_2 Y_{11i_mkj}]\,;\ 2 \leqslant k \leqslant j_m-1$$

The equations that couple the linearized far-field equations with finite differencing near-field equations for mesh stations that are located one station downstream of the upstream boundary are given by the expression

$$\varphi_{2j} = \exp(i\lambda_1 M x_1)\left[(1+i\lambda_1 M \Delta x_1/2)\psi(x_1,y_j) + \frac{\Delta x_1}{2}\,\psi_x(x_1,y_j)\right] \tag{B78}$$

$$+ \varphi_w - \Delta x_1 \varphi_{wx}/2.$$

Inserting the expressions for $\psi(x_1,y_j)$ and $\psi_x(x_1,y_j)$ of equations 67 and 68 into equation 78 yields the expression

$$\varphi_{2j} = \exp(i\lambda_1 M x_1) \left\{ -\bar{C}_1 \left[\sum_{i=2}^{i_m-1} (\sigma_{ui} X_{01ij_mj} + \sigma_{di} X_{01i1j}) \right.\right.$$

$$\left. + \sum_{k=2}^{j_{max}-1} (\sigma_{\ell k} Y_{011kj} + \sigma_{rk} Y_{01i_mkj}) \right] - \frac{\Delta x_i}{4\sqrt{K}} \sigma_{\ell j}$$

$$- C_2 \left[\sum_{i=2}^{i_{max}-1} (\sigma_{ui} \tilde{X}_{11ij_mj} + \sigma_{di} \tilde{X}_{11i1j}) \right. \qquad \text{(B79)}$$

$$\left.\left. + (x_1 - x_{j_{max}}) \sum_{k=2}^{j_{max}-2} \sigma_{rk} Y_{11i_mkj} \right] \right\} + \varphi_w + \Delta x_1 \varphi_{wx}/2,$$

where $\bar{C}_1$ is the conjugate of C_1.

The W coefficients of the source strengths are then defined by the equation

$$\varphi_{2j} = \sum_{k=1}^{NS} W(j_m+j-3,k)\sigma_k + \varphi_w + \Delta x_1 \varphi_{wx}/2,$$

where

$$W(j_m+j-3,i-1) = \exp(i\lambda_1 M x_1) [-\bar{C}_1 X_{01ij_mj} - C_2 \tilde{X}_{11ij_mj}] ; 2 \leqslant i \leqslant i_m - 1,$$

$$W(j_m+j-3,i_m+i-3) = \exp(i\lambda_1 M x_1) [-\bar{C}_1 X_{01i1j} - C_2 \tilde{X}_{11i1j}] ; 2 \leqslant i \leqslant i_m - 1,$$

$$W(j_m+j-3,2i_m+k-5) = \exp(i\lambda_1 M x_1) \left[-\bar{C}_1 Y_{011kj} - \frac{\Delta x_1}{4\sqrt{K}} \delta_{ik} \right] ; 2 \leqslant k \leqslant j_m - 1,$$

and

$$W(j_m+j-3,2i_m+j_m+k-7) = \exp(i\lambda_1 M x_1) [-\bar{C}_1 Y_{01i_mkj} - (x_1 - x_{i_m}) C_2 Y_{11i_mkj}]; 2 \leqslant k \leqslant j_m - 1. \qquad \text{(B80)}$$

In like manner, we now establish the W coefficients for the mesh potentials located on either side of the downstream boundary. The equations for the potentials at mesh stations that are one station upstream and one station downstream of the downstream boundary are obtained from equation 10 as

$$\varphi_{i_m-1,j} = \exp(i\lambda_1 M x_{i_m}) [(1 - i\lambda_1 M \Delta x_m/2)\psi(x_{i_m},y_j) - \Delta x_m \psi_x(x_{i_m},y_j)/2]$$

$$+ \varphi_w - \Delta x_m \varphi_{wx}/2 \qquad \text{(B81)}$$

and

$$\varphi_{i_m,j} = \exp(i\lambda_1 M x_{i_m}) [(1 + i\lambda_1 M \Delta x_m/2)\psi(x_{i_m},y_j) + \Delta x_m \psi(x_{i_m},y_j)/2]$$

$$+ \varphi_w + \Delta x_m \varphi_{wx}/2. \qquad \text{(B82)}$$

Inserting the expressions for ψ and ψ_x at the downstream boundary (equations 67 and 69) into the first of equations 81 results in the equation that defines the potential along a vertical line of mesh stations located one station ahead of the downstream boundary.

$$\varphi_{i_m-1,j} = \exp(i\lambda_1 M x_{1_m}) \left\{ C_3 \left[\sum_{i=2}^{i_m-1} (\sigma_{ui} X_{0i_m i j_m j} + \sigma_{di} X_{01_m i 1 j}) \right.\right.$$

$$\left. + \sum_{k=2}^{j_m-1} (\sigma_{\ell k} Y_{0i_m 1 k j} + \sigma_{rk} Y_{0i_m i_m k j}) \right]$$

$$+ C_4 \left[\sum_{i=2}^{i_m} (\sigma_{ui} \tilde{X}_{1i_m i j_m j} + \sigma_{di} \tilde{X}_{1i_m i 1 j}) + (x_{i_m} - x_1) \sum_{k=2}^{j_m-1} \sigma_{\ell k} Y_{1i_m 1 k j} \right]$$

$$\left. + \varphi_w - \Delta x_m \varphi_{wx}/2, \right. \tag{B84}$$

where

$$C_3 = i(1 - i\lambda_1 M \Delta x_m/2)/4,$$

$$C_4 = i\Delta x_m \lambda_1^2/16,$$

and

$$i = \sqrt{-1}.$$

The W coefficients are then defined by

$$\varphi_{i_m-1,j} = \sum_{k=1}^{NS} W(2j_m + j - 5, k)\sigma_k + \varphi_w - \Delta x_m \varphi_{wx}/2,$$

where

$$W(2j_m + j - 5, i - 1) = \exp(i\lambda_1 M x_{i_m}) [C_3 X_{0i_m i j_m j} + C_4 \tilde{X}_{1i_m i j_m j}] \; ; \; 2 \leq i \leq i_m - 2,$$

$$W(2j_m + j - 5, i_m + i - 3) = \exp(i\lambda_1 M x_{i_m}) [C_3 X_{0i_m i 1 j} + C_4 \tilde{X}_{1i_m i 1 j}] \; ; \; 2 \leq i \leq i_m - 2,$$

$$W(2j_m + j - 5, 2i_m + k - 5) = \exp(i\lambda_1 M x_{i_m}) [C_3 Y_{0i_m 1 k j} + (x_{i_m} - x_1) C_4 Y_{1i_m 1 k j}] \; ; \; 2 \leq k \leq j_m - 1, \tag{B85}$$

and

$$W(2j_m + j - 5, 2i_m + j_m + k - 7) = \exp(i\lambda_1 M x_{i_m}) [C_3 Y_{0i_m i_m k j} - \Delta x_m \delta_{jk}/(4\sqrt{K})] \; ; \; 2 \leq k \leq j_m - 1.$$

The equations for the potentials along a vertical line one mesh station aft of the downstream boundary are obtained by inserting equations 67 and 69 into the second expression of equation 81, which yields

$$\varphi_{i_m j} = \exp(i\lambda_1 M x_{i_m}) \left\{ -\bar{C}_3 \left[\sum_{i=2}^{i_m-1} (\sigma_{ui} x_{0 i_m i j_m j} + \sigma_{di} x_{0 i_m i 1 j}) \right.\right.$$

$$\left. + \sum_{k=2}^{J_m-1} (\sigma_{\ell k} Y_{0 i_m 1 k j} + \sigma_{rk} Y_{0 i_m i_m k j}) \right]$$

$$-C_4 \left[\sum_{i=2}^{i_m-1} (\sigma_{ui} \tilde{X}_{1 i_m i j_m j} + \sigma_{di} \tilde{X}_{1 i_m i 1 j}) \right.$$

$$\left.\left. + (x_{i_m} - x_1) \sum_{k=2}^{j_m-1} (\sigma_{\ell k} Y_{1 i_m 1 k j}) \right] + \Delta x_m \delta_{kj} / (4\sqrt{K}) \right\} \qquad \text{(B86)}$$

$$+ \varphi_w + \Delta x_m \varphi_{wx}/2.$$

The potentials given in terms of the W coefficients are then defined as

$$\varphi_{i_m j} = \sum_{k=1}^{NS} W(3j_m + j - 7, k)\, \sigma_k + \varphi_w + \Delta x_m \varphi_{wx}/2;$$

where

$$W(3j_m + j - 7, i - 1) = \exp(i\lambda_1 M x_{i_m}) [-\bar{C}_3 X_{0 i_m i j_m j} - C_4 \tilde{X}_{1 i_m i j_m j}],$$

and

$$W(3j_m + j - 7, i_m + i - 3) = \exp(i\lambda_1 M x_{i_m}) [-\bar{C}_3 X_{0 i_m i 1 j} - C_4 \tilde{X}_{1 i_m i 1 j}], \qquad \text{(B87)}$$

where $2 \leq i \leq i_m - 1$; and where

$$W(3j_m + j - 7, 2i_m + k - 5) = \exp(i\lambda_1 M x_{i_m}) [-\bar{C}_3 Y_{0 i_m 1 k j} - C_4 (x_{i_m} - x_1) Y_{1 i_m 1 k j}],$$

and

$$W(3j_m + k - 7, 2i_m + j_m + k - 7) = \exp(i\lambda_1 M x_{i_m}) [-\bar{C}_3 Y_{0 i_m i_m k j} + \Delta x_m \delta_{jk} / (4\sqrt{K})],$$

where $2 \leq k \leq j_m - 1$.

We now establish the equations that couple the linearized far-field equations with the finite difference equations across the lower boundary by inserting equation 15 into equation 13 and obtaining

$$\varphi_{i1} = \exp(i\lambda_1 M x_i) \left\{ \psi(x_i,y_1) - \frac{\Delta y_1}{2} \psi_y(x_i,y_1) \right\} + \varphi_w - \Delta y_1 \varphi_{wy}/2$$

(B88)

and

$$\varphi_{i2} = \exp(i\lambda_1 M x_i) \left\{ \psi(x_i,y_1) + \frac{\Delta y_1}{2} \psi_y(x_i,y_1) \right\} + \varphi_w + \Delta y_1 \varphi_{wy}/2.$$

Inserting equations 67 and 71 into the first of equation 88 yields an expression that is applicable for stations located one station below the lower boundary.

$$\begin{aligned}
\varphi_{i1} = \exp(i\lambda_1 M x_i) \Bigg\{ & C_5 \Bigg[\sum_{k=2}^{i_m-1} (\sigma_{uk} x_{0ikj_m1} + \sigma_{dk} x_{0ik11}) \\
& + \sum_{j=2}^{j_m-1} (\sigma_{\ell j} Y_{0i1j1} + \sigma_{rj} Y_{0ii_mj1}) \Bigg] \\
& + \Delta y_1 \sqrt{K}\, \sigma_{di}/4 \\
& + C_6 \Bigg[\sum_{j=2}^{j_m-1} (\sigma_{\ell j} \tilde{Y}_{1i1j1} + \sigma_{rj} \tilde{Y}_{1ii_mj1}) \\
& + (y_1 - y_m) \sum_{k=2}^{j_m-1} [\sigma_{uk} x_{1ikj_m1}] \Bigg] \Bigg\} \\
& + \varphi_w - \Delta y_1 \varphi_{wy}/2,
\end{aligned} \tag{B89}$$

where $C_5 = i/4$; $C_6 = i\lambda_1^2 K \Delta y_1/16$.

The W coefficients for equations numbered $4(j_m-2)+i-1$, where i ranges between $i = 2$ and $i = i_m-1$, are given by

$$W(4j_m+i-9,k-1) = \exp(i\lambda_1 M x_i) [C_5 x_{0ikj_m1} + C_6(y_1-y_m) x_{1ikj_m1}],$$

and

$$W(4j_m+i-9,i_m+k-3) = \exp(i\lambda_1 M x_i) [C_5 x_{0ik11} + \Delta y_1 \sqrt{K}\, \delta_{ik}/4],$$

where the range of k is $2 \leq k \leq i_m-1$; and by

(B90)

$$W(4j_m+i-9,2i_m+j-5) = \exp(i\lambda_1 M x_i) [C_5 Y_{0i1j1} + C_6 \tilde{Y}_{1i1j1}]$$

and

$$W(4j_m+i-9,2i_m+j_m+j-7) = \exp(i\lambda_1 Mx_i)\,[C_5 Y_{0ii_mj1} + C_6 \tilde{Y}_{1ii_mj1}],$$

where the range of j is $2 \leq j \leq j_m-1$.

The second expression of equation 88 provides the coupling relationships between the near-field and far-field equations for mesh stations located one station above the lower boundary. Inserting equations 67 and 71 into the second expression of equation 88 yields the coupling expression given as

$$\begin{aligned}\varphi_{i2} = \exp(i\lambda_1 Mx_i) \Bigg\{ C_5 \Bigg[& \sum_{k=2}^{i_m-1} (\sigma_{uk} x_{0ikj_m1} + \sigma_{dk} x_{0ik11}) \\ & + \sum_{j=2}^{j_m-1} (\sigma_{\ell j} Y_{0i1j1} + \sigma_{rj} Y_{0ii_mj1}) \Bigg] \\ & - \Delta y_1 \sqrt{K}\, \sigma_{di}/4 \\ & - C_6 \Bigg[\sum_{j=2}^{i_m-1} (\sigma_{\ell j} \tilde{Y}_{1i1j1} + \sigma_{rj} \tilde{Y}_{1ii_mj1}) \\ & + (y_1 - y_{j_m}) \sum_{k=2}^{i_m-1} \sigma_{uk} x_{1ikj_m1} \Bigg] \Bigg\} \\ & + \varphi_w + \Delta y_1 \varphi_{wy}/2.\end{aligned} \tag{B91}$$

The mesh potentials are related to the W coefficients and unknown source strengths by the relationship given as

$$\varphi_{i2} = \sum_{k=1}^{NS} W(4j_m+i_m+i-11,k)\,\sigma_k + \varphi_w + \Delta y_1 \varphi_{wy}/2. \tag{B92}$$

For equations numbered as $(4(j_m-2) + (i_m-2) + i - 1)$ for i ranging between $i = 2$ and $i = i_m-1$, the W coefficients are given as

$$W(4j_m+i_m+i-11,k-1) = \exp(i\lambda_1 Mx_i)\,[C_5 x_{0ikj_m1} - C_6(y_1-y_{j_m})x_{1ikj_m1}]$$

and

$$W(4j_m+i_m+i-11,i_m+k-3) = \exp(i\lambda_1 Mx_i)\,[C_5 x_{0ik11} - \Delta y_1 \sqrt{K}\, \delta_{ik}/4]$$

$$\text{for } 2 \leq k \leq i_m-1, \text{ and as} \tag{B93}$$

$$W(4j_m+i_m+i-11,2i_m+j-5) = \exp(i\lambda_1 Mx_i)\,[C_5 Y_{0i1j1} - C_6 \tilde{Y}_{1i1j1}]$$

and

$$W(4j_m+i_m+i-11,2i_m+j_m+j-7) = \exp(i\lambda_1 Mx_i)\,[C_5 Y_{0ii_mj1} - C_6 \tilde{Y}_{1ii_mj1}]$$

$$\text{for } 2 \leq j \leq j_m-1.$$

The final two sets of W coefficients are obtained by inserting equation 15 into equation 12, which results in the expressions given by

$$\varphi_{i,j_m-1} = \exp(i\lambda_1 Mx_i)\,[\psi(x_i,y_m) - \Delta y_m \psi_y(x_i,y_m)/2] + \varphi_w - \Delta y_m \varphi_{w_y}/2$$

and (B94)

$$\varphi_{i,j_m} = \exp(i\lambda_1 Mx_i)\,[\psi(x_i,y_m) + \Delta y_m \psi_y(x_i,y_m)/2] + \varphi_w + \Delta y_m \varphi_{w_y}/2.$$

Inserting the expressions for $\psi(x_i,y_m)$ and $\psi_y(x_i,y_m)$ from equations 67 and 70 into the first of equation 94 results in

$$\begin{aligned}\varphi_{i,j_m-1} = \exp(i\lambda_1 Mx_i) \Bigg\{ C_5 \Bigg[&\sum_{k=2}^{i_m-1} (\sigma_{uk} x_{0ikj_mj_m} + \sigma_{dk} x_{0ikij_m}) \\ &+ \sum_{j=2}^{j_m-1} (\sigma_{\ell j} Y_{0i1ijj_m} + \sigma_{rj} Y_{0ii_mij_m}) \Bigg] \\ &- \Delta y_m \sqrt{K}\, \sigma_{ui}/4 \\ &+ C_7 \Bigg[\sum_{j=2}^{j_m-1} (\sigma_{\ell j} \tilde{Y}_{1i1jj_m} + \sigma_{rj} \tilde{Y}_{1ii_mij_m}) \\ &+ (y_{j_m} - y_1) \sum_{k=2}^{i_m-1} \sigma_{dk} x_{1ikij_m} \Bigg] \Bigg\} \\ &+ \varphi_w - \Delta y_m \varphi_{wy}/2,\end{aligned} \tag{B95}$$

where $C_7 = i\lambda_1^2 K \Delta y_m/16$.

The mesh potentials (developed for stations that are located one station below the upper boundary) are related to the W coefficients and unknown source strengths by the relationship given as

$$\varphi_{i,j_m-1} = \sum_{k=1}^{NS} W(4j_m+2i_m+i-13,k)\,\sigma_k + \varphi_w - \Delta y_m \varphi_{wy}/2.$$

The equations range in number from $(4(j_m-2) + 2(i_m-2) + 1$ to $4(j_m-2) + 3(i_m-2)$ along the strip that is located one station below the upper boundary, and the W coefficients are given as

$$W(4j_m+2i_m+i-13,k-1) = \exp(i\lambda_1 Mx_i)\,[C_5 x_{0ikj_mj_m} - \Delta y_m \sqrt{K}\,\delta_{ik}/4]$$

and

$$W(4j_m+2i_m+i-13,i_m+k-3) = \exp(i\lambda_1 Mx_i)\,[C_5 x_{0ikij_m} + C_7(y_{j_m}-y_1)x_{1ikij_m}]$$

$$\text{for } 2 \leqslant k \leqslant i_m-1, \text{ and as} \qquad \text{(B96)}$$

$$W(4j_m+2i_m+i-13,2i_m+j-5) = \exp(i\lambda_1 Mx_i)\,[C_5 Y_{0ii_jj_m} + C_7 \tilde{Y}_{1ii_jj_m}]$$

and

$$W(4j_m+2i_m+i-13,2i_m+j_m+j-7) = \exp(i\lambda_1 Mx_i)\,[C_5 Y_{0ii_mj_m} + C_7 \tilde{Y}_{1ii_mj_m}]$$

$$\text{for } 2 \leqslant j \leqslant j_{m-1}.$$

Inserting equations 67 and 70 into the second expression of equation 94 results in the relationship for the potentials of mesh stations located one station above the upper boundary which is given as

$$\begin{aligned}\varphi_{i,j_m} = \exp(i\lambda_1 Mx_i)\,\Bigg\{ C_5 \Bigg[&\sum_{k=2}^{i_m-1} (\sigma_{uk} x_{0ikj_mj_m} + \sigma_{dk} x_{0ikij_m}) \\ &+ \sum_{j=2}^{j_m-1} (\sigma_{\ell j} Y_{0iij_j m} + \sigma_{rj} Y_{0ii_mj_m}) \Bigg] \\ &+ \Delta y_m \sqrt{K}\,\sigma_{ui}/4 \\ &- C_7 \Bigg[\sum_{j=2}^{j_m-1} (\sigma_{\ell j} \tilde{Y}_{1iij_m} + \sigma_{rj} \tilde{Y}_{1ii_mj_m}) \\ &+ (y_{j_m}-y_1) \sum_{k=2}^{i_m-1} \sigma_{dk} x_{1ikij_m} \Bigg] \Bigg\} \\ &+ \varphi_w + \Delta y_m \varphi_{wy}/2.\end{aligned} \qquad \text{(B97)}$$

The last set of equations developed to couple the near-field and far-field potentials is given in terms of the W coefficients by the expression

$$\varphi_{i,j_m} = \sum_{k=1}^{NS} W(4j_m+3i_m+i-15,k)\,\sigma_k + \varphi_w + \Delta y_m \varphi_{wy}/2,$$

where the equation number begins at $4(j_m-2) + 3(i_m-2) + 1$ and ends up at $4(j_m-2) + 4(i_m-2)$.

The W coefficients are then defined as

$$W(4j_m+3i_m+i-15,k-1) = \exp(i\lambda_1 M x_i)\,[C_5 x_{0ikj_mj_m} - \Delta y_m \sqrt{K}\,\delta_{ik}/4]$$

and

$$W(4j_m+3i_m+i-15,i_m+k-3) = \exp(i\lambda_1 M x_i)\,[C_5 x_{0ik1j_m} - C_7(y_{j_m}-y_1)x_{1ik1jm}]$$

$$\text{for } 2 \leqslant k \leqslant i_m-1, \text{ and as} \qquad \text{(B98)}$$

$$W(4j_m+3i_m+i-15,2i_m+j-5) = \exp(i\lambda_1 M x_i)\,[C_5 Y_{0i1j\bar{j}_m} - C_7 \bar{Y}_{1i1j\bar{j}_m}]$$

and

$$W(4j_m+3i_m+i-15,2i_m+j_m+j-7) = \exp(i\lambda_1 M x_i)\,[C_5 Y_{0i\bar{i}_m\bar{j}_m} - C_7 \bar{Y}_{1i\bar{i}_m\bar{j}_m}]$$

$$\text{for } 2 \leqslant j \leqslant j_{m-1}.$$

Note that the quantities Δx_1, Δx_m, Δy_1, Δy_m derive from the differencing of the normal derivative across the boundary. The formulas as written for the w array represent these quantities as being computed before the x variables for $i = 1$ and $i = i_m$ are replaced by the values of the mesh boundaries, a_1 and a_2. If they are computed after these variables are changed, then a factor 2 must be removed from the denominators of the coefficients in the preceding formulas. The same thing holds for the y differences.

The only things yet to be defined are the expressions for the wake potential and its derivatives in order to complete the expressions for coupling the near-field and far-field equations at the boundary of the grid network. Expressions for the potential of the wake and its derivatives are developed in the following appendix.

APPENDIX C

EVALUATION OF THE INTEGRAL FOR THE INFINITE WAKE FOR TWO-DIMENSIONAL FLOW

The wake integral is defined in Appendix A by the expression

$$\varphi_w = \frac{\Delta\varphi_{te}}{4i} \int_{x_{te}}^{\infty} \exp(-i\omega(x_1'-x_{te}))\, \psi_{y_1'} dx_1', \tag{C1}$$

which is put in the framework of our grid definition by setting $x_{te} = a_2$ (the downstream boundary) and evaluating the integral from $x = a_2$ to $x \to \infty$.

The function ψ is given in terms of coordinate differences, that is, $\psi = \psi(x_1-x_1', y_1-y_1')$ with $x_1 = x$ and $y_1 = \sqrt{K}y$.

Note that

$$\frac{\partial\psi}{\partial y_1'} = \frac{-\partial\psi}{\partial y_1}.$$

Thus the wake integral reduces to

$$\varphi_w = \frac{i\Delta\varphi_{te}}{4} \int_{a_2}^{\infty} \exp(-i\omega(x_1'-a_2))\, \psi_{y_1} dx_1'. \tag{C2}$$

ψ is given in Appendix A by the expression

$$\psi = \exp(i\lambda_1 M(x_1-x_1'))\, H_0^{(2)}(\lambda_1\sqrt{((x_1-x_1')^2 + y_1^2)}), \tag{C3}$$

where $H_0^{(2)}(\lambda_1 r)$ is the Hankel function of the second type.

We make a change in variables by letting

$$\eta = y_1 \equiv \sqrt{K}y$$

and

$$t = x_1'-x,$$

which transforms the wake integral into the expression

$$\varphi_w = \frac{i\Delta\varphi_{te}}{4} \exp(i\omega(a_2-x)) \frac{\partial}{\partial\eta} \int_{a_2-x}^{\infty} \exp(-i\omega t)\exp(-i\lambda_1 Mt) H_0^{(2)}(\lambda_1\sqrt{(t^2+\eta^2)})dt.$$

Note: Unless otherwise stated, references made in Appendices A, B, C, and D to equations in these appendices do not include the appendix letter or parenthesis. For example, in Appendix A, equation (A5) would be referred to as "equation 5."

Using the definition $\lambda_1 = \omega M/(1-M^2)$, we combine the two exponentials into a single exponential and then replace the single integral by two equivalent integrals to obtain the expression

$$\varphi_w = \frac{i\Delta\varphi_{te}}{4} \exp(iw(a_2-x)) \frac{\partial}{\partial\eta} \left\{ \int_0^{\infty} \exp(-i\lambda_1 t/M) H_0^{(2)}(\lambda_1\sqrt{(t^2+\eta^2)})dt \right.$$

$$\left. - \int_0^{a_2-x} \exp(-i\lambda_1 t/M) H_0^{(2)}(\lambda_1\sqrt{(t^2+\eta^2)})dt \right\}. \qquad \text{(C4)}$$

The second integral can easily be evaluated using standard integration quadrature procedures. However, it is more difficult to evaluate the first integral due to its slow rate of convergence along the real t axis.

The integral can be evaluated more readily if the device of contour integration is applied to reduce the integration of a slowly convergent integral defined for real variable integration to an integration of a rapidly convergent integral defined in the complex plane.

In applying contour integration, we first identify any poles or branch point singularities in the complex plane so that we can choose a contour that will allow an accurate integral evaluation without having to evaluate singular functions at localized poles in the complex plane. Fortunately, the integrand becomes singular only at the branch points $t = \pm i|\eta|$. Therefore, we select a contour developed to enclose an area free of point singularities. The contour shown in the following sketch appears satisfactory for performing the contour integration.

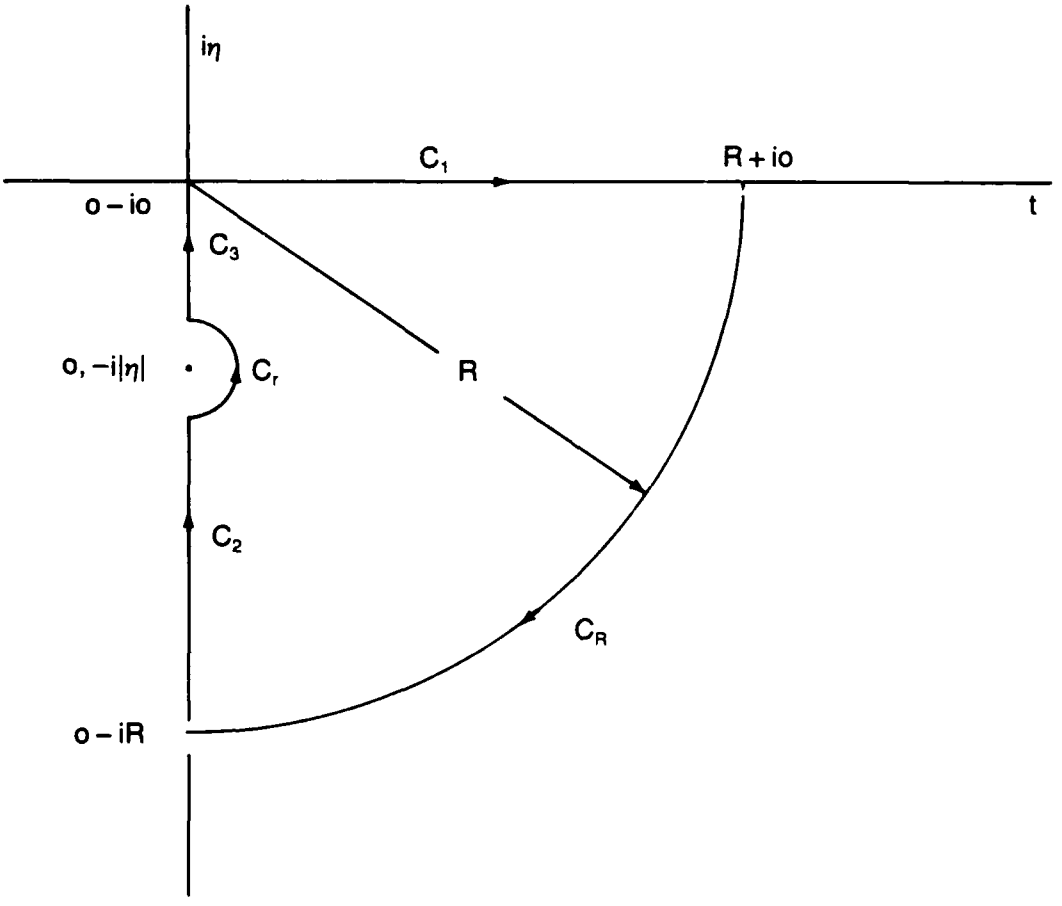

The sum of line integrals around the closed contour equals zero since the area enclosed by the above contour is free of singularities (poles).

That is,

$$\oint_C f(t)dt = 0, \text{ which is represented by}$$

$$I_{C_1} + I_{C_R} + I_{C_2} + I_{C_r} + I_{C_3} = 0. \tag{C5}$$

If R is allowed to approach ∞, then $I_{C_R} \to 0$. Also if $r \to 0$, then $I_{C_r} \to 0$; and we obtain

$$\lim_{R\to\infty} \{I_{C_1} + I_{C_2} + I_{C_3}\} = 0.$$

In terms of individual line integrals, the contour integration becomes

$$\lim_{R\to\infty} \left\{ \int_0^R \exp(-i\lambda_1 t/M) H_0^{(2)}(\lambda_1\sqrt{(t^2+\eta^2)})\, dt + \int_{-iR}^{-i|\eta|} \exp(-i\lambda_1 t/M) H_0^{(2)}(\lambda_1\sqrt{(t^2+\eta^2)})\, dt \right.$$

$$\left. + \int_{-i|\eta|}^{-0i} \exp(-i\lambda_1 t/M) H_0^{(2)}(\lambda_1\sqrt{(t^2+\eta^2)})\, dt \right\} = 0. \tag{C6}$$

We transform the last two integrals using the transformation $t = -iv$ to obtain

$$\int_{-iR}^{-i|\eta|} \exp(-i\lambda_1 t/M) H_0^{(2)}(\lambda_1\sqrt{(t^2+\eta^2)})\, dt = +i \int_{|\eta|}^{R} \exp(-\lambda_1 v/M) H_0^{(2)}(\lambda_1\sqrt{((-iv)^2+\eta^2)})\, dv$$

and

$$\int_{-i|\eta|}^{-0i} \exp(-i\lambda_1 t/M) H_0^{(2)}(\lambda_1\sqrt{(t^2+\eta^2)})\, dt = +i \int_0^{|\eta|} \exp(-\lambda_1 v/M) H_0^{(2)}(\lambda_1\sqrt{((-iv)^2+\eta^2)})\, dv.$$

When $v > \eta$ and the integration ranges between $v = |\eta|$ to $v = R$, the square root term is evaluated as

$$\sqrt{((-iv)^2+\eta^2)} = \sqrt{((-iv+i\eta)(-iv-i\eta))}$$

$$= \sqrt{((-i)^2(v^2-\eta^2))}$$

$$= -i\sqrt{(v^2-\eta^2)}.$$

When $v \leq \eta$ and the integration limits are $v = 0$ and $v = |\eta|$, the square root term is evaluated as

$$\sqrt{((-iv)^2+\eta^2)} = \sqrt{(((-iv)+\eta)\,((-iv)-\eta))} = \sqrt{((-i)^2(v^2-\eta^2))}$$

$$= \sqrt{((-i)^2(i)^2(\eta^2-v^2))}$$

$$= \sqrt{(\eta^2-v^2)}.$$

Inserting the expressions for the square root terms into the appropriate integrals results in integrands having Hankel functions of both real and complex functions.

The Hankel function of a complex function is changed into a modified Bessel function of a real function by making use of the relations of section 9.6.4 of Abramowitz and Stegun (ref. 13), where we observe that

$$H_0^{(2)}(-iz) = \frac{2i}{\pi} K_0(z).$$

The $K_0(z)$ function converges very rapidly, as is shown in figure 9.7 of Reference 13.

Thus the slowly convergent integral defined along the real axis of the variable can be evaluated as a rapidly convergent integral defined along the negative imaginary axis that is given by

$$\int_0^\infty \exp(-i\lambda_1 t/M) H_0^{(2)}(\lambda_1\sqrt{(t^2+\eta^2)})dt = \frac{2}{\pi}\int_{|\eta|}^\infty \exp(-\lambda_1 v/M) K_0(\lambda\sqrt{(v^2-\eta^2)})\, dv$$

$$-i\int_0^{|\eta|} \exp(-\lambda_1 v/M) H_0(\lambda_1\sqrt{(\eta^2-v^2)})\, dv. \tag{C7}$$

Inserting equation 7 into equation 4, we obtain a revised form of the wake integral given as

$$\varphi_w = -\frac{i\Delta\phi_{te}}{4}\exp(i\omega(a_2-x))\frac{\partial}{\partial\eta}\left\{-\int_0^{a_2-x}\exp(-i\lambda_1 t/M)H_0^{(2)}(\lambda_1\sqrt{(t^2+\eta^2)})\, dt\right.$$

$$-i\int_0^{|\eta|}\exp(-\lambda_1 v/M)H_0^{(2)}(\lambda_1\sqrt{(\eta^2-v^2)})\, dv$$

$$\left.+\frac{2}{\pi}\int_{|\eta|}^\infty \exp(-\lambda_1 v/M)K_0(\lambda_1\sqrt{(v^2-\eta^2)})\, dv\right\}. \tag{C8}$$

The expression for the wake integral is simplified to the form

$$\varphi_w = \frac{i\Delta\phi_{te}}{4}\{\psi_1(x,\eta)+\psi_2(\eta)\}\exp(i\omega(a_2-x)), \tag{C9}$$

where

$$\psi_1 = \eta\lambda_1\int_0^{a_2-x}\exp(-i\lambda_1 t/M)H_1^{(2)}(\lambda_1\sqrt{(t^2+\eta^2)})/\sqrt{(\eta^2+t^2)}\, dt, \tag{C10}$$

and

$$\psi_2 = \frac{\partial}{\partial \eta} \left\{ -i \int_0^{|\eta|} \exp(-\lambda_1 t/M) H_0^{(2)} (\lambda_1 \sqrt{(\eta^2 - t^2)}) \, dt \right.$$

$$\left. + \frac{2}{\pi} \int_{|\eta|}^{\infty} \exp(-\lambda_1 t/M) K_0(\lambda \sqrt{(t^2 - \eta^2)}) \, dt \right\}. \tag{C11}$$

We now apply transformations to simplify the numerical integrations. We first eliminate the variable of integration from the integration limits by inserting the transformation $t = |\eta| t'$ into equation 11 to obtain

$$\psi_2 = \frac{\partial}{\partial \eta} \left\{ -i|\eta| \int_0^1 \exp(-\lambda_1 |\eta| t/M) H_0^{(2)} (\lambda_1 |\eta| \sqrt{(1 - t^2)}) \, dt \right.$$

$$\left. + \frac{2|\eta|}{\pi} \int_1^{\infty} \exp(-\lambda_1 |\eta| t/M) K_0(\lambda_1 |\eta| \sqrt{(t^2 - 1)}) \, dt \right\}, \tag{C12}$$

where the primes have been dropped.

A new variable is introduced to simplify the expression even further; we let $\zeta = \lambda_1 \eta$. Then the equation is reduced to

$$\psi_2 = \frac{\partial}{\partial \zeta} \left\{ -i|\zeta| \int_0^1 \exp(-|\zeta| t/M) H_0^{(2)} (|\zeta| \sqrt{(1 - t^2)}) \, dt \right.$$

$$\left. + \frac{2|\zeta|}{\pi} \int_1^{\infty} \exp(-|\zeta| t/M) K_0(|\zeta| \sqrt{(t^2 - 1)}) \, dt \right\}. \tag{C13}$$

The singularities that exist at $t = 1$ are moved to the origin in the first integral by introducing $t' = 1 - t$ and by using $t' = t - 1$ in the second integral. This leads to

$$\psi_2 = \frac{\partial}{\partial \zeta} \left\{ -i|\zeta| \exp(-|\zeta|/M) \int_0^1 \exp(|\zeta| t/M) H_0^{(2)} (|\zeta| \sqrt{(t(2 - t))}) \, dt \right.$$

$$\left. + 2|\zeta| \exp(-|\zeta|/M) \int_0^{\infty} \exp(-|\zeta| t/M) K_0(|\zeta| \sqrt{(t(2 + t))}) \, dt \right\}, \tag{C14}$$

where the primes have been dropped. Equation 14 may be expressed in terms of a new function defined by

$$\psi_0 = -i\int_0^1 \exp(|\zeta|t/M)H_0^{(2)}(|\zeta|\sqrt{(t(2-t))})\,dt$$

$$+ \frac{2}{\pi}\int_0^\infty \exp(-|\zeta|t/M)K_0(|\zeta|\sqrt{(t(2+t))})\,dt. \qquad \text{(C15)}$$

That is,

$$\psi_2 = \frac{\partial}{\partial \zeta}[|\zeta|\exp(-|\zeta|/M)\psi_0], \qquad \text{(C16)}$$

or

$$\psi_2 = \exp(-|\zeta|/M)\,[(1-|\zeta|/M)\psi_0 + |\zeta|\psi_{0|\zeta|}]\,\mathrm{sgn}\zeta. \qquad \text{(C17)}$$

For convenience in numerical integrations, the integrals are combined as follows:

$$\psi_0 = \int_0^1 \left[\frac{2}{\pi}\exp(-\zeta t/M)K_0(\zeta\sqrt{(t(2+t))} - i\exp(\zeta t/M)H_0^{(2)}(\zeta\sqrt{(t(2-t))}\right]dt$$

$$+ \frac{2}{\pi}\int_1^\infty \exp(-\zeta t/M)K_0(\zeta\sqrt{(t(2+t))})\,dt, \qquad \text{(C18)}$$

where the absolute sign has been dropped for convenience.

Then the derivative with respect to ζ takes the form

$$\frac{\partial \psi_0}{\partial \zeta} = -\int_0^1 \Big\{\exp(-\zeta t/M)(2/\pi)[(t/M)K_0(\zeta\sqrt{(t(2+t))} + \sqrt{(t(2+t))}\,K_1(\zeta\sqrt{(t(2+t))}]$$

$$+ i\exp(\zeta t/M)\,[(t/M)H_0^{(2)}(\zeta\sqrt{(t(2-t))} - \sqrt{(t(2-t))}\,H_1^{(2)}(\zeta\sqrt{(t(2-t))}]\Big\}\,dt$$

$$-\frac{2}{\pi}\int_1^\infty \exp(-\zeta t/M)[(t/M)K_0(\zeta\sqrt{(t(2+t))} + \sqrt{(t(2+t))}\,K_1(\zeta\sqrt{(t(2+t))}]\,dt. \qquad \text{(C19)}$$

We simplify the expressions by letting

$$z_1 = \sqrt{(t(2-t))},$$

$$z_2 = \sqrt{(t(2+t))},$$

and

$$\alpha = t/M$$

and obtain

$$\psi_{0\zeta} = -\int_0^1 \Big\{ \exp(-\zeta\alpha)(2/\pi)\,[\alpha K_0(\zeta z_2) + z_2 K_1(\zeta z_2)]$$

$$+ i\exp(\zeta\alpha)[\alpha H_0^{(2)}(\zeta z_1) - z_1 H_1^{(2)}(\zeta z_1)] \Big\}\, dt$$

$$- \frac{2}{\pi}\int_1^\infty \exp(-\zeta\alpha)[\alpha K_0(\zeta z_2) + z_2 K_1(\zeta z_2)]\, dt. \tag{C20}$$

SUMMARY OF THE DERIVATION

The potential induced by the wake is given by equation 9 as

$$\varphi_w = \frac{i\Delta\varphi_{te}}{4}\,\{\psi_1(x,\eta) + \psi_2(\zeta)\}\,\exp(i\omega(a_2 - x)), \tag{C21}$$

where $\eta = \sqrt{K}y$ and $\zeta = \lambda_1\eta$.

The derivatives with respect to x and y are given as

$$\varphi_{wx} = -i\omega\varphi_w + \frac{i\Delta\varphi_{te}}{4}\,\psi_{1x}\exp(i\omega(a_2 - x)) \tag{C22}$$

and

$$\varphi_{wy} = \frac{i\Delta\varphi_{te}}{4}\,\{\psi_{1y} + \lambda_1\sqrt{K}\,\psi_{2\zeta}\}\,\exp(i\omega(a_2 - x)), \tag{C23}$$

where

$$\psi_1 = \eta\lambda_1\int_0^{a_2 - x}\exp(-i\lambda_1 t/M)H_1^{(2)}(\lambda_1\sqrt{(t^2+\eta^2)})/\sqrt{(t^2+\eta^2)}\, dt, \tag{C24}$$

$$\psi_{1x} = -\lambda_1\eta\,\exp(-i\lambda_1(a_2 - x)/M)H_1^{(2)}(\lambda_1\sqrt{(\eta^2 + (a_2 - x)^2)})/\sqrt{(\eta^2 + (a_2 - x)^2)}, \tag{C25}$$

$$\psi_{1y} = \psi_1/y - \lambda_1^2\sqrt{K}\eta^2\int_0^{a_2 - x}\exp(-i\lambda_1 t/M)H_2^{(2)}(\lambda_1\sqrt{(t^2+\eta^2)})/(t^2+\eta^2)\, dt, \tag{C26}$$

and

$$\psi_2 = \exp(-|\zeta|/M)\{(1 - |\zeta|/M)\psi_0 + |\zeta|\psi_{0|\zeta|}\}\,\mathrm{sgn}\zeta, \tag{C27}$$

where ψ_0 is obtained from equation 18 as

$$\psi_0 = \frac{2}{\pi}\int_0^\infty \exp(-\alpha|\zeta|)K_0(|\zeta|z_2)dt - i\int_0^1 \exp(\alpha|\zeta|)H_0^{(2)}(|\zeta|z_1)\, dt \tag{C28}$$

and

$$\psi_{0\zeta} = \frac{-2}{\pi}\int_0^\infty \exp(-a\zeta)[aK_0(\zeta z_2)+z_2K_1(\zeta z_2)]\,dt$$

$$-i\int_0^1 \exp(a\zeta)[aH_0^{(2)}(\zeta z_1)-z_1H_1^{(2)}(\zeta z_1)]\,dt. \qquad \text{(C29)}$$

(Absolute value signs have been dropped for convenience.)

Inserting equations 28 and 29 into equation 27 yields the final form of ψ_2, given by

$$\psi_2 = \exp(-\zeta/M)\left\{\frac{2}{\pi}\int_0^\infty \exp(-a\zeta)[(1-\zeta/M-a\zeta)K_0(\zeta z_2)-\zeta z_2K_1(\zeta z_2)]\,dt\right.$$

$$\left.-i\int_0^1 \exp(a\zeta)[(1-\zeta/M+a\zeta)H_0^{(2)}(\zeta z_1)-z_1\zeta H_1^{(2)}(\zeta z_1)]\,dt\right\} \qquad \text{(C30)}$$

and making use of the differentiation formulas

$$\frac{d}{dz}\{zJ_1(z)\} = zJ_0(z)$$

and

$$\frac{d}{dz}\{zK_1(z)\} = zK_0(z).$$

We obtain the derivative of ψ_2 with respect to ζ in the form of

$$\psi_{2\zeta} = -\psi_2/M+\exp(-\zeta/M)\left\{\frac{2}{\pi}\int_0^\infty \exp(-a\zeta)\left[(a^2\zeta+a\zeta/M-2a-\frac{1}{M}+\zeta z_2^2)K_0(\zeta z_2)\right.\right.$$

$$\left.+\,z_2(a\zeta+\zeta/M-1)K_1(\zeta z_2)\right]dt$$

$$-i\int_0^1 \exp(a\zeta)[a^2\zeta-a\zeta/M+2a-1/M-\zeta z_1^2)H_0^{(2)}(\zeta z_1)$$

$$\left.-z_1(a\zeta-\zeta/M+1)H_1^{(2)}(\zeta z_1)dt\right\}. \qquad \text{(C31)}$$

APPENDIX D

MODIFICATION OF COUPLING EQUATIONS FOR THE INCLUSION OF THE POTENTIALS DUE TO THE INFINITE WAKE FOR TWO-DIMENSIONAL FLOW

Wake potential contained in equations 72, 81, 88, and 94 of Appendix B are terms that are designated as φ_w, φ_{wx}, and φ_{wy}. These terms will now be put in a form that is suitable for inclusion in the W matrix. For equations $1 \leq j \leq j_m - 1$ (that apply to grid points located one station ahead of the upstream boundary), the first of equation 72 of Appendix B has the form

$$-\varphi_{1,j} + \varphi_w(x_1, y_j) - \frac{\Delta x_1}{2}\varphi_{wx}(x_1, y_j) + \sum_{k=1}^{NS} W(j-1, k)\sigma_k = 0. \tag{D1}$$

For equations $(j_m - 1) \leq (j_m - 2 + j - 1) \leq 2(j_m - 2)$ defined for points located one station downstream of the upstream boundary, we use the second part of equation 72 of Appendix B to obtain

$$-\varphi_{2,j} + \varphi_w(x_1, y_j) + \frac{\Delta x_1}{2}\varphi_{wx}(x_1, y_j) + \sum_{k=1}^{NS} W(j_m + j - 3, k)\sigma_k = 0. \tag{D2}$$

For equations $2(j_m - 2) + 1 \leq 2(j_m - 2) + j - 1 \leq 3(j_m - 2)$ that apply to points located one station upstream of the downstream boundary, the first expression of equation 81 of Appendix B gives the form

$$-\varphi_{i_m-1,j} + \varphi_w(x_{i_m}, y_j) - \frac{\Delta x_m}{2}\varphi_{w_x}(x_{i_m}, y_j) + \sum_{k=1}^{NS} W(2(j_m - 2) + j - 1, k)\sigma_k = 0. \tag{D3}$$

For equations $3(j_m - 2) + 1 \leq 3(j_m - 2) + j - 1 \leq 4(j_m - 2)$ that are applicable for grid points located one station downstream of the downstream boundary, we use the second expression of equation 81 of Appendix B and obtain

$$-\varphi_{i_m,j} + \varphi_w(x_{i_m}, y_j) + \frac{\Delta x_m}{2}\varphi_{wx}(x_{i_m}, y_j) + \sum_{k=1}^{NS} W\left(3(j_m - 2) + j - 1, k\right)\sigma_k = 0. \tag{D4}$$

For equations $4(j_m - 2) + 1 \leq 4(j_m - 2) + i - 1 \leq 4(j_m - 2) + (j_m - 2)$ that apply to grid points located one station below the lower boundary, we use the first expression of equation 88 of Appendix B to obtain

$$-\varphi_{i,1} + \varphi_w(x_i, y_1) - \frac{\Delta y_1}{2}\varphi_{wy}(x_i, y_1) + \sum_{k=1}^{NS} W\left(4(j_m - 2) + i - 1, k\right)\sigma_k = 0. \tag{D5}$$

For equations $4(j_m - 2) + (i_m - 2) + 1 \leq 4(j_m - 2) + (i_m - 2)\, i - 1 \leq 4(j_m - 2) + 2(i_m - 2)$ that are valid for points located lone station above the lower boundary, we made use of the second expression of equation 88 of Appendix B to establish the equation

---

Note: Unless otherwise stated, references made in Appendices A, B, C, and D to equations in these appendices do not include the appendix letter or parenthesis. For example, in Appendix A, equation (A5) would be referred to as "equation 5."

$$-\varphi_{i,2} + \varphi_w(x_i, y_1) + \frac{\Delta y_1}{2}\,\varphi_{wy}(x_i, y_1) + \sum_{k=1}^{NS} W\left(4(j_m-2) + (i_m-2) + i - 1, k\right)\sigma_k = 0. \quad \text{(D6)}$$

For equations $4(j_m - 2) + 2(i_m - 2) + 1 \le 4(j_m - 2) + 2(i_m - 2)\,i - 1 \le 4(j_m - 2) + 3(i_m - 2)$ that define the potentials at grid points located one station below the upper boundary, we use the first expression of equation 94 of Appendix B to derive the expression

$$-\varphi_{i,j_m-1} + \varphi_w(x_i, y_{j_m}) - \frac{\Delta y_m}{2}\,\varphi_{wy}(x_i, y_{j_m}) + \sum_{k=1}^{NS} W\left(4(j_m-2) + 2(i_m-2) + i - 1, k\right)\sigma_k = 0. \quad \text{(D7)}$$

For equations $4(j_m - 2) + 3(i_m - 2) + 1 \le 4(j_m - 2) + 3(i_m - 2)\,i - 1 \le 4(j_m - 2) + 4(i_m - 2)$ that represent the equations that define the potentials at grid points located one station above the upper boundary, we use the second expression of equation 94 of Appendix B which provides the expression

$$-\varphi_{i,j_m} + \varphi_w(x_i, y_{j_m}) + \frac{\Delta y_m}{2}\,\varphi_{wy}(x_i, y_{j_m}) + \sum_{k=1}^{NS} W\left(4(j_m-2) + 3(i_m-2) + i - 1, k\right)\sigma_k = 0. \quad \text{(D8)}$$

Using equation 9 of Appendix C, the wake integral is given as

$$\varphi_w = \frac{i\Delta\varphi}{4}\{\psi_1(x,\eta)+\psi_2(\zeta)\}\exp(i\omega(x_{i_m}-x)), \quad \text{(D9)}$$

where $\eta = \sqrt{K}y$; $\zeta = \lambda_1\eta$.

$\Delta\varphi$ is the jump in potential at the downstream boundary. In terms of $\Delta\varphi_{i_1+1}$ at the trailing edge,

$$\Delta\varphi = \Delta\varphi_{i_1+1}\exp(-i\omega(x_{i_m}-x_{i_1+1})).$$

Equation 9 then becomes

$$\varphi_w = \frac{i\Delta\varphi_{i_1+1}}{4}\{\psi_1(x,\eta)+\psi_2(\zeta)\}\exp(i\omega(x_{i_1+1}-x)), \quad \text{(D10)}$$

and the derivatives of the wake potential are given by

$$\varphi_{wx} = -i\omega\varphi_w + \frac{i\Delta\varphi_{i_1+1}}{4}\,\psi_{1x}\exp(i\omega(x_{i_1+1}-x)), \quad \text{(D11)}$$

and

$$\varphi_{wy} = \frac{i\Delta\varphi_{i_1+1}}{4}\{\psi_{1y}+\psi_2'(\zeta)\lambda\sqrt{K}\,\mathrm{sg}\eta y\}\exp(i\omega(x_{i_1+1}-x)). \quad \text{(D12)}$$

Substituting equations 10 and 11 into equation 1 yields

$$-\varphi_{1j}+\varphi_w+\frac{\Delta x_1}{2}\,i\omega\varphi_w-\frac{i\Delta x_1}{8}\,\Delta\varphi_{i_1+1}\psi_{1x}\exp(i\omega(x_{i_1+1}-x_1))+\sum_{k=1}^{NS}W(j-1,k)\sigma_k=0,$$

$$-\varphi_{1j}+(1+i\omega\Delta x_{1/2})\varphi_w-\frac{i\Delta x_1}{8}\,\Delta\varphi_{i_1+1}\psi_{1x}\exp(i\omega(x_{i_1+1}-x_1))+\sum_{k=1}^{NS}W(j-1,k)\sigma_k=0,$$

and

$$-\varphi_{1j}-\frac{i\Delta\varphi_{i1+1}}{4}\left\{(\psi_1+\psi_2)(1+i\omega\Delta x_{1/2})-\frac{\Delta x_1}{2}\psi_{1x}\right\}\exp(i\omega(x_{i_1+1}-x_1))+\sum_{k=1}^{NS}W(j-1,k)\sigma_k=0. \tag{D13}$$

Similarly, from equation 2, we obtain

$$-\varphi_{2j}+\frac{i\Delta\varphi_{i1+1}}{4}\left\{[\psi_1(x_1,\eta_j)+\psi_2(\xi_j)](1-i\psi\Delta x_{1/2})+\frac{\Delta x_1}{2}\psi_{1x}\right\}\exp(i\omega(x_{i_1+1}-x_1))$$

$$+\sum_{k=1}^{NS}W((j_m-2)+j-1,k)\sigma_k=0. \tag{D14}$$

Substituting equations 10 and 11 into equation 3 yields

$$-\varphi_{i_m-1,j}+\frac{i\Delta\varphi_{i1+1}}{4}\left\{[\psi_1(x_{i_m},\eta_j)+\psi_2(\xi_j)](1+i\omega\Delta x_{m/2})-\frac{\Delta x_m}{2}\psi_{1x}\right\}\exp(i\omega(x_{i_1+1}-x_{i_m}))$$

$$+\sum_{k=1}^{NS}W(2(j_m-2)+j-1,k)\sigma_k=0. \tag{D15}$$

Similarly, for equation 4, we obtain

$$-\varphi_{i_mj}+\frac{i\Delta\varphi_{i1+1}}{4}\left\{[\psi_1(x_{i_m},\eta_j)+\psi_2(\xi_j)](1-i\Delta x_m\omega/2)\right.$$

$$\left.+\frac{\Delta x_m}{2}\psi_{1x}\right\}\exp(i\omega(x_{i_1+1}-x_{i_m}))+\sum_{k=1}^{NS}W(3(j_m-2)+j-1,k)\sigma_k=0. \tag{D16}$$

Substituting equations 10 and 11 into equation 5 leads to

$$-\varphi_{i1}+\frac{i\Delta\varphi_{i1+1}}{4}\left\{[\psi_1(x_i,\sqrt{K}y_1)+\psi_2(\lambda_1\sqrt{K}y_1)]-\frac{\Delta y_1}{2}[\psi_{1y}+\psi_{2y}]\right\}\exp(i\omega(x_{i_1+1}-x_i))$$

$$+\sum_{k=1}^{NS}W(4(j_m-2)+i-1,k)\sigma_k=0. \tag{D17}$$

Similarly, equation 6 becomes

$$-\varphi_{i2} + \frac{i\Delta\varphi_{i_1+1}}{4}\left\{[\psi_1(x_i,\sqrt{K}y_1)+\psi_2(\lambda_1\sqrt{K}y_1)] + \frac{\Delta y_1}{2}[\psi_{1y}+\psi_{2y}]\right\}\exp(i\omega(x_{1_{1+1}}-x_i))$$

$$+\sum_{k=1}^{NS} W(4(j_m-2)+(i_m-2)+i-1,k)\sigma_k = 0. \qquad \text{(D18)}$$

Substituting equations 10 and 12 into equation 7 yields

$$-\varphi_{i,j_m-1} + \frac{i\Delta\varphi_{i_1+1}}{4}\left\{[\psi_1(x_i,\sqrt{K}y_{j_m})+\psi_2(\lambda_1\sqrt{K}y_{j_m}]\right.$$

$$\left.-\frac{\Delta y_m}{2}[\psi_{1y}+\psi_{2y}]\right\}\exp(i\omega(x_{i_{1+1}}-x_i))$$

$$+\sum_{k=1}^{NS} W(4(j_m-2)+2(i_m-2)+i-1,k)\sigma_k = 0. \qquad \text{(D19)}$$

Similarly, equation 8 becomes

$$-\varphi_{i,j_m} + \frac{i\Delta\varphi_{i_1+1}}{4}\left\{[\psi_1(x_i,\sqrt{K}y_{j_m})+\psi_2(\lambda_1\sqrt{K}y_{j_m})]\right.$$

$$\left.+\frac{\Delta y_m}{2}[\psi_{1y}+\psi_{2y}]\right\}\exp(i\omega(x_{i_{1+1}}-x_i))$$

$$+\sum_{k=1}^{NS} W(4(j_m-2)+3(i_m-2)+i-1,k)\sigma_k = 0. \qquad \text{(D20)}$$

We now identify the W coefficients that are due to the wake terms of equations 13 to 20 by the following expressions.

$$W(j-1,NS+1) = \frac{i}{4}\left\{(\psi_1(x_1,\eta_j)+\psi_2(\xi_j))(1+i\omega\Delta x_1/2) - \frac{\Delta x_1}{2}\psi_{1x}\right\}\exp(i\omega(x_{i_{1+1}}-x_1)) \qquad \text{(D21)}$$

$$W((j_m-2)+j-1,NS+1) = \frac{i}{4}\left\{[\psi_1(x_1,\eta_j)+\psi_2(\xi_j)](1-i\omega\Delta x_1/2) + \frac{\Delta x_1}{2}\psi_{1x}\right\}\exp(i\omega(x_{i_{1+1}}-x_1)) \qquad \text{(D22)}$$

$$W(2(j_m-2)+j-1,NS+1) = \frac{i}{4}\left\{[\psi_1(x_{i_m},\eta_j)+\psi_2(\xi_j)](1+i\omega\Delta x_m/2) - \frac{\Delta x_m}{2}\psi_{1x}\right\}\exp(i\omega(x_{i_{1+1}}-x_{i_m})) \qquad \text{(D23)}$$

$$W(3(j_m-2)+j-1,NS+1) = \frac{i}{4}\left\{[\psi_1(x_{i_m},\eta_j)+\psi_2(\zeta_j)](1-i\omega\Delta x_m/2) + \frac{\Delta x_m}{2}\psi_{1x}\right\}\exp(i\omega(x_{i_{1+1}}-x_{i_m})) \quad (D24)$$

$$W(4(j_m-2)+i-1,NS+1) = \frac{i}{4}\left\{\psi_1(x_i,\eta_1)+\psi_2(\zeta_1) - \frac{\Delta y_1}{2}[\psi_{1y}+\psi_{2y}]\right\}\exp(i\omega(x_{i_{1+1}}-x_i)) \quad (D25)$$

$$W(4(j_m-2)+(i_m-2)+i-1,NS+1) = \frac{i}{4}\left\{\psi_1(x_i,\eta_1)+\psi_2(\zeta_1) + \frac{\Delta y_1}{2}[\psi_{1y}+\psi_{2y}]\right\}\exp(i\omega(x_{i_{1+1}}-x_i)) \quad (D26)$$

$$W(4(j_m-2)+2(i_m-2)+i-1,NS+1) = \frac{i}{4}\left\{\psi_1(x_i,\eta_{j_m})+\psi_2(\zeta_{j_m}) - \frac{\Delta y_m}{2}[\psi_{1y}+\psi_{2y}]\right\}\exp(i\omega(x_{i_{1+1}}-x_i)) \quad (D27)$$

$$W(4(j_m-2)+3(i_m-2)+i-1,NS+1) = \frac{i}{4}\left\{\psi_1(x_i,\eta_{j_m})+\psi_2(\zeta_{j_m}) + \frac{\Delta y_m}{2}[\psi_{1y}+\psi_{2y}]\right\}\exp(i\omega(x_{i_{1+1}}-x_i)) \quad (D28)$$

We now collect the W coefficients, and we write the equations for the potentials at grid stations that are located inside of the boundaries as

$$-\varphi_{2,j}+\sum_{k=1}^{NS} W((j_m-2)+j-1,k)\sigma_k+\Delta\varphi_{i_{1+1}}W((j_m-2)+j-1,NS+1) = 0, \quad (D29)$$

$$-\varphi_{i_m-1,j}+\sum_{k=1}^{NS} W(2(j_m-2)+j-1,k)\sigma_k+\Delta\varphi_{i_{1+1}}W(2(j_m-2)+j-1,NS+1) = 0, \quad (D30)$$

$$-\varphi_{i,2}+\sum_{k=1}^{NS} W(4(j_m-2)+(i_m-2)+i-1,k)\sigma_k+\Delta\varphi_{i_{1+1}}W(4(j_m-2)+(i_m-2)+i-1,NS+1) = 0, \quad (D31)$$

and

$$-\varphi_{i,j_m-1}+\sum_{k=1}^{NS} W(4(j_m-2)+2(i_m-2)+i-1,k)\sigma_k+\Delta\varphi_{i_{1+1}}W(4(j_m-2)+2(i_m-2)+i-1,NS+1) = 0. \quad (D32)$$

The terms $\varphi_{i,j}$, $\varphi_{i_m-1,j}$, $\varphi_{i,2}$, and φ_{i,j_m-1} are variables in the finite differencing procedures; but they are not free variables since these variables must also satisfy the boundary conditions specified by equations 29, 30, 31, and 32. The number of equations involved in satisfying the boundary conditions at grid points located one station inside of the boundaries is $2(j_m-2)+2(i_m-2)$.

We collect the remaining W coefficients and write the equations for the potentials at grid points that are located one station outside of the interface boundary.

$$\varphi_{1,j} = \sum_{k=1}^{NS} W(j-1,k)\sigma_k+\Delta\varphi_{i_{1+1}}W(j-1,NS+1) \quad (D33)$$

$$\varphi_{i_m,j} = \sum_{k=1}^{NS} W(3(j_m-2)+j-1,k)\sigma_k+\Delta\varphi_{i_{1+1}}W(3(j_m-1)+j-1,NS+1) \quad (D34)$$

$$\varphi_{i,1} = \sum_{k=1}^{NS} W(4(j_m-2)+i-1,k)\sigma_k + \Delta\varphi_{i_1+1} W(4(j_m-1)+i-1,NS+1) \tag{D35}$$

$$\varphi_{i,j_m} = \sum_{k=1}^{NS} W(4(j_m-2)+3(i_m-2)+i-1,k)\sigma_k + \Delta\varphi_{i_1+1} W(4(j_m-2)+3(i_m-2)+i-1,NS+1) \tag{D36}$$

The terms on the left-hand side of the above equations are eliminated from the finite differencing procedures by replacing them with the coupling boundary conditions given by the expressions on the right-hand side. The expressions on the right-hand side represent the potentials at the outer stations that are derived using the potentials of the wake and applied source distributions evaluated at the boundary. The number of equations involved by imposing the above boundary conditions is $2(j_m-2)+2(i_m-2)$.

The total number of equations involved in this coupling procedure is then equal to $(i_m-2)*(j_m-2)+4(j_m-2)+4(i_m-2)$, which equals the sum of finite-differencing potentials and exterior applied source distributions.

APPENDIX E

EQUATIONS FOR THE FINITE DIFFERENCE POTENTIALS FOR THE INTERIOR REGION IN THREE-DIMENSIONAL FLOW

The mathematical derivation of the procedures required for the solution of the unsteady velocity potential for the flow about a harmonically oscillating wing is given in reference 1. The following discussion is limited to a brief outline of those procedures. The complete nonlinear differential equation has been simplified by applying the assumption that the unsteady flow can be represented by a small perturbation about the steady flow condition.

The perturbation velocity potential is given by

$$\left[K - (\gamma - 1)\phi_t - (\gamma + 1)\phi_x\right]\phi_{xx} + \phi_{yy} + \phi_{zz} - (2\phi_{xt} - \phi_{tt})/\epsilon = 0 \tag{E1}$$

where $K = (1 - M^2)/M^2\epsilon$, M is the freestream Mach number of velocity U_o in the x direction and x, y are dimensionless coordinates. Time is nondimensionalized by b/U_o.

The airfoil shape and displacement are defined in terms of time by the relation

$$z_o(x,y,t) = \delta f(x,y,t)$$

The boundary conditions are linearized and defined by

$$\phi_z = f_x(x,y,t) + f_t(x,y) \tag{E2}$$

The quantity δ associated with airfoil properties such as thickness ratio, camber, and angle of attack is assumed to be small. The y, z coordinates are scaled to the dimensionless physical coordinates by the relationship

$$y = \delta^{1/3}M^{2/3}y_o \; ; \; z = \delta^{1/3}M^{2/3}z_o$$

and ϵ is defined in terms of δ by

$$\epsilon = (\delta/M)^{2/3}$$

The pressure coefficient is given by

$$C_p = -2\epsilon(\phi_x + \phi_t)$$

The differential equation of flow (E1) is simplified by assuming harmonic motion and by assuming that the velocity potential can be separated into a steady and unsteady potential representation. That is, we assume that the potential can be represented by the expression

$$\phi = \phi_o(x,y,z) + \phi_1(x,y,z)\exp(i\omega t) \tag{E3}$$

where the body shape definition is given by

$$z_o = \delta f_x(x,y,z,t) = \delta\left[f_o(x,y) + f_1(x,y)\exp(i\omega t)\right] \tag{E3A}$$

In the absence of oscillations, the steady state terms must satisfy the differential equation and boundary condition given by

$$\left[K - (\gamma + 1)\phi_{o_x}\right]\phi_{o_{xx}} + \phi_{o_{yy}} + \phi_{o_{zz}} = 0$$

$$\phi_{o_z} = f_o(x,y) \text{ on } z = 0 \text{ and } -1 \le x \le 1 \tag{E4}$$

For the unsteady condition, it is assumed that the oscillations are small and that higher order terms may be neglected. The differential equation and associated boundary condition that must be satisfied by the unsteady potential ϕ_1 is then given by

$$\left[\left[K - (\gamma + 1)\varphi_{o_x}\right]\varphi_{1_x}\right]_x + \phi_{1_{yy}} + \phi_{1_{zz}} - (2i\omega/\epsilon)\phi_{1_x} + q\phi_1 = 0$$

$$\phi_{1_z} = f_{1_x} + i\omega f_1(x,y) \text{ on } z = 0, \text{ for } -1 \le x \le 1 \text{ and } 0 \le y \le y_{tip}$$

where $q = \omega^2/\epsilon - i\omega(\gamma - 1)\phi_{0_{xx}}$ (E5)

The differential equation of (E5) is of a mixed type, being elliptic or hyperbolic whenever the steady state equation (E4) is elliptic or hyperbolic. The finite difference equations are formulated by using central differencing in defining the y and z derivatives, whereas the x derivatives are evaluated using central differencing whenever the region is subsonic (having elliptic characteristics). Upstream (or backward) differences are applied in defining the x derivative at all hyperbolic stations.

The finite difference form of equation (E5) that is applicable to subsonic flow regions is given by

$$a_{z_k}\phi_{1_{ijk-1}} - (a_{y_j} + b_{y_j} + a_{z_k} + b_{z_k} + E_1 + E_2 - q_{ijk}/2) + b_{z_k}\phi_{1_{ijk+1}}$$

$$= -E_1\phi_{1_{i+1jk}} - E_2\phi_{1_{i-1jk}} - a_{y_j}\phi_{1_{ij-1k}} - b_{y_j}\phi_{1_{ij+1k}} \tag{E6}$$

The finite difference form applicable to supersonic regions is given by

$$a_{z_k}\phi_{1_{ijk-1}} - (a_{y_j} + b_{y_j} + a_{z_k} + b_{z_k} - E_3 - q_{ijk}/2)\phi_{1_{ijk}} + b_{z_k}\phi_{1_{ijk+1}}$$

$$= (E_3 + E_4)\phi_{1_{i-1jk}} - E_4\phi_{1_{i-2jk}} - a_{y_j}\phi_{1_{ij-1k}} - b_{y_j}\phi_{1_{ij+1k}} \tag{E7}$$

where

$$a_{z_k} = 1/(z_{k+1} - z_{k-1})(z_k - z_{k-1}) ; \quad a_{y_j} = 1/(y_{j+1} - y_{j-1})(y_j - y_{j-1}) ;$$

$$b_{z_k} = 1/(z_{k+1} - z_{k-1})(z_{k+1} - z_k) ; \quad b_{y_j} = 1/(y_{j+1} - y_{j-1})(y_{j+1} - y_j) ;$$

$$\mathrm{E}_1 = c_i u_{i+1/2jk} - i\omega c_{1_i}/\epsilon ; \quad \mathrm{E}_2 = d_i u_{i+1/2jk} + i\omega d_{1_i}/\epsilon ;$$

$$\mathrm{E}_3 = c_{i-1} u_{i-1/2jk} - i\omega c_{2_i}/\epsilon ; \quad \mathrm{E}_4 = d_{i-1} u_{i-3/2jk} - i\omega d_{2_i}/\epsilon ;$$

$$c_i = 1/(x_{i+1} - x_{i-1})(x_{i+1} - x_i) ; \quad c_{i_1} = (x_i - x_{i-1})c_i ;$$

$$d_i = 1/(x_{i+1} - x_{i-1})(x_i - x_{i-1}) ; \quad d_{i_1} = (x_{i+1} - x_i)d_i$$

$$u_{i+1/2jk} = \mathrm{K} - (\gamma+1)(\phi_{o_{i+1jk}} - \phi_{o_{ijk}})/(x_{i+1} - x_i)$$

$$u_{i-1/2jk} = \mathrm{K} - (\gamma+1)(\phi_{o_{ijk}} - \phi_{o_{i-1jk}})/(x_i - x_{i-1})$$

$$c_{2_i} = 1/(x_i - x_{i-1}) + 1/(x_i - x_{i-2})$$

$$d_{2_i} = - d_{1_{i-1}}$$

Boundary conditions on the upper and lower wing surfaces lead to the following equations for subsonic flow. The finite difference equation at grid points below and adjacent to the wing surface at $z = z_{k_m}$ is given by

$$a_{z_{k_m}} \phi_{i_{ijk_m-1}} - (a_{y_j} + b_{y_j} + a_{z_{k_m}} + \mathrm{E}_1 + \mathrm{E}_2 - q_{ijk}/2)\phi_{1_{ijk_m}}$$

$$= - \mathrm{E}_1 \phi_{1_{i+1jk_m}} - \mathrm{E}_2 \phi_{1_{i-1jk_m}} - a_{y_j} \phi_{1_{ij-1k_m}} - b_{y_j} \phi_{1_{ij+1k_m}} - h_1 b_{z_{k_m}} \mathrm{F}_{ij}^{(\mathrm{L})} \qquad \text{(E8)}$$

The finite difference boundary condition equation applicable to grid points above and adjacent to the wing surface is given by

$$- (a_{y_j} + b_{y_j} + a_{z_{k_{m+1}}} + \mathrm{E}_1 + \mathrm{E}_2 - q_{ijk_m+1}/2)\phi_{1_{ijk_m+1}} + b_{z_{k_m}} \phi_{1_{ijk_m+2}}$$

$$= (- \mathrm{E}_1 \phi_{1_{i+1jk_m+1}} - \mathrm{E}_2 \phi_{1_{i-1jk_m+1}} - a_{y_j} \phi_{1_{ij-1k_m+1}} - b_{y_1} \phi_{1_{ij+1k_m+1}} + h_1 a_{z_{k_m+1}} \mathrm{F}_{ij}^{(\mathrm{U})}$$

where $\mathrm{F}_{ij}^{(\mathrm{L})} = f_{1_x}^{(\mathrm{L})}(x_i, y_j) + i\omega f_1^{(\mathrm{L})}(x_i, y_j)$

$$\mathrm{F}_{ij}^{(\mathrm{U})} = f_{1_x}^{(\mathrm{U})}(x_i, y_j) + i\omega f_1^{(\mathrm{U})}(x_i, y_j)$$

$$h_1 = z_{k_{m+1}} - z_{k_m} \qquad \text{(E9)}$$

The (L) and (U) superscripts refer to the lower and upper wing surfaces respectively.

Additional terms need to be added to equations (E6) and (E7) to satisfy continuity of normal flow across the wake vortex sheet.

The term $bz_{k_m}\Delta\phi 1_{ij}$
is added to the finite difference stations just below the wing, and $-az_{k_m}\Delta\phi 1_{ij}$ is added to stations just above the wing.

The jump in potential is given by

$$\Delta\phi 1_{ij} = \Delta\phi 1_{i_1+1j} \exp\Big(- i\omega(x_i - x_{i_1+1})\Big)$$

where $\Delta\phi 1_{i_1+1j}$ is the jump in potential at the first station downstream of the trailing edge and is determined in such a manner that the Kutta condition is satisfied at the trailing edge. The jump in potential at x_{i_1+1} is determined from the condition of a zero pressure jump across the wake as given by the pressure equation

$$\frac{\partial\Delta\phi_1}{\partial x} + i\omega\Delta\phi_1 = 0 \tag{E10}$$

The finite difference form of equation (E10) is given by

$$c_{1i_1}(\Delta\phi_{i_1+1j} - \Delta\phi_{i_1j}) + d_{1i_1}(\Delta\phi_{i_1j} - \Delta\phi_{i_1-1j}) + i\omega\Delta\phi_{i_1j} = 0$$

$$\text{where } c_{1i_1} = (x_{i_1} - x_{i_1-1})/(x_{i_1+1} - x_{i_1-1})(x_{i_1+1} - x_{i_1})$$

$$d_{1i_1} = (x_{i_1+1} - x_{i_1})/(x_{i_1+1} - x_{i_1-1})(x_{i_1} - x_{i_1-1}) \tag{E11}$$

The potential jump at the first finite difference station downstream of the trailing edge then becomes

$$\Delta\phi_{i_1+1j} = c_{kc1}\,\Delta\phi_{i_1j} + c_{kc2}\Delta\phi_{i_1-1j}$$

$$\text{where } c_{kc1} = 1 - d_{1i_1}/c_{1i_1} - i\omega/c_{1i_1}$$

$$c_{kc2} = d_{1i_1}/c_{1i_1} \tag{E12}$$

The potential jump terms on the right-hand side of equation (E12) are the potential jump terms across the wing at stations forward of the trailing edge.

The potential jump for stations on the wing is given in reference 1 by

$$\Delta\phi_{ij} = \phi_{ijk_m+1} - \phi_{ijk_m} - c_{s1}(\phi_{ijk_m+2} - \phi_{ijk_m+1})$$

$$- c_{s2}(\phi_{ijk_m} - \phi_{ijk_m-1}) - (d_{s1}F_{ij}^{(U)} + d_{s2}F_{ij}^{(L)}) \tag{E13}$$

where

$$c_{s1} = 1/\left(4s_1(s_1 + 1)\right); \quad c_{s2} = 1/\left(4s_2(s_2 + 1)\right);$$

$$d_{s1} = h(2s_1 + 1)/4(s_1 + 1); \quad d_{s2} = h(2s_2 + 1)/4(s_2 + 1);$$

$$s_1 = (z_{k_m+2} - z_{k_m+1})/h; \quad s_2 = (z_{k_m} - z_{k_m-1})/h;$$

$$h = (z_{k_m+1} - z_{k_m})$$

The jump in potential given by equation (E12) at the first finite difference station downstream of the trailing edge is given as follows

$$\begin{aligned}\Delta\phi_{i_1+1j} = {} & A_{11}\phi_{i_1-1jk_m-1} + A_{12}\phi_{i_1-1jk_m} + A_{13}\phi_{i_1-1jk_m+1} \\ & + A_{14}\phi_{i_1-1jk_m+2} + A_{21}\phi_{i_1jk_m-1} + A_{22}\phi_{i_1jk_m} \\ & + A_{23}\phi_{i_1jk_m-1} + A_{24}\phi_{i_1jk_m+2} - c_{kc1}(d_{s1}F^{(U)}_{i_1j} + d_{s2}F^{(L)}_{i_1j}) \\ & - c_{kc2}(d_{s1}F^{(U)}_{i_1-1j} + d_{s2}F^{(L)}_{i_1-1j})\end{aligned} \tag{E14}$$

where

$$A_{11} = c_{kc2}c_{s2}; \quad A_{12} = -c_{kc2}(1 + c_{s2}); \quad A_{13} = c_{kc2}(1 + s_1); \quad A_{14} = -c_{kc2}c_{s1};$$

$$A_{21} = c_{kc1}c_s; \quad A_{22} = -c_{kc1}(1 + c_{s2}); \quad A_{23} = c_{kc1}(1 + c_{s1}); \quad A_{24} = -c_{kc1}c_{s1}$$

As before, for stations below the wing surface and for $i \geq i_1 + 1$, an additional term is added having the form

$$-b_{z_{k_m}}\Delta\phi_{i_1+1j}\exp\left(-i\omega(x_i - x_{i_1+1})\right)$$

for values of y_j that are less than the wingtip station.

For finite difference stations located above the surface for $i > i_1 + 1$ and j less than the tip station value, the additional term to be added is

$$a_{z_{k_m}}\Delta\phi_{i_1+1j}\exp\left(-i\omega(x_i - x_{i_1+1})\right)$$

APPENDIX F

SOURCE AND DOUBLET DISTRIBUTIONS TO BE APPLIED TO THE OUTER MESH BOUNDARIES OF THE FINITE DIFFERENCE REGION FOR A WING

A combination of source and doublet distributions is to be applied to the outer surface of the reduced-size grid network in order to provide a means for matching inner and outer solutions on the grid boundary. The source distribution applied on the surface $z' = \text{constant}$ is given by

$$\varphi_s(x,y,z) = (\exp(i\lambda Mx)/4\pi)\int_{b_1}^{b_2}\int_{a_1}^{a_2}\sigma(x',y')\,\frac{\exp(-i\lambda r)}{r}\,dx'dy' \tag{F1}$$

where $$r^2 = (x'-x)^2 + K(y'-y)^2 + K(z'-z)^2$$

The doublet distribution is defined as

$$\varphi_{dz}(x,y,z) = (\exp(i\lambda Mx)/4\pi)\int_{b_1}^{b_2}\int_{a_1}^{a_2}\mu(x',y')\,\frac{\partial}{\partial z'}\left(\frac{\exp(-i\lambda r)}{r}\right)dx'dy' \tag{F2}$$

which becomes

$$\varphi_{dz}(x,y,z) = -(\exp(i\lambda Mx))\,(K/4\pi)\int_{b_1}^{b_2}\int_{a_1}^{a_2}\frac{\mu(x',y')\,(z'-z)}{r^2}\left(i\lambda + \frac{1}{r}\right)\exp(-i\lambda r)\,dx'dy' \tag{F3}$$

We introduce new variables in order to evaluate the limiting values of the source and doublet expressions when z approaches z'.

We let $$x_1 = (x'-x)\,/\,|z'-z|\;;\; y_1 = (y'-y)\,/\,|z'-z|$$

then $$r^2 = (z'-z)^2 r_o^2 \text{ where } r_o^2 = x_1^2 + Ky_1^2 + K \tag{F4}$$

The limits of the doublet integral are then transformed to

$$\begin{aligned} y_{1u} &= (b_2-y)\,/\,|z'-z|\;;\; x_{1u} = (a_2-x)\,/\,|z'-z| \\ y_{1\ell} &= (b_1-y)\,/\,|z'-z|\;;\; x_{1\ell} = (a_1-x)\,/\,|z'-z| \end{aligned} \tag{F5}$$

and the integral becomes

$$\varphi_{dz}(x,y,z) = -(\exp(i\lambda Mx))\,(K/4\pi)\int_{y_{1\ell}}^{y_{1u}}\int_{x_{1\ell}}^{x_{1u}}\frac{\mu(x+y_1|z'-z|,y+y_1|z'-z|)}{r_o^2}\left(i\lambda|z'-z| + \frac{\operatorname{sgn}|z'-z|}{r_o}\right)dx_1dy_1 \tag{F6}$$

Letting z approach z' for $a_1 < x < a_2$ and $b_1 < y < b_2$, we obtain

$$\varphi_{dz}(x,y,z') = -\exp(i\lambda Mx)\,(K/4\pi)\int_{-\infty}^{\infty}\int_{-\infty}^{\infty}\mu(x,y)\,\operatorname{sgn}|z'-z|\,/r_o^3\,dx_1dy_1 \tag{F7}$$

Integrating with respect to x_1 yields

$$\int_{-\infty}^{\infty}\frac{dx_1}{[x_1^2 + K(y_1^2+1)]^{3/2}} = \frac{x_1}{K(y_1^2+1)\sqrt{x_1^2 + K(y_1^2+1)}}\Bigg|_{-\infty}^{\infty} = \frac{2}{K(y_1^2+1)} \tag{F8}$$

Then integrating with respect to y_1 leads to

$$\varphi_{dz}(x,y,z') = [\exp(i\lambda M x)\ \mu(x,y)\ \mathrm{sgn}(z-z')] / 2 \tag{F9}$$

In a similar fashion the limiting value of the doublet distribution, applied to the $y' =$ constant plane and having y approach y', is given by

$$\varphi_{dz}(x,y',z) = \exp(i\lambda M x)\ \mu(x,z)\ \mathrm{sgn}(y-y') / 2 \tag{F10}$$

Considering the doublet distribution applied to the $x = x'$ surface, we obtain

$$\varphi_{dx}(x,y,z) = -\exp(i\lambda M x)/4\pi \int_{b_1}^{b_2}\int_{c_1}^{c_2} \mu(y',z')\,\frac{(x'-x)}{r^2}\left(i\lambda + \frac{1}{r}\right)\exp(-i\lambda r)dy'dz' \tag{F11}$$

We then make a change in variables to facilitate the process in evaluating the limit as x approaches x'. That is, we define

$$y_1 = (y'-y) / |x'-x| \text{ and } z_1 = (z'-z) / |x'-x| \tag{F12}$$

which changes r^2 to $\quad r^2 = (x'-x)^2\, r_o^2$ where $r_o^2 = 1 + K(y_1^2+z_1^2)$

The integral then becomes

$$\varphi_{dx}(x,y,z) = -\exp(i\lambda M x)/4\pi \int_{y_{1\ell}}^{y_{1u}}\int_{z_{1\ell}}^{z_{1u}} \frac{\mu(y+y_1|x'-x|, z+z_1|x'-x|)}{r_o^2}$$

$$\left(i\lambda|x'-x| + \frac{\mathrm{sgn}(x'-x)}{r_o}\right)\exp(-i\lambda r_o)dy_1dz_1 \tag{F13}$$

where

$$y_{1\ell} = \frac{b_1-y}{|x'-x|};\ y_{1u} = \frac{b_2-y}{|x'-x|}$$

$$z_{1\ell} = \frac{c_1-z}{|x'-x|};\ z_{1u} = \frac{c_2-z}{|x'-x|}$$

Then, letting x approach x' for $b_1 < y < b_2$ and $c_1 < z < c_2$, we obtain

$$\varphi_{dx}(x',y,z) = \frac{-\exp(i\lambda M x)\mu(y,z)}{4\pi}\int_{-\infty}^{\infty}\int_{-\infty}^{\infty}\frac{\mathrm{sgn}(x'-x)}{r_o^3}\,dy_1dz_1 \tag{F14}$$

Integrating with respect to z_1 yields

$$\int_{-\infty}^{\infty}\frac{dz_1}{(Kz_1^2+(Ky_1^2+1))^{3/2}} = \frac{2}{\sqrt{K}(Ky_1^2+1)} \tag{F15}$$

Then integrating with respect to y_1 yields

$$\varphi_{dx}(x',y,z) = \exp(i\lambda M x')\ \mu(y,z)\ \mathrm{sgn}(x-x') / 2K \tag{F16}$$

The potential at a point x, y, z due to a unit source at x', y', z' is given as

$$\psi_s(x'-x,y'-y,z'-z) = \exp(-i\lambda r) / 4\pi r \tag{F17}$$

where $$r^2 = (x'-x)^2 + K(y'-y)^2 + K(z'-z)^2$$

The potential due to a doublet aligned with the x', y', z' planes is then given as

$$\psi_{dx} = \frac{-(x'-x)}{4\pi r^2}\left(i\lambda + \frac{1}{r}\right)\exp(-i\lambda r) \tag{F18}$$

$$\psi_{dy} = \frac{-K(y'-y)}{4\pi r^2}\left(i\lambda + \frac{1}{r}\right)\exp(-i\lambda r) \tag{F19}$$

$$\psi_{dz} = \frac{-K(z'-z)}{4\pi r^2}\left(i\lambda + \frac{1}{r}\right)\exp(-i\lambda r) \tag{F20}$$

We now indicate the potentials at x, y, z due to the distribution on each of the outer surfaces. For the potential at x, y, z due to sources distributed over the forward face, we have

$$S_f(a_1-x,y,z) = \int_{c_1}^{c_2}\int_{b_1}^{b_2} \sigma_f(y',z')\psi_s(a_1-x,y'-y,z'-z)\,dy'dz' \tag{F21}$$

The potential expression due to sources distributed on the downstream face becomes

$$S_r(a_2-x,y,z) = \int_{c_1}^{c_2}\int_{b_1}^{b_2} \sigma_r(y',z')\psi_s(a_2-x,y'-y,z'-z)dy'dz' \tag{F22}$$

For sources distributed on the upper face, the expression becomes

$$S_u(x,y,c_2-z) = \int_{a_1}^{a_2}\int_{b_1}^{b_2} \sigma_u(x',y')\psi_s(x'-x,y'-y,c_2-z)dx'dy' \tag{F23}$$

For sources distributed on the lower surface, the expression for the potential is given as

$$S_d(x,y,c_1-z) = \int_{a_1}^{a_2}\int_{b_1}^{b_2} \sigma_d(x',y')\psi_s(x'-x,y'-y,c_1-z)dx'dy' \tag{F24}$$

For sources distributed on the left-hand outboard face, the potential expression is

$$S_o(x,b_1-y,z) = \int_{a_1}^{a_2}\int_{c_1}^{c_2} \sigma_o(x',z')\psi_s(x'-x,b_1-y,z'-z)dx'dz' \tag{F25}$$

and, for the right-hand side source distribution, the potential is

$$S_o(x,b_2-y,z) = \int_{a_1}^{a_2}\int_{c_1}^{c_2} \sigma_o(x',z')\psi_s(x'-x,b_2-y,z'-z)dx'dz' \tag{F26}$$

Similar expressions may be constructed for the doublet distributions. For example, for the potential due to a doublet distribution applied to the downstream face, we have the expression

$$D_r(a_2-x,y,z) = \int_{c_1}^{c_2}\int_{b_1}^{b_2} \mu_r(y',z')\psi_{dx}(a_2-x,y'-y,z'-z)dy'dz' \tag{F27}$$

The general expression for the potential at a station x, y, z due to source and doublet distributions applied to the external mesh boundaries is given by

$$\begin{aligned}\varphi_o(x,y,z) = \exp(i\lambda \mathrm{M}x) \Big\{ & \mathrm{S}_r(a_2-x,y,z) + \mathrm{S}_t(a_1-x,y,z) + \mathrm{D}_r(a_2-x,y,z) \\ & + \mathrm{D}_t(a_1-x,y,z) + \mathrm{S}_u(x,y,c_2-z) + \mathrm{S}_d(x,y,c_1-z) + \mathrm{D}_u(x,y,c_2-z) \\ & + \mathrm{D}_d(x,y,c_1-z) + \mathrm{S}_{or}(x,b_2-y,z) + \mathrm{S}_{ot}(x,b_1-y,z) \\ & + \mathrm{D}_{or}(x,b_2-y,z) + \mathrm{D}_{ot}(x,b_1-y,z) + \psi_w \Big\} \end{aligned} \tag{F28}$$

where ψ_w is the potential due to the wake.

To obtain the external potential on the upstream face, we note from equation (F16) that $\mathrm{D}_t(a_1-x,y,z) = -\mu(y,z) / 2\mathrm{K}$ for values of $x < a_1$.

Therefore the external potential on the upstream face is given as

$$\begin{aligned}\varphi_o(a_1,y,z) = \exp(i\lambda \mathrm{M}a_1) \Big\{ & \mathrm{S}_r(a_2-a_1,y,z) + \mathrm{S}_t(o,y,z) + \mathrm{D}_r(a_2-a_1,y,z) \\ & - \mu(y,z) / 2\mathrm{K} + \mathrm{S}_u(a_1,y,c_2-z) + \mathrm{S}_d(a_1,y,c_1-z) \\ & + \mathrm{D}_u(a_1,y,c_2-z) + \mathrm{D}_d(a_1,y,c_1-z) + \mathrm{S}_{or}(a_1,b_2-y,z) \\ & + \mathrm{S}_{ot}(a_1,b_1-y,z) + \mathrm{D}_{or}(a_1,b_2-y,z) + \mathrm{D}_{ot}(a_1b_1-y,z) \\ & + \psi_w(a_1,y,z) \Big\} \end{aligned} \tag{F29}$$

In a similar fashion, we evaluate the potential at stations downstream of the forward face and note from equation (F16) that $\mathrm{D}_t = +\mu(y,z) / 2\mathrm{K}$ for values of $x > a_1$ and thus obtain

$$\begin{aligned}\varphi_o(a_1,y,z) = \exp(i\lambda \mathrm{M}a_1) \Big\{ & \mathrm{S}_r(a_2-a_1,y,z) + \mathrm{S}_t(o,y,z) + \mathrm{D}_r(a_2-a_1,y,z) \\ & + \mu_t(y,z) / 2\mathrm{K} + \mathrm{S}_u(a_1,y,c_2-z) + \mathrm{S}_d(a_1,y,c_1-z) \\ & + \mathrm{D}_u(a_1,y,c_2-z) + \mathrm{D}_d(a_1,y,c_1-z) + \mathrm{S}_{or}(a_1,b_2-y,z) \\ & + \mathrm{D}_{ot}(a_1,b_1-y,z) + \mathrm{D}_{or}(a_1,b_2-y,z) \\ & + \mathrm{S}_{ot}(a_1,b_1-y,z) + \psi_w(a_1,y,z) \Big\} \end{aligned} \tag{F30}$$

We now set the external potential on the interior of the grid equal to zero by imposing the boundary condition

$$\varphi_o(a_1+,y,z) = 0 \tag{F31}$$

and couple equation (F31) with equation (F29) to arrive at the potential expression on the outer face as

$$\varphi_o(a_1-,y,z) = -\exp(i\lambda \mathrm{M}a_1)\mu_t(y,z) / \mathrm{K} \tag{F32}$$

which must be used together with the interior potential expression that is set to zero

$$S_r(a_2-a_1,y,z) + S_t(o,y,z) + D_r(a_2-a_1,y,z) + \mu_t(y,z) / 2K$$
$$+ S_u(a_1,y,c_2-z) + S_d(a_1,y,c_1-z) + D_u(a_1,y,c_2-z) + D_d(a_1,y,c_1-z)$$
$$+ D_{ot}(a_1,b_1-y,z) + D_{or}(a_1,b_2-y,z)$$
$$+ S_{or}(a_1,b_2-y,z) + S_{ot}(a_1,b_1-y,z) + \psi_w(a_1,y,z) = 0 \qquad \text{(F33)}$$

The potential is set equal to zero just inside of the downstream face, and we arrive at an expression for the potential on the outer surface of the downstream face given as

$$\varphi_o(a_2+,y,z) = \exp(i\lambda M a_2)\mu_r(y,z) / K \qquad \text{(F34)}$$

subject to the condition defined for the interior potential expression given as

$$S_t(a_1-a_2,y,z) + S_r(o,y,z) - \mu_r(y,z) / 2K + D_t(a_1-a_2,y,z)$$
$$+ S_u(a_2,y,c_2-z) + S_d(a_2,y,c_1-z) + D_u(a_2,y,c_2-z) + D_d(a_2,y,c_1-z)$$
$$+ S_{or}(a_2,b_2-y,z) + S_{ot}(a_2,b_1-y,z) + D_{or}(a_2,b_2-y,z)$$
$$+ D_{ot}(a_2,b_1-y,z) + \psi_w(a_2,y,z) = 0 \qquad \text{(F35)}$$

To obtain similar expressions for the region of the lower grid surface, we employ equation (F9), allowing z to approach c_1 through values of $z<c_1$, which results in the expression for external potential given as

$$\varphi_o(x,y,c_1-) = - \exp(i\lambda Mx)\mu_d(x,y) \qquad \text{(F36)}$$

subject to the condition that the interior potential is zero as defined by

$$S_r(a_2-x,y,c_1) + S_t(a_1-x,y,c_1) + D_r(a_2-x,y,c_1) + D_t(a_1-x,y,c_1)$$
$$+ D_{ot}(x,b_1-y,c_1) + D_{or}(x,b_2-y,c_1)$$
$$+ S_u(x,y,c_2-c_1) + S_d(x,y,o) + D_u(x,y,c_2-c_1) + \mu_d(x,y) / 2$$
$$+ S_{or}(x,b_2-y,c_1) + S_{ot}(x,b_1-y,c_1) + \psi_w(x,y,c_1) \equiv 0 \qquad \text{(F37)}$$

In a similar fashion, the potential (exterior and interior) on the upper surfaces is given by

$$\varphi_o(x,y,c_2+) = \exp(i\lambda Mx)\mu_u(x,y) \qquad \text{(F38)}$$

and subject to having the interior potential set to zero, which is given as

$$S_r(a_2-x,y,c_2) + S_t(a_1-x,y,c_2) + D_r(a_2-x,y,c_2) + D_t(a_1-x,y,c_1)$$
$$+ S_u(x,y,o) + S_d(x,y,c_1-c_2) - \mu_u(x,y) / 2 + D_d(x,y,c_1-c_2)$$
$$+ S_{or}(x,b_2-y,c_2) + S_{ot}(x,b_1-y,c_2) + D_{or}(x,b_2-y,c_2)$$
$$+ D_{ot}(x,b_1-y,c_2) + \psi_w(x,y,c_2) = 0 \qquad \text{(F39)}$$

For the potential (external and internal) at $y = b_2$, we obtain

$$\varphi_o(x,b_2+,z) = \exp(i\lambda \mathrm{M}x)\mu(x,z) \tag{F40}$$

subject to having the internal potential set to zero as defined by

$$\begin{aligned} &\mathrm{S}_r(a_2-x,b_2,z) + \mathrm{S}_t(a_1-x,b_2,z) + \mathrm{D}_r(a_2-x,b_2,z) \\ &+ \mathrm{D}_t(a_1-x,b_2,z) + \mathrm{S}_u(x,b_2,c_2-z) + \mathrm{S}_d(x,b_2,c_1-z) \\ &+ \mathrm{D}_u(x,b_2,c_2-z) + \mathrm{D}_d(x,b_2,c_1-z) + \mathrm{S}_{or}(x,o,z) \\ &+ \mathrm{S}_{ot}(x,b_1-b_2,z) - \mu_{or}(x,z)/2 + \mathrm{D}_{ot}(x,b_1-b_2,z) \\ &+ \psi_w(x,b,z) = 0 \end{aligned} \tag{F41}$$

APPENDIX G

EQUATIONS COUPLING THE POTENTIALS FROM THE SOURCE AND DOUBLET DISTRIBUTIONS TO THE FINITE DIFFERENCE BOUNDARY POTENTIALS

The linear exterior solution is set equal to the interior finite differencing solution by equating potentials and normal derivatives at the boundary that separates the two solution procedures.

The exterior potential that is developed from applying sources and doublets to the exterior boundary of the grid network is defined as ϕ_o.

The potential at a general finite differencing grid station (ijk) of the interior grid network is represented by ϕ_{ijk}.

On the forward boundary face that is located halfway between $x = x_1$ and $x = x_2$, the exterior potential and normal derivative are equated to the interior potential and normal derivative of the finite-differencing solution as follows:

$$\phi_o(a_1,y,z) = (\phi_{2jk} + \phi_{1jk})/2$$

$$\phi_{ox}(a_1,y,z) = (\phi_{2jk} - \phi_{1jk})/(x_2 - x_1) \tag{G1}$$

which is rearranged to a form

$$\phi_{1jk} = \phi_o - \Delta x_1 \phi_{ox}/2$$

$$\phi_{2jk} = \phi_o + \Delta x_1 \phi_{ox}/2 \tag{G2}$$

where $\Delta x_1 = x_2 - x_1$.

The exterior potential ϕ_o is given in the form

$$\phi_o = \exp(i\lambda \mathrm{M} x)\psi_o \tag{G3a}$$

and its derivative is given as

$$\phi_{ox} = \left[(1 - i\lambda \mathrm{M}\Delta x_1/2)\psi_o + \psi_{ox}\right] \exp(i\lambda \mathrm{M} x) \tag{G3b}$$

We substituted equations (G3a) and (G3b) into equation (G2) to produce

$$\phi_{1jk} = \left[(1 - i\lambda \mathrm{M}\Delta x_1/2)\,\psi_o - \Delta x_1\,\psi_{ox}/2\right] \exp(i\lambda \mathrm{M} a_1)$$

$$\phi_{2jk} = \left[(1 + i\lambda \mathrm{M}\Delta x_1/2)\,\psi_o + \Delta x_1\,\psi_{ox}/2\right] \exp(i\lambda \mathrm{M} a_1) \tag{G4}$$

By taking the x derivative of the ϕ_o expression given in equation (F28), ψ_{ox} is obtained. That is,

$$\psi_{ox} = \frac{\partial}{\partial x}\left\{S_t(a_1-x,y,z) + S_r(a_2-x,y,z) + D_t(a_1-x,y,z)\right.$$

$$+ D_r(a_2-x,y,z) + S_u(x,y,c_2-z) + S_d(x,y,c_1-z)$$

$$+ D_u(x,y,c_2-z) + D_d(x,y,c_1-z) + S_{or}(x,b_2-y,z)$$

$$\left. + S_{ot}(x,b_1-y,z) + D_{or}(x,b_2-y,z) + D_{ot}(x,b_1-y,z) + \psi_{wake}\right\} \quad \text{(G5)}$$

All terms of equation (G5) are continuous at $x=a_1$ except the term which takes the form

$$\frac{\partial}{\partial x}\left(S_t(a_1-x,y,z)\right) = - D_t(a_1-x,y,z) \quad \text{(G6)}$$

Since ψ_{ox} vanishes identically inside of the grid region, we obtain the expression for the derivative ψ_{ox} given as

$$\psi_{ox} = \sigma_t(y,z)/K \quad \text{(G7)}$$

as x approaches a_1 through values of x that are less than a_1. For values of $x > a_2$, the derivative expression becomes

$$\psi_{ox} = - \sigma_r(y,z)/K \quad \text{(G8)}$$

Substituting equation (F32) for the definition of $\phi_o\,(a_1,y,z)$ along with the expression for ψ_{ox} of equation (G7) into equation (G4), we obtain the expressions relating the potentials of the finite-differencing grid to the external potentials in the upstream face given as

$$\phi_{1jk} = \left[-(1 - i\lambda M\Delta x_1/2)\mu_t(y_j,z_k) - \Delta x_1\sigma_t(y_j,z_k)/2\right]\exp(i\lambda M a_1)/K$$

$$\phi_{2jk} = \left[-(1 + i\lambda M\Delta x_1/2)\mu_t(y_j,z_k) + \Delta x_1\sigma_t(y_j,z_k)/2\right]\exp(i\lambda M a_1)/K \quad \text{(G9)}$$

To obtain the relationship between external and internal potentials on the downstream face, we equate the potentials and normal derivatives at a plane that lies halfway between $x = x_{i_m}$ and $x = x_{i_m-1}$ as follows:

$$\phi_o(a_2,y_j,z_k) = (\phi_{i_m jk} + \phi_{i_m-1jk})/2$$

$$\phi_{ox}(a_2,y_j,z_k) = (\phi_{i_m jk} - \phi_{i_m-1jk})/(x_{i_m} - x_{i_m-1}) \quad \text{(G10)}$$

which results in

$$\phi_{i_m jk} = \left[(1 + i\lambda M\Delta x_m/2)\psi_o + \Delta x_m \psi_{ox}/2\right] \exp(i\lambda M a_2)$$

$$\phi_{i_m - 1jk} = \left[(1 - i\lambda M\Delta x_m/2)\psi_o - \Delta x_m \psi_{ox}/2\right] \exp(i\lambda M a_2) \quad \text{(G11)}$$

The expressions for the external potential and its derivative (obtained from equations (F34) and (G8)) are inserted into (G11) to produce

$$\phi_{i_m jk} = \left[(1 + i\lambda M\Delta x_m/2)\mu_r(y_j,z_k) - \Delta x_m \sigma_r(y_j,z_k)/2\right] \exp(i\lambda M a_2)/K$$

$$\phi_{i_m - 1jk} = \left[(1 - i\lambda M\Delta x_m/2)\mu_r(y_j,z_k) + \Delta x_m \sigma_r(y_j,z_k)/2\right] \exp(i\lambda M a_2)/K \quad \text{(G12)}$$

The equations applicable to the remaining faces of the network are developed following the above procedures. Solution coupling equations developed for the lower boundary and located on a plane $z = c_1$ situated halfway between the first and second finite-differencing stations $z = z_1$ and $z = z_2$ are given as

$$\phi_o(x_i,y_j,c_1) = (\phi_{ij1} + \phi_{ij2})/2$$

$$\phi_{oz}(x_i,y_j,c_1) = (\phi_{ij2} - \phi_{ij1})/(z_2 - z_1) \quad \text{(G13)}$$

and reorganized into

$$\phi_{ij1} = \phi_o(x_i,y_j,c_1) - \Delta z_1 \phi_{oz}(x_i,y_j,c_1)/2$$

$$\phi_{ij2} = \phi_o(x_i,y_j,c_1) + \Delta z_1 \phi_{oz}(x_i,y_j,c_1)/2 \quad \text{(G14)}$$

where $\Delta z_1 = z_2 - z_1$.

The potential derivative, ϕ_{oz}, is obtained by taking the derivative of equation (F28) with respect to z.

$$\frac{\partial}{\partial z}\phi_o(x,y,z) = \exp(i\lambda Mx)\frac{\partial}{\partial z}\left\{S_r(a_2 - x,y,z) + S_\ell(a_1 - x,y,z)\right.$$

$$+ D_r(a_2 - x,y,z) + D_\ell(a_1 - x,y,z) + S_u(x,y,c_2 - z) + S_d(x,y,c_1 - z)$$

$$+ D_u(x,y,c_2 - z) + D_d(x,y,c_1 - z) + S_{or}(x,b_2 - y,z) + S_{o\ell}(x,b_1 - y,z)$$

$$\left. + D_{or}(x,b_2 - y,z) + D_{o\ell}(x,b_1 - y,z) + \psi_w\right\} \quad \text{(G15)}$$

All derivatives of equation (G15) are continuous across the boundary, with the exception of

$$\frac{\partial}{\partial z} S_d(x,y,c_1 - z) = - D_d(x,y,c_1 - z) \tag{G16}$$

which is evaluated using equation (F9) with $\sigma(x,y)$ replaced by $\mu(x,y)$. On the inside of the network, ϕ_{oz} is set to zero, and this allows the derivative on the outside to be given as

$$\phi_{oz} = \exp(i\lambda \mathrm{M} x)\sigma(x,y) \tag{G17}$$

The potential on the outside of the lower surface is given by equation (F36) as

$$\phi_o = - \exp(i\lambda \mathrm{M} x)\mu_d(x,y) \tag{G18}$$

Inserting (G17) and (G18) into (G14) yields

$$\begin{aligned} \phi_{ij1} &= \left[- \mu_d(x_i,y_j) - \Delta z_1 \sigma_d(x_i,y_j)/2 \right] \exp(i\lambda \mathrm{M} x_i) \\ \phi_{ij2} &= \left[- \mu_d(x_i,y_j) + \Delta z_1 \sigma_d(x_i,y_j)/2 \right] \exp(i\lambda \mathrm{M} x_i) \end{aligned} \tag{G19}$$

Coupling equations applicable to the upper boundary are determined in a similar manner. The upper boundary is located on the plane $z = c_2$ situated halfway between the two top finite-differencing stations $z = z_{k_m}$ and $z = z_{k_m - 1}$ (where k_m represents the maximum value of k). The boundary equations are given as

$$\begin{aligned} \phi_o(x_i,y_j,c_2) &= (\phi_{ijk_m} + \phi_{ijk_m{}^{-1}})/2 \\ \phi_{oz}(x_i,y_j,c_2) &= (\phi_{ijk_m} - \phi_{ijk_m{}^{-1}})/(z_{k_m} - z_{k_m{}^{-1}}) \end{aligned} \tag{G20}$$

from which we obtain

$$\begin{aligned} \phi_{ijk_m} &= \phi_o + \Delta z_m \phi_{oz}/2 \\ \phi_{ijk_m{}^{-1}} &= \phi_o - \Delta z_m \phi_{oz}/2 \\ \Delta z_m &= z_{k_m} - z_{k_m{}^{-1}} \end{aligned} \tag{G21}$$

The derivative of the external potential is evaluated by taking the derivative of the potential equation (F28) with respect to z and noting that all derivatives are continuous across the upper boundary except for the derivative defined by

$$\frac{\partial}{\partial z} S_u(x,y,c_2).$$

This term is evaluated using the relationship

$$\frac{\partial}{\partial z} S_u = - D_u$$

of equation (F9) where $\mu(x,y)$ is replaced by $\sigma(x,y)$ in (F9). Using an additional condition that the derivative on the inside of the grid is identically zero, we then have the result that the derivative of the potential in the region exterior of the grid becomes

$$\phi_{oz} = - \exp(i\lambda M x_i)\sigma_u(x_i,y_j)$$

with the external potential $\phi_o(x,y,c_2)$ given in equation (F38) by $\phi_o(x,y,c_2) = \exp(i\lambda M x_i)\ \mu_u(x_i y_j)$.

The above external potential and derivative are inserted into equation (G21) to produce relationships between the finite-differencing potentials and the exterior potentials on the upper boundary, which are given as

$$\phi_{ijk_m} = \left[\mu_u(x_i,y_j) - \Delta z_m \sigma_u(x_i,y_j)/2\right] \exp(i\lambda M x_i)$$

$$\phi_{ijk_m^{-1}} = \left[\mu_u(x_i,y_j) + \Delta z_m \sigma_u(x_i,y_j)/2\right] \exp(i\lambda M x_i) \qquad \text{(G22)}$$

Coupling equations applicable to the outboard boundary are developed on a plane defined as $y = b_2$ that is situated halfway between $y = y_{j_m}$ and $y = y_{j_m^{-1}}$. The equations that provide continuity between potentials and normal derivatives of the interior and exterior regions are given by

$$\phi_o(x_i,b_2,z_k) = (\phi_{ij_m k} + \phi_{ij_m^{-1}k})/2$$

$$\phi_{oy}(x_i,b_2,z_k) = (\phi_{ij_m k} - \phi_{ij_m^{-1}k})/(y_{j_m} - y_{j_m^{-1}}) \qquad \text{(G23)}$$

which may be reorganized into the form

$$\phi_{ij_m k} = \phi_o + \Delta y_m \phi_{oy}/2$$

$$\phi_{ij_m^{-1}k} = \phi_o - \Delta y_m \phi_{oy}/2 \qquad \text{(G24)}$$

where $\Delta y_m = y_{j_m} - y_{j_m^{-1}}$.

From equation (F10), with the conditions that

$$\frac{\partial}{\partial y} S_{or} = - D_{or}$$

and the interior derivative is zero, we obtain boundary conditions for the outboard boundary defined as

$$\phi_{ij_m k} = \left[\mu_o(x_i,z_k) - \Delta y_m \sigma_o(x_i,z_k)/2\right] \exp(i\lambda M x_i)$$

$$\phi_{ij_m - 1k} = \left[\mu_o(x_i,z_k) + \Delta y_m \sigma_o(x_i,z_k)/2\right] \exp(i\lambda M x_i) \qquad \text{(G25)}$$

The wing is assumed to be symmetrical about the wing root chord at $y = 0$. Thus, we combine and simplify some of the integrals. For example, on the aft boundary at $x = a_2$, the integral for the potential due to a source distribution applied to the aft boundary face is expressed as

$$S_r(a_2-x,y,z) = \int_{c_1}^{c_2}\int_{o}^{b_2} \sigma_r(y',z') \left[\psi_s(a_2-x,y'-y,z'-z) + \psi_s(a_2-x,y'+y,z'-z)\right] dy'dz' \qquad \text{(G26)}$$

Redefining the inner expression to

$$\psi_{ss}(a_2-x,y',y,z'-z) = \psi_s(a_2-x,y'-y,z'-z) + \psi_s(a_2-x,y'+y,z'-z) \qquad \text{(G27)}$$

we obtain the above integral in the form

$$S_r(a_2-x,y,z) = \int_{c_1}^{c_2}\int_{o}^{b_2} \sigma_r(y',z')\, \psi_{ss}(a_2-x,y',y,z'-z)dy'dz' \qquad \text{(G28)}$$

The other potential integrals may be put in a similar form as indicated by the following.

$$S_t(a_1-x,y,z) = \int_{c_1}^{c_2}\int_{o}^{b_2} \sigma_t(y',z')\, \psi_{ss}(a_1-x,y',y,z'-z)dy'dz'$$

$$S_u(x,y,c_2-z) = \int_{a_1}^{a_2}\int_{o}^{b_2} \sigma_u(x',y')\, \psi_{ss}(x'-x,y',y,c_2-z)dy'dx'$$

$$S_d(x,y,c_1-z) = \int_{a_1}^{a_2}\int_{o}^{b} \sigma_d(x',y')\, \psi_{ss}(x'-x,y',y,c_1-z)dy'dx' \qquad \text{(G29)}$$

For convenience, we retain separate source and doublet relations for the outboard boundary faces located at $y = b_1$ and $y = b_2$ and note that

$$\sigma_{ot}(x',z') = \sigma_{or}(x',z') = \sigma_o(x',z')$$

$$\mu_{ot}(x',z') = \mu_{or}(x',z') = \mu_o(x',z') \qquad \text{(G30)}$$

We represent the distribution of sources and doublets applied to the external boundaries by a combination of global functions that are sectionally continuous over each outer boundary face. The applied source distributions are represented by

$$\sigma_t(y',z') = \sum_{n=1}^{NL} \alpha_n^t f_n^t(y',z')$$

$$\sigma_r(y',z') = \sum_{n=1}^{NR} \alpha_n^r f_n^r(y',z')$$

$$\sigma_d(x\ ,y') = \sum_{n=1}^{ND} \alpha_n^d f_n^d(x',y')$$

$$\sigma_u(x',y') = \sum_{n=1}^{NU} \alpha_n^u f_n^u(x',y')$$

$$\sigma_o(x',z') = \sum_{n=1}^{NO} \alpha_n^o f_n^o(x',z') \qquad \text{(G31)}$$

The doublet distributions applied to the individual boundary faces are defined as

$$\mu_f(y',z') = \sum_{n=1}^{NL} \beta_n^f f_n^f(y',z')$$

$$\mu_r(y',z') = \sum_{n=1}^{NR} \beta_n^r f_n^r(y',z')$$

$$\mu_d(x',y') = \sum_{n=1}^{ND} \beta_n^d f_n^d(x',y')$$

$$\mu_u(x',y') = \sum_{n=1}^{NU} \beta_n^u f_n^u(x',y')$$

$$\mu_o(x',z') = \sum_{n=1}^{NO} \beta_n^o f_n^o(x',z') \qquad \text{(G32)}$$

where α and β quantities are parameters to be determined to satisfy the boundary conditions on the five faces of the reduced-size grid boundary.

Doublet integrals may now be developed in the manner corresponding to the S integrals ((G28) and (G29)) having source distributions defined by (G27). For example, the potential due to the doublet distribution applied to the aft boundary face is defined as

$$D_r(a_2 - x,y,z) = \int_{c_1}^{c_2}\int_{o}^{b_2} \mu_r(y',z') \left[\psi_{dx}(a_2-x,y'-y,z'-z) + \psi_{dx}(a_2-x,y'+y,z'-z)\right]dy'dz'$$

which is rewritten as

$$D_r(a_2-x,y,z) = \int_{c_1}^{c_2}\int_{o}^{b_2} \mu_r(y',z')\psi_{sx}(a_2-x,y',y,z'-z)dy'dz' \qquad \text{(G33)}$$

where

$$\psi_{sx}(a_2-x,y',y,z'-z) = \psi_{dx}(a_2-x,y'-y,z'-z) + \psi_{dx}(a_2-x,y'+y,z'-z)$$

The remaining potential expressions are described in a similar fashion.

In order to shorten the notation, the integrals of the global functions are designated as follows:

$$W_n^f(a_1-x,y,z) = \int_{c_1}^{c_2}\int_{o}^{b_2} f_n^f(y',z')\,\psi_{ss}(a_1-x,y',y,z'-z)dy'dz'$$

$$W_n^r(a_2-x,y,z) = \int_{c_1}^{c_2}\int_{o}^{b_2} f_n^r(y',z')\,\psi_{ss}(a_2-x,y',y,z'-z)dy'dz'$$

$$W_n^d(x,y,c_1-z) = \int_{a_1}^{a_2}\int_{o}^{b_2} f_n^d(x',y')\,\psi_{ss}(x'-x,y'y,c_1-z)dy'dx'$$

$$W_n^u(x,y,c_2-z) = \int_{a_1}^{a_2}\int_{o}^{b_2} f_n^u(x',y')\,\psi_{ss}(x'-x,y',y,c_2-z)dy'dx'$$

$$W_n^{or}(x,b_2-y,z) = \int_{a_1}^{a_2}\int_{c_1}^{c_2} f_n^{or}(x',z')\,\psi_{ss}(x'-x,b_2-y,z'-z)dz'dx'$$

$$W_n^{of}(x,b_1-y,z) = \int_{a_1}^{a_2}\int_{c_1}^{c_2} f_n^{of}(x',z')\,\psi_{ss}(x'-x,b_1-y,z'-z)dz'dx' \qquad \text{(G34)}$$

Similar expressions may be constructed for the doublet distributions; for example, the potential due to the global sheet of doublets applied to the aft boundary face is given by

$$V_n^r(a_2-x,y,z) = \int_{c_1}^{c_2}\int_o^{b_2} f_n^r(y',z')\,\psi_{sx}(a_2-x,y',y,z'-z)dy'dz' \tag{G35}$$

The source integral then becomes (for the aft face boundary)

$$S_r(a_2-x,y,z) = \sum_{n=1}^{NR} \alpha_n^r W_n^r(a_2-x,y,z) \tag{G36}$$

and the doublet integral becomes

$$D_r(a_2-x,y,z) = \sum_{n=1}^{NR} \beta_n^r V_n^r(a_2-x,y,z) \tag{G37}$$

The boundary condition equations of equations (F32) and (F33) are revised to include the above notation to describe the potentials on either side of the upstream boundary face:

for $x < a_1$,

$$\phi_o(a_1,y,z) = -\exp(i\lambda Ma_1)\mu_t(y,z)/K \tag{G38}$$

for $x > a_1$,

$$\begin{aligned}\psi_o(a_1,y,z) = &\sum_{n=1}^{NL} \alpha_n^t W_n^t(o,y,z) + \sum_{n=1}^{NR} \alpha_n^r W_n^r(a_2-a_1,y,z) \\ &+ \sum_{n=1}^{ND} \alpha_n^d W_n^d(a_1,y,c_1-z) + \sum_{n=1}^{NU} \alpha_n^u W_n^u(a_1,y,c_2-z) \\ &+ \sum_{n=1}^{NL} \beta_n^t f_n^t(y,z)/2K + \sum_{n=1}^{NR} \beta_n^r V_n^r(a_2-a_1,y,z) + \sum_{n=1}^{ND} \beta_n^d V_n^d(a_1,y,c_1-z) \\ &+ \sum_{n=1}^{NU} \beta_n^u V_n^u(a_1,y,c_2-z) + \sum_{n=1}^{NO} \alpha_n^o \left[W_n^o(a_1,b_2-y,z) + W_n^o(a_1,b_1-y,z)\right] \\ &+ \sum_{n=1}^{NO} \beta_n^o \left[V_n^o(a_1,b_2-y,z) + V_n^o(a_1,b_1-y,z)\right] + \psi_w(a_1,y,z) = 0\end{aligned} \tag{G39}$$

Equations (F34) and (F35), which describe the potentials on either side of the downstream or aft boundary face, are revised as follows:

for $x > a_2$,

$$\phi_o(a_2,y,z) = \exp(i\lambda Ma_2)\mu_r(y,z)/K \tag{G40}$$

for $x < a_2$,

$$\psi_o(a_2,y,z) = \sum_{n=1}^{NL} \alpha_n^l W_n^l (a_1-a_2,y,z) + \sum_{n=1}^{NR} \alpha_n^r W_n^r (o,y,z)$$

$$+ \sum_{n=1}^{ND} \alpha_n^d W_n^d (a_2,y,c_1-z) + \sum_{n=1}^{NU} \alpha_n^u W_n^u (a_2,y,c_2-z) + \sum_{n=1}^{NL} \beta_n^l V_n^l (a_1-a_2,y,z)$$

$$- \sum_{n=1}^{NR} \beta_n^r f_n^r (y,z)/2K + \sum_{n=1}^{ND} \beta_n^d V_n^d (a_2,y,c_1-z) + \sum_{n=1}^{NU} \beta_n^u V_n^u (a_2,y,c_2-z)$$

$$+ \sum_{n=1}^{NO} \alpha_n^o \left[W_n^o (a_2,b_2-y,z) + W_n^o (a_2,b_1-y,z) \right]$$

$$+ \sum_{n=1}^{NO} \beta_n^o \left[V_n^o (a_2,b_2-y,z) + V_n^o (a_2,b_1-y,z) \right] + \psi_w(a_2,y,z) = 0 \qquad \text{(G41)}$$

Equations (F36) and (F37), which describe the potentials on either side of the lower boundary, are revised into the following forms:

for $z < c_1$,

$$\psi_o(x,y,c_1) = - \mu_d(x,y) \qquad \text{(G42)}$$

for $z > c_1$,

$$\psi_o(x,y,c_1) = \sum_{n=1}^{NL} \alpha_n^l W_n^l (a_1-x,y,c_1) + \sum_{n=1}^{NR} \alpha_n^r W_n^r (a_2-x,y,c_1)$$

$$+ \sum_{n=1}^{ND} \alpha_n^d W_n^d (x,y,0) + \sum_{n=1}^{NU} \alpha_n^u W_n^u (x,y,c_2-c_1) + \sum_{n=1}^{NL} \beta_n^l V_n^l (a_1-x,y,c_1)$$

$$+ \sum_{n=1}^{NR} \beta_n^r V_n^r (a_2-x,y,c_1) + \sum_{n=1}^{ND} \beta_n^d f_n^d (x,y)/2 + \sum_{n=1}^{NU} \beta_n^u V_n^u (x,y,c_2-c_1)$$

$$+ \sum_{n=1}^{NO} \alpha_n^o \left[W_n^o (x,b_2-y,c_1) + W_n^o (x,b_1-y,c_1) \right]$$

$$+ \sum_{n=1}^{NO} \beta_n^o \left[V_n^o (x,b_2-y,c_1) + V_n^o (x,b_1-y,c_1) \right] + \psi_w(x,y,c_1) = 0 \qquad \text{(G43)}$$

Potentials on either side of the upper boundary face defined by equations (F38) and (F39) are revised to the following forms:

for $z > c_2$,

$$\psi_o(x,y,c_2) = \mu_u(x,y) \tag{G44}$$

for $z < c_2$,

$$\begin{aligned}\psi_o(x,y,c_2) = &\sum_{n=1}^{NL} \alpha_n^l \mathrm{W}_n^l(a_1-x,y,c_2) + \sum_{n=1}^{NR} \alpha_n^r \mathrm{W}_n^r(a_2-x,y,c_2) \\ &+ \sum_{n=1}^{ND} \alpha_n^d \mathrm{W}_n^d(x,y,c_1-c_2) + \sum_{n=1}^{NU} \alpha_n^u \mathrm{W}_n^u(x,y,0) + \sum_{n=1}^{NL} \beta_n^l \mathrm{V}_n^l(a_1-x,y,c_2) \\ &+ \sum_{n=1}^{NR} \beta_n^r \mathrm{V}_n^r(a_2-x,y,c_2) + \sum_{n=1}^{ND} \beta_n^d \mathrm{V}_n^d(x,y,c_1-c_2) - \sum_{n=1}^{NU} \beta_n^u f_n^u(x,y)/2 \\ &+ \sum_{n=1}^{NO} \alpha_n^o \left[\mathrm{W}_n^o(x,b_2-y,c_2) + \mathrm{W}_n^o(x,b_1-y,c_2)\right] \\ &+ \sum_{n=1}^{NO} \beta_n^o \left[\mathrm{V}_n^o(x,b_1-y,c_2) + \mathrm{V}_n^o(x,b_1-y,c_2)\right] + \psi_w(x,y,c_2) = 0\end{aligned} \tag{G45}$$

Equations (F40) and (F41) are also reformatted into the following forms:

for $y > b_2$,

$$\psi_o(x,b_2,z) = \mu_o(x,z) \tag{G46}$$

for $y < b_2$,

$$\begin{aligned}\psi_o(x,b_2,z) = &\sum_{n=1}^{NL} \alpha_n^l \mathrm{W}_n^l(a_1-x,b_2,z) + \sum_{n=1}^{NR} \alpha_n^r \mathrm{W}_n^r(a_2-x,b_2,z) \\ &+ \sum_{n=1}^{ND} \alpha_n^d \mathrm{W}_n^d(x,b_2,c_1-z) + \sum_{n=1}^{NU} \alpha_n^u \mathrm{W}_n^u(x,b_2,c_2-z) + \sum_{n=1}^{NL} \beta_n^l \mathrm{V}_n^l(a_1-x,b_2,z) \\ &+ \sum_{n=1}^{NR} \beta_n^r \mathrm{V}_n^r(a_2-x,b_2,z) + \sum_{n=1}^{ND} \beta_n^d \mathrm{V}_n^d(x,b_2,c_1-z) + \sum_{n=1}^{NU} \beta_n^u \mathrm{V}_n^u(x,b_2,c_2-z) \\ &+ \sum_{n=1}^{NO} \alpha_n^o \left[\mathrm{W}_n^o(x,o,z) + \mathrm{W}_n^o(x,b_1-b_2,z)\right] \\ &+ \sum_{n=1}^{NO} \beta_n^o \left[\mathrm{V}_n^o(x,b_1-b_2,z) - f_n^o(x,z)/2\right] + \psi_w(x,b_2,z) = 0\end{aligned} \tag{G47}$$

The expressions associated with boundary conditions and relating the finite differencing values to the exterior potentials are now written using the above α and β variables.

We now define new constants to shorten the equation writeup; that is, we let

$$c_1 = 1 + i\lambda M\Delta x_1/2$$

$$\bar{c}_1 = 1 - i\lambda M\Delta x_1/2$$

$$c_2 = 1 + i\lambda M\Delta x_m/2$$

$$\bar{c}_2 = 1 - i\lambda M\Delta x_m/2 \tag{G48}$$

Then the coupling equations applicable to the left-hand boundary as defined by equation (G9) are reformatted into

$$\phi_{1jk} = - \exp(i\lambda M a_1) \sum_{n=1}^{NL} (\bar{c}_1\beta_n^l + \Delta x_1\alpha_n^l/2) f_n^l(y_j,z_k)/K \tag{G49a}$$

$$\phi_{2jk} = - \exp(i\lambda M a_1) \sum_{n=1}^{NL} (c_1\beta_n^l - \Delta x_1\alpha_n^l/2) f_n^l(y_j,z_k)/K \tag{G49b}$$

Downstream boundary coupling equations defined in equation (G12) are revised to include the α and β definitions which now take the form

$$\phi_{i_m jk} = \exp(i\lambda M a_2) \sum_{n=1}^{NR} (c_2\beta_n^r - \Delta x_m\alpha_n^r/2) f_n^r(y_j,z_k)/K \tag{G50a}$$

$$\phi_{i_m-1jk} = \exp(i\lambda M a_2) \sum_{n=1}^{NR} (\bar{c}_2\beta_n^r + \Delta x_m\alpha_n^r/2) f_n^r(y_j,z_k)/K \tag{G50b}$$

The lower surface boundary conditions described by equation (G19) are revised into the following forms.

$$\phi_{ij2} = \exp(i\lambda M x_i) \sum_{n=1}^{ND} (- \beta_n^d + \Delta z_1 \alpha_n^d/2) f_n^d(x_i,y_j) \tag{G51a}$$

$$\phi_{ij1} = \exp(i\lambda M x_i) \sum_{n=1}^{ND} (- \beta_n^d - \Delta z_1 \alpha_n^d/2) f_n^d(x_i,y_j) \tag{G51b}$$

Coupling equations applicable to the upper boundary face are changed from the form given by equation (G22) into the following expressions.

$$\phi_{ijk_m} = \exp(i\lambda M x_i) \sum_{n=1}^{NU} (\beta_n^u - \Delta z_m \alpha_n^u/2) f_n^u(x_i,y_j) \tag{G52a}$$

$$\phi_{ijk_m-1} = \exp(i\lambda M x_i) \sum_{n=1}^{NU} (\beta_n^u + \Delta z_m \alpha_n^u/2) f_n^u(x_i,y_j) \tag{G52b}$$

The boundary conditions to be satisfied on the outboard face are now defined as

$$\phi_{ij_m k} = \exp(i\lambda M x_i) \sum_{n=1}^{NO} (\beta_n^o - \Delta y_m \alpha_n^o/2) f_n^o(x_i, z_k) \tag{G53a}$$

$$\phi_{ij_m{}^{-1}k} = \exp(i\lambda M x_i) \sum_{n=1}^{NO} (\beta_n^o + \Delta y_m \alpha_n^o/2) f_n^o(x_i, z_k) \tag{G53b}$$

APPENDIX H

EQUATIONS FOR THE EXTERNAL APPLIED POTENTIAL USING A LEAST SQUARES APPROACH

The grid network is composed of $(i_m)(j_m)(k_m)$ grid stations. The boundaries that separate exterior and interior solution regions are located between the first two and last two grid stations of each coordinate axis; that is, the forward boundary is located halfway between the grid stations x_1 and x_2; the aft boundary is located halfway between x_{j_m-1} and x_{j_m}; the lower boundary is located between z_1 and z_2; the upper boundary is located between z_{k_m-1} and z_{k_m}; and the outboard boundary is located between y_{j_m-1} and y_{j_m}.

Boundary equations (G49a), (G50a), (G51b), (G52a), and (G53a) are used to eliminate the potential equations of the finite differencing grid that are exterior of the boundaries. This results in $(i_m-2)(j_m-2)(k_m-2)$ potentials to be evaluated for the finite differencing grid. There are 2(NL+NR+NU+ND+NO) parameters associated with the source and doublet distributions applied to the exterior boundary that need to be evaluated. Potentials are specified for the interior finite differencing grid stations that are directly adjacent to the boundaries, as indicated by equations (G49b), (G50b), (G51a), (G52b), and (G53b), which make up a total number of equations indicated by $2(i_m-)(j_m-2) + 2(j_m-2)(k_m-2) + (i_m-2)(k_m-2)$.

The global distributions of sources and doublets applied to the boundary exterior have strengths that are determined using least-squares error procedures. For convenience, we define a new set of functions that describes the boundary conditions of equations (G49b), G50b), (G51a), (G52b), and (G53b) in the form

$$\psi_{2jk} = \phi_{2jk} + \exp(i\lambda \mathrm{M} a_1)\sum_{n=1}^{NL}(c_1\beta_n^t - \Delta x_1\alpha_n^t/2)\, f_n^t(y_j,z_k)/\mathrm{K} = 0$$

$$\psi_{i_m-1jk} = -\phi_{i_m-1jk} + \exp(i\lambda \mathrm{M} a_2)\sum_{n=1}^{NR}(\bar{c}_2\beta_n^r + \Delta x_m\alpha_n^r/2)\, f_n^r(y_j,z_k)/\mathrm{K} = 0$$

$$\psi_{ij2} = -\phi_{ij2} + \exp(i\lambda \mathrm{M} x_i)\sum_{n=1}^{ND}(-\beta_n^d + \Delta z_1\alpha_n^d/2)\, f_n^d(x_i,y_j) = 0$$

$$\psi_{ijk_m-1} = -\phi_{ijk_m-1} + \exp(i\lambda \mathrm{M} x_i)\sum_{n=1}^{NU}(\beta_n^u + \Delta z_m\alpha_n^u/2)\, f_n^u(x_i,y_j) = 0$$

$$\psi_{ij_m-1k} = -\phi_{ij_m-1k} + \exp(i\lambda \mathrm{M} x_i)\sum_{n=1}^{NO}(\beta_n^o + \Delta y_m\alpha_n^o/2)\, f_n^o(x_i,z_k) = 0 \qquad \text{(H1)}$$

We now apply a least-squares approach to obtain the best approximation to the boundary conditions. The stations used in the least-squares approximation are defined to be located at x_t, y_m, z_n and do not necessarily coincide with the mesh grid points. The function to be minimized is developed by combining the sums of the squares of equations (G39), (G41), (G43), (G45), (G47), and (H1). This leads to

$$F(\alpha,\beta) = \sum_{m,n} \psi_o^2(a_1,y_m,z_n) + \sum_{m,n} \psi_0^2(a_2,y_m,z_n) + \sum_{t,m} \psi_o^2(x_t,y_m,c_1)$$

$$+ \sum_{t,m} \psi_o^2(x,y_m,c_2) + \sum_{t,n} \psi_0^2(x_t,b_2,z_n) + \sum_{i=2}^{i_m^{-1}} \sum_{k=2}^{k_m^{-1}} \psi_{ij_m^{-1}k}^2$$

$$+ \sum_{j=2}^{j_m^{-1}} \sum_{k=2}^{k_m^{-1}} (\psi_{2jk}^2 + \psi_{i_m^{-1}jk}^2) + \sum_{i=2}^{i_m^{-1}} \sum_{j=2}^{j_m^{-1}} (\psi_{ijk_m^{-1}}^2 + \psi_{ij2}^2) = 0 \qquad \text{(H2)}$$

The function $F(\alpha,\beta)$ is minimized by equating the partial derivatives with respect to α and β to zero. The number of equations developed within this procedure is 2(NL+NR+ND+NU+NO), which provides for a system of equations that is determinate.

The variables are numbered for purposes of computation. A single variable, σ_k, is designated to represent both source and doublet parameters.

Thus for source parameters α, we have the following α to σ_k correspondence.

α_n^l; for n = 1 *to* NL	σ_k; for k = 1 *to* NL
α_n^r; for n = 1 *to* NR	σ_k; for k = NL + 1 *to* NL + NR
α_n^d; for n = 1 *to* ND	σ_k; for k = NL + NR + 1 *to* NL + NR + ND
α_n^u; for n = 1 *to* NU	σ_k; for k = NL + NR + ND + 1 *to* NL + NR + ND + NU
α_n^o; for n = 1 *to* NO	σ_k; for k = NL + NR + ND + NU + 1 *to* NS (H3)

For the doublet parameters β, we have the β to σ_k relationship designated as

β_n^l; for n = 1 *to* NL	σ_k; for k = NS + 1 *to* NS + NL
β_n^r; for n = 1 *to* NR	σ_k; for k = NS + NL + 1 *to* NS + NL + NR
β_n^d; for n = 1 *to* ND	σ_k; for k = NS + NL + NR + 1 *to* NS + NL + NR + ND
β_n^u; for n = 1 *to* NU	σ_k; for k = NS + NL + NR + ND + 1 *to* NS + NL + ND + NR + NU
β_n^o; for n = 1 *to* NO	σ_k; for k = NS + NL + NR + ND + NU + 1 *to* 2NS (H4)

Interior potentials of equations (G39), (G41), (G43), (G45), and (G47) are put in a more compact form associated with new coefficients defined in the following equation set.

$$\psi_o(a_1,y,z) = \sum_{k=1}^{2NS} \sigma_k\, a_{1k}(y,z) + \psi_w(a_1,y,z)$$

$$\psi_o(a_2,y,z) = \sum_{k=1}^{2NS} \sigma_k\, a_{2k}(y,z) + \psi_w(a_2,y,z)$$

$$\psi_o(x,y,c_1) = \sum_{k=1}^{2NS} \sigma_k\, a_{3k}(x,y) + \psi_w(x,y,c_1)$$

$$\psi_o(x,y,c_2) = \sum_{k=1}^{2NS} \sigma_k\, a_{4k}(x,y) + \psi_w(x,y,c_2)$$

$$\psi_o(x,b_2,z) = \sum_{k=1}^{2NS} \sigma_k\, a_{5k}(x,z) + \psi_w(x,b_2,z) \qquad \text{(H5)}$$

The arrays a_{1k},a_{2k},a_{3k},a_{4k}, and a_{5k}, are defined in terms of the source and doublet integrals by the chart in Appendix I.

The equation set of (H1) is also revised to shorten the notation by letting

$$n1 = n; \quad n2 = \mathrm{NL} + n; \quad n3 = \mathrm{NL} + \mathrm{NR} + n$$

$$n4 = \mathrm{NL} + \mathrm{NR} + \mathrm{ND} + n; \quad n5 = \mathrm{NL} + \mathrm{NR} + \mathrm{ND} + \mathrm{NU} + n$$

$$c3 = \Delta x_1/2; \quad c4 = \Delta x_m/2; \quad c5 = \Delta z_1/2$$

$$c6 = \Delta z_m/2; \quad c7 = \Delta y_m/2 \qquad \text{(H6)}$$

Thus the equations of (H1) are redefined as

$$\psi_{2jk} = \phi_{2jk} + \exp(i\lambda \mathrm{Ma}_1) \sum_{n=1}^{NI} (c_1\sigma_{NS+n1} - c_3\sigma_{n1})\, f_n^t(y_j,z_k)/\mathrm{K}$$

$$\psi_{i_m-1jk} = -\phi_{i_m-1jk} + \exp(i\lambda \mathrm{Ma}_2) \sum_{n=1}^{NR} (\bar{c}_2\sigma_{NS+n2} + c_4\sigma_{n2})\, f_n^r(y_j,z_k)/\mathrm{K}$$

$$\psi_{ij2} = -\phi_{ij2} + \exp(i\lambda \mathrm{Mx}_i) \sum_{n=1}^{ND} (-\sigma_{NS+n3} + c_5\sigma_{n3})\, f_n^d(x_i,y_j)$$

$$\psi_{ijk_m-1} = -\phi_{ijk_m-1} + \exp(i\lambda \mathrm{Mx}_i) \sum_{n=1}^{NU} (\sigma_{NS+n4} + c_6\sigma_{n4})\, f_n^u(x_i,y_j)$$

$$\psi_{ij_m-1k} = -\phi_{ij_m-1k} + \exp(i\lambda \mathrm{Mx}_i) \sum_{n=1}^{NO} (\sigma_{NS+n5} + c_7\sigma_{n5})\, f_n^o(x_i,z_k) \qquad \text{(H7)}$$

Equation (H2) is separated into two parts for convenience in taking the respective derivatives. Equation (H2) is redefined as

$$F(\sigma) = F_1(\sigma) + F_2(\sigma)$$

where $F_1(\sigma)$ represents the sum of the squares of the terms that vanish on the interior of the grid boundary; that is,

$$F_1(\sigma) = \sum_{m,n} \psi_o^2(a_1, y_m, z_n) + \sum_{m,n} \psi_o^2(a_2, y_m, z_n)$$

$$+ \sum_{\ell,m} \psi_o^2(x_\ell, y_m c_1) + \sum_{\ell,m} \psi_o^2(x_\ell, y_m, c_2) + \sum_{\ell,n} \psi_o^2(x_\ell, b_2, z_n) \tag{H8}$$

And $F_2(\sigma)$ represents the sum of the squares of the terms that provide continuity between inner and outer potentials at the boundary of the grid; that is,

$$F_2(\sigma) = \sum_{j=2}^{j_m-1} \sum_{k=2}^{k_m-1} (\psi_{2jk}^2 + \psi_{i_m-1jk}^2)$$

$$+ \sum_{i=2}^{i_m-1} \sum_{j=2}^{j_m-1} (\psi_{ijk_m-1}^2 + \psi_{ij2}^2) + \sum_{i=2}^{i_m-1} \sum_{k=2}^{k_m-1} \psi_{ij_m-1k}^2 \tag{H9}$$

Minimization of $F(\sigma)$ is accomplished by equating the partial derivatives of $F(\sigma)$ with respect to σ_k to zero using the definition

$$\frac{1}{2} \frac{\partial F}{\partial \sigma_{k'}} = \frac{1}{2} \frac{\partial F_1}{\partial \sigma_{k'}} + \frac{1}{2} \frac{\partial F_2}{\partial \sigma_{k'}} = 0 \tag{H10}$$

The first term becomes

$$\frac{1}{2} \frac{\partial F_1}{\partial \sigma_{k'}} = \sum_{m,n} \psi_o(a_1, y_m, z_n)\, \partial \psi_o(a_1, y_m, z_n)/\partial \sigma_{k'}$$

$$+ \sum_{m,n} \psi_o(a_2, y_m, z_n)\, \partial \psi_o(a_2, y_m, z_n)/\partial \sigma_{k'}$$

$$+ \sum_{\ell,m} \psi_o(x_\ell, y_m, c_1)\, \partial \psi_o(x_\ell, y_m, c_1)/\partial \sigma_{k'}$$

$$+ \sum_{\ell,m} \psi_o(x_\ell, y_m, c_2)\, \partial \psi_o(x_\ell, y_m, c_2)/\partial \sigma_{k'}$$

$$+ \sum_{\ell,n} \psi_o(x_\ell, b_2, z_n)\, \partial \psi_o(x_\ell, b_2, z_n)/\partial \sigma_{k'} \tag{H11}$$

Substituting the expressions of (H5) into (H11) yields

$$\frac{1}{2}\frac{\partial F_1}{\partial \sigma_{k'}} = \sum_{m,n}\Bigg\{\Big[\sum_{k=1}^{2NS}\sigma_k\, a_{1k}(y_m,z_n) + \psi_w(a_1,y_m,z_n)\Big]\, a_{1k'}(y_m,z_n)$$

$$+ \Big[\sum_{k=1}^{2NS}\sigma_k\, a_{2k}(y_m,z_n) + \psi_w(a_2,y_m,z_n)\Big]\, a_{2k'}(y_m,z_n)\Bigg\}$$

$$+ \sum_{\ell,m}\Bigg\{\Big[\sum_{k=1}^{2NS}\sigma_k\, a_{3k}(x_\ell,y_m) + \psi_w(x_\ell,y_m,c_1)\Big]\, a_{3k'}(x_\ell,y_m)$$

$$+ \Big[\sum_{k=1}^{2NS}\sigma_k\, a_{4k}(x_\ell,y_m) + \psi_w(x_\ell,y_m,c_2)\Big]\, a_{4k'}(x_\ell,y_m)\Bigg\}$$

$$+ \sum_{\ell,n}\Big[\sum_{k=1}^{2NS}\sigma_k\, a_{5k}(x_\ell,z_n) + \psi_w(x_\ell,b_2,z_n)\Big]\, a_{5k'}(x_\ell,z_n) \qquad \text{(H12)}$$

Equation (H12) is rearranged into a form defining coefficients of σ_k as follows.

$$\frac{1}{2}\frac{\partial F_1}{\partial \sigma_{k'}} = \sum_{k=1}^{2NS}\sigma_k\Big\{a_{1k}(y_m,z_n)\, a_{1k'}(y_m,z_n)$$

$$+ \sum_{m,n} a_{2k}(y_m,z_n)\, a_{2k'}(y_m,z_n) + \sum_{\ell,m} a_{3k}(x_\ell,y_m)\, a_{3k'}(x_\ell,y_m)$$

$$+ \sum_{\ell,m} a_{4k}(x_\ell,y_m)\, a_{4k'}(x_\ell,y_m) + \sum_{\ell,n} a_{5k}(x_\ell,z_n)\, a_{5k'}(x_\ell,z_n)\Big\}$$

$$+ \sum_{m,n}\Big[\psi_w(a_1,y_m,z_n)\, a_{1k'}(y_m,z_n) + \psi_w(a_2,y_m,z_n)\, a_{2k'}(y_m,z_n)\Big]$$

$$+ \sum_{\ell,m}\Big[\psi_w(x_\ell,y_m,c_1)\, a_{3k'}(x_\ell,y_m) + \psi_w(x_\ell,y_m,c_2)\, a_{4k'}(x_\ell,y_m)\Big]$$

$$+ \sum_{\ell,n}\psi_w(x_\ell,b_2,z_n)\, a_{5k'}(x_\ell,z_n) \qquad \text{(H13)}$$

The derivative of F_2 with respect to $\sigma_{k'}$ is given by

$$\frac{1}{2}\frac{\partial F_2}{\partial \sigma_{k'}} = \sum_{j=2}^{j_m-1}\sum_{k=2}^{k_m-1}\left[\psi_{2jk}\,\partial\psi_{2jk}/\partial\sigma_{k'} + \psi_{i_m-1jk}\,\partial\psi_{i_m-1jk}/\partial\sigma_{k'}\right]$$

$$+ \sum_{i=2}^{i_m-1}\sum_{j=2}^{j_m-1}\left[\psi_{ijk_m-1}\,\partial\psi_{ijk_m-1}/\partial\sigma_{k'} + \psi_{ij2}\partial\psi_{ij2}/\partial\sigma_{k'}\right]$$

$$+ \sum_{i=2}^{i_m-1}\sum_{k=2}^{k_m-1}\psi_{ij_m-1k}\,\partial\psi_{ij_m-1k}/\partial\sigma_{k'} \qquad \text{(H14)}$$

We insert the expression for ψ_{2jk} that is contained in equation (H7) to obtain the derivatives with respect to $\sigma_{k'}$ for $1 \le k' \le NL$ given by

$$\frac{1}{2}\frac{\partial F_2}{\partial \sigma_{k'}} = -\sum_{j=2}^{j_m-1}\sum_{k=2}^{k_m-1}\exp(i\lambda Ma_1)\left\{\phi_{2jk} + \exp(i\lambda Ma_1)\sum_{n=1}^{NL}(c_1\sigma_{NS+n1} - c_3\sigma_{n1})\,f_n'(y_j,z_k)/K\right\} c_3\,f_{k'}'(y_j,z_k)/K \qquad \text{(H15)}$$

These derivatives now define new terms,

$$c_{W1jkn} = \exp(i\lambda Ma_1)\,f_n'(y_j,z_k)/K$$

$$W_{1nr} = \sum_{j=2}^{j_m-1}\sum_{k=2}^{k_m-1} c_{W1jkn}\,c_{W1jkr} \qquad \text{(H16)}$$

which are inserted into (H15) to provide the shortened expression

$$\frac{1}{2}\frac{\partial F_2}{\partial \sigma_{k'}} = -c_3\sum_{j=2}^{j_m-1}\sum_{k=2}^{k_m-1} c_{W1jkk'}\,\phi_{2jk} - c_3\sum_{n=1}^{NL}(c_1\sigma_{NS+n1} - c_3\sigma_{n1})W_{1nk'} \qquad \text{(H17)}$$

Equations applicable to the aft boundary face and numbering between $k' = NL+1$ and $k' = NL+NR$ are given by

$$\frac{1}{2}\frac{\partial F_2}{\partial \sigma_{k'}} = \sum_{j=2}^{j_m-1}\sum_{k=2}^{k_m-1}\left[-\phi_{i_m-1jk} + \exp(i\lambda Ma_2)\sum_{n=1}^{NR}(\bar{c}_2\sigma_{NS+n2} + c_4\sigma_{n2})f_n'(y_j,z_k)/K\right] c_4\exp(i\lambda Ma_2)\,f_{k'-NL}'(y_j,z_k)/K \qquad \text{(H18)}$$

With

$$c_{W2jkn} = \exp(i\lambda \mathrm{M} a_2)\, f_n^r(y_j, z_k)/\mathrm{K}$$

$$\mathrm{W}_{2nr} = \sum_{j=2}^{j_m^{-1}} \sum_{k=2}^{k_m^{-1}} c_{W2jkn}\, c_{W2jkr} \tag{H19}$$

we obtain the shortened expressions

$$\frac{1}{2}\frac{\partial \mathrm{F}_2}{\partial \sigma_{k'}} = -\, c_4 \sum_{j=2}^{j_m^{-1}} \sum_{k=2}^{k_m^{-1}} c_{W2jk,k'-NL}\, \phi_{i_m^{-1}jk}$$

$$+\, c_4 \sum_{n=1}^{NR} (\bar{c}_2 \sigma_{NS+n2} + c_4 \sigma_{n2})\, \mathrm{W}_{2n,k'-NL} \tag{H20}$$

The source derivative equations applicable to the lower surface and ranging in number between $k' = \mathrm{NL+NR+1}$ and $k' = \mathrm{NL+NR+ND}$ are given by

$$\frac{1}{2}\frac{\partial \mathrm{F}_2}{\partial \sigma_{k'}} = \sum_{i=1}^{i_m^{-1}} \sum_{j=1}^{j_m^{-1}} \left[-\, \phi_{ij2} + \exp(i\lambda \mathrm{M} x_i) \sum_{n=1}^{ND} (-\, \sigma_{NS+n3} + c_5 \sigma_{n3})\, f_n^d(x_i, y_j) \right] \exp(i\lambda \mathrm{M} x_i) c_5 f_n^d(x_i, y_j) \tag{H21}$$

With

$$c_{W3ijn} = \exp(i\lambda \mathrm{M} x_i)\, f_n^d(x_i, y_j)$$

$$\mathrm{W}_{3nr} = \sum_{i=2}^{i_m^{-1}} \sum_{j=2}^{j_m^{-1}} c_{W3ijn}\, c_{W3ijr} \tag{H21a}$$

we obtain the expressions in reduced form as

$$\frac{1}{2}\frac{\partial \mathrm{F}_2}{\partial \sigma_{k'}} = -\, c_5 \sum_{i=2}^{i_m^{-1}} \sum_{j=2}^{j_m^{-1}} c_{W3ijn'}\, \phi_{ij2} + c_5 \sum_{n=1}^{ND} (-\, \sigma_{NS+n3} + c_5 \sigma_{n3})\, \mathrm{W}_{3nn'} \tag{H22}$$

where $n' = k' - \mathrm{NL} - \mathrm{NR}$.

Equations pertaining to the derivatives of the source terms that number from $k' = \mathrm{NL+NR+ND+1}$ to $k' = \mathrm{NL+NR+ND+NU}$ are given by

$$\frac{1}{2}\frac{\partial \mathrm{F}_2}{\partial \sigma_{k'}} = \sum_{i=2}^{i_m^{-1}} \sum_{j=2}^{j_m^{-1}} \left[-\, \phi_{ijk_m^{-1}} + \exp(i\lambda \mathrm{M} x_i) \sum_{n=1}^{NU} (\sigma_{NS+n4} + c_6 \sigma_{n4})\, f_n^u(x_i, y_j) \right] c_6 \exp(i\lambda \mathrm{M} x_i)\, f_{n'}^u(x_i, y_j) \tag{H23}$$

where $n' = k' - NL - NR - ND$

and

$$c_{W4ijn} = \exp(i\lambda M x_i)\, f_n^u(x_i, y_j)$$

$$W_{4nr} = \sum_{i=2}^{i_m^{-1}} \sum_{j=2}^{j_m^{-1}} c_{W4ijn}\, c_{W4ijr} \tag{H24}$$

Thus we obtain

$$\frac{1}{2}\frac{\partial F_2}{\partial \sigma_{k'}} = -c_6 \sum_{i=2}^{i_m^{-1}} \sum_{j=2}^{j_m^{-1}} c_{w4ijn}\, \phi_{ijk_m^{-1}} + c_6 \sum_{n=1}^{NU} (\sigma_{NS+n4} + c_6\sigma_{n4})\, W_{4nn'} \tag{H25}$$

where again $n' = k' - NL - NR - ND$.

We then come to the equations of the source derivatives applicable to the outboard boundary and ranging in number between $k' = NL+NR+ND+NU+1$ and $k' = NL+NR+ND+NU+NO \equiv NS$, which are obtained from (H14) and use the definition for ψ_{ij_m-1k} of equation (H7):

$$\frac{1}{2}\frac{\partial F_2}{\partial \sigma_{k'}} = \sum_{i=2}^{i_m^{-1}} \sum_{k=2}^{k_m^{-1}} \Big[-\phi_{ij_m^{-1}k} + \exp(i\lambda M x_i) \sum_{n=1}^{NO} (\sigma_{NS+n5} + c_7\sigma_{n5})\, f_n^o(x_i, z_k) \Big]\, c_7 \exp(i\lambda M x_i)\, f_{n'}^o(x_i, z_k) \tag{H26}$$

With

$$c_{W5ikn} = \exp(i\lambda M x_i)\, f_n^o(x_i, z_k)$$

$$W_{5nr} = \sum_{i=2}^{i_m^{-1}} \sum_{k=2}^{k_m^{-1}} c_{W5ikn}\, c_{W5ikr} \tag{H27}$$

we obtain the expressions

$$\frac{1}{2}\frac{\partial F_2}{\partial \sigma_{k'}} = -c_7 \sum_{i=2}^{i_m^{-1}} \sum_{k=2}^{k_m^{-1}} c_{W5ikn'}\, \phi_{ij_m^{-1}k} + c_7 \sum_{n=1}^{NO} (\sigma_{NS+n5} + c_7\sigma_{n5})\, W_{5nn'} \tag{H28}$$

where $n' = k' - NL - NR - ND - NU$.

Derivatives of the F_2 doublet terms with respect to $\sigma_{k'}$ are obtained in a similar fashion. For the forward face, the equations that range in number between $k' = NS+1$ and $k' = NS+NL$ have been derived from (H14) and (H7) and are given by

$$\frac{1}{2}\frac{\partial F_2}{\partial \sigma_{k'}} = c_1 \sum_{j=2}^{j_m-1} \sum_{k=2}^{k_m-1} c_{W1jk,k'-NS}\, \phi_{2jk}$$

$$+ c_1 \sum_{n=1}^{NL} (c_1\sigma_{NS+n1} - c_3\sigma_{n1})\, W_{1n,k'-NS} \qquad \text{(H29)}$$

Equations applicable to the aft face are developed in a similar manner and range in number between $k' = NS+NL+1$ and $k' = NS+NL+NR$. These equations are given by

$$\frac{1}{2}\frac{\partial F_2}{\partial \sigma_{k'}} = -\bar{c}_2 \sum_{j=2}^{j_m-1} \sum_{k=2}^{k_m-1} c_{W2jkn'}\, \phi_{i_m-1jk}$$

$$+ \bar{c}_2 \sum_{n=1}^{NR} (\bar{c}_2\sigma_{NS+n2} + c_4\sigma_{n2})\, W_{2nn'} \qquad \text{(H30)}$$

where $n' = k' - NS - NL$.

Equations developed for the lower face and ranging in number between $k' = NS+NL+NR+1$ and $k' = NS+NL+NR+ND$ are given by

$$\frac{1}{2}\frac{\partial F_2}{\partial \sigma_{k'}} = \sum_{i=2}^{i_m-1} \sum_{j=2}^{j_m-1} c_{W3ijn'}\, \phi_{ij2} + \sum_{n=1}^{ND} (\sigma_{NS+n3} - c_5\sigma_{N3})\, W_{3nn'} \qquad \text{(H31)}$$

where $n' = k' - NS - NL - NR$.

Equations applicable to the upper face and ranging in number between $k' = NS+NL+NR+ND+1$ and $k' = NS+NL+NR+ND+NU$ are obtained in a similar fashion:

$$\frac{1}{2}\frac{\partial F_2}{\partial \sigma_{k'}} = -\sum_{i=2}^{i_m-1} \sum_{j=2}^{j_m-1} c_{W4ijn'}\, \phi_{ijk_m-1} + \sum_{n=1}^{NU} (\sigma_{NS+n4} + c_6\sigma_{n4})\, W_{4nn'} \qquad \text{(H32)}$$

where $n' = k' - NS - NL - NR - ND$.

The final set of equations applicable to the outboard face and having equation numbers between $k' = NS+NL+NR+ND+NU+1$ and $k' = 2NS$ is given as

$$\frac{1}{2}\frac{\partial F_2}{\partial \sigma_{k'}} = -\sum_{i=2}^{i_m-1} \sum_{k=2}^{k_m-1} c_{W5ikn'}\, \phi_{ij_m-1k} + \sum_{n=1}^{NO} (\sigma_{NS+n5} + c_7\sigma_{n5})\, W_{5nn'} \qquad \text{(H33)}$$

where $n' = k' - NS - NL - NR - ND - NU$.

APPENDIX I

DEFINITION OF THE a_{nk} COEFFICIENTS

The a_{nk} coefficients that appear in the (H5) equation set are now defined in terms of the integrals of the source and doublet global functions using equation (G34) and (G35).

The accumulated effect of all source and doublet distributions acting on the upstream grid boundary is represented by a_{1k}. The total effect of all source and doublet distributions acting on the downstream boundary is represented by a_{2k}. The total effect on the lower boundary is a_{3k}, a_{4k} is the accumulated effect on the upper boundary, and a_{5k} is the total effect on the outboard boundary.

The number of global functions applied to the forward surface is NL source and NL doublet distributions. There are NR source and doublet distributions applied to the downstream boundary. Also, there are ND, NU, and NO distributions of sources and doublets applied to the lower, upper, and outboard boundaries respectively. We construct a set of constants formed from various combinations of applied distributions in order to shorten the notation used to identify a particular equation number.

That is, we define a set of acronyms to denote various combinations of the externally applied source and doublet distributions as follows.

$$\begin{aligned}
NL &= NL \\
NLR &= NL + NR \\
NLRD &= NL + NR + ND \\
NLRDU &= NL + NR + ND + NU \\
NS &= NL + NR + ND + NU + NO \\
NSL &= NS + NL \\
NSLR &= NS + NL + NR \\
NSLRD &= NS + NL + NR + ND \\
NSLRDU &= NS + NL + NR + ND + NU
\end{aligned}$$

Also, we identify a new set of constants kn in order to shorten the notation used in identifying the index number associated with the a_{nk} coefficients. These constants are identified as follows.

$$\begin{aligned}
k0 &= k \\
k1 &= k - NL \\
k2 &= k - (NL + NR) \\
k3 &= k - (NL + NR + ND) \\
k4 &= k - (NL + NR + ND + NU) \\
k5 &= k - (NL + NR + ND + NU + NO) \\
&= k - NS \\
k6 &= k - (NS + NL) \\
k7 &= k - (NS + NL + NR) \\
k8 &= k - (NS + NL + NR + ND) \\
k9 &= k - (NS + NL + NR + ND + NU)
\end{aligned}$$

Definitions of the various constants and acronyms are included in the a_{nk} coefficients definitions listed in Table 1 in terms of integrals of the applied source and doublet distributions.

Table 1 — Definition of a_{nk} Coefficients

k - Index Number	$a_{1k}(y,z)$	$a_{2k}(y,z)$	$a_{3k}(x,y)$	$a_{4k}(x,y)$	$a_{5k}(x,z)$
$1 \le k \le NL$	$W^{l}_{ko}\ (o,y,z)$	$W^{l}_{ko}\ (a_1-a_2,y,z)$	$W^{l}_{ko}\ (a_1-x,y,c_1)$	$W^{l}_{ko}\ (a_1-x,y,c_2)$	$W^{l}_{ko}\ (a_1-x,b_2,z)$
$NL+1 \le k \le NLR$	$W^{r}_{k1}\ (a_2-a_1,y,z)$	$W^{r}_{k1}\ (o,y,z)$	$W^{r}_{k1}\ (a_2-x,y_1,c_1)$	$W^{r}_{k1}\ (a_2-x,y,c_2)$	$W^{r}_{k1}\ (a_2-x,b_2,z)$
$NLR+1 \le k \le NLRD$	$W^{d}_{k2}\ (a_1,y,c_1-z)$	$W^{d}_{k2}\ (a_2,y,c_1-z)$	$W^{d}_{k2}\ (x,y,o)$	$W^{d}_{k2}\ (x,y,c_1-c_2)$	$W^{d}_{k2}\ (x,b_2,c_1-z)$
$NLRD+1 \le k \le NLRDU$	$W^{u}_{k3}\ (a_1,y,c_2-z)$	$W^{u}_{k3}\ (a_2,y,c_2,-z)$	$W^{u}_{k3}\ (x,y,c_2-c_1)$	$W^{u}_{k3}\ (x,y,o)$	$W^{u}_{k3}\ (x,b_2,c_2,-z)$
$NLRDU+1 \le k \le NS$	$W^{o}_{k4}\ (a_1,b_1-y,z)$ $+W^{o}_{k4}\ (a_1,b_2-y,z)$	$W^{o}_{k4}\ (a_2,b_2-y,z)$ $+W^{o}_{k4}\ (a_2,b_2-y,z)$	$W^{o}_{k4}\ (x,b_1-y,c_1)$ $+W^{o}_{k4}\ (x,b_2-y,c_1)$	$W^{o}_{k4}(x,b_1-y,c_2)$ $+W^{o}_{k4}\ (x,b_2-y,c_2)$	$W^{o}_{k4}\ (x,b_1-b_2,z)$ $+W^{o}_{k4}\ (x,o,z)$
$NS+1 \le k \le NSL$	$f^{l}_{k5}\ (y,z)/2$	$V^{l}_{k5}\ (a_1-a_2,y,z)$	$V^{l}_{k5}\ (a_1-x,y,c_1)$	$V^{l}_{k5}\ (a_1-x,y,c_2)$	$V^{l}_{k5}\ (a_1-x,b_2,z)$
$NSL+1 \le k \le NSLR$	$V^{r}_{k6}\ (a_2-a_1,y,z)$	$-f^{r}_{k6}\ (y,z)/2$	$V^{r}_{k6}\ (a_2-x,y,c_1)$	$V^{r}_{k6}\ (a_2-x,y,c_2)$	$V^{r}_{k6}\ (a_2-x,b_2,z)$
$NSLR+1 \le k \le NSLRD$	$V^{d}_{k7}\ (a_1,y,c_1-z)$	$V^{d}_{k7}\ (a_2,y,c_1-z)$	$f^{d}_{k7}\ (x,y)/2$	$V^{d}_{k7}\ (x,y,c_1-c_2)$	$V^{d}_{k7}\ (x,b_2,c_1-z)$
$NSLRD+1 \le k \le NSLRDU$	$V^{u}_{k8}\ (a_1,y,c_2-z)$	$V^{u}_{k8}\ (a_2,y,c_2-z)$	$V^{u}_{k8}\ (x,y,c_2-c_1)$	$-f^{u}_{k8}\ (x,y)/2$	$V^{u}_{k8}\ (x,b_2,c_2-z)$
$NSLRDU+1 \le k \le 2NS$	$V^{o}_{k9}\ (a_1,b_1-y,z)$ $+V^{o}_{k9}\ (a_1,b_2-y,z)$	$V^{o}_{k9}\ (a_2,b_1-y,z)$ $+V^{o}_{k9}\ (a_2,b_2-y,z)$	$V^{o}_{k9}\ (x,b_1-y,c_1)$ $+V^{o}_{k9}\ (x,b_2-y,c_1)$	$V^{o}_{k9}\ (x,b_1-y,c_2)$ $+V^{o}_{k9}\ (x,b_2-y,c_2)$	$V^{o}_{k9}\ (x,b_1-b_2,z)$ $-f^{o}_{k9}\ (x,z)/2$

APPENDIX J

EVALUATION OF THE CONTRIBUTION FROM THE INFINITE WAKE

The potential induced by the wake extending beyond the finite difference box containing the wing is given by

$$\phi_w(x,y,z) = \frac{1}{4\pi}\int_{-y_t}^{y_t} \exp(i\omega a_2)\Delta\phi_1(a_2,y_1')\,dy_1' \cdot$$

$$\int_{a_2}^{\infty} \exp(-i\omega x')\,[\partial\psi_1(x-x',y_1-y_1',z_1-z_1')/\partial z_1']\,dx' \qquad \text{(J1)}$$

where a_2 is the x coordinate of the downstream face of the box. The jump in potential at the downstream face is $\Delta\phi_1(a_2,y_1')$. The fundamental solution is ψ_1, given as

$$\psi_1 = \exp\left(-i\lambda(R_1 + M(x'-x))\right)/R_1 \qquad \text{(J2)}$$

with

$$R_1^2 = (x-x')^2 + (y_1-y_1')^2 + (z_1-z_1')^2$$

$$\lambda = \omega M/(1-M^2)$$

The subscript 1 denotes scaled variables; $y_1 = \sqrt{K}\,y$, $z_1 = \sqrt{K}\,z$.

The above definitions are then inserted into the infinite integral to produce

$$I_w = \frac{\partial}{\partial z_1'}\int_{a_2}^{\infty} \exp\left(-i\omega(x'-x)\right) \cdot \exp\left(-i\lambda(R_1 + M(x'-x))\right)/R_1 dx' \qquad \text{(J3)}$$

where an extra exponential is added to provide for a single definition of the dummy variable $(x' - x)$.

J.1 EVALUATION OF THE FLOWWISE INFINITE INTEGRAL

Numerical evaluation of equation (J3) is very difficult. The derivation of the procedure presented here for its evaluation begins by rewriting (J3) as

$$I_w = \exp(-i\omega(x_1-a_2)) \cdot \frac{\partial}{\partial z_1'}\int_{a_2}^{\infty} \exp(i\omega(x_1-a_2)) \cdot \frac{\exp(-i\lambda(R_1 - M(x_1-x_1')))}{R_1}\,dx_1'$$

A transformation of the form $\tau = (x_1 - x_1')$ is applied to (J3), which results in the expression

$$I_w = \exp(-i\omega(x_1-a_2)) \cdot \frac{\partial}{\partial z_1'}\int_{(x_1-a_2)}^{-\infty} \exp(i\omega\tau) \cdot \frac{\exp(i\lambda(\tau^2+r_o^2)^{1/2} - M\tau))}{R_1}\,d\tau \qquad \text{(J4)}$$

where $r_o^2 = (y_1-y_1')^2 + (z_1-z_1')^2$

The exponentials are combined and a transformation of the form $\tau = -\tau$ is applied to produce the expression

$$I_w = \exp(-i\omega(x_1 - a_2)) \cdot \frac{\partial}{\partial z_1'} \int_{-(x_1-a_2)}^{\infty} \frac{\exp(-i\bar{\omega}(\tau + M(\tau^2 + r_o^2)^{1/2}))}{(\tau^2 + r_o^2)^{1/2}} d\tau \tag{J5}$$

$$\text{where } \bar{\omega} = \lambda/M$$

Equation (J5) is then separated into two parts as given by

$$I_w = \exp(-i\omega(x_1 - a_2)) \cdot \left\{ \frac{\partial}{\partial z_1'} \int_o^{\infty} \frac{\exp(-i\bar{\omega}(\tau + M(\tau^2 + r_o^2)^{1/2})}{(\tau^2 + r_o^2)^{1/2}} d\tau \right.$$

$$\left. + \frac{\partial}{\partial z_1'} \int_o^{x_1 - a_2} \frac{\exp(i\bar{\omega}(\tau - M(\tau^2 + r_o^2)^{1/2})}{(\tau^2 + r_o^2)^{1/2}} d\tau \right\} \tag{J6}$$

where a transformation of the form $\tau = -\tau$ has been applied to the finite limit integral.

The two integrals given in (J6) are identical with the integrals used to evaluate the downwash at a field point (x,y) in the $z = 0$ plane of subsonic lifting surface theory in reference 7, with the exception that a double derivative

$$\frac{\partial^2}{\partial z_1 \partial z_1'}$$

is applied to each of the integrals instead of applying a single derivative as indicated in (J6).

The final expression developed for the kernel of the potential function is identically equal to the kernel of the downwash integral multiplied by z_1. That is, the wake integral is given by

$$I_w = z_1 * \exp(-i\omega(x_1 - a_2)) * \left\{ \frac{\alpha}{r_o^2} \left[K_1(\alpha) + i\frac{\pi}{2}(I_1(\alpha) - L_1(\alpha)) \right] \right.$$

$$- \frac{i\alpha}{r_o^2} + \frac{1}{r_o^2} \frac{(x_1 - a_2)}{((x_1 - a_2)^2 + r_o^2)^{1/2}} \exp\left[\frac{i\alpha}{r_o^2} \left((x_1 - a_2)^2 - M\left((x_1 - a_2)^2 + r_o^2\right)^{1/2} \right) \right]$$

$$\left. + \frac{i\alpha}{r_o^2} \int_o^{((x_1 - a_2) - M((x_1 - a_2) + r_o^2)^{1/2}) r_o \beta} \tau/(1 + \tau^2)^{1/2} * \exp(i\omega r_o \tau/\beta)\, d\tau \right\}$$

$$\text{where } \alpha = \omega r_o/\beta \tag{J7}$$

The finite limit integral may be reduced to a closed form expression by applying the approximation of $\tau/(1 + \tau^2)^{1/2}$ that is given in reference 12.

To perform the integration in equation (J7) we consider

$$\int_0^T \tau e^{i\alpha\tau} d\tau / \sqrt{1 + \tau^2} \tag{J8}$$

where $T = \left[x_1 - a_2 - M\sqrt{(x_1 - a_2)^2 + r_o^2} \right] / r_o\beta$, $\alpha = \omega r_o/\beta$ (J9)

Following reference (12), we approximate the integrand by

$$\tau/\sqrt{1 + \tau^2} \cong 1 - c_1 e^{-a\tau} - c_2 e^{-b\tau} - c_3 e^{-c\tau} \sin(\pi\tau) \tag{J10}$$

where $C_1 = 0.101$, $C_2 = 0.899$, $C_3 = 0.09480933$, $a = 0.329$, $b = 1.4067$, and $c = 2.90$

The upper limit may take on negative values. For this case we must introduce a new variable $t = -\tau$ before using the approximation in equation (J10). For the case $(x_i - a) > Mr_o/\beta$, we have

$$\int_0^T \tau e^{i\alpha\tau}\, d\tau \,/\, \sqrt{1+\tau^2} = \int_0^T \left[e^{i\alpha\tau} - c_1 e^{(i\alpha - a)\tau} - c_2 e^{(i\alpha - b)\tau} - c_3 e^{(i\alpha - c)\tau} \sin(\pi\tau) \right] d\tau$$

$$= (e^{i\alpha\tau} - 1)/(i\alpha) - c_1(e^{(i\alpha - a)T} - 1)/(i\alpha - a) - c_2(e^{(i\alpha - b)} - 1)/(i\alpha - b)$$

$$- c_3 \left\{ e^{(i\alpha - c)T} \left[(i\alpha - c) \sin(\pi T) - \pi\cos(\pi T) \right] + \pi \right\} / \left[\pi^2 + (i\alpha - c)^2 \right] \tag{J12}$$

For $(x - a) < Mr_o/\beta$, we write

$$\int_0^T \frac{\tau e^{i\alpha\tau}}{\sqrt{1+\tau^2}}\, d\tau = \int_0^{|T|} \frac{\tau e^{-i\alpha\tau}}{\sqrt{1+\tau^2}}\, d\tau \tag{J13}$$

We see that this is the same as the left hand side of (J12) with α replaced by $-\alpha$.

J.2 SPANWISE INTEGRATION OF THE WAKE INTEGRAND

The potential induced by the wake as defined by equation (J1) can now be expressed in terms of I_w.

$$\phi_w(x,y_1,z_1-z_1') = (1/4\pi)\int_{-y_t}^{y_t} \exp(i\omega a_2)\Delta\phi_1(a_2,y_1')\,dy_1'$$

$$\cdot \exp(-i\omega x)\int_{a_2}^{\infty} \exp\big(-i\omega(x'-x)\big)\cdot\big(\partial\psi_1(x-x',y_1-y_1',z_1-z_1')/\partial z_1'\big)\,dx' \qquad \text{(J14)}$$

This integral is modified by assuming symmetry about the planform centerline ($y' = o$) and takes the form

$$\phi_w(x,y_1,z_1-z_1') = (1/4\pi)\int_{o}^{y_t} \exp(i\omega a_2)\Delta\phi_1(a_2,y_1')\,dy_1'$$

$$\cdot \exp(-i\omega x)\int_{a_2}^{\infty} \exp\big(-i\omega(x'-x)\big)\cdot\big(\partial\psi_1(x-x',y_1-y_1',z_1-z_1')/\partial z_1'$$

$$+\ \partial\psi_1(x-x',y_1+y_1',z_1-z_1')/\partial z_1'\big)\,dx' \qquad \text{(J15)}$$

The infinite integral of equation (J14) has the functional form

$$I_w(x,y_1-y_1',z_1-z_1') = I_{wj}^-$$

The second part of equation (J15) has the functional form

$$I_w(x,y_1+y_1',z_1-z_1') = I_{wj}^+$$

Thus equation (J15) takes the form

$$\phi_w(x,y_1,z_1-z_1') = \exp(-i\omega x)/4\pi\int_{o}^{y_t} \exp(i\omega a_2)\Delta\phi_1(a_2,y_1')\,(I_{wj}^- + I_{wj}^+)dy_1' \qquad \text{(J16)}$$

The jump in potential at the downstream face of the grid network may be expressed in terms of the jump in potential at the trailing edge of the wing.

That is,

$$\Delta\phi_1(a_2,y_1') = \Delta\phi_{i_1+1}(y_1')\cdot\exp\big(i\omega(x_{i_1+1}-a_2)\big) \qquad \text{(J17)}$$

Integration in the spanwise direction is replaced by a finite sum integration procedure that makes use of trapezoidal integration techniques that yield

$$\psi_w(x,y_1,z_1 - z_1') = exp\big(-i\lambda Mx - i\omega(x - x_{i_1+1})\big)\sum_{j=2}^{j_{s1}}\Big\{\Delta\phi_{i_1+1,j}\,(I_{wj}^- + I_{wj}^+)$$

$$+\ \Delta\phi_{i_1+1,j+1}(I_{wj+1}^- + I_{wj+1}^+)\Big\}\,(y_{1j+1} - y_{1j})/8\pi \qquad \text{(J18)}$$

where ψ_w is related to ϕ_w by

$$\phi_w = \exp(i\lambda M x)\psi_w \tag{J19}$$

Note that the spanwise grid has been devised such that the wingtip is located at the midstation between the grid stations defined by $y_{j_{s1}}$ and $y_{j_{s1}+1}$. The potential jump exists only along the trailing edge up to the tip of the wing. Thus the summation indicated in equation (J18) is revised into the following form.

$$\begin{aligned}\psi_w(x,y_1,z_1-z_1') = \exp(-i\lambda x/M + i\omega x_{i_1+1}) \cdot \Big\{ & \Delta\phi_{i_1+1,2}(\bar{I}_{w2} + I^{+}_{w2})\,(y_{1,3}-y_{1,2})/8\pi \\ & + \sum_{j=3}^{j_{s1}-1} \Delta\phi_{i_1+1j}\,(\bar{I}_{wj} + I^{+}_{wj})\,(y_{1j+1}-y_{1j-1})/8\pi \\ & + \Delta\phi_{i_1+1j_{s1}}(\bar{I}_{wj_{s1}} + I^{+}_{wj_{s1}})\,(y_{1j_{s1}+1}+y_{1j_{s1}}-2y_{1j_{s1}-1})/16\pi\Big\}\end{aligned} \tag{J20}$$

The $z = 0$ wing plane lies within the same plane that contains the wake; consequently $z_1' \equiv 0$.

The wake expression is then defined for stations at

$$x = x_i;\ y_1 = y_{1j};\ \text{and}\ z_1 = z_{1k}$$

by the expression

$$\psi_{wijk} = \sum_{\ell=2}^{j_{s1}} \Delta\phi_{i_1+1,\ell}\,\mathrm{WAK}_{\ell ijk} \tag{J21}$$

where for $\ell = 2$ (midspan station)

$$\begin{aligned}\mathrm{WAK}_{2ijk} = \exp(-i\lambda x_i/M + i\omega x_{i_1+1}) \\ \cdot\Big(I_w(x_i,y_{1j}-y_{1,2},z_{1k}) + I_w(x_i,y_{1j}+y_{1,2},z_{1k})\Big)\,(y_{1,3}-y_{1,2})/8\pi\end{aligned} \tag{J22A}$$

For $\ell = \ell$ (the general integration station)

$$\begin{aligned}\mathrm{WAK}_{\ell ijk} = \exp(-i\lambda x_i/M + i\omega x_{i_1+1}) \\ \cdot\Big(I_w(x_i,y_{1j}-y_{1\ell},z_{1k}) + I_w(x_i,y_{1j}+y_{1\ell},z_{1k})\Big)\,(y_{1\ell+1}-y_{1\ell-1})/8\pi\end{aligned} \tag{J22B}$$

For $\ell = j_{s1}$ (the station next to the wingtip),

$$\begin{aligned}\mathrm{WAK}_{j_{s1}ijk} = \exp(-i\lambda x_i/M + i\omega x_{i_1+1}) \\ \cdot\Big(I_w(x_i,y_{1j}-y_{1j_{s1}},z_{1k}) + I_w(x_i,y_{1j}+y_{1j_{s1}},z_{1k})\Big) \\ \cdot(y_{1j_{s1}+1}+y_{1j_{s1}}-2y_{1j_{s1}-1})/16\pi\end{aligned} \tag{J22C}$$

The trapezoidal rule of integration proved inadequate and Legendre integration was applied with special treatment of the singularity. However, the basic form of equation (J22) still holds.

Because of the singularity in the integrand for points near the wake plane $z = 0$, special care must be applied to obtain sufficient accuracy in evaluating the wake integral. The jump in potential at the first point downstream of the trailing edge is determined to satisfy the Kutta condition.

The quantity

$$\Delta\phi(x_{i+1},y_j)$$

is therefore given in terms of the potentials

$$\phi_{i_1-1jk_m-1}\ ,\ \phi_{i_1-1jk_m}\ ,\ \phi_{i_1-1jk_m+1}\ ,\ \phi_{i_1-1jk_m+2}\ ,$$

$$\phi_{i_1jk_m-1}\ ,\ \phi_{i_1jk_m}\ ,\ \phi_{i_1jk_m+1}\ ,\ \phi_{i_1jk_m+2}\ ,$$

whose coefficients must be calculated in the construction of the matrix.

Consider a point y_B lying between the plane of symmetry and the wing tip. We assume

$$y_{j_c} < y_B < y_{j_c}+1$$

In the range of integration $y = 0$ to $y = y_{j_c-1}$, the integrand is smooth and we apply Legendre integration. This is also true of the range y_{j_c+1} to y_T. In the range y_{j_c-1} to y_{j_c+1}, we make the integrand regular by subtracting a singular term which can be added to the result in a closed form integral.

To apply the Legendre quadrature formula we must evaluate the integrand at points y_N, N = 1 to NLEG, which cover the span of integration. For this purpose we need the values of $\Delta\phi$ at the spanwise points y_N. Since $\Delta\phi$ is only defined at the points y_j we must use a Lagrange interpolation polynomial. For each y_N, we determine a J(N) such that

$$y(\mathrm{J(N)}) < y_N < y(\mathrm{J(N)}+1)$$

Then the value of $\Delta\phi$ at $y = y_N$ is given by

$$\begin{aligned}\Delta\phi(x_{i_1+1},y_N) = {} & \Delta\phi(x_{i_1+1},y_{\mathrm{J(N)}-1}) * \mathrm{GL1}\ (y_N,\mathrm{J(N)}) \\ & + \Delta\phi(x_{i_1+1})\ y_{\mathrm{J(N)}}) * \mathrm{GL2}(y_N,\mathrm{J(N)}) \\ & + \Delta\phi(x_{i_1+1},y_{\mathrm{J(N)}+1}) * \mathrm{GL3}(y_N,\mathrm{J(N)})\end{aligned} \tag{J23}$$

where

$$\begin{aligned}\mathrm{GL1}\ (y,\mathrm{J}) &= (y-y_j)\ (y-y_{j+1})\ /\ \left[(y_{j-1}-y_j)\ (y_{j-1}-y_{j+1})\right] \\ \mathrm{GL2}\ (y,\mathrm{J}) &= (y-y_{j-1})\ (y-y_{j+1})\ /\ \left[(y_j-y_{j-1})\ (y_j-y_{j+1})\right] \\ \mathrm{GL3}\ (y,\mathrm{J}) &= (y-y_{j-1})\ (y-y_j)\ /\ \left[(y_{j+1}-y_{j-1})\ /\ (y_{j+1}-y_j)\right]\end{aligned} \tag{J24}$$

The integral we are evaluating is given in equation (J16) which is modified to be

$$\psi_W(x,y_B,z) = \exp\left[-i\,(\lambda x/M-\omega x_{i_1+1})\right] * \int_0^{y_T} \Delta\phi_1\left(x_{i_1+1},y'\right)\left(I_w^- + I_w^+\right) dy'/4\pi \qquad \text{(J25)}$$

Here we have applied equations (J17) and (J19). The portion of this integral for 0 to y_{j_c-1}, then, is given by

$$\exp\left[-i\,(\lambda x/M-\omega x_{i_1+1})\right] \sum_{N=1}^{NLEG} \Delta\phi\,(x_{i_1+1},y_N)\left[I_w^-\,(y_N) + I_w^+\,(y_N)\right] WT\,(N) * (y_{j_c-1}-0) \qquad \text{(J26)}$$

where WT(N) are the Legendre weight coefficients. The quantities $\Delta\phi$ are replaced by equation (J23) to yield

$$\begin{aligned}\exp\left[-i(\lambda x/M-\omega x_{i_1+1})\right] \sum_{N=1}^{NLEG} \Big\{&\Delta\phi(x_{i_1+1},y_{J(N)-1})\ GL1\left(y_N,J(N)\right)\\ &+\Delta\phi(x_{i_1+1},y_{J(N)})\ GL2\left(y_N,J(N)\right)\\ &+\Delta\phi(x_{i_1+1},y_{J(N)+1})\ GL3\left(y_N,J(N)\right)\Big\}\left[I_w^-\,(y_N) + I_w^+\,(y_N)\right] WT(N) y_{j_c-1}\end{aligned} \qquad \text{(J27)}$$

To construct the coefficients of the matrix we need the coefficients of $\Delta\phi\,(x_{i_1+1},y_j)$. For j = J (N) −1, we have

$$\exp\left[-i(\lambda x/M-\omega x_{i_1+1})\right] * GL1\left(y_N,J(N)\right) * \left[I_w^-(y_N) + I_w^+\,(y_N)\right] WT(N) y_{j_c-1} \qquad \text{(J28)}$$

For j = J (N), we have

$$\exp\left[-i\left(\lambda x/M-\omega x_{i_1+1}\right)\right] * GL2\left(y_N,J(N)\right) * \left[I_w^-(y_N) + I_w^+(y_N)\right] WT(N) y_{j_c-1} \qquad \text{(J29)}$$

and for j = J (N) +1, we have

$$\exp\left[-i(\lambda x/M-\omega x_{i_1+1})\right] * GL3\left(y_N,J(N)\right) * \left[I_w^-(y_N) + I_w^+(y_N)\right] WT(N) y_{j_c-1} \qquad \text{(J30)}$$

For some values of j, there may be more than one contribution from the numerical integration; hence these contributions must be summed to obtain the wake terms

WAK1, WAK2, WAK3, WAK4, and WAK5

defined in equation (J21) for ψ on the 5 planar boundaries of the grid.

The integration from y_{j_c+1} to y_T is performed in the same manner. For the singular integral y_{j_c-1} to y_{j_c+1}, the integrand $I_w^- + I_w^+$ is first evaluated at $y = y_B$, the singular point. Then we compute a constant

$$I_{wo} = r_o^2\left(I_w^- + I_w^+\right)$$

where $r_o^2 = Kz^2$. For the numerical integration we use the regular integrand

$$I_w^- + I_w^+ - I_{wo}/r_o^2 \tag{J31}$$

where, now, $r_o^2 = K(y - y_B)^2 + z^2$. The jump in potential is defined at the Legendre points y_N lying in the interval $y_{j_c-1} \le y \le y_{j_c+1}$ by

$$\begin{aligned}\Delta\phi(x_{i_1+1}, y_n) = {} & \Delta\phi(x_{i_1+1}, y_{j_c-1}) * GL1(y_N, J_c) \\ & + \Delta\phi(x_{i_1+1}, y_{j_c}) * GL2(y_N, J_c) \\ & + \Delta\phi(x_{i_1+1}, y_{j_c+1}) * GL3(y_N, J_c)\end{aligned} \tag{J32}$$

Thus for the closed form integral to be added to the integration of equation (J31) we must evaluate

$$\begin{aligned}&I_{wo}\int_{y_{j_c-1}}^{y_{j_c+1}} GL1(y, J_c)\, dy/r_o^2 \\ &I_{wo}\int_{y_{j_c-1}}^{y_{j_c+1}} GL2(y, J_c)\, dy/r_o^2 \\ &I_{wo}\int_{y_{j_c-1}}^{y_{j_c+1}} GL3(y, J_c)\, dy/r_o^2\end{aligned} \tag{J33}$$

Since the numerical integration is performed in the scaled variables, the first integral becomes

$$I_{wo}\int_{y_{j_c-1}}^{y_{j_c+1}} \frac{(y-y_{j_c})\,(y-y_{j_c+1})\,\sqrt{K}\,dy}{(y_{j_c-1}-y_{j_c})(y_{j_c-1}-y_{j_c+1})\,K\left[(y-y_B)^2+z^2\right]}$$

Let $(y - y_B)/|z| = t$, $(y_j - y_B)/|z| = \alpha_j$, and $D_j = y_j - y_{j-1}$. Then the integral above reduces to

$$\frac{|z|\,I_{wo}}{\sqrt{K}D_{j_c}(D_{j_c} + D_{j_c+1})}\int_{\alpha_{j_c-1}}^{\alpha_{j_c+1}} \frac{(t-\alpha_{j_c})\,(t-\alpha_{j_c+1})}{(t^2+1)}\,dt$$

Expanding the numerator and using the relation

$$t^2/(1 + t^2) = 1 - 1/(1+t^2)$$

we obtain

$$\frac{|z|\,I_{wo}}{\sqrt{K}D_{j_c}(D_{j_c} + D_{j_c+1})}\int_{\alpha_{j_c-1}}^{\alpha_{j_c+1}} \left[1 - \frac{(\alpha_{j_c}+\alpha_{j_c+1})t}{1+t^2} + \frac{\alpha_{j_c}\alpha_{j_c+1}-1}{1+t^2}\right] dt \tag{J34}$$

integration yields

$$\frac{|z|\ I_{wo}}{\sqrt{K}\ D_{j_c}(D_{j_c}+D_{j_c+1})}\Bigg[\ \alpha_{j_c+1}\ -\ \alpha_{j_c-1}\ -\ \frac{(\alpha_{j_c}+\alpha_{j_c+1})}{2}\log\left(\frac{1+\alpha_{j_c+1}^2}{1+\alpha_{j_c-1}^2}\right)$$

$$+\ (\alpha_{j_c}\alpha_{j_c+1}-1)(\tan^{-1}\alpha_{j_c+1}\ -\ \tan^{-1}\alpha_{j_c-1})\Bigg] \qquad \text{(J35)}$$

The second integral becomes

$$\frac{I_{wo}}{\sqrt{K}}\int_{y_{j_c-1}}^{y_{j_c+1}}\frac{(y-y_{j_c-1})\,(y-y_{j_c+1})}{(y_{j_c}-y_{j_c-1})\,(y_{j_c}-y_{j_c+1})}\frac{dy}{|(y-y_B)^2+z^2|}$$

Introducing the same variables yields

$$\frac{-|z|I_{o\omega}}{\sqrt{K}\ D_{j_c}D_{j_c+1}}\int_{\alpha_{j_c-1}}^{\alpha_{j_c+1}}\frac{(t-\alpha_{j_c-1})\,(t-\alpha_{j_c+1})}{t^2+1}\,dt$$

Integration then gives us

$$\frac{-|z|I_{wo}}{\sqrt{K}\ D_{j_c}D_{j_c+1}}\Big[\alpha_{j_c+1}-\alpha_{j_c-1}-\frac{(\alpha_{j_c-1}+\alpha_{j_c+1})}{2}\log\left(\frac{1+\alpha_{j_c+1}^2}{1+\alpha_{j_c-1}^2}\right)$$

$$+\ \left(\alpha_{j_c-1}\alpha_{j_c}\ -\ 1\right)\left(\tan^{-1}\alpha_{j_c+1}\ -\ \tan^{-1}\alpha_{j_c-1}\right)\Big] \qquad \text{(J36)}$$

Similarly, the third integral yields

$$\frac{I_{wo}}{\sqrt{K}}\int_{y_{j_c-1}}^{y_{j_c+1}}\frac{(y-y_{j_c-1})\,(y-y_{j_c})}{(y_{j_c+1}-y_{j_c-1})\,(y_{j_c+1}-y_{j_c})}\frac{dy}{|(y-y_B)^2+z^2|}$$

$$=\frac{-|z|I_{wo}}{\sqrt{K}\ D_{j_c+1}(D_{j_c+1}+D_{j_c})}\Big[\ \alpha_{j_c+1}-\ \alpha_{j_c-1}\ -\ \frac{(\alpha_{j_c-1}+\alpha_{j_c})}{2}\log\left(\frac{1+\alpha_{j_c+1}^2}{1+\alpha_{j_c-1}^2}\right)$$

$$+\ \left(\alpha_{j_c-1}\alpha_{j_c}-1\right)\left(\tan^{-1}\alpha_{j_c+1}-\ \tan^{-1}\alpha_{j_c-1}\right)\Big] \qquad \text{(J37)}$$

J.3 DETERMINATION OF THE POTENTIAL JUMP AT THE TRAILING EDGE

The required jump in potential necessary to satisfy smooth flow conditions at the trailing edge is obtained from the derivation given by equation (37), page 46, of Reference 1. It is given in terms of the potential jump on the wing by the expression

$$\Delta\phi_{i_1+1j} = (1 - d_{1i_1}/c_{1i_1} - i\omega/c_{1i_1})\Delta\phi_{i_1j} + (d_{1i_1}/c_{1i_1})\Delta\phi_{i_1-1j} \tag{J38}$$

or is written as

$$\Delta\phi_{i_1+1j} = c_{kc1}\Delta\phi_{i_1j} + c_{kc2}\Delta\phi_{i_1-1j}$$

where

$$c_{1i} = (x_i - x_{i-1})/c_i \quad ; \quad c_i = 1/(x_{i+1} - x_{i-1})(x_{i+1} - x_i)$$

$$d_{1i} = (x_{i+1} - x_i)/d_i \quad ; \quad d_i = 1/(x_{i+1} - x_{i-1})(x_i - x_{i-1})$$

The potential jump at the first differencing station downstream of the wing trailing edge is represented by $\Delta\phi_{i_1+1}$. The potential jump at a point (i,j) on the wing is obtained from the derivation shown on page 66 of Reference 1 and has the form

$$\Delta\phi_{ij} = c_{s2}\phi_{ijk_m-1} - (1 + c_{s2})\phi_{ijk_m} + (1 + c_{s1})\phi_{ijk_m+1}$$

$$- c_{s1}\phi_{ijk_m+1} - (d_{s1}F_{ij}^{(U)} + d_{s2}F_{ij}^{(L)}) \tag{J39}$$

where

$$c_{s1} = 1/4s_1(s_1 + 1) \quad ; \quad c_{s2} = 1/4s_2(s_2 + 1)$$

$$d_{s1} = h(2s_1 + 1)/4(s_1 + 1) \quad ; \quad d_{s2} = h(2s_2 + 1)/4(s_2 + 1)$$

$$s_1 = (z_{k_m+2} - z_{k_m+1})/h \quad ; \quad s_2 = (z_{k_m} - z_{k_m-1})/h$$

$$h = (z_{k_m+1} - z_{k_m})$$

where $F_{ij}^{(U)}$ and $F_{ij}^{(L)}$ are boundary conditions on the upper and lower surfaces.

Thus the potential jump at the first station downstream of the trailing edge in the wake is given by

$$\begin{aligned}\Delta\phi_{i_1+1j} = c_{kc2}\Big(&c_{s2}\phi_{i_1-1jk_m-1} - (1+c_{s2})\phi_{i_1-1jk_m} + (1+c_{s1})\phi_{i_1-1jk_m+1} \\ &- c_{s1}\phi_{i_1-1jk_m+2} - (d_{s1}F^{(U)}_{i_1-1j} + d_{s2}F^{(L)}_{i_1-1j})\Big) \\ &+ c_{kc1}\Big(c_{s2}\phi_{i_1jk_m-1} - (1+c_{s2})\phi_{i_1jk_m} + (1+c_{s1})\phi_{i_1jk_m+1} \\ &- c_{s1}\phi_{i_1jk_m+2} - (d_{s1}F^{(U)}_{i_1j} + d_{s2}F^{(L)}_{i_1j})\Big) \end{aligned} \tag{J40}$$

where

$$c_{kc1} = 1 - d_{1i_1}/c_{1i_1} - i\omega/c_{1i_1}$$

$$c_{kc2} = d_{1i_1}/c_{1i_1}$$

The potential jump at the first finite differencing station downstream of the trailing edge is now defined in terms of the A_{ij} coefficients described in the section on wake boundary conditions and takes the form

$$\begin{aligned}\Delta\phi_{i_1+1j} = &A_{11}\phi_{i_1-1jk_m-1} + A_{12}\phi_{i_1-1jk_m} + A_{13}\phi_{i_1-1jk_m+1} \\ &+ A_{14}\phi_{i_1-1jk_m+2} + A_{21}\phi_{i_1jk_m-1} + A_{22}\phi_{i_1jk_m} + A_{23}\phi_{i_1jk_m+1} \\ &+ A_{24}\phi_{i_1jk_m+2} - c_{kc2}(d_{s1}F^{(U)}_{i_1-1j} + d_{s2}F^{(L)}_{i_1-1j}) \\ &- c_{kc1}(d_{s1}F^{(U)}_{i_1j} + d_{s2}F^{(L)}_{i_1j}) \end{aligned} \tag{J41}$$

Definition of the wake potential is finalized by inserting (J41) into (J21).

$$\begin{aligned}\psi_{wijk} = \sum_{\ell=2}^{J_{s1}} \mathrm{WAK}_{\ell ijk}\Big[&A_{11\ell}\phi_{i_1-1\ell k_m-1} + A_{12\ell}\phi_{i_1-1\ell k_m} \\ &+ A_{13\ell}\phi_{i_1-1\ell k_m+1} + A_{14\ell}\phi_{i_1-1\ell k_m+2} + A_{21\ell}\phi_{i_1\ell k_m-1} \\ &+ A_{22\ell}\phi_{i_1\ell k_m} + A_{23\ell}\phi_{i_1\ell k_m+1} + A_{24\ell}\phi_{i_1\ell k_m+2} \\ &- c_{kc2}\left(d_{s1}F^{(U)}_{i_1-1\ell} + d_{s2}F^{(L)}_{i_1-1\ell}\right) \\ &- c_{kc1}\left(d_{s1}F^{(U)}_{i_1\ell} + d_{s2}F^{(L)}_{i_1\ell}\right) \end{aligned} \tag{J42}$$

Let $$\mathrm{RHS1}_{j_c} = c_{kc2}\left(d_{s1}\mathrm{F}^{(\mathrm{U})}_{i_1-1j_c} + d_{s2}\mathrm{F}^{(\mathrm{L})}_{i_1-1j_c}\right) + c_{kc1}\left(d_{s1}\mathrm{F}^{(\mathrm{U})}_{i_1j_c} - d_{s2}\mathrm{F}^{(\mathrm{L})}_{i_1j_c}\right) \tag{J43}$$

In equation (J42), then

$$\begin{aligned}\psi_{wijk} = \sum_{j_c=2}^{j_{s1}} \Big[& \mathrm{A}_{11j_c}\phi_{i_1-1j_ck_m-1} + \mathrm{A}_{12j_c}\phi_{i_1-1j_ck_m} \\ & + \mathrm{A}_{13j_c}\phi_{i_1-1j_ck_m+1} + \mathrm{A}_{14j_c}\phi_{i_1-1j_ck_m+2} + \mathrm{A}_{21j_c}\phi_{i_1j_ck_m-1} \\ & + \mathrm{A}_{22j_c}\phi_{i_1j_ck_m} + \mathrm{A}_{23j_c}\phi_{i_1j_ck_m+1} + \mathrm{A}_{24j_c}\phi_{i_1j_ck_m+2} \\ & - \mathrm{RHS1}_{j_c}\Big] * \mathrm{WAK}_{j_cijk}\end{aligned} \tag{J44}$$

J.4 INCORPORATION OF THE WAKE INTEGRAL INTO THE EQUATIONS FOR THE APPLIED SOURCE AND DOUBLET DISTRIBUTIONS

Substituting equations (J44) into equation (H13) yields

$$\begin{aligned}\frac{1}{2}\frac{\partial \mathrm{F}_1}{\partial \sigma_r} = & \sum_{k=1}^{2\mathrm{NS}} \sigma_k \mathrm{W}'(k,r) + \sum_{j_c=2}^{j_{s1}} \Big[\mathrm{A}_{11j_c}\phi_{i_1-1j_ck_m-1} \\ & + \mathrm{A}_{12j_c}\phi_{i_1-1j_ck_m} + \mathrm{A}_{13j_c}\phi_{i_1-1j_ck_m+1} + \mathrm{A}_{14j_c}\phi_{i_1-1j_ck_m+2} \\ & + \mathrm{A}_{21j_c}\phi_{i_1j_ck_m-1} + \mathrm{A}_{22j_c}\phi_{i_1j_ck_m} + \mathrm{A}_{23j_c}\phi_{i_1j_ck_m+1} + \mathrm{A}_{24j_c}\phi_{i_1j_ck_m+2} \\ & - \mathrm{RHS1}_{j_c}\Big] \Big\{ \sum_{m,n} \left[a_{1r}(y_m,z_n)\,\mathrm{WAK}_{j_c1mn} + a_{2r}(y_m,z_n)\,\mathrm{WAK}_{j_cj_{max}mn} \right] \\ & + \sum_{\ell,m} \left[a_{3r}(x_\ell,y_m)\,\mathrm{WAK}_{j_c\ell m1} + a_{4r}(x_\ell,y_m)\,\mathrm{WAK}_{j_c\ell mk_{max}} \right] \\ & + \sum_{\ell,n} \left[a_{5r}(x_\ell,z_n)\,\mathrm{WAK}_{j_cj_{max}n} \right] \Big\}\end{aligned} \tag{J45}$$

Here, we defined the array $\mathrm{W}'(k,r)$ as follows:

$$\begin{aligned}\mathrm{W}'(k,r) = & \sum_{m,n} \left[a_{1kmn}a_{1rmn} + a_{2kmn}a_{2rmn} \right] \\ & + \sum_{\ell,m} \left[a_{3k\ell m}a_{3r\ell m} + a_{4k\ell m}a_{4r\ell m} \right] \\ & + \sum_{\ell,n} a_{5k\ell n}a_{5r\ell n}\end{aligned} \tag{J46}$$

where $a_{1kmn} = a_{1k}(y_m, z_n)$, etc. Let

$$\mathrm{WA}_{j_c r} = \sum_{m,n}\left[\mathrm{WAK}_{j_c 1mn} a_{1rmn} + \mathrm{WAK}_{j_c i_{max} mn} a_{2rmn}\right]$$

$$+ \sum_{\ell,m}\left[\mathrm{WAK}_{j_c \ell m,2} a_{3r\ell m} + \mathrm{WAK}_{j_c \ell m k_{max}} a_{4r\ell m}\right]$$

$$+ \sum_{\ell,n} \mathrm{WAK}_{j_c \ell j_{max} n} a_{5r\ell n} \tag{J47}$$

then equation (J45) becomes

$$\frac{1}{2}\frac{\partial \mathrm{F}_1}{\partial \sigma_r} = \sum_{k=1}^{2NS} \sigma_k \mathrm{W}'(k,r) + \sum_{j_c=2}^{J_{s1}} \left[\mathrm{A11}_{j_c} \phi_{i_1-1 j_c k_m - 1} + \mathrm{A12}_{j_c} \phi_{i_1-1 j_c k_m}\right.$$

$$+ \mathrm{A13}_{j_c} \phi_{i_1-1 j_c k_m+1} + \mathrm{A14}_{j_c} \phi_{i_1-1 j_c k_m+2} + \mathrm{A21}_{j_c} \phi_{i_1 j_c k_m-1}$$

$$\left. + \mathrm{A22}_{j_c} \phi_{i_1 j_c k_m} + \mathrm{A23}_{j_c} \phi_{i_1 j_c k_m+1} + \mathrm{A24}_{j_c} \phi_{i_1 j_c k_m+2}\right] WA_{j_c r} - \mathrm{RHSW}(r) \tag{J48}$$

where

$$\mathrm{RHSW}(r) = \sum_{j_c=2}^{J_{s1}} \mathrm{RHS1}_j \, \mathrm{WA}_{j_c r} \tag{J49}$$

The *r th* equation is actually given by

$$\frac{1}{2}\frac{\partial \mathrm{F}_1}{\partial \sigma_r} + \frac{1}{2}\frac{\partial \mathrm{F}_2}{\partial \sigma_r} = 0 \tag{J50}$$

In this equation there are contributions to the coefficients of σ in equation (J48) from $\partial \mathrm{F}_2/\partial \sigma_r$. Thus, for $1 \le r \le \mathrm{NL}$, $1 \le n \le \mathrm{NL}$, we have from equation (H17)

$$\sum_{k=1}^{2ns} \sigma_k \mathrm{W}'(k,r) + \sum_{j=2}^{J_{s1}} (\mathrm{WAKE}\ \phi\ \mathrm{TERMS}) - \mathrm{RHSW}(r)$$

$$- c_3 \sum_{j=2}^{j_{max}-1} \sum_{k=2}^{k_{max}-1} c_{W1\ jkr} \phi_{2jk} - c_3 \sum_{n=1}^{\mathrm{NL}} \left(c_1 \sigma_{\mathrm{NS}+n} - c_3 \sigma_n\right) \mathrm{W}_{1nr} \tag{J51}$$

Hence for equations $r=1$ to NL, we drop the prime on $W(k,r)$ and modify W according to

$$W_{nr} = W_{nr} + c_3^2 W_{1nr} \qquad n=1, \text{NL}$$

$$W_{n+\text{NS}\,r} = W_{n+\text{NS}\,r} - c_1 c_3 W_{1nr} \tag{J52}$$

and the coefficients of ϕ_{2jk} for $2 \le j \le j_{\max}-1$, $2 \le k \le k_{max}-1$ are

$$-c_3\, c_{W1jkr} \tag{J53}$$

We now follow the shortened notation in equation (H6). Thus for $1 \le r \le$ NR, and $1 \le n \le$ NR and for equations NL + r, we have, according to equation (H20).

$$W_{n2\ r+\text{NL}} = W_{n2\ r+\text{NL}} + c_4^2 W_{2nr}$$

$$W_{n2+\text{NS}\ r+\text{NL}} = W_{n2+\text{NS}\ r+\text{NL}} + c_2 c_4 W_{2nr} \tag{J54}$$

and the coefficients $\phi_{i_{\max}-1jk}$ for $2 \le j \le j_{\max}-1$, $2 \le k \le k_{\max}-1$ are

$$-c_4\, c_{W2jkr} \tag{J55}$$

For equations NLR + r and for $1 \le r \le$ ND we modify W according to equation (H23) and obtain

$$W_{n3\ \text{NLR}+r} = W_{n3\ \text{NLR}+r} + c_5^2 W_{3nr}$$

$$W_{n3+\text{NS NLR}+r} = W_{n3+\text{NS NLR}+r} - c_5 W_{3nr} \tag{J56}$$

and the coefficients of ϕ_{ij2} are

$$-c_5\, c_{W3ijr} \tag{J57}$$

For equations NLRD + r and for $1 \le r \le$ NU, $1 \le n \le$ NU, we have from equation (H25)

$$W_{n4\ \text{NLRD}+r} = W_{n4\ \text{NLRD}+r} + c_6^2 W_{4nr}$$

$$W_{n4+\text{NS NLRD}+r} = W_{n4+\text{NS NLRD}+r} + c_6 W_{4nr} \tag{J58}$$

and the coefficients of $\phi_{ijk_{\max}-1}$ are

$$-c_6\, c_{W4ijr} \tag{J59}$$

For equations NLRDU + r and for $1 \le r \le$ NO, $1 \le n \le$ NO, we have from equation (H28)

$$W_{n5\ \mathrm{NLRDU}+r} = W_{n5\ \mathrm{NLRDU}} + c_7^2 W_{5nr}$$

$$W_{n5+\mathrm{NS\ NLRDU}+r} = W_{n5+\mathrm{NS\ NLRDU}+r} + c_7 W_{5nr} \tag{J60}$$

and the coefficients of $\phi_{ij_{\max}-1k}$ are

$$-c_7\, c_{W5ikr} \tag{J61}$$

For equations NS + r and for $1 \le r \le$ NL, $1 \le n \le$ NL, we have from equation (H29)

$$W_{n\ \mathrm{NS}+r} = W_{n\ \mathrm{NS}+r} - c_1 c_3 W_{1nr}$$

$$W_{n+\mathrm{NS\ NS}+r} = W_{n+\mathrm{NS\ NS}+r} + c_1^2 W_{1nr} \tag{J62}$$

and the coefficients of ϕ_{2jk} are

$$c_1\, c_{W1jkr} \tag{J63}$$

For equations NS + NL + r and for $1 \le r \le$ NR, $1 \le n \le$ NR, equation (H30) yields

$$W_{n+\mathrm{NL\ NSL}+r} = W_{n+\mathrm{NL\ NSL}+r} + \tilde{c}_2 c_4 W_{2nr}$$

$$W_{n2+\mathrm{NS\ NSL}+r} = W_{n2+\mathrm{NS\ NSL}+r} + \tilde{c}_2^2 W_{2nr} \tag{J64}$$

and the coefficients of $\phi_{i_{max}-1jk}$ are

$$-\tilde{c}_2 c_{W2jkr} \tag{J65}$$

For equations NSLR + r and for $1 \le r \le$ ND, $1 \le n \le$ ND, equation (H31) leads to

$$W_{n3\ \mathrm{NSLR}+r} = W_{n3\ \mathrm{NSLR}+r} - c_5 W_{3nr}$$

$$W_{n3+\mathrm{NS\ NSLR}+r} = W_{n3+\mathrm{NS\ NSLR}+r} + W_{3nr} \tag{J66}$$

and the coefficients of ϕ_{ij2} are

$$c_{W3ijr} \tag{J67}$$

For equations NSLRD + r and for $1 \le r \le$ NU, $1 \le n \le$ NU, equation (H32) leads to

$$W_{n4\ \mathrm{NSLRD}+r} = W_{n4\ \mathrm{NSLRD}+r} + c_6 W_{4nr}$$

$$W_{n4+\mathrm{NS\ NSLRD}+r} = W_{n4+\mathrm{NS\ NSLRD}+r} + W_{4nr} \tag{J68}$$

and the coefficients of $\phi_{ijk_{\max}-1}$ are

$$-c_{W4ijr} \tag{J69}$$

Finally for equations NSLRU + r and for $1 \leq r \leq$ NO, $1 \leq n \leq$ NO, equations (H33) gives us

$$W_{n5\ \mathrm{NS\ NSLRDU}+r} = W_{n5\ \mathrm{NSLRDU}+r} + c_7 W_{5nr}$$

$$W_{n5+\mathrm{NS\ NSLRDU}+r} = W_{n5+\mathrm{NS\ NSLRDU}+r} + W_{5nr} \tag{J70}$$

and the coefficients of $\phi_{ij_{\max}-1k}$ are

$$-c_{W5ikr} \tag{J71}$$

Equations (J46), (J47), and (J52) through (J71) are computed in the program by the subroutine labeled WMATRX.

APPENDIX K

INTEGRATION OF SOURCE DISTRIBUTIONS FOR RECEIVING POINTS IN THE PLANE OF INTEGRATION

When we integrate the influence of a source distribution on itself, we have to treat the integration separately because of the 1/r singularity. It is possible to eliminate this singularity by introducing polar coordinates about the point where the influence is to be calculated. For a source distribution of the form $x^m y^n$, the integral to be evaluated takes the form

$$\int_{y_1}^{y_2}\int_{x_1}^{x_2} \xi^m \eta^n \exp(-i\lambda r)\, d\xi d\eta/4\pi r \tag{K1}$$

where $r^2 = (x-\xi)^2 + (y-\eta)^2$. Introduction of polar coordinates about $\xi = x$, $\eta = y$ yields integrals of the form

$$\int_{\theta_1}^{\theta_2}\int_{0}^{(y_2-y)/\cos\theta} (x-r\sin\theta)^m (y+r\cos\theta)^n \exp(-i\lambda r)\, dr d\theta \tag{K2}$$

Integration with respect to r leads to four line integrals along the edges of the rectangle that must be evaluated numerically. This procedure turned out to be too costly so a simpler method was derived.

Equation (K1) can be expressed in a more convenient form by a translation of the coordinates. Thus we have

$$\int_{y_1-y}^{y_2-y}\int_{x_1-x}^{x_2-x} \frac{(\xi+x)^m (\eta+y)^n \exp(-i\lambda\sqrt{\xi^2+\eta^2})}{\sqrt{\xi^2+\eta^2}}\, d\xi d\eta \tag{K3}$$

Expanding the numerator and retaining the first order terms in ξ and η yields

$$\int_{y_1-y}^{y_2-y}\int_{x_1-x}^{x_2-x} \frac{[x^m y^n + m x^{m-1} y^n \xi + n x^m y^{n-1}\eta + \ldots.]\, d\xi d\eta}{r} \tag{K4}$$

where r^2 now is $\xi^2 + \eta^2$. This can be integrated in closed form. When the integrand of equation (K4) is subtracted from equation (K3), the resulting integral is nonsingular and can be integrated numerically. Adding the closed form integration of equation (K4) then leads to an accurate way of integrating equation (K1). Thus we integrate numerically the integral

$$\int_{y_1-y}^{y_2-y}\int_{x_1-x}^{x_2-x} [(\xi+x)^m (\eta+y)^n \exp(-i\lambda r) - x^m y^n - m x^{m-1} y^n \xi - n x^m y^{n-1}\eta] d\xi d\eta/r \tag{K5}$$

and add the closed form integration of equation (K4).

By integration by parts we obtain

$$\iint \frac{d\xi d\eta}{r} = \int \log(\xi + r)\, d\eta$$
$$= \eta \log(\xi + r) + \xi \log(\eta + r) - \xi - \eta$$
$$= F_1(\xi.\eta) \tag{K6}$$

Also we have,

$$\iint \frac{\xi d\xi d\eta}{r} = \int r d\eta = \eta r/2 + (\xi^2/2) \log(\eta + r)$$
$$= F_2(\xi.\eta) \tag{K7}$$

Similarly,

$$\iint \frac{\eta d\xi d\eta}{r} = \frac{\xi r}{2} + \frac{\eta^2}{2} \log(\xi + r)$$
$$= F_2(\eta,\xi) \tag{K8}$$

Applying the integration limits of equation (K4) yields for the closed form solution

$$\begin{aligned} & x^m y^n \left[F_1(x_2 - x, y_2 - y) - F_1(x_1 - x, y_2 - y) \right. \\ & \left. - F_1(x_2 - x, y_1 - y) + F_1(x_1 - x, y_1 - y) \right] \\ & + m x^{m-1} y^n \left[F_2(x_2 - x, y_2 - y) - F_2(x_1 - x, y_2 - y) \right. \\ & \left. - F_2(x_2 - x, y_1 - y) + F_2(x_1 - x, y_1 - y) \right] \\ & + n x^m y^{n-1} \left[F_2(y_2 - y, x_2 - x) - F_2(y_2 - y, x_1 - x) \right. \\ & \left. - F_2(y_1 - y, x_2 - x) + F_2(y_1 - y, x_1 - x) \right] \end{aligned} \tag{K9}$$

Since the integrand of equation (K5) goes rapidly to zero at $\xi = \eta = 0$, the range of integration is divided into four rectangles by the lines $\xi = 0$ and $\eta = 0$. The Legendre integration formulas are applied to each rectangle.

APPENDIX L

CONTRIBUTIONS OF THE SOURCES AND DOUBLETS OF THE EXTERIOR SOLUTION TO THE MESH BOUNDARY CONDITIONS IN THE FINITE DIFFERENCE EQUATIONS

We now change notation to a more convenient form. For the source and doublet distributions in Appendix F, we choose the following:

$$a_1 \rightarrow x_1 \qquad a_2 \rightarrow x_{i_{max}}$$

$$b_2 \rightarrow y_{j_{max}} \qquad c_1 \rightarrow z_1 \qquad c_2 \rightarrow z_{k_{max}}$$

For the upstream boundary plane and $1 \leq n \leq NL$,

$$\sigma = \sigma_n^{\ell} f_n^{\ell}(y,z) \tag{L1}$$

$$\mu = \mu_n^{\ell} f_n^{\ell}(y,z) \tag{L2}$$

For the downstream boundary plane and $1 \leq n \leq NR$,

$$\sigma = \sigma_n^{r} f_n^{r}(y,z) \tag{L3}$$

$$\mu = \mu_n^{r} f_n^{r}(y,z) \tag{L4}$$

For the lower boundary plane and $1 \leq n \leq ND$,

$$\sigma = \sigma_n^{d} f_n^{d}(x,y) \tag{L5}$$

$$\mu = \mu_n^{d} f_n^{d}(x,y) \tag{L6}$$

For the upper boundary plane and $1 \leq n \leq NU$,

$$\sigma = \sigma_n^{u} f_n^{u}(x,y) \tag{L7}$$

$$\mu = \mu_n^{u} f_n^{u}(x,y) \tag{L8}$$

For the outboard plane and $1 \leq n \leq NO$,

$$\sigma = \sigma_n^{o} f_n^{o}(x,z) \tag{L9}$$

$$\mu = \mu_n^{o} f_n^{o}(x,z) \tag{L10}$$

Using equations (G49a), (G50a), (G51b), (G52a), and (G53a) and then applying the ordering of the parameters of Appendix I, we obtain for the exterior boundary conditions of the mesh

$$\phi_{1jk} = -\exp\left(i\lambda_1 \mathrm{M} x_1\right) \sum_{n=1}^{\mathrm{NL}} \left[\bar{c}_1 \sigma_{\mathrm{NS}+n} + (\Delta x_1/2)\,\sigma_n\right] f_n^{\ell}(y_j, z_k)/\mathrm{K} \tag{L11}$$

$$\phi_{i_{\max}jk} = \exp\left(i\lambda_1 \mathrm{M} x_{i_{\max}}\right) \sum_{n=1}^{\mathrm{NR}} \left[c_2 \sigma_{\mathrm{NS}+\mathrm{NL}+n} - (\Delta x_m/2)\,\sigma_{\mathrm{NL}+n}\right] f_n^{r}(y_j, z_k)/\mathrm{K} \tag{L12}$$

$$\phi_{ij1} = \exp\left(i\lambda_1 \mathrm{M} x_i\right) \sum_{n=1}^{\mathrm{ND}} \left[-\sigma_{\mathrm{NS}+\mathrm{NLR}+n} - (\Delta z_1/2)\,\sigma_{\mathrm{NLR}+n}\right] f_n^{d}(x_i, y_j) \tag{L13}$$

$$\phi_{ijk_{\max}} = \exp\left(i\lambda_1 \mathrm{M} x_i\right) \sum_{n=1}^{\mathrm{NU}} \left[\sigma_{\mathrm{NS}+\mathrm{NLRD}+n} + (\Delta z_m/2)\,\sigma_{\mathrm{NLRD}+n}\right] f_n^{u}(x_i, y_j) \tag{L14}$$

$$\phi_{ij_{\max}\mathrm{k}} = \exp\left(i\lambda_1 \mathrm{M} x_i\right) \sum_{n=1}^{\mathrm{ND}} \left[\sigma_{\mathrm{NS}+\mathrm{NLRD}U+n} + (\Delta y_m/2)\,\sigma_{\mathrm{NLRDU}+n}\right] f_n^{o}(x_i, z_k) \tag{L15}$$

where NLR = NL + NR, NLRD = NL + NR + ND, and similarly for the other terms. We also define NS = NL + NR + ND + NU + NO.

We now apply these boundary conditions to the finite difference equations along the boundary of the mesh. We begin by rewriting equations (E6) and (E7) in a general form for programming as

$$\begin{aligned}&\mathrm{DIAG}(\mathrm{K}) * \phi_{ijk} + \mathrm{SUB}(\mathrm{K}) * \phi_{ijk-1} + \mathrm{SUPER}(\mathrm{K}) * \phi_{ijk+1} + \mathrm{CIN}(\mathrm{K}) * \phi_{ij-1k} \\ &+ \mathrm{COUT}(\mathrm{K}) * \phi_{ij+1k} + \mathrm{CFOR2}(\mathrm{K}) * \phi_{i-2jk} + \mathrm{CFOR}(\mathrm{K}) * \phi_{i-1jk} + \mathrm{CAFT}(\mathrm{K}) * \phi_{i+1jk} \\ &+ \mathrm{RHS}(\mathrm{K}) = 0\end{aligned}$$

For the upstream boundary, $i = 2$,

$$\mathrm{CFOR(K)} * \phi_{1jk} \text{ must be replaced by}$$

$$-\mathrm{CFOR(K)} * \exp\left(i\lambda_1 \mathrm{M} x_1\right) \sum_{n=1}^{\mathrm{NL}} \left[\bar{c}_1\, \sigma_{\mathrm{NS}+n} + (\Delta x_1/2)\,\sigma_n\right] f_n^{\ell}(y_j, z_k)\ /\mathrm{K}$$

From equation (H16) this becomes

$$= -\mathrm{CFOR(K)} * \sum_{n=1}^{\mathrm{NL}} \left[\bar{c}_1\, \sigma_{\mathrm{NS}+n} + c_3 \sigma_n\right] c_{W1jkn} \tag{L16}$$

where $c_3 = \Delta x_1/2$ and then CFOR(K) must be set to zero.

For $i = i_{max} - 1$ and all j, k, we note that

$$\text{CAFT (K)} * \phi_{i_{\max} jk}$$

must be replaced by

$$\text{CAFT(K)} * \exp\left(i\lambda_1 \text{M} x_{i_{\max}}\right) \sum_{n=1}^{\text{NR}} \left(c_2\, \sigma_{\text{NS+NL}+n} - \frac{\Delta x_m}{2}\, \sigma_{\text{NL}+n}\right) f_n^r\,(y_j, z_k)\ /\text{K}$$

Using equation (H19) with $c_4 = \dfrac{\Delta x_m}{2}$ leads to

$$\text{CAFT(K)} * \sum_{n=1}^{\text{NR}} \left(c_2\, \sigma_{\text{NS+NL}+n} - c_4 \sigma_{\text{NL}+n}\right) c_{W2jkn} \tag{L17}$$

and then CAFT (K) is set to zero.

Similarly, for $k = 2$ and all i, j, we have

$$\text{SUB(2)} * \phi_{ij1} \text{ replaced by}$$

$$-\text{SUB(2)} * \exp\left(i\lambda_1 \text{M} x_i\right) \sum_{n=1}^{\text{ND}} \left(\sigma_{\text{NS+NLR}+n} + \frac{\Delta z_1}{2}\, \sigma_{\text{NLR}+n}\right) f_n^d\,(x_i, y_j)$$

Using equations (H21a) with $c_5 = \Delta z_1/2$ leads to

$$-\text{SUB(2)} * \sum_{n=1}^{\text{ND}} \left(\sigma_{\text{NS+NLR}+n} + c_5\, \sigma_{\text{NLR}+n}\right) c_{W3ijn} \tag{L18}$$

and SUB(2) is set to zero.

For $k = k_{max} - 1$ and all i, j, we have

$$\text{SUPER (KMAX1)} * \phi_{ijk_{\max}} \text{ replaced by}$$

$$\text{SUPER (KMAX1)} * \exp\left(i\lambda_1 \text{M} x_i\right) \sum_{n=1}^{\text{NU}} \left(\sigma_{\text{NS+NLRD}+n} - \frac{\Delta z_m}{2}\, \sigma_{\text{NLRD}+n}\right) f_n^u\,(x_i, y_j) \tag{L19}$$

Using equation (H24) with $c_6 = \Delta z_m\ /2$ yields for equation (L19)

$$\text{SUPER (KMAX1)} \sum_{n=1}^{\text{NU}} \left(\sigma_{\text{NS+NLRD}+n} - c_6 \sigma_{\text{NLRD}+n}\right) c_{W4ijn} \tag{L20}$$

and SUPER (KMAX1) is set to zero.

For $j = j_{max} - 1$ and all i,k,

COUT (K) * $\phi_{ij_{\max}k}$ is replaced by

$$\text{COUT (K)} * \exp\left(i\lambda_1 \text{M} x_i\right) \sum_{n=1}^{\text{NO}} \left(\sigma_{\text{NS+NLRDU}+n} - \frac{\Delta y_m}{2}\sigma_{\text{NLRDU}+n}\right) f_n^o\,(x_i, z_k)$$

Using equation (H27) with $c_7 = \Delta z_1/2$ leads to

$$\text{COUT (K)} \sum_{n=1}^{\text{NO}} \left(\sigma_{\text{NS+NLRDU}+n} - c_7\sigma_{\text{NLRU}+n}\right) c_{W5ikn} \tag{L21}$$

and COUT(K) is set to zero.